FLUID-STRUCTURE INTERACTION OF SUBMERGED SHELLS

A Thesis submitted for the degree of Doctor of Philosophy

by

Richard John Randall

Department of Mechanical Engineering.
Brunel University

April 1990

ACKNOWLEDGEMENTS

I would like to take this opportunity to thank my supervisor, Professor W.G.Price, who has consistently guided ,assisted and supported my efforts for the duration of this study.

Similar sentiments are offered to Dr. B.J.Dobson, my external supervisor, who sowed the seed and was still around at the end to proof read the thesis.

Dr P.Temarel and Mr. A.Ergin who have helped ease the difficulties of being Plymouth-based by their cooperation and adaptability whenever I was in Uxbridge. I look forward to working with them in the next stage of this work.

Mr M.Day who has been a stalwart on many aspects of the experimental design and manufacture.

Finally I forgive my wife Jane and children Charlotte, Louis, Edward and Charles for being noisy and demanding and hope they forgive me for my numerous sins exacerbated by this research.

ABSTRACT

Brunel University, Dept. of Mech. Engineering,Uxbridge

Author: R.J.Randall

Title: Fluid-structure interaction of submerged shells

Degree: Ph.D.

Year: 1990

A general three-dimensional hydroelasticity theory for the evaluation of responses has been adapted to formulate hydrodynamic coefficients for submerged shell-type structures. The derivation of the theory has been presented and is placed in context with other methods of analysis.

The ability of this form of analysis to offer an insight into the physical behaviour of practical systems is demonstrated. The influence of external boundaries and fluid viscosity was considered separately using a flexible cylinder as the model. When the surrounding fluid is water, viscosity was assessed to be significant for slender structural members and flexible pipes and in situations where the clearance to an outer casing was slight.

To validate the three-dimensional hydroelasticity theory, predictions of resonance frequencies and mode shapes were compared with measured data from trials undertaken in enclosed tanks. These data exhibited differences due to the position of the test structures in relation to free and fixed boundaries. The rationale of the testing programme and practical considerations of instrumentation, capture and storage of data are described in detail.

At first sight a relatively unsophisticated analytical method appeared to offer better correlation with the measured data than the hydroelastic solution. This impression was mistaken, the agreement was merely fortuitous as only the hydroelastic approach is capable of reproducing the trends recorded in the experiments. The significance of an accurate dynamic analysis using finite elements and the influence of physical factors such as buoyancy on the predicted results are also examined.

CONTENTS

LIST OF FIGURES

LIST OF TABLES

NOTATION

$[\ ]$	matrix
$[\ ]^T$	transpose matrix
$[\ ]^{-1}$	inverse matrix
$\{\ \}$	vector
∇	Laplace operator = d/dx+d/dy+d/dz in rectangular coordinates
$\dot{}$	temporal derivative
*	complex conjugate

Coordinate systems

x,y,z	rectangular coordinate system
r,θ,z	cylindrical coordinate system

Roman

a	radius
A	surface area or cross-sectional area
A	acoustic damping matrix derived from Sommerfeld radiation condition
$A(\omega)$	accelerance
rA_{jk}	modal constant between points j and k of rth. mode
B	diagonal fitting matrix in IDCA
c	acoustic wavespeed
c_p	low frequency phase velocity of compressional waves ($= \sqrt{K/\rho}$)
c	structural (viscous) damping
C	hydrodynamic damping
C^{-1}	diagonal fitting matrix in DAA2
C_m	coefficient of inertia

C_v	coefficient of damping
D	diagonal fitting matrix in IDCA
E	Youngs modulus of elasticity
F_r,F	generalised fluid force
F_{DR}	Diffraction force
F_{OR}	Froude-Krylov force
g	acceleration due to gravity
G	Green's function
h	thickness
Hn	cylindrical Hankel function of the first kind
H(ω)	frequency response function
I	second moment of area
I_n,K_n	modified Bessel function of order n
J_n,Y_n	Bessel functions of order n
k	structural stiffness
km	wave number
K	hydrodynamic (or acoustic) stiffness
K	bulk modulus
l	length
m	structural mass
M	hydrodynamic (or acoustic) mass
n	normal taken positive into fluid
N	shape function
p	acoustic pressure
p_i	pressure in incident wave
p_R	pressure in reflected wave
p_r	pressure in radiated wave

p_r	rth. principal cordinate
Q	applied force
Q	source strength
R	Reynolds number
R	distance from body ($=\sqrt{x^2 + y^2}$)
s	surface
S	coupling matrix for fluid finite elements
S	Strouhal number
t	time
u,v,w	displacement in coordinate directions
U,V,W	normal velocity on shell surface
U_M	inertial component of normal velocity
U_D	damping component of normal velocity
W_r	rth. characteristic function (mode shape)
x	position of field point
Y	position of integration point
$Y(\omega)$	mobility
Z	total fluid force

Greek

α	damping matrix in DAA
α_r	rth. root of frequency eqn. (2.3)
$\alpha(\omega)$	receptance
β^2	(=h/12a)
γ	virtual mass matrix in DAA
γ^2	coherence
Γ	boundary
δ	delta function

ε	strain
ζ	vorticity
Θ	externally applied fluid force
κ	bulk modulus
λ	non-zero diagonal fitting matrix in IDCA
μ	mass density
ν	Poissons' ratio
ν	viscosity
ν	damping ratio
ρ	fluid density
ρ_s	material density
σ	source density
ϕ	velocity potential
ϕ_r	rth. orthogonal mode shape
ψ	stream function
ω_r	rth. natural frequency
Ω	non-dimensional frequency

CHAPTER 1 - INTRODUCTION

1.1 Preview

Situations in which flexible structures are in contact with a fluid are commonplace. The response of water retaining structures under earthquake loading or the behaviour of flexible pipelines in normal operation being just two examples. Wherever it occurs the presence of the fluid invariably modifies the dynamic behaviour of the structure and it is usual to classify fluid-structure interaction problems into categories determined by the nature of the fluid actions.

The first class of problems is that in which the motion of the fluid is relatively large. It may include the study of flow-induced noise or flutter, boundary layer stability, ship manoeuvrability and forces on propellers. The fluid actions are governed by the flow characteristics which may be described by a linearized form of the Navier-Stokes equation which simplifies nonlinear convective momentum terms but retains the effect of viscosity.

In all other cases the fluid action is governed by a form of the wave equation.

$$\nabla^2 p - \ddot{p}/c^2 = 0 \qquad (1.1)$$

where p(t) is pressure, c is the wavespeed, ($= \sqrt{K/\rho}$), K is the bulk modulus and ρ is the density

The applied forces may be due to mechanical or acoustical sources and there is no difference, within linear acoustic theory, between sound radiation and acoustic scattering phenomena. For problems dealing with the transient response of a structure an incident pressure pulse is often considered. This may emanate from a point source or be represented by a plane wave, neither of which will satisfy the wave equation everywhere. This can be overcome by considering the pressure field in three parts; incident pressure, (p_i), (which would occur in the absence of the structure), reflected pressure, (p_R), (due to the presence of a structure with rigid boundaries) and a radiated pressure, (p_r), (that accounts for the remainder of the total pressure field). Thus,

$$p_{TOT} = p_i + p_R + p_r = p_i + p \qquad (1.2)$$

The incident wave pressure, p_i, is prescribed, and therefore only the scattered parts of the total pressure field are unknown and need to satisfy the wave equation.

Further sub-divisions in the categories of fluid-structure interaction problems are possible to differentiate between situations, such as shock or impact effects, where compressibility of the fluid is significant.

The fluid itself will have differing effects on the

behaviour of the structure depending on its relative density. A light fluid, such as air, will have a comparatively small influence on the structural vibration, but may be important if the acoustic noise produced adversely affects the working environment, e.g. within the cabin of an aircraft.

The radiated pressure in a heavier acoustic medium, such as water, will be significant and will both influence and be influenced by the structural response. The radiated pressure field and the structural response are therefore inexorably linked and neither can be solved independently of the other without making some gross assumptions or approximations. Unfortunately the complexity of the problem is such that attempts to solve simultaneously in the fluid and structural domains are only possible for certain idealised sections such as spherical bodies and infinitely long cylinders in an infinite extent of fluid.

In this work the fluid will generally be taken to be water, which will be deemed to be incompressible but not necessarily inviscid. The structures which are immersed in this fluid will be cylindrical or beam-like and the steady-state rather than the transient structural response will be considered. However the methodology presented will be general and capable of adaptation to many other cases.

The remainder of this chapter reviews the solution methods that have been proposed including analytical techniques, decoupling schemes, approximations, fluid finite elements and boundary elements.

In chapter 2 a two-dimensional fluid-structure interaction problem is analysed in which a circular cross-section is contained within a rigid outer boundary and the annular gap contains a fluid. The linearized Navier-Stokes equation mentioned above is used so that the influence of viscosity can be assessed. By considering adjacent sections as a series of thin strips, a crude three dimensional representation of a free-free beam can be achieved.

A more rigorous treatment of three dimensional shapes appears in the next chapter where the choices to be made when modelling a flexible shell-type structure using finite elements are considered. The determination of hydrodynamic coefficients is explained.

Chapter 4 looks at the requirements for measuring the structural response or the radiated pressure field from a vibrating cylinder submerged in water. The influence of the free surface and rigid side and bottom boundaries on hydrodynamic coefficients is recognised.

The structural responses measured in a series of model tests and predicted from hydroelasticity theory

are presented in the next chapter and finally these are compared and conclusions drawn in chapters 6 & 7.

1.2 Background

Reviewers into the subject of fluid-structure interaction have been faced with a vast amount of literature which has been difficult to categorise or classify. Most of the available references deal with a specific problem or a technique emphasizing certain particular aspects.

There was a plethora of reviews in the mid 1970s since when the bulk of material available has restricted attempts to present an extensive overview. Noor & Dwoyer(1989) have edited the most recent review of fluid-structure interaction which concentrates solely on recent advances, as does Petyt(1980).

Other reviewers like Krajcinovic(1975) and Klosner(1976) have limited themselves to one particular aspect, such as investigations concerned with the response to acoustic shocks of shells submerged in a fluid of infinite expanse.

In other cases where the reviewers attempted to be more encompassing there is still disagreement as to the most satisfactory format for presenting the material. Menton & Magrab(1973), Firth(1975) and Geers(1975) favoured a listing in chronological order whereas

Zienkiewicz & Bettes(1978) classified the subject according to the amplitude and duration of the relative motion of the two media. Chen & Pierucci(1977) chose to differentiate between the action of the exciting force which can be mechanically, acoustically or hydrodynamically applied. Kalinowski(1975) looked at the solution techniques that were available at the time and listed the commercial and research computer programmes that used them.

For these reasons the review which follows does not attempt to be totally comprehensive. The information has been presented according to the various solution techniques, starting with analytical techniques, through approximations, fluid finite elements and boundary element methods to boundary integral methods and hydroelasticity.

1.3 Analytical methods

When considering the response of a submerged structure the crux of the problem is in the applied loading. For the same structure in air, the external forces will be specified and will not be altered by the dynamic response. This is no longer true when the structure is immersed in a fluid whose specific acoustic impedance approaches that of the structural material. The pressure loading due to the fluid is not known a priori but depends on the surface motions. The

equations of structural and fluid motion are inexorably linked and must be solved simultaneously unless certain assumptions are made which decouple them.

Analytical methods do not contain any assumptions of this sort and because they require a solution at every point in the spatial continuum they are necessarily limited. They can only be used sensibly when the wet surface of the submerged structure can be defined in terms of a single coordinate, for example describing a spherical surface or an infinite circular cylindrical surface.

The free vibration of a submerged spherical shell has been studied by Lou & Su(1966) and Berger(1969) and more recently by Felippa & Geers(1980), in which the complex natural frequencies of the sphere are obtained from the roots of polynomial equations. Junger(1952), Bleich & Baron(1954) and Warburton(1961) have obtained results for the vibration of infinite flexible cylinders surrounded by, or containing, a fluid by matching solutions at the interface for standing waves in the fluid and vibrations of the cylinder.

Similarly the transient response of spheres and infinite cylinders has provided exact solutions which are benchmarks against which alternative solutions can be matched. The earliest work was presented by Carrier(1951) who considered a plane wave incident on a

cylindrical shell. Carrier formulated the equations but he did not provide any numerical examples. Lax, Sette & Gooding(1953), Murray(1955), Forrestal & Alzheimer(1968) and Forrestal(1968) did derive results but only for the first few circumferential modes of vibration.

Huang(1970) and Huang & Wang(1970) were among the first to produce results for a significant number of modes by taking the Laplace transform of the coupled field equations and then expressing quantities as Fourier series in the angular coordinate. The resulting algebraic equations can be solved but transforming back into the time domain presents some difficulties. Geers(1969) employed a more indirect approach transforming back into the time domain before solving the equations. The exact solutions obtained have been compared with approximations which neglect one of the components of the external pressure field. Geers found that neglecting the scattered wave results in underestimates of the post-envelopment shell velocity by factors greater than two, whereas failure to account for the radiated wave yielded results which were only slightly over-estimates. From this was conceived the idea that approximations could be used which would give reasonable results even though their physical basis may be ill-founded.

1.4 Approximations

The earliest work in which an approximation for the generalised forces due to pressure loading exerted on a shell is used to uncouple the motion of the fluid from that of the shell is by Mindlin & Bleich(1953). The main effect of the approximation is to give the reflected and radiated waves associated with each mode of the shell the propagation characteristics of plane waves rather than cylindrical or spherical waves. Hence it is known as the plane wave approximation (PWA). It has been shown that this approximation is accurate at the early stages of envelopment by an incident shock wave and become progressively less accurate at later times. Separating the total pressure field in a manner similar to eqn(1.2) into a prescribed (or incident) part, p_i, and an unknown scattered (or radiated and reflected) part, p, on the shell surface, there will be corresponding generalised force matrices F_i and F. The normal veocity on the shell surface will also be made up of an incident part $U_i(s,t)$ and a radiated part U(s,t) corresponding to p_i and p. The radiated generalised fluid force predicted by the PWA is directly proportional to the radiated velocity through a matrix α

$$F = \alpha U \qquad (1.3)$$

so that the sole effect of the fluid on the structure is radiation damping.

An improved short-time approximation was proposed by Haywood(1958) who introduced an after-flow coefficient which accounted in part for the cylindrical nature of the scattered wave. This approximation is known as the curved wave approximation (CWA). There has been considerable effort into assessing, through numerical examples, the accuracy of the PWA and CWA compared with exact solutions. (Herrman & Russell(1967), Berglund & Klosner(1968), Bedrosian & Dimaggio(1972) and Grigoluik & Gorshkov(1974)). There have however been very few comparisons in the open literature with practical tests. Chertock(1970) reviews some experimental work that was done more than 15 years earlier and which on the theoretical side uses a different approximation to uncouple the motion of shell and fluid. In this approximation the fluid is considered incompressible and pressures are transmitted with infinite velocity. The virtual mass approximation (VMA) in which radiated generalised fluid force is proportional to the acceleration of the fluid introduces an added mass term into the equations of motion and is valid for low frequency modes

$$F = \gamma \ddot{U} \tag{1.4}$$

The doubly asymptotic approximation (DAA) proposed by Geers(1971) is an amalgam of the PWA and VMA

$$\dot{U} = \alpha^{-1}\dot{F} + \gamma^{-1}F \tag{1.5}$$

so that it has the advantage of accuracy at early and late times but at intermediate times it overpredicts the fluid resistance and thus overdamps the structural vibration. This approximation has been widely adopted despite its limitations and has been proposed and used as a tool for predicting the dynamic response of complex structures by Ranlet, DiMaggio, Bleich & Baron(1977) and Geers(1978).

Further developments in this area have accepted that the DAA offers the best compromise between computational cost and accuracy and have only attempted to improve the accuracy at intermediate frequencies and times. The improved doubly asymptotic approximation (DAA2) (Geers(1978)) and the inertial-damping collocation approximation (IDCA) (Dimaggio, Ranlet, Bleich & Baron(1978)) are the most recent variations. DAA2 uses a diagonal fitting matrix, C, to match one of the two components of the impedance with the exact value at an intermediate frequency.

$$\ddot{U} + C^{-1}\dot{U} = \alpha^{-1}(\ddot{F} + \alpha\gamma^{-1}\dot{F}) + C^{-1}\gamma^{-1}F \qquad (1.6)$$

with $C^{-1} = 0$ this reduces to DAA.

The IDCA uses two fitting matrices and by splitting the induced normal velocity, U, into inertial and damping components U_M and U_D can be used to match both the acoustic reactance and resistance at two selected frequencies

$$\dot{U}_M - B\lambda\ddot{U}_M = \gamma^{-1}F + B\ddot{F} \tag{1.7}$$

$$\ddot{U}_D - D\,U_D = \alpha^{-1}\ddot{F} \tag{1.8}$$

$$U = U_M + U_D \tag{1.9}$$

B and D are the diagonal fitting matrices and λ is a non-zero diagonal matrix introduced to permit the IDCA to approach the correct asymptotic limits at zero and infinite frequencies. Matrices B and D are chosen so that exact solutions for the resistive and reactive components of response are obtained, respectively, at two intermediate driving frequencies. If B and D are set to zero, eqns(1.8)-(1.10) reduce to the DAA of eqn(1.6). Vasudevan & DiMaggio(1981) have compared the approximations DAA, DAA2 and IDCA with exact solutions for the transient response of a spherical shell under a plane step shock wave.

1.5 Fluid finite elements

As one moves away from relatively straightforward geometric shapes it is necessary to resort to methods which yield solutions at only a finite number of spatial points rather than every location. Finite element analysis is now well established and finite element/DAA formulations have been presented (DeRuntz, Geers & Felippa (1980)); however it is not the only alternative.

Both the fluid and the structure can be represented

with finite elements. The structural analysis is invariably performed using a Lagrangian approach based on displacement. The fluid analysis can be performed in one of two ways. Either a Lagrangian approach can be adopted so that the fluid is treated as an elastic solid with negligible shear modulus (Akkas, Akay & Yilmaz(1979)). A disadvantage of this method is that the fluid finite element mesh may become highly contorted as it follows the fluid motion. Thus, the use of fluid finite elements is more applicable to examples in which the fluid is totally contained within the structure. However the coupling is simplified as no special distinction is made between solid and fluid elements other than the fact that the material constants used to define the element fluid stiffness are selected in a particular manner (Miller, Constantino & Fey(1967)).

Alternatively an Eulerian approach can be employed with the fluid characterised by a single variable (pressure or potential) and coupling achieved by consideration of interface forces. Discretising the wave equation (1.1), leads to

$$[\ M\ ]\{\ \ddot{p}\ \} + [\ K\ ]\{\ p\ \} - \{\ f\ \} = 0 \qquad (1.10)$$

where [M], [K] are acoustic mass and stiffness matrices that are functions of fluid topology and wave speed, c.

{ p } is pressure

and { f } is a forcing function which is determined from the fluid structure interaction.

As the fluid motion is constrained to move with the structure at the interface, the forcing function {f} can be related to the structure surface motion through

$$\{ f \} = [S]\{ \ddot{u} \} \qquad (1.11)$$

where [S] is determined from the appropriate shape functions in both fluid and structural regimes.

Finally, the fluid interface pressure {p} can be related to the equivalent interaction nodal force, {F}, by the principle of virtual work.

$$\{ F \} = - [S]^T \{ p \} \qquad (1.12)$$

Therefore simultaneous equations relating structural and fluid motion can be written

$$\begin{bmatrix} m & 0 \\ -S & M \end{bmatrix} \begin{Bmatrix} \ddot{u} \\ \ddot{p} \end{Bmatrix} + \begin{bmatrix} c & 0 \\ 0 & 0 \end{bmatrix} \begin{Bmatrix} \dot{u} \\ \dot{p} \end{Bmatrix} + \begin{bmatrix} k & S^T \\ 0 & K \end{bmatrix} \begin{Bmatrix} u \\ p \end{Bmatrix} = \begin{Bmatrix} Q_{ext} \\ 0 \end{Bmatrix} \qquad (1.13)$$

where [m], [c], [k] are structural mass, damping and stiffness matrices respectively.

Q_{ext} is an external force vector.

Unfortunately the solution of eqn.(1.13) cannot be accomplished using the standard solution techniques of finite element structural analysis as these utilise the

fact that coefficient matrices are symmetric and banded. Nor can time-marching algorithms such as the Newmark-Beta method be used for transient analysis, as spurious oscillations arise from the asymmetric matrices. Extensive manipulation is required to get the matrices into symmetric form; alternatively eqn.(1.13) can be reduced to two symmetric equations dealing separately with structural displacement or the pressure variable in an iterative manner. (Park,DeRuntz & Felippa(1977), Babu & Reddy(1981) and Zienkiewicz & Taylor(1985)).

In the absence of external forces eqn.(1.13) yields a real eigenvalue problem of the form

$$\left(-\omega^2\begin{bmatrix} m & 0 \\ -S & M \end{bmatrix} + \begin{bmatrix} k & S^T \\ 0 & K \end{bmatrix}\right)\begin{Bmatrix} u \\ p \end{Bmatrix} = 0 \qquad (1.14)$$

solution of which determines the natural frequencies.

A method whereby the matrices in eqn.(1.14) can be expressed in a symmetrical form was suggested by Irons(1970) and requires [K] to be invertible. Felippa(1985) gives three alternative methods of symmetrization, each of which requires one of the matrices [m], [k], [M] to be invertible.

The equation of motion of a small element of fluid, ignoring viscosity is

$$\rho\, u = -\nabla p \qquad (1.15)$$

from which it can be seen that an Eulerian approach based on pressure is almost identical to an acceleration potential formulation. Alternative Eulerian formulations for modelling the fluid in fluid-structure interaction problems are possible. Olsen & Bathe(1985) present a method based on velocity potential, with one pressure nodal variable. This produces a symmetric formulation and appears to lead to the existence of a "damping" matrix, however, the non-standard eigenvalue problem derived does have real roots. Felippa(1985) uses displacement potential to arrive at equations similar to (1.13) and (1.14). Morand & Ohayon(1979) and Geradin , Robert & Huck(1984) work with both displacement potential and pressure as variables in the fluid. This leads to larger, very sparse matrices, which require no special symmetrization, but which are highly singular.

A Lagrangian formulation can be used for the fluid domain, where displacement is the unknown variable and coupling is ensured by matching normal displacements at the fluid-structure interface. Unfortunately the irrotational condition in the fluid is not satisfied and the eigensolution contains many zeros corresponding to purely circulatory modes. Careful examination of the results is required to extract the relevant information. This problem can be overcome by modifying the variational principle to include a penalty function, as

pointed out by Zienkiewicz & Bettes(1978), Hamdi, Ousset & Verchery(1978) and Deshpande, Belkune & Ramesh(1981).

1.5.1 Regions with infinite boundaries

Special consideration must be given to problems involving an unbounded fluid domain as either the mesh must be truncated at some distance relatively near to the submerged structure or an inordinate amount of computer space must be allocated to modelling the fluid with little remaining for the structure itself.

Zienkiewicz & Newton(1969) developed a radiation condition for boundaries a large distance, compared with an acoustic wavelength, from the vibrating structure. Assuming that the boundary is far enough away, the radiation pressure wave can be considered to have a plane wavefront. The outgoing pressure wave crossing the boundary will be a function of direction and time,

$$p = f(n - ct) \tag{1.16}$$

n being the direction normal to the boundary, taken positive in the direction of the out-going wave.

There will be no incoming waves (by assumption)

so $\partial p/\partial x = f'$

and $\partial p/\partial t = -cf'$

giving the boundary condition

$$\frac{\partial p}{\partial x} = -\frac{1}{c}\frac{\partial p}{\partial t} \tag{1.17}$$

For a periodic solution with frequency ω this becomes

$$\frac{\partial p}{\partial n} + i\omega\frac{p}{c} = 0 \qquad (1.18)$$

which can be incorporated into the Somerfeld(1949) radiation condition

$$\lim_{r\to\infty} \quad r\left(\frac{\partial p}{\partial n} + i\omega\frac{p}{c}\right) = 0 \qquad (1.19)$$

which simultaneously satisfies eqn.(1.18) and the condition that pressure should tend to zero as the distance from the source, r, tends to infinity.

Zienkiewicz & Bettes(1975) have shown that this condition can be applied with some approximation at a finite distance from the disturbance and can be easily incorporated into the discretised equations of motion. Eqn.(1.10) is modified to

$$[M]\ddot{p} + [A]\dot{p} + [K]p - [S]\ddot{u} = 0 \qquad (1.20)$$

where $[A] = 1/(\rho c)\int_{\Gamma_r}[N]^T[N]\,d\Gamma$

and Γ_r is the distant boundary used to model the radiation. The equations of motion are the same as eqn.(1.13) except that the lower right partition of the $\{\dot{u}\}$ vector has [A] in place of [0].

Alternative ways of handling the infinite boundary problem for methods that consider both the structure and the fluid to be comprised of finite elements are

"infinite elements" (Zienkiewicz & Bettes(1975), Bettes(1980) and Goransson & Davidsson(1987)) and boundary integral methods.

1.5.2 Boundary integral methods

Boundary integral methods are means by which the fluid pressure can be assessed at the fluid-structure interface and divide into two categories; simple source methods and Helmholtz-formulation methods.

In the simple source method described by Chen & Schweikert(1963) the pressure in the fluid region surrounding the structure is represented as the integral of a source density, σ, over the surface

$$p(\tilde{x}) = \int_{\Gamma} \sigma(\tilde{x},\tilde{y})\, G(\tilde{x},\tilde{y})\, d\Gamma(\tilde{y})$$

$$i\omega\rho U(\tilde{x}) = \sigma(\tilde{x})/2 - \int_{\Gamma} \sigma(\tilde{y}) \frac{\partial G(\tilde{x},\tilde{y})}{\partial n(\tilde{x})} d\Gamma(\tilde{y}) \qquad (1.21)$$

in which $G(\tilde{x},\tilde{y}) = e^{(-ik(\tilde{x}-\tilde{y}))}/4\pi(\tilde{x}-\tilde{y})$ is the free-field Greens function which satisfies the wave equation and the conditions that only outgoing waves are allowed from a point source and that pressure tends to zero at an infinite distance from the source, and $\tilde{x},\tilde{y}$ are points on the closed surface Γ

p is pressure

U is velocity

n is the outward normal at the fluid-structure interface.

The principal values of integrals are to be taken, since they are singular when x and y coincide. The discrete form of eqns(1.21) may be written as a pair of matrix equations

$$p(\tilde{x}) = P\,\sigma(\tilde{y})$$

$$U(\tilde{x}) = R\,\sigma(\tilde{y}) \qquad (1.22)$$

The elements of the matrices P and R are surface integrals involving the integrands G and dG/dn respectively and which can be solved to determine σ and then p. However,it is pointed out by Copley(1968) and Schenck(1968) that this method breaks down at certain (critical) frequencies. Copley proves that these frequencies are the eigenvalues of the interior problem with condition p=0 on Γ. As the frequency approaches a critical frequency the source density becomes infinite. If a finite source density were used in the case of a critical frequency there would be no effect outside Γ as the interior would provide zero impedance to this configuration. Jones(1974) suggests a modification, replacing $G(\tilde{x},\tilde{y})$ by a similar function, which prevents this failure for a certain frequency range.

In the Helmholtz-formulation method, the pressure distribution is given by the surface Helmholtz integral equation (Baker & Copson(1950))

$$p(\tilde{x}) = 2\int_{\Gamma} p(\tilde{y})\,\frac{\partial G(\tilde{x},\tilde{y})}{\partial n(\tilde{x})}\,d\Gamma(\tilde{y}) + 2i\omega\rho\int_{\Gamma} U(\tilde{y})\,G(\tilde{x},\tilde{y})\,d\Gamma(\tilde{y}) \qquad (1.23)$$

This equation can be solved numerically (Seybert, Soenarko, Rizzo & Shippy(1985)) but fails at the same critical frequencies as the simple source method. Schenck(1968) has presented a method which avoids the cavity resonance problem by simultaneously solving the surface Helmholtz integral eqn(1.24) and the interior Helmholtz integral (Kupradze(1952)).

Finally, in this section, it is noted that evaluation of the Helmholtz equation is complicated and must be undertaken by numerical means for anything other than simple geometric shapes. A method of modelling infinite regions of fluid is to use fluid finite elements from the submerged structure out to a spherical surface surrounding it. A standard series solution for the Helmholtz equation outside a spherical cavity, is then used to model the external region out to infinity. Hunt, Knittel, & Barach(1974) and Hunt, Knittel, Nichols & Barach(1975) have used this method for acoustic radiation and scattering problems.

1.6 Hydroelasticity

The preceding section describing boundary integral methods provides some of the background for the recent developments (Bishop, Price & Wu(1986)) relating to a general theory of hydroelasticity.

Hydroelasticity is the study of the behaviour of a

flexible body moving through a fluid. Hydroelasticity theory has been established in an attempt to unify hitherto disparate parts of Naval Architecture; namely, theory of manoeuvring and seakeeping and structural analysis. In seakeeping analysis the ship has been treated as a rigid body (Korvin-Kroukovsky (1961), Gerritsma & Beukelman(1964) and Lewis(1967)), whereas ship structural analysis was considered as a problem of statics solved by techniques that were to some extent empirical (Murray (1965)). The approach suggested by Bishop & Price (1979) was to apply established techniques of dynamics to the overall subject of hull response, so that determination of symmetric motions of heave and pitch of a rigid hull formed just part of the hydroelastic analysis.

Fundamental to the problem of structural ship dynamics is determination of the applied fluid forces, Betts, Bishop & Price(1977) adopted strip theory of which there are several formulations. Elementary (Gerritsma & Beukelman(1964) and Lewis(1967)), revised (Salvesen, Tuck & Faltinsen(1970) and Vugts(1971)) and rational strip theories (Ogilvie & Tuck(1969)) have been developed and evaluated (Faltinsen (1974)). It is, however, an approximate procedure as it assesses the two-dimensional hydrodynamic properties of a strip of fluid on to the hull. The resultant fluid actions derived by semi-empirical means are then summed along

the length of the hull without consideration of the longitudinal motions.

These limitations were partially responsible for the decision to employ "dry" rather than "wet" modes in the modal analysis used in the current theory (Bishop & Price(1976)). As the fluid forces determine the mode shapes, the orthogonality condition will rely on the strip theory, with all its inherent weaknesses, in a "wet modes" analysis. With the chosen technique, all hydrodynamic forces and forces due to structural damping are regarded as being applied to the structure whose dynamic undamped vibration characteristics have been established in vacuo. The orthogonality properties of the dry modes are uncomplicated and one of the great imponderables, structural damping, is isolated in the analysis.

A unified dynamic analysis of ship response in waves was presented by Bishop, Price & Tam(1977) which enabled symmetric responses and associated bending moments and shear forces to be determined at any section of a "beam-like" hull. This was extended by Bishop, Price & Temarel(1979) to include asymmetric modes for ships with port-starboard symmetry and extended again to admit asymmetric structures, e.g. aircraft carriers (Bishop, Price & Temarel(1984) or ships having an angle of heel (Conceicao, Price & Temarel (1984)). The transient response of a ship slamming in heavy seas has also been

considered (Bishop, Price & Tam(1978) and Belik, Bishop & Price(1980)) and compared with measured data obtained from trials on board frigates at sea (Bishop, Clarke & Price(1984)).

In all of the analyses performed up to this date strip theory had been employed with the hull of the ship represented as either a Timoshenko or a Vlasov beam (Bishop, Price & Zhang Xicheng(1983)). A major development was the work produced by Bishop, Price & Wu(1986) in which strip theory was superceded by a three dimensional potential theory which allows a variety of floating or submersible structures such as small water area twin hull vessels (SWATHs) (Price,Temarel & Wu(1985), flexible jack-up rigs (Fu, Price & Temarel(1986) and cantilever plates (Fu & Price(1987)) to be analysed. The traditional potential theory used in rigid body dynamics (Newman (1978)) has been extended to include distortion modes. The boundary value problem postulated is solved by boundary integral equations using the singularity distribution technique, with free surface and forward speed effects included.

This work seeks to extend this progression by developing the existing theory to situations in which the responses of a submerged flexible shell-type structure are analysed. A new class of structure is thereby introduced into the analyses and the predictions are compared with a series of experimental tests.

CHAPTER 2 - VISCOUS MODEL

2.1 Introduction

The Navier-Stokes equations and the equation of continuity completely describe the plane flow of an incompressible Newtonian fluid with constant viscosity. They are used here as the basis on which to determine the added mass and damping associated with the vibration of a beam in a confined fluid. The work that is included in this chapter has been published in reports (Randall(1986,1987)) and a paper (Hosoda, Price & Randall(1989)) that is included at Appendix E. Full details are available in the references and to avoid repetition only an outline will be included in this portion of the text.

Added mass is a well-known concept and can be traced back to Stokes(1843). For a structural body in an infinite, inviscid fluid it can be easily evaluated. In certain circumstances, this simple approach may be all that is required. However in reality there will invariably be an external boundary to consider. When this outer boundary comes into close proximity with the structure it greatly increases the magnitude of the added mass. In this situation it is also appropriate to consider the effects of viscosity in the fluid. The inclusion of viscosity related terms into the formulation increases the added mass in a frequency

dependant manner; furthermore hydrodynamic damping is introduced.

2.2 Mathematical model

Adopting the system studied by Chen, Wambsganss & Jendrzejczyk(1978), a flexible cylindrical rod is considered vibrating in a viscous fluid enclosed by a rigid concentric cylindrical shell. However, to enable variations in the response of a projectile emerging from an outer tube to be studied, the length of the cylinder was finite and the outer boundary may be totally removed or a transitional state with the cylinder partially enclosed can be considered.

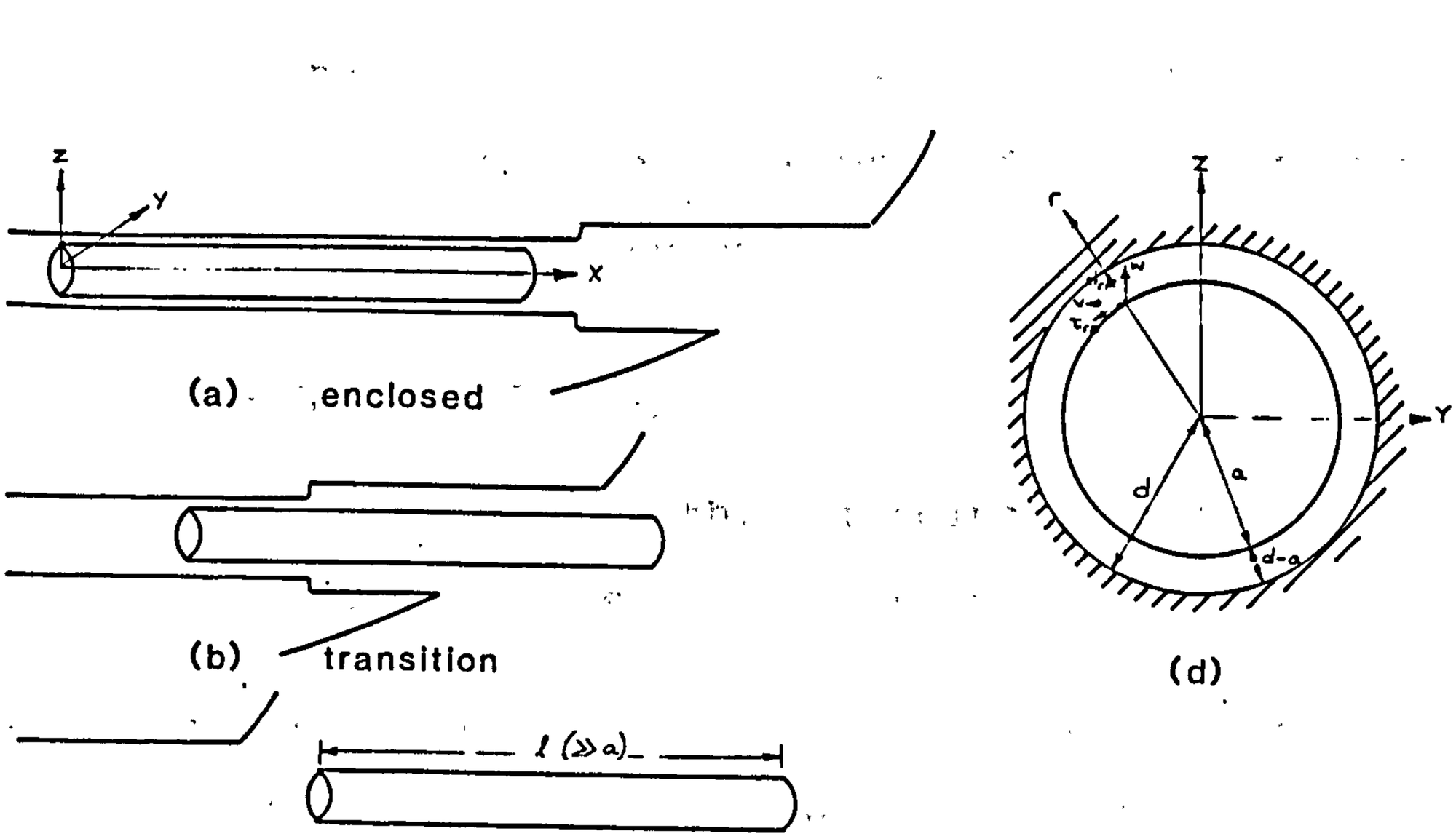

Figure 2.1

Schematic and coordinate system for cylinder in rigid water-filled tube

2.2.1 Dry analysis

The structure under consideration has a simple geometric shape for which closed form solutions for the dynamic response exist. The governing equation is given by

$$\frac{\delta^2 w}{\delta t^2} + \frac{EI_{NA}}{\rho_b A_b} \frac{\delta^4 w}{\delta x^4} = Q(t) \qquad (2.1)$$

where w = deflection

E = Youngs modulus

I = Moment of inertia

A = Sectional area

ρ = mass density

Q = external excitation

The theorem given by Rayleigh(1894) shows that the solution of eqn(2.1) may be expressed as an aggregate of distortions in its principal modes.

$$w(x,t) = \Sigma\, p_r(t).\Phi_r(x) \qquad (2.2)$$

where $p_r(t)$ is the rth. principal coordinate

$\Phi_r(x)$ is the rth. principal mode shape

The principal modes and natural frequencies obtained from eqn(2.1) with the appropriate boundary conditions for a free-free beam can be obtained from standard solutions (Bishop & Johnson(1960)). The natural frequency of the rth. mode of vibration is given by

$$\omega_r = \frac{\alpha_r^2}{l^2}\sqrt{(EI/\mu)} \qquad (2.3)$$

where αr is the rth. root of the frequency equation

$$\cos \alpha_r \cosh \alpha_r - 1 = 0 \qquad (2.4)$$

The corresponding characteristic functions wr(x), scaled to give wr(0)=1, are

$$w_r(x) = 0.5(\cosh(\alpha_r x/l) + \cos(\alpha_r x/l) - \sigma_r[\sinh(\alpha_r x/l) + \sin(\alpha_r x/l)]) \qquad (2.5)$$

$$\text{where } \sigma_r = \frac{\cosh \alpha_r - \cos \alpha_r}{\sinh \alpha_r - \sin \alpha_r} \quad (r = 2,3,\ldots)$$

2.2.2 Wet analysis

The fluid forces are derived by considering the two dimensional flow of the fluid defined by velocity components v,w along the axis directions Oy and Oz respectively.

The Navier-Stokes equations, mass conservation and angular rotation of the fluid flow are combined to obtain

$$\frac{\partial \zeta}{\partial t} + \dot{v}\frac{\partial \zeta}{\partial y} + \dot{w}\frac{\partial \zeta}{\partial y} = \nu\left(\frac{\partial^2 \zeta}{\partial z^2} + \frac{\partial^2 \zeta}{\partial y^2}\right) \qquad (2.6)$$

By defining a stream function such that

$$\dot{v} = \frac{\partial \psi}{\partial z} \qquad \dot{w} = -\frac{\partial \psi}{\partial y} \qquad (2.7)$$

and assuming small amplitudes of motion eqn(2.6) can be expressed as

$$\frac{\partial}{\partial t}\nabla^2\psi - \nu\nabla^4\psi = 0 \qquad (2.8)$$

The solution of eqn(2.8) is known to be

$$\psi = V\left(A\left(\frac{a^2}{r}\right) + Br + CaI_1(kr) + DaK_1(kr) \right) \sin\theta . e^{i\omega t} \qquad (2.9)$$

where $k^2 = i\omega/\nu$

V is the amplitude of the velocity of the oscillating beam

A,B,C,D are constants to be determined from the boundary conditions.

I_1, K_1 are modified Bessels functions of the first kind.

From which the pressure at the surface of the beam and hence the force producing vertical motion can be obtained

$$F_z(x,t) = -i\omega mV(-A + B + CI_1(ka) + DK_1(ka)) e^{i\omega t} \qquad (2.10)$$
$$= -i\omega mVHe^{i\omega t}$$

The complex quantity,

$$H = \{-A + B + CI_1(ka) + DK_1(ka)\} \qquad (2.11)$$

has real and imaginary components H^R and H^I respectively which are used to establish the generalised hydrodynamic coefficient

$$M_{rs} = \int_0^1 w_r(x) w_s(x) H^R(x,\omega,\nu)\, dx \qquad (2.12)$$

and generalised damping coefficient

$$C_{rs} = \int_0^1 w_r(x) w_s(x) H^I(x,\omega,\nu)\, dx \qquad (2.13)$$

from which the generalised vertical fluid force can be obtained

$$F_r(t) = -\sum_{s=0}^{n-1} (M_{rs}\ddot{p}_s(t) + C_{rs}\dot{p}_s(t)) \qquad (2.14)$$

The equation of motion for the rth. mode of vibration is

$$m_{rr}\ddot{p}_r(t) + c_{rr}\dot{p}_r(t) + k_{rr}p_r(t) = Z_r(t) \qquad (2.15)$$

where the total external loading is

$$Z_r(t) = F_r(t) + Q_r(t) \qquad (2.16)$$

Combining eqns(2.14)-(2.16) the equation of motion in the rth. mode is given by

$$\left(m_{rr} + \sum_{k=0}^{\infty} M_{rk}\right)\ddot{p}_r(t) + \left(c_{rr} + \sum_{k=0}^{\infty} C_{rk}\right)\dot{p}_r(t) + \omega_r^2 m_{rr} p(t) = Q_r(t) \qquad (2.17)$$

In matrix terms

$$[m + M]\ddot{p} + [c + C]\dot{p} + [k]p = [Q(t)] \qquad (2.18)$$

where M and C may be non-diagonal matrices. The residual external excitation can take any form but if a steady harmonic input force is considered, at one distinct point on the beam. Then,

$$Q_r(t) = \int_0^1 P(x,t)\, w_r(x)\, dx \qquad (2.19)$$

If P(x,t) has unit magnitude and is applied at $x=x'$ from one end, $(x'<1)$ then

$$P(x,t) = 1.\delta(x-x').e^{i\omega t} \qquad (2.20)$$

where $\delta(x-x')$ is a delta function such that

$$\delta = 1 \quad (x=x') \qquad \bar{\delta} = 0 \quad \text{(elsewhere)}$$

So

$$Q_r(t) = \int_0^l \delta(x-x').w_r(x).e^{i\omega t}.dx = w_r(x').e^{i\omega t} \qquad (2.21)$$

Now as the steady state response is such that

$$p_r(t) = p_r e^{i\omega t} \qquad (2.22)$$

the amplitude matrix p satisfies the equation

$$[\,-\omega^2(m+M) + i\omega(c+C) + k\,]\,p = D\,p = Q \qquad (2.23)$$

or

$$I\,p = D^{-1}Q = \frac{\text{adj } D}{\det D}Q = J(\omega)Q \qquad (2.24)$$

where adj denotes the adjoint matrix and the determinant is $\det D = \det\left|-\omega^2(m+M) + i\omega(c+C) + k\right|$

2.3 Calculations

The complex quantity H in eqn(2.11) is a function of frequency of oscillation, ω, coefficient of viscosity, ν, and the ratio of the radii, d/a. This will be reflected in the generalised hydrodynamic coefficients M_{rs}, C_{rs} given in eqns(2.12) and (2.13), however for a uniform beam of sufficient length so that end effects are negligible H^R and H^I will be constant. Then due to the orthogonality relationships that exist for the dry modes, the generalised hydrodynamic coefficient matrices M and C are diagonal.

From eqn(2.11) the added mass coefficient C_m and damping coefficient C_v are defined as

$$C_m = \text{Real}(H) = H^R/m$$
$$C_v = -m\omega.\text{Imag}(H) = H^I \qquad (2.25)$$

These coefficients will be assessed in the following set of figures against gap clearance d/a and another non-dimensional parameter $RS = \omega a^2/\nu$ which is the product of Reynolds number ($R = Ua/\nu$) and Strouhal number ($S = \omega a/U$) at some representative velocity, U.

2.3.1 Gap clearance

In the absence of viscosity it can be shown that eqn(2.11) reduces to

$$H = (1+\gamma^2)/(1-\gamma^2) \text{ where } \gamma = a/d \qquad (2.26)$$

that is C_m, the added mass parameter is independent of frequency and $C_v = 0$. There is a very rapid change in added mass as the gap clearance narrows as shown below.

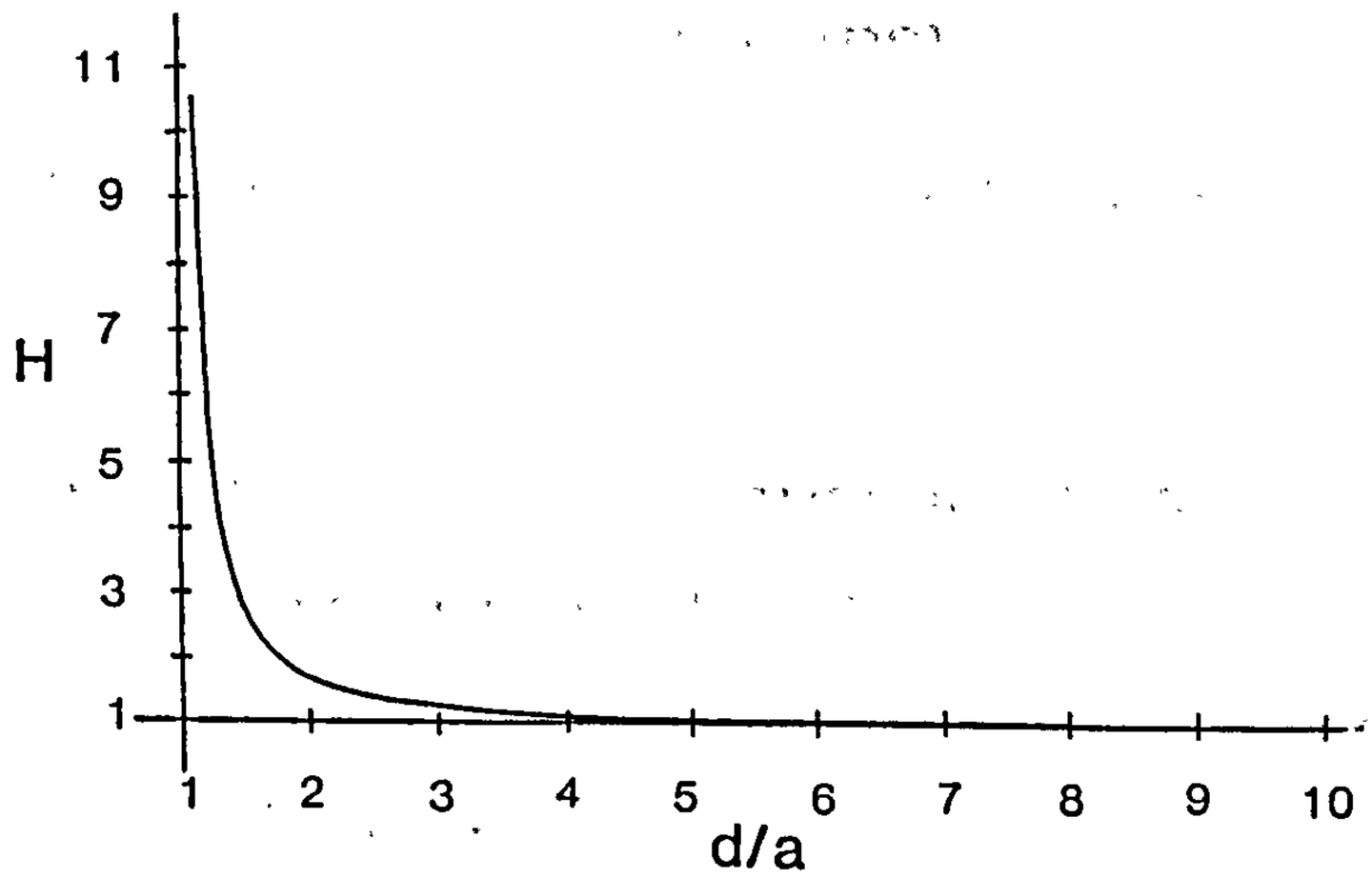

Figure 2.2

Changes in added mass coefficient, C_m, due to variation in annular clearance : inviscid fluid.

2.3.2 Viscosity or frequency

Next the frequency dependent effect of viscosity on added mass and damping coefficients is shown in isolation by removing the outer boundary. When $d \to \infty$; $\beta = kd \to \infty$ and $\gamma = a/d \to 0$, then

$$H = 1 + 4K_1(\alpha)/\alpha K_0(\alpha) \quad , \quad \alpha = ka \qquad (2.27)$$

As $\nu \to 0$ so $RS \to \infty$ and the real part of H, as shown in figure 2.3, tends to unity, which is the limiting

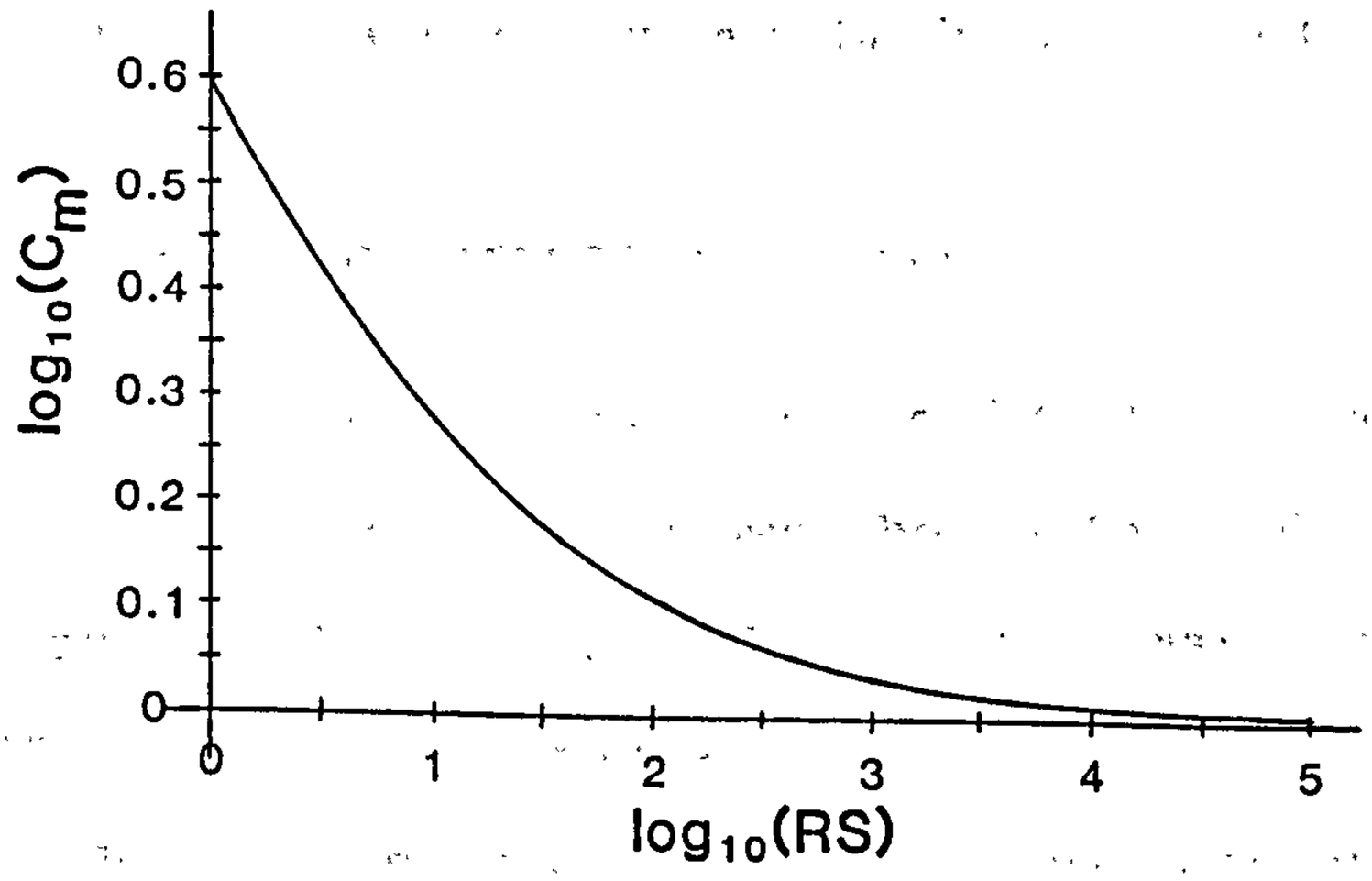

Figure 2.3

Variation of added mass coeffient, C_m, for viscous fluid (d/a at infinity)

value in figure 2.2 at large gap clearances. Figure 2.4 shows an opposite trend with increasing magnitude of the damping coefficient with frequency, providing ν and a are kept constant.

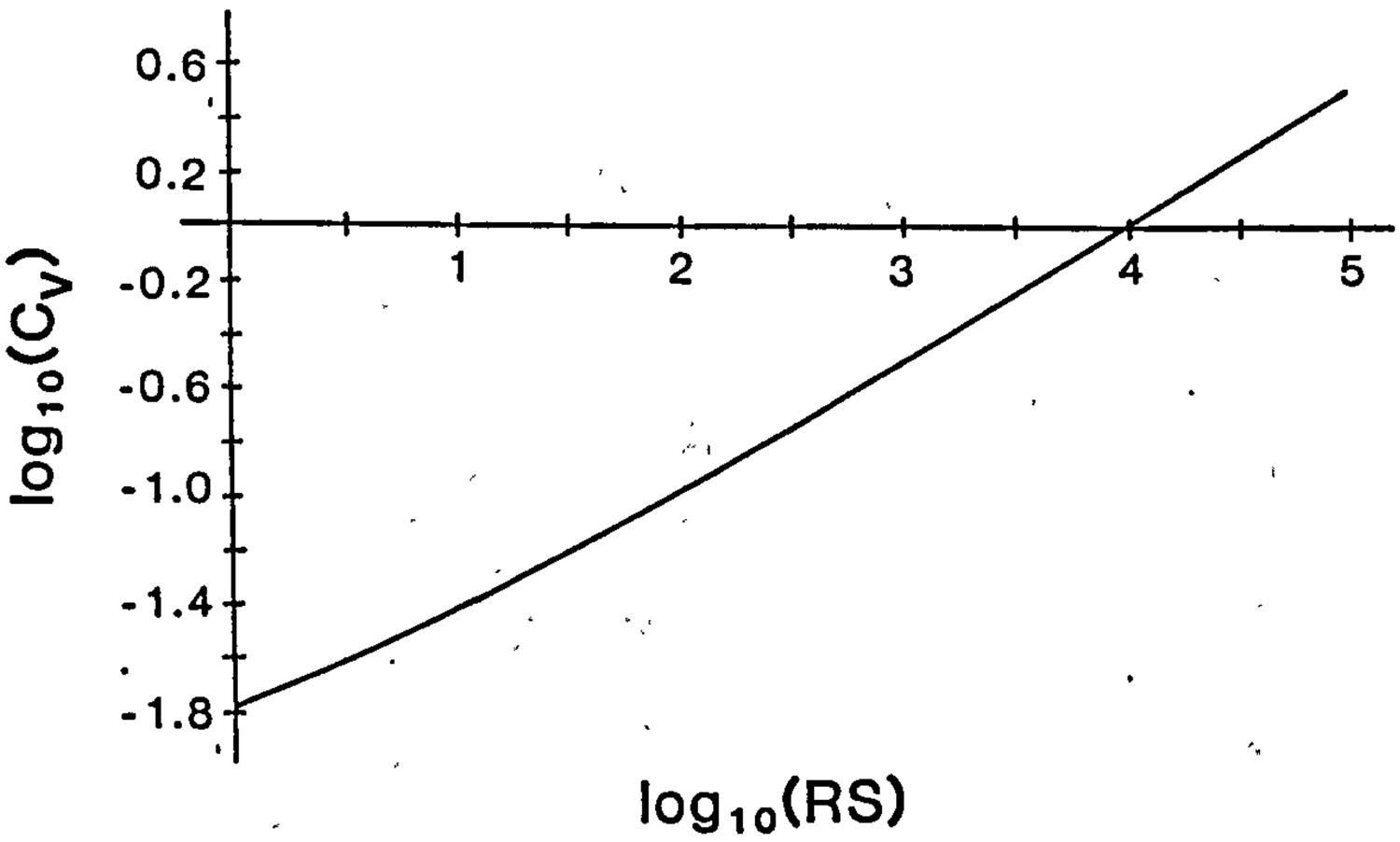

Figure 2.4

Variation of damping coefficient, C_v, for viscous fluid (d/a at infinity)

2.3.3 Gap clearance and viscosity

In the general case when $d \neq \infty$, H is evaluated from eqn(2.11). Figure 2.5 shows the effect different gap clearances have on the added mass and damping coefficients over a range of viscosities or frequencies. The added mass coefficient attains constant values at either end of the frequency range, with the high frequency limit being that which would be obtained from fig. 2.2 for an inviscid fluid.

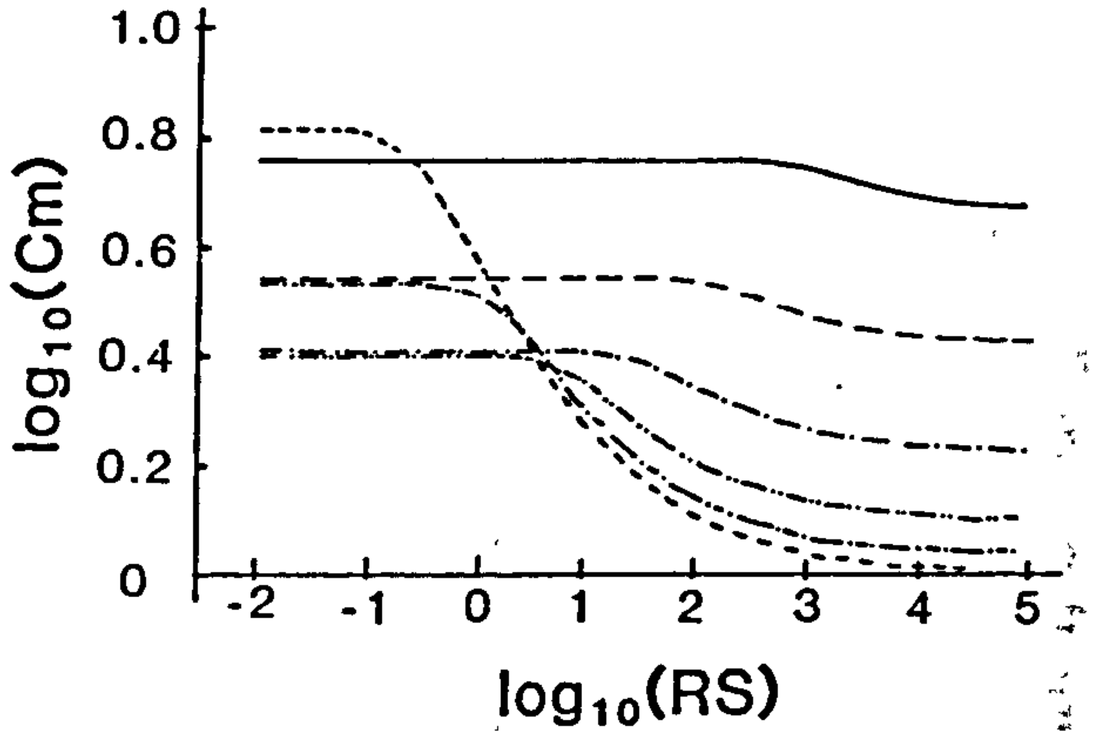

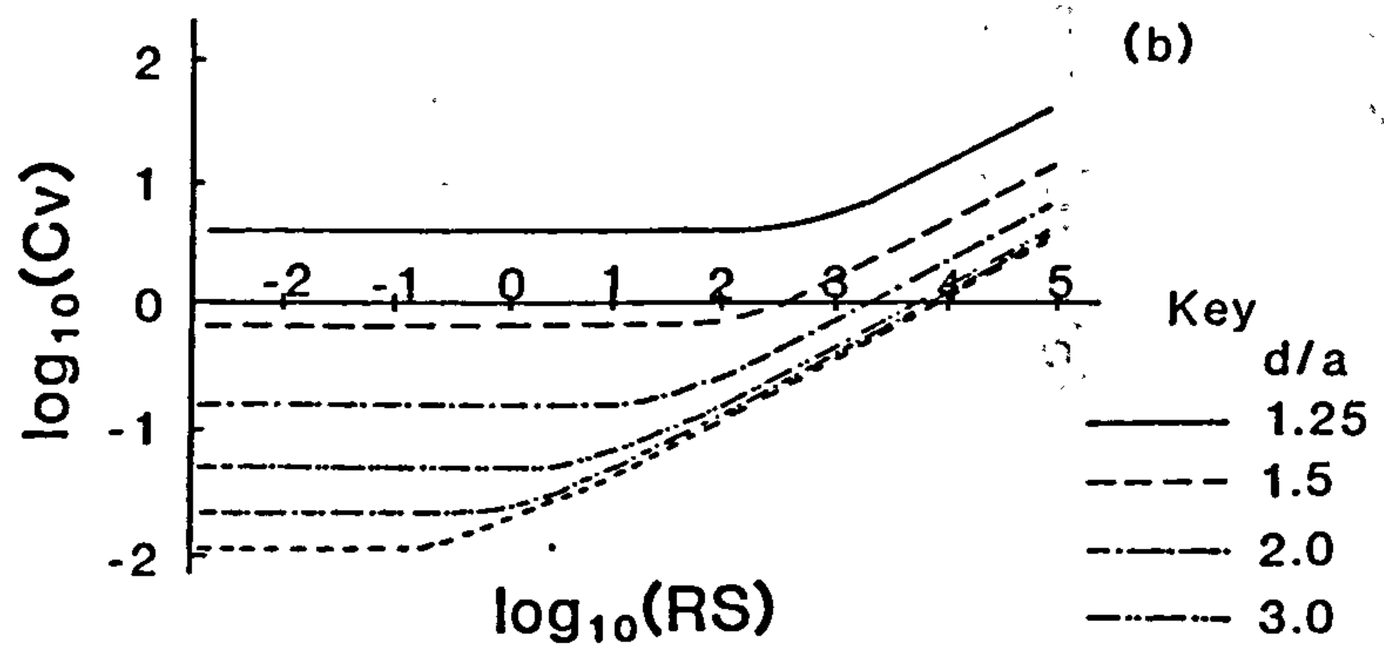

Figure 2.5

Changes in (a) added mass coefficient, Cm, and (b) damping coefficient, Cv, for selected values of d/a

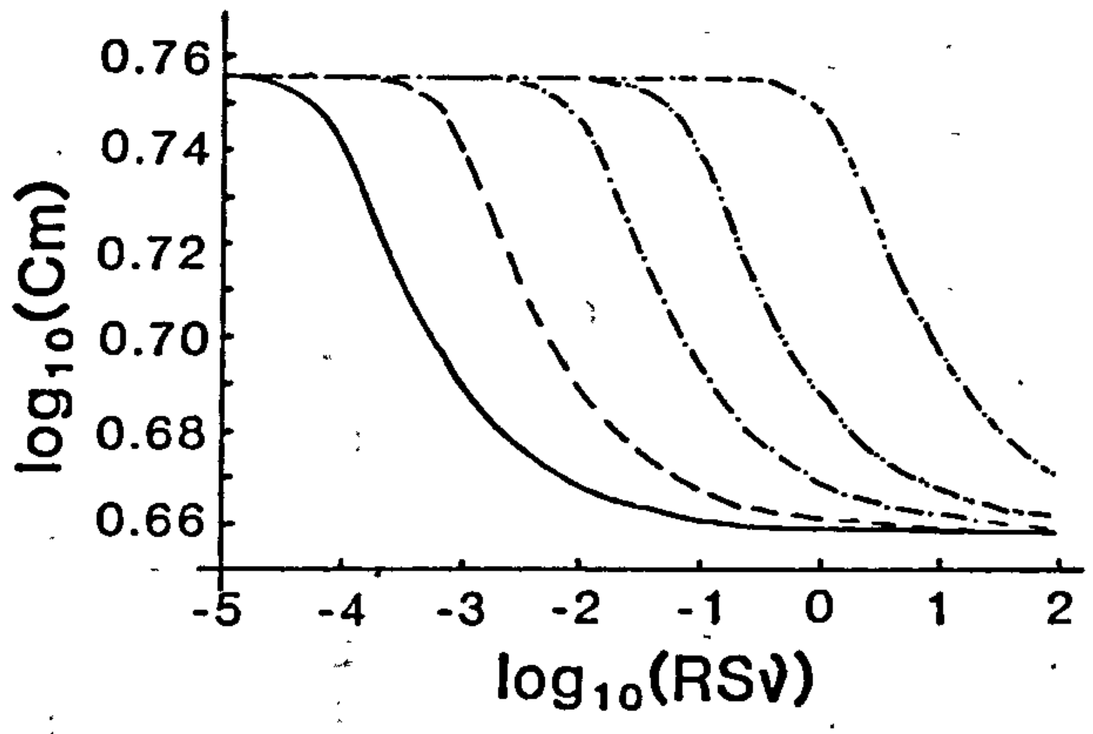

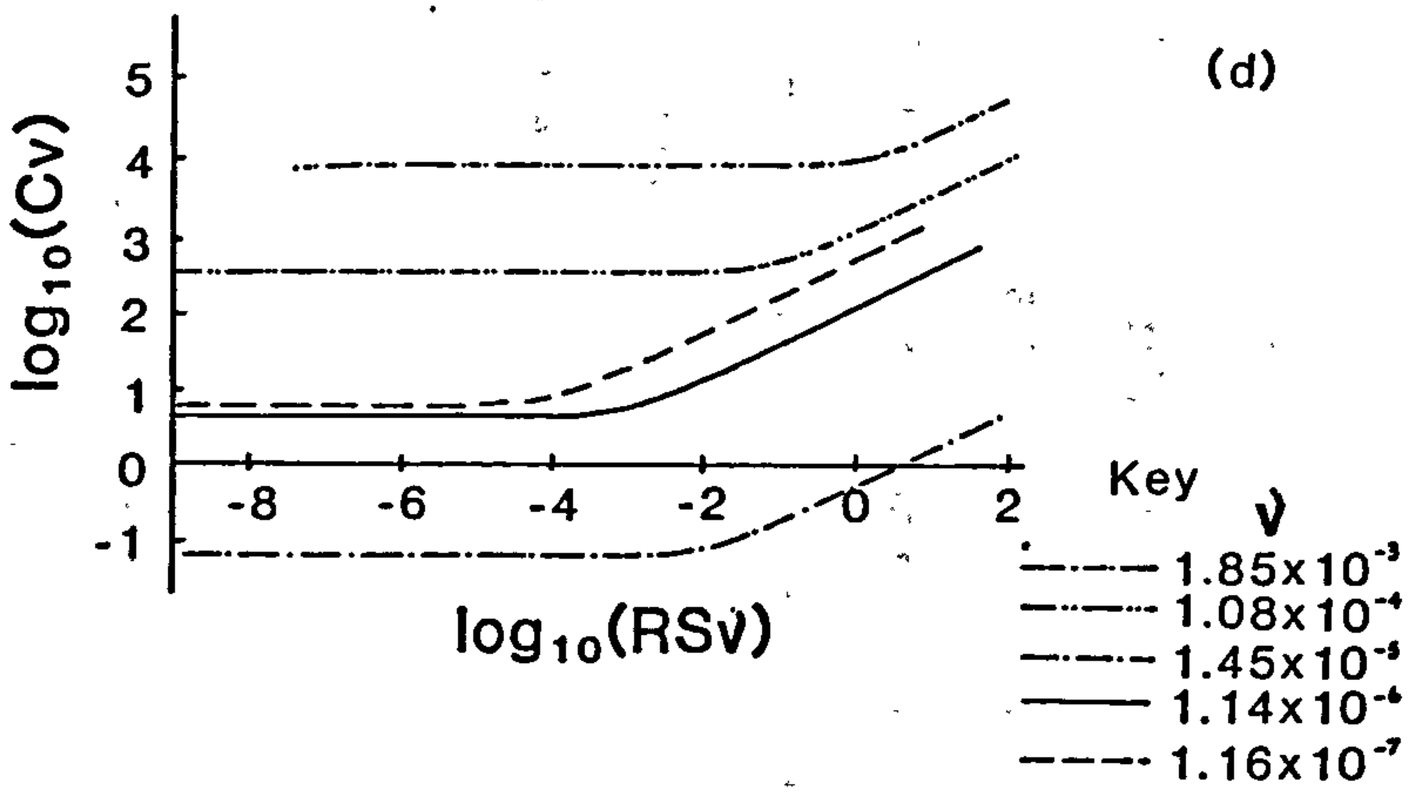

Variation of (c) added mass coefficient Cm, and (d) damping coefficient, Cv, for different viscous fluids

2.3.4 Principal coordinates of uniform beams.

The principal coordinates given by eqn(2.24) will reach a peak when detD reaches a minimum. The first three distortion modes r=2,3,4 are shown in fig. 2.6 for a cylinder of length 1.0m and beam radius 0.1m. in a tube radius 2.0m. The cylinder was assumed lightly damped with $\nu_r = 10^{-4}$, the elements of the assumed diagonal structural damping matrix, c, are

$$c_{rr} = 2\nu_r \omega_r m_{rr} \qquad (2.28)$$

in accordance with Bishop & Johnson(1960). The excitation is provided by a point load at a point x'=0.651 measured from one end.

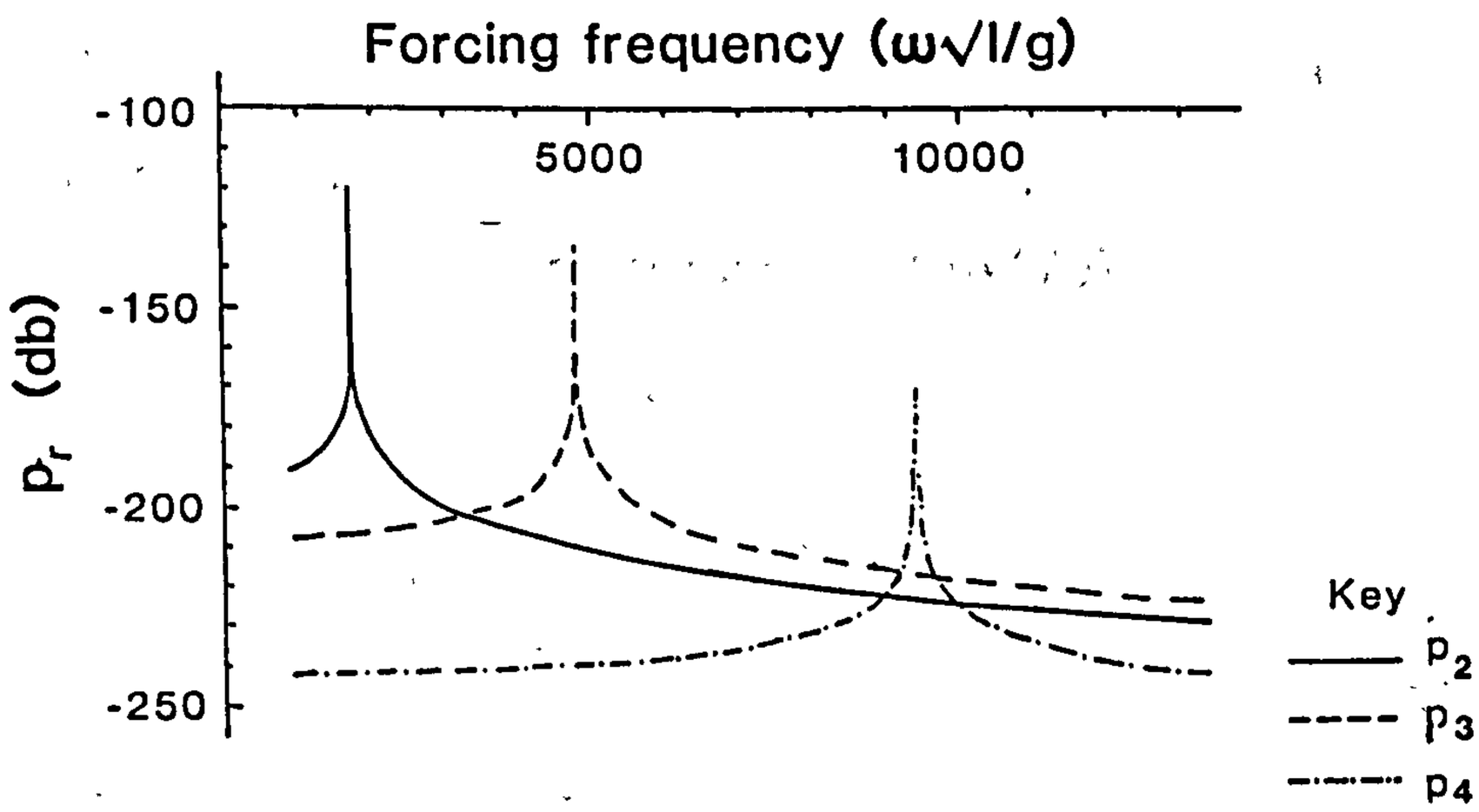

Figure 2.6

Variation of principal coordinates p_r, r=2,3,4 for uniform beam

From fig.2.6 the principal coordinates are uncoupled and these curves could represent the cylinder surrounded by an inviscid fluid or water ($\nu = 1.14\times10^{-6}$ m^2/s) as the results are identical. There will only be coupling between principal coordinates if M or C contain off-diagonal terms; which will only happen if H varies along the length of the beam. Also, appreciable differences between viscous and inviscid fluid models only occur if the hydrodynamic coefficient matrices M or C are significant compared to structural mass and damping m and c.

To demonstrate this latter point the same beam data as given above were used except that the radius was progressively reduced. This lowers the structural mass and damping and at the same time increases H^R and H^I as the non-dimensional parameter RS decreases from $10^{4.7}$ to $10^{1.7}$ (see figs. 2.3 & 2.4 for appropriate changes in C_m and C_v).

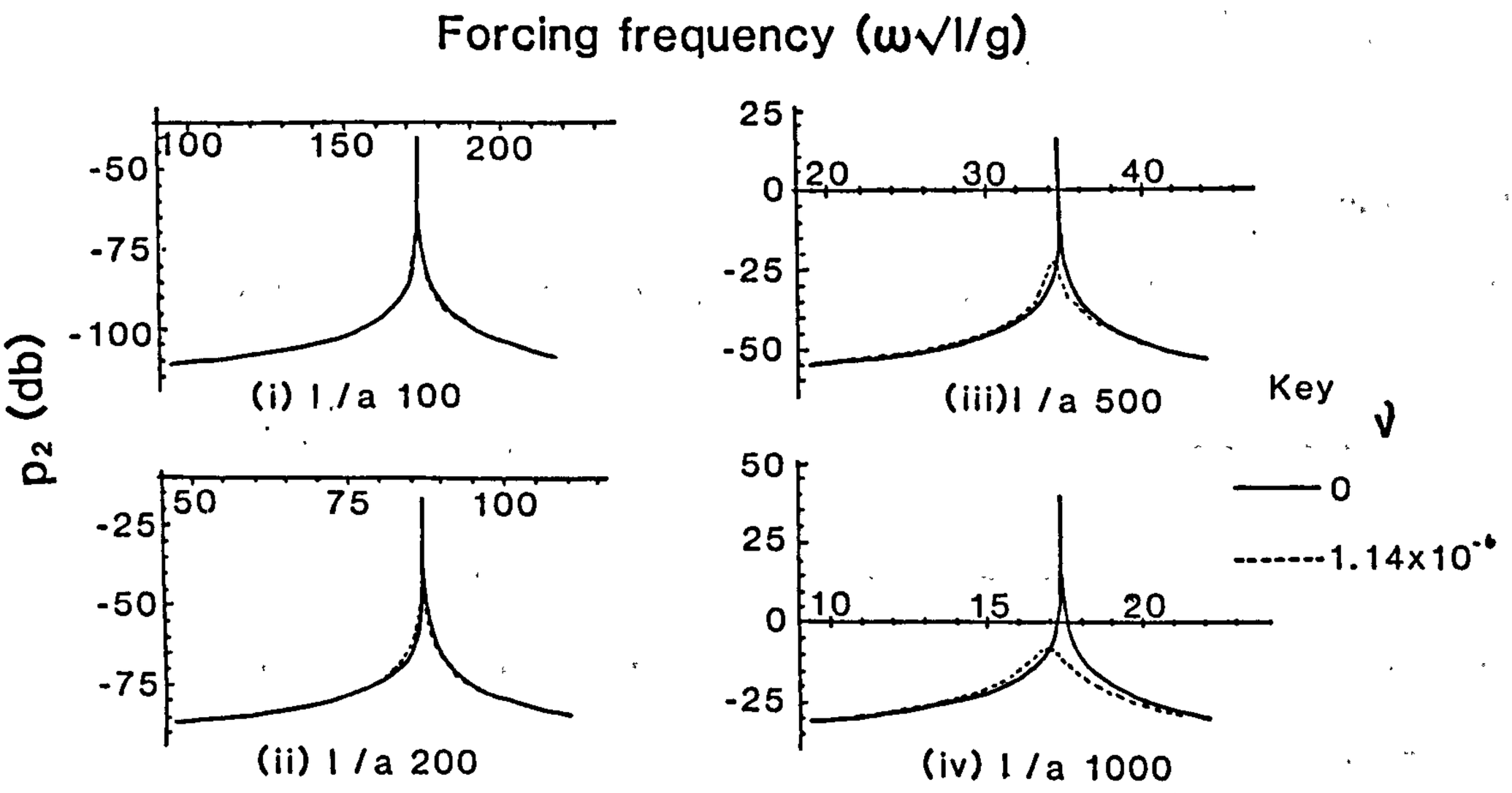

Figure 2.7

Effect of viscosity on principal coordinate p_2 for slender beams

The effect of the changes can be seen to be primarily related to changing the damping charateristics of the beam compared with the inviscid case and has relevance to the behaviour of long flexible tubes or pipes. The same effect could have been achieved by increasing the viscosity of the surrounding medium but using a physically realisable and commonly occuring fluid such as water retains the significance of the study to maritime engineering. The effect of annular clearance on the resonance frequency value of p_2 is clearly demonstrated in fig.2.8.

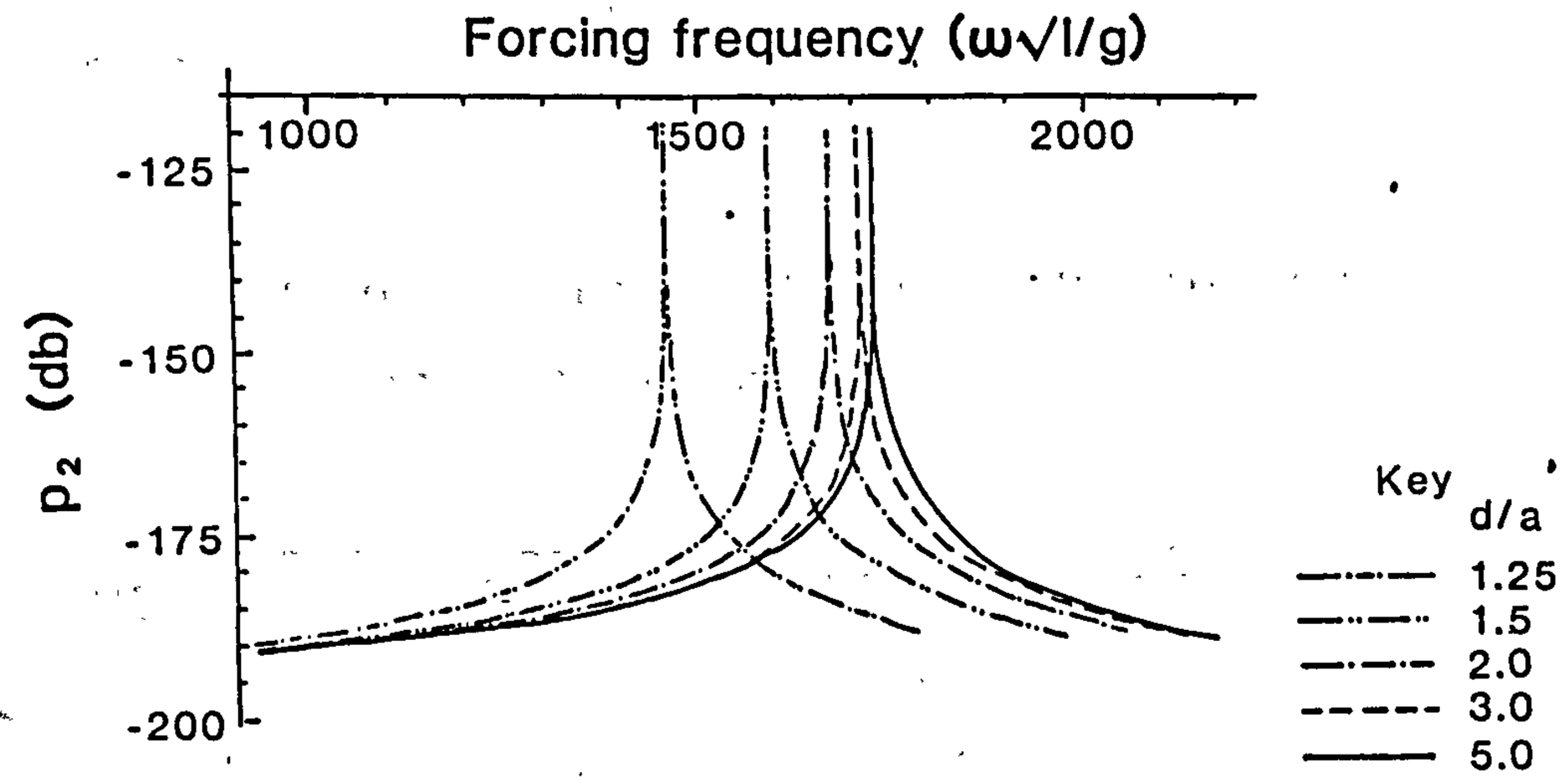

Figure 2.8

Variation of principal coordinate p_2 for uniform beam at selected values of d/a

2.3.4 Principal coordinates of non-uniform beams.

To demonstrate the coupling between the principal coordinates, changes have been made to the homogeneous nature or uniform section of the beam. The beam

modelled in fig. 2.9a has a 50% increase in density over one half of the beam. The recalculated amplitude p_4 clearly shows the coupling associated with the coordinates p_2 and p_3. To illustrate the effect of geometric variation a uniformly tapered beam (a_1=0.1m, x=0; a_2=0.2m, x=1) of constant density was considered and

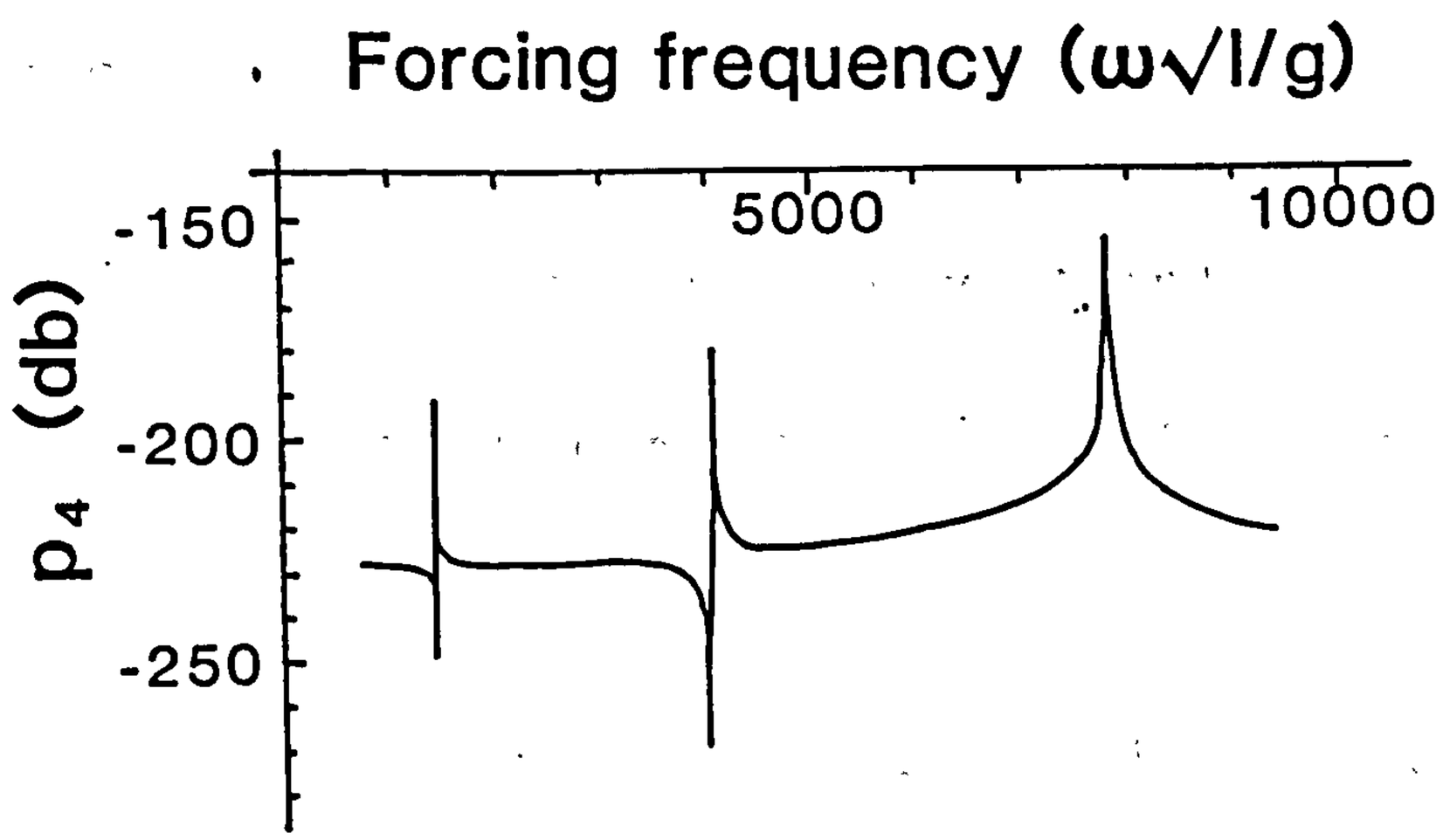

(a) Constant radius beam with non-uniform mass distribution

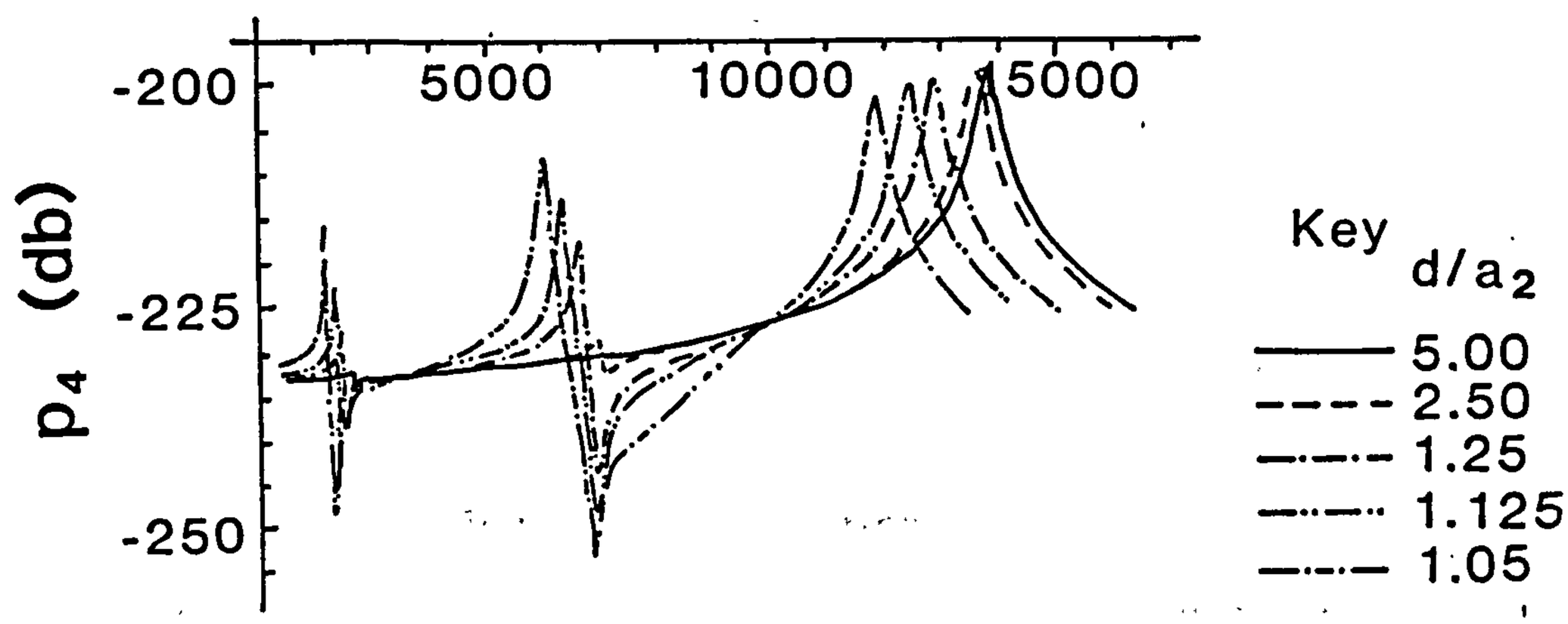

(b) Tapered beam with varying annular clearance

Figure 2.9 Variation of principal coordinate $\bar{p}_4$ for non-uniform beams

the annular clearance varied from 0.21m<d<2.0m. The beam was again surrounded by water and fig.2.9b summarizes the role of coupling in the principal coordinate p4 for different values of the annular clearance. The coupling between the coordinates increases as the annular clearance decreases. This effect is due to the increasing influence of the off-diagonal contributions arising in the generalised hydrodynamic coefficient matrices M and C.

2.3.5 Non-uniform beam with discontinuous outer boundary.

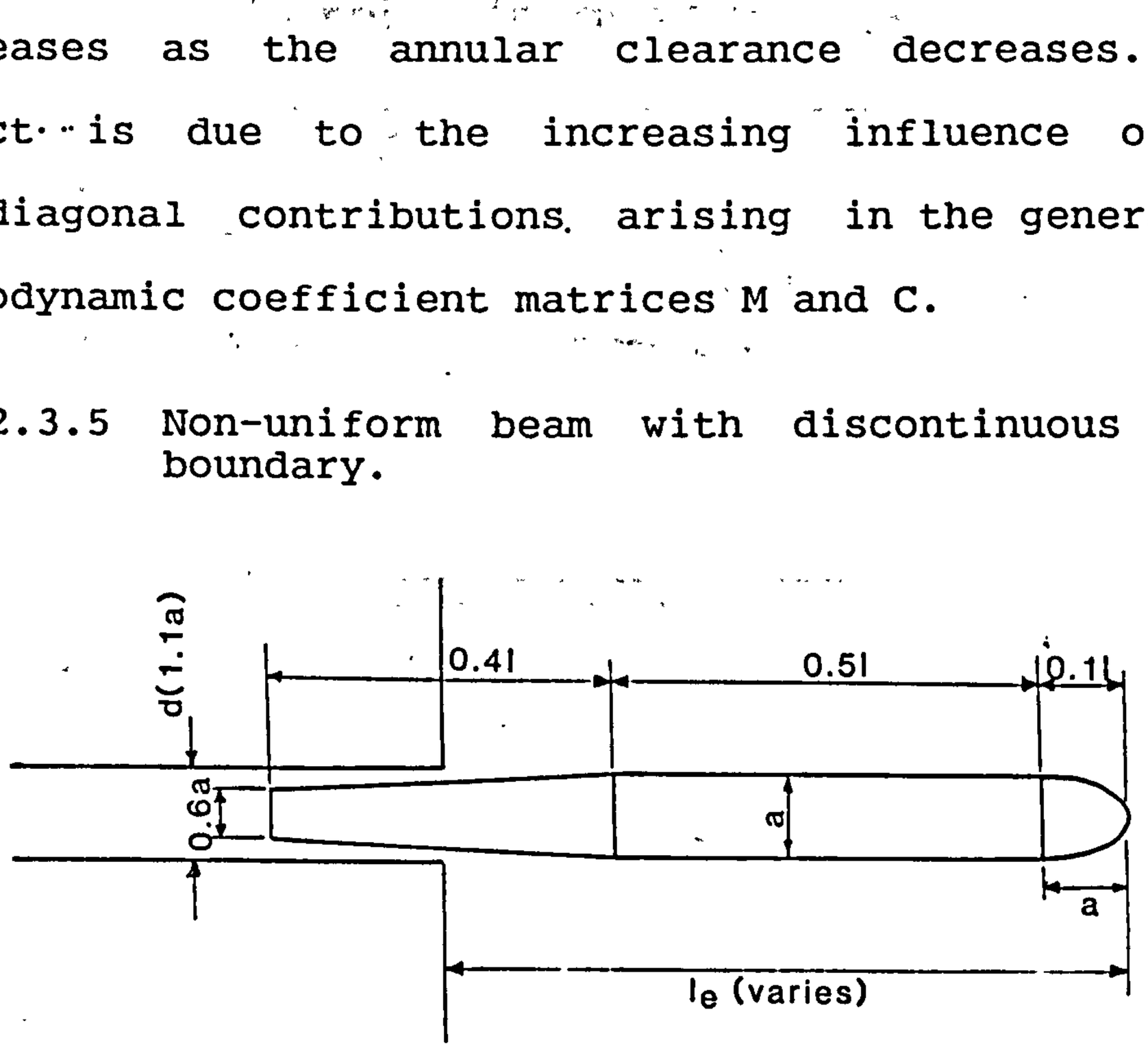

Figure 2.10 Non-uniform beam with discontinuous outer boundary

Finally to demonstrate a practical illustration of the foregoing, fig. 2.10 illustrates a situation in which the faired shape of an underwater projectile is represented by a non-uniform beam which is partially enclosed by a constraining outer tube. The projectile is surrounded by fluid and as the outer boundary is

moved to the right, a crude simulation in a quasi-static manner of the launch of the projectile becomes possible. This allows changes in the amplitude of the principal coordinate p_r and the resonance frequencies ω_r to be monitored.

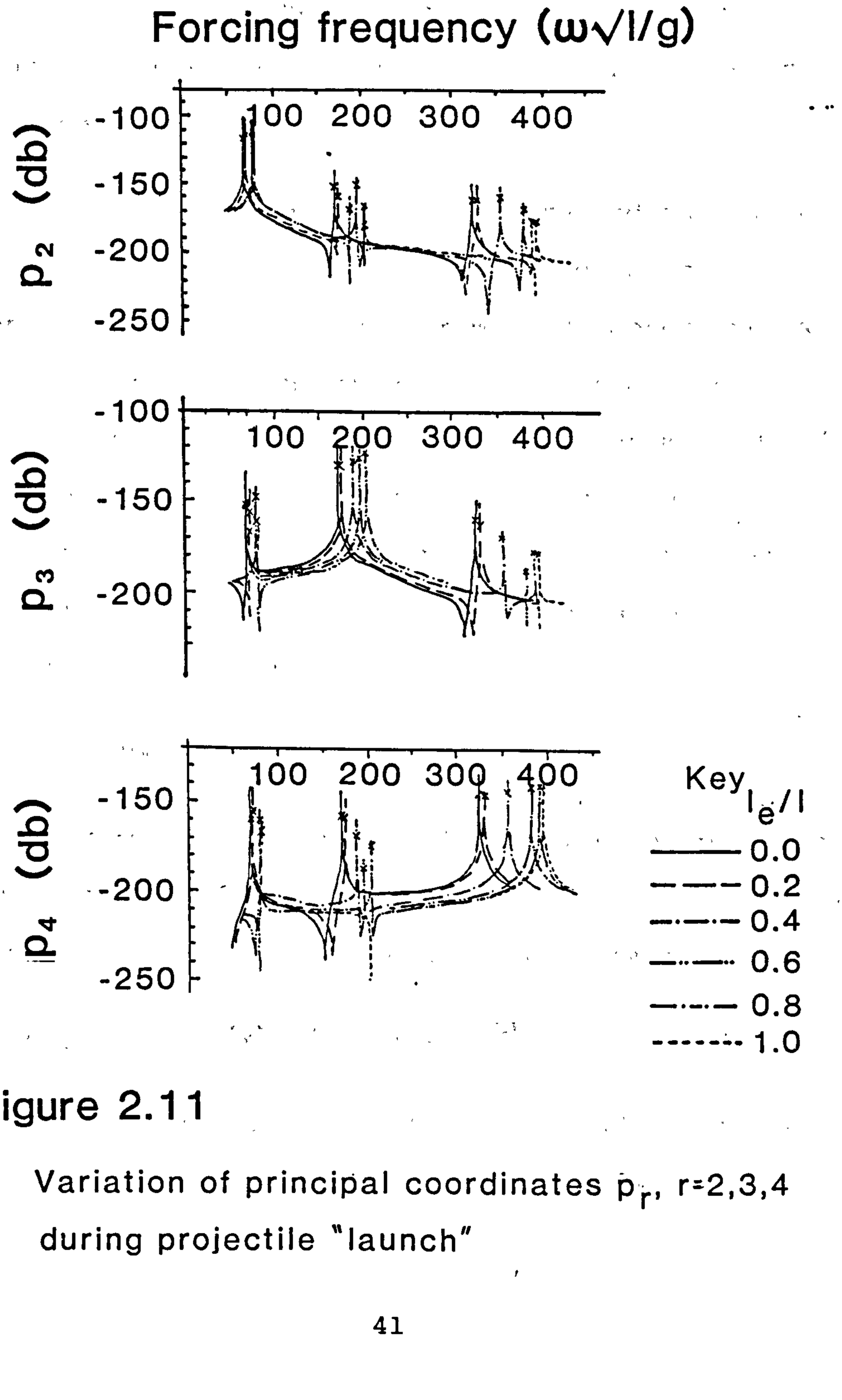

Figure 2.11

Variation of principal coordinates p_r, r=2,3,4 during projectile "launch"

Figure 2.11 shows the variation in p_r, r=2,3,4 as the projectile moves from a state of enclosure within the tube to one of complete emergence. The resulting increase in resonance frequencies as the coefficients of hydrodynamic inertia reduce is evident, but what is not as predictable is the irregular way in which the resonance frequencies change or the variations in the coupling between modes.

When the surrounding water is treated as a viscous fluid no noticeable differences are observed in the resonance frequency values from those determined with the inviscid model. The only change that occurs is an increase in the generalised hydrodynamic damping coefficient values, producing a reduction in the peak values of p_r. A mark is shown on each of the curves in fig. 2.11 to indicate a lower amplitude associated with the viscid fluid model.

2.3.7 Response

The symmetrical vertical displacement at position x to an oscillatory applied unit ampitude force at position x' is given by Bishop, Price & Temarel(1984).

$$w(x,x',t) = w^T(x)\,[J(\omega)]\,w(x')\,e^{i\omega t} \qquad (2.29)$$

where the complex valued function $J(\omega)$ is defined in equation (2.24).

A resonance condition is identified when det $D(\omega)$ in eqn.(2.24) is a minimum, at $\omega = \Omega$, and the resonance displacement may be expressed as

$$w(x,x',t) = W(x,x',\Omega)\, e^{i\varepsilon(x,x',\Omega)}\, e^{i\Omega t} \qquad (2.30)$$

Here $W(x,x',\Omega)$ denotes the displacement amplitude associated with the "wet" resonance frequency Ω and $\varepsilon(x,x',\Omega)$ is the phase angle between the applied force at x' and the response at x measured from the stern.

If the complex receptance is expressed in the form

$$J(\Omega) = J^R(\Omega) + iJ^I(\Omega) \qquad (2.31)$$

it follows that

$$\begin{aligned} W(x,x',\Omega)\cos\varepsilon(x,x',\Omega) &= w^T(x)\,[J^R(\Omega)]\,w(x') = A_1 \\ W(x,x',\Omega)\sin\varepsilon(x,x',\Omega) &= w^T(x)\,[J^I(\Omega)]\,w(x') = A_2 \end{aligned} \qquad (2.32)$$

where the phase angle satisfies the relationship

$$\tan\varepsilon(x,x',\Omega) = A_2/A_1 \qquad (2.33)$$

and the vertical amplitude is

$$W(x,x',\Omega) = \sqrt{(A_1^2 + A_2^2)} \qquad (2.34)$$

In a full-scale measurement it is the displacement amplitude which is measured and this is commonly referred to as a "mode shape", being associated with a resonance condition. Figure 2.13 displays the complex characteristics of the vertical displacement at the first three lowest resonance frequencies. The "twist" observed in the mode shapes is due to the influence of the viscous fluid and structural damping.

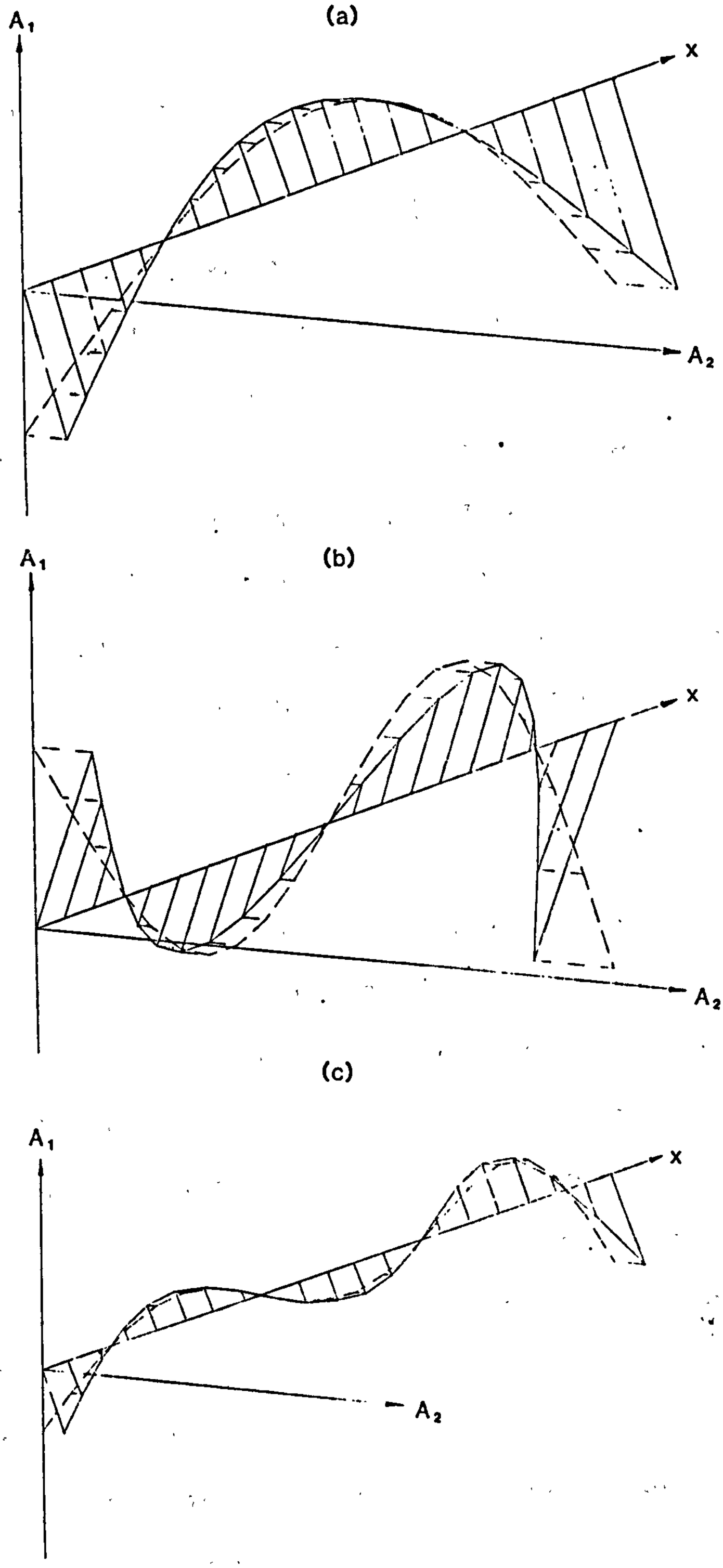

Figure 2.12

Mode shapes including phase relationships at (a) first (b) second and (c) third resonance frequencies

CHAPTER 3 - NUMERICAL ANALYSIS

3.1 Introduction

Fluid-structure interaction is concerned with determining how the dynamic response characteristics of a structure are affected by the presence of a surrounding fluid. There are many factors that will affect the dynamic response of a thin-walled flexible structure when it is submerged. They can be divided into effects that are influenced by the geometry of the structure and whether the external loading is transient or periodic, and those which are dependant on the fluid; its physical properties and the proximity of fixed and free boundaries.

Initially, therefore, it is expedient to consider one of the simplest geometric shapes, an infinitely long cylinder and determine the forced vibration of that structure in an infinite domain of water. Bleich & Baron(1954), Warburton(1961) and Junger(1972) have all derived analytical solutions for the response of a cylinder in contact with an internal or an external fluid. For application to submarine vessels it is obviously the latter that is of the greater interest. However it is difficult to extend the results to the practically more realistic case of cylinders of finite length because the effect of the ends on the motion of the fluid are not known.

Despite these drawbacks it can be shown that resonable correlation can be obtained between results calculated for this simplistic model and measured data. The underlying assumptions and differences in the theoretical formulations will be examined to see whether they can shed any light on this apparent inconsistency.

Rayleigh(1851) considered the problem of free vibration of infinitely long thin cylindrical shells for the case of negligible bending stiffness. Bleïch & Baron(1954) use the mode shapes derived from membrane theory to derive a correction which can be used to include the effects of bending stiffness. The results obtained are an upper limit to the solution given in the more rigorous treatment by Warburton(1961).

3.2 Analytical predictions

The equations of motion for a cylindrical shell can be assessed by studying the middle surface deflections. The prime assumption being that variations across the thickness of the shell are negligible compared with displacements of the middle surface. In detail, this assumption will not be violated providing

(i) Displacements are small in comparison with the thickness of the shell so that linear theory of shell deformation can be applied.

(ii) Shell thickness is small compared with the radius of the cylinder (aspect ratio < 0.05, more

typically 1/100).

(iii) Fibres of the shell initially perpendicular to the shell middle surface remain so after deformation and are not subject to elongation.

(iv) Normal stresses on planes parallel to the shell middle surface are negligible in comparison with other stresses.

The equations of motion are derived, applying the above assumptions, from Hamiltons' variational principle in which expressions are obtained for the total kinetic and potential energies of the system in terms of the unknown middle surface deflections. Discrepancies in the differential equations derived in this way which appear in the literature are due to small differences in the strain-displacement relationships and are not generally significant.

3.2.1 Cylindrical shell in-vacuo

Using the strain-displacement relationships given by Fung(1965) for the cylindrical coordinate system shown in figure 3.1.

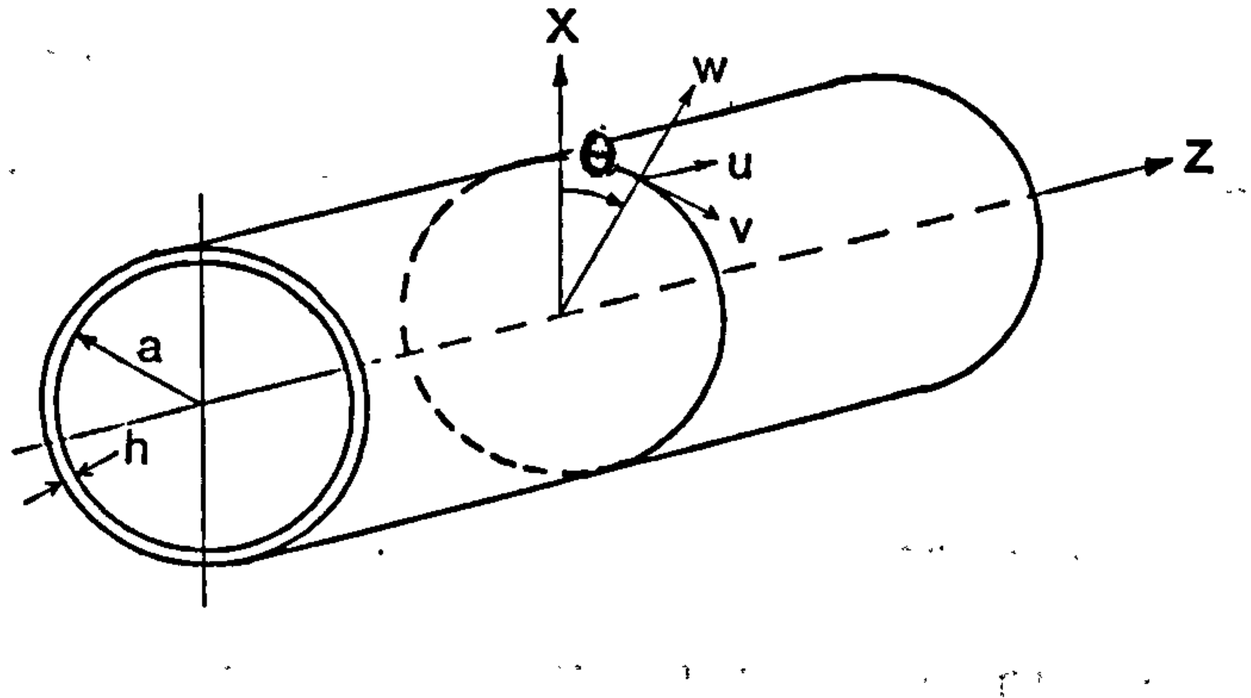

Figure 3.1

Geometry of cylindrical shell showing direction of displacement components

$$\varepsilon_{zz} = \frac{\delta u}{\delta z} - x\frac{\delta^2 w}{\delta z^2}$$

$$\varepsilon_{\theta\theta} = \frac{1}{a}\frac{\delta v}{\delta\theta} + w - \frac{x}{a^2}\frac{\delta^2 w}{\delta\theta^2} - \frac{\delta v}{\delta\theta} \qquad (3.1)$$

$$\varepsilon_{z\theta} = \frac{1}{a}\frac{\delta u}{\delta\theta} + \frac{\delta v}{\delta z} - \frac{x}{a}2\frac{\delta^2 w}{\delta z\delta\theta} - \frac{\delta v}{\delta z}$$

The three equations of motion are then given by (Junger & Feit(1972))

$$\frac{\delta^2 u}{\delta z^2} + \frac{1-\nu}{2a^2}\frac{\delta^2 u}{\delta\theta^2} + \frac{1+\nu}{2a}\frac{\delta^2 v}{\delta z\delta\theta} + \frac{\nu}{a}\frac{\delta w}{\delta z} - \frac{\ddot{u}}{c_p^2} = 0$$

$$\frac{1+\nu}{2a}\frac{\delta^2 u}{\delta z\delta\theta} + \frac{1-\nu}{2}(1+\beta^2)\frac{\delta^2 v}{\delta z^2} + \frac{1}{a^2}(1+\beta^2)\frac{\delta^2 v}{\delta\theta^2} + \frac{1}{a^2}\frac{\delta w}{\delta\theta} - \beta^2\left(\frac{\delta^3 w}{\delta z^2\delta\theta} + \frac{1}{a^2}\frac{\delta^3 w}{\delta\theta^3}\right) - \frac{\ddot{v}}{c_p^2} = 0 \qquad (3.2)$$

$$-\frac{\nu}{a}\frac{\delta u}{\delta z} - \frac{1}{a^2}\frac{\delta v}{\delta\theta} + \beta^2\left(\frac{\delta^3 v}{\delta z^2\delta\theta} + \frac{1}{a^2}\frac{\delta^3 v}{\delta\theta^3}\right) - \frac{w}{a^2} - \beta^2\left(a^2\frac{\delta^4 w}{\delta z^4} + 2\frac{\delta^4 w}{\delta z^2\delta\theta^2} + \frac{1}{a^2}\frac{\delta^4 w}{\delta\theta^4}\right) - \frac{\ddot{w}}{c_p^2} = -p_a\frac{(1-\nu^2)}{Eh}$$

in which

u,v,w are components of displacement in axial, tangential and radial direction

r,θ,z are cylindrical coordinates

β^2 h /12a

h thickness

a radius

ν Poissons ratio

c_p low-frequency phase velocity of compressional waves in an elastic plate

E Youngs modulus

p_a radial force per unit area, positive outward, it only being necessary to consider forces acting in this direction.

Terms containing the quantity β^2 represent contributions from bending stresses as opposed to membrane stresses. Warburton uses the equation of motion in eqn.(3.2) in their full generality, including a v-dependent flexural term not shown here and with little penalty in computational effort. Junger produces slightly simpler equations by assuming $1 + x/a \approx 1$ in the strain-displacement relationship.

Then assuming displacements of the form

$$u = \sum_{m,n} U_{mn} \cos n\theta \sin k_m z$$
$$v = \sum_{m,n} V_{mn} \sin n\theta \cos k_m z \qquad (3.3)$$
$$w = \sum_{m,n} W_{mn} \cos n\theta \cos k_m z$$

which describe motion in standing waves in both radial and axial directions. Radial displacement node lines in the circumferential direction are separated by the distances $\pi.a/n$ and the axial wavelength is $2.\pi/k_m$, where $k_m = 2.\pi/L$ is the axial wave number.

Substitution of (3.3) into (3.2) yields a homogeneous set of three linear algebraic equations in U_{mn}, V_{mn} and W_{mn}. For a non-trivial solution to exist, the determinant of the coefficients must vanish

$$\begin{vmatrix} -\Omega^2 + k_m^2a^2 + 0.5(1-\nu)n^2 & 0.5(1+\nu)k_ma & \nu k_ma \\ 0.5(1+\nu)nk_ma & -\Omega^2 + 0.5(1-\nu)k_m^2a^2 + n^2 & n \\ \nu k_ma & n & -\Omega^2 + 1 + \beta^2(k_ma^2+n^2)^2 \end{vmatrix} = 0 \qquad (3.4)$$

which produces a cubic equation in Ω^2,

$$(\Omega^2)^3 + A(\Omega^2)^2 + B(\Omega^2) + C = 0 \qquad (3.5)$$

where Ω is non-dimensional frequency such that

$$\Omega = \frac{\omega a}{c_p} = \frac{\bar{c}}{c_p} ka \qquad (3.6)$$

The three roots of equation(3.5) are all solutions having different mode shapes given by the ratios V/U, W/U indicating which modes are predominantly radial, tangential or of mixed origin.

3.2.2 Cylindrical shell in acoustic medium

Once the cylinder is submerged the first two of equations (3.2) are unchanged but the third equation will have additional terms due the pressure acting on the shell. It is the determination of this pressure loading effect which is the crux of the fluid-structure interaction problem.

Approximate expressions for the frequencies and mode shapes of the submerged shell are obtained by Junger & Feit(1972) but here we follow the more rigorous approach adopted by Warburton(1961).

The displacements of the shell are given in cylindrical polar coordinates in a manner similar to equation (3.3) and fluid motion is described by defining a velocity potential, Ψ, which satisfies the wave

equation

$$\nabla^2\psi = \frac{1}{c^2}\frac{\delta^2\psi}{\delta t^2} \qquad (3.7)$$

Internal or external fluids are considered and determination of whether the inequality

$$\omega/c > n/L$$

is satisfied or not determines the form of the pressure wave i.e. whether it is a standing or diverging wave.

If attention is restricted to the situation in which only an external fluid field exists, then the solution of the wave equation is

$$\psi = F(r) \cos n\theta \sin nz/L \, e^{i\omega t} \qquad (3.8)$$

with $F(r) = A.J_n(kr) + B\,Y_n(kr)$ if $\omega/c > n/L$

or $F(r) = C.I_n(k_1 r) + D\,K_n(k_1 r)$ if $\omega/c < n/L$

where $k^2 = \omega^2/c^2 - n^2/L^2$

and $k_1^2 = n^2/L^2 - \omega^2/c^2$

The constants A, B, C and D are determined by consideration of boundary conditions. For example, the velocity potential reduces to zero at infinity

$$\psi \longrightarrow 0 \text{ as } r \longrightarrow \infty \qquad (3.9)$$

and radial fluid velocity at the shell surface equals

the shell velocity when there is no cavitation.

$$\frac{\partial w}{\partial t} = \left(\frac{\partial \psi}{\partial r}\right)_{r=a} \tag{3.10}$$

The pressures due to the external field can be obtained from

$$p = -\rho\left(\frac{\partial \psi}{\partial t}\right)_{r=a} \tag{3.11}$$

which when substituted into the equations of motion along with the relevant strain-displacement relationships from eqn.(3.1) yields

$$\begin{aligned}
&(k_m^2a^2 + 0.5(1-\nu)n^2 - \Omega^2)U_{mn} - (0.5(1+\nu)nk_ma)V_{mn} - \nu k_maW_{mn} = 0 \\
&(-0.5(1+\nu)k_ma)U_{mn} + (0.5(1-\nu)k_m^2a^2 + n^2 - \Omega^2 \\
&\quad + \beta^2(n^2 + 2(1-\nu)k_m^2a^2))V_{mn} + (n + \beta^2(n^3 + (2-\nu)k_m^2a^2n))W_{mn} = 0 \\
&-\nu k_maU_{mn} + (n + \beta^2(n^3 + (2-\nu)k_m^2a^2n))V_{mn} \\
&\quad + (1 + \beta^2(k_m^2a^2 + n^2)^2 - \Omega^2(1+f(x)))W_{mn} = P_3
\end{aligned} \tag{3.12}$$

The presence of an external pressure field leads to the f(x) term in the last of eqn(3.12) above, which is defined as

$$f(x) = -\frac{\rho}{\rho_s}\frac{a}{h}\frac{1}{x}\frac{H_n^2(x)}{H_n'^2(x)} \quad \text{if } \omega/c > \pi/L$$

$$\text{or} \quad f(x) = -\frac{\rho}{\rho_s}\frac{a}{h}\frac{1}{x_1}\frac{K_n(x_1)}{K_n'(x_1)} \quad \text{if } \omega/c < \pi/L \tag{3.13}$$

where $x^2 = a^2(k^2 - k_m^2)$

and $x_1^2 = a^2(k_m^2 - k^2)$

The solution to equations(3.12) can be expressed as

$$W = \frac{-P_3((\Omega^2)^2 - C_1(\Omega^2) + C_0)}{(\Omega^2)^3 - K_2(\Omega^2)^2 + K_1(\Omega^2) - K_0 + f(x).\Omega^2((\Omega^2)^2 - C_1(\Omega^2) + C_0)} \tag{3.14}$$

Resonance occurs when the denominator in (3.14) is zero. Therefore for the cylinder in-vacuo f(x) = 0 and the natural frequency of free vibration will be given by

$$(\Omega^2)^3 - K_2(\Omega^2)^2 + K_1(\Omega^2) - K_0 = 0 \qquad (3.15)$$

As in the solution to eqn(3.5) the lowest root will correspond to a mode shape in which the radial component of the amplitude of vibration, W is considerably larger than the other two components U and V. When the cylinder is considered in a fluid, resonance frequencies are obtained when the real part of the denominator is 0.

$$(\Omega^2)^3 - K_2(\Omega^2)^2 + K_1(\Omega^2) - K_0 + \Omega^2((\Omega^2)^2 - C_1(\Omega^2) + C_0).\mathrm{Re}[f(x)] = 0 \qquad (3.16)$$

For an external fluid and $\omega/c < \pi/L$, f(x) is given by the second of eqn(3.13). The limiting values for $K_n(x)$ for small values of x are (Abramowitz & Stegun(1965))

$$K_n(x_1) \approx 0.5\,\Gamma(n)\,(x_1/2)^{-n}$$
$$K_n'(x_1) \approx 0.5\,\Gamma(n)\,\frac{2^n}{(x_1)^{n+1}}\,(-n) \qquad (3.17)$$

therefore $$\frac{K_n(x_1)}{K_n'(x_1)} \approx -\frac{x_1}{n}$$

Rearranging equation(3.16)

$$= -\Delta\, F(\Omega^2) = \gamma_n(x)$$

where $$\Delta = \frac{\rho_s}{\rho}\,\frac{h}{a}\,x_1\,, \qquad (3.18)$$

$$F(\Omega^2) = ((\Omega^2)^3 - K_2(\Omega^2)^2 + K_1(\Omega^2) - K_0)/\Omega^2((\Omega^2)^2 - C_1(\Omega^2) + C_0)\,,$$

$$\gamma_n(x) = -1/n\,.$$

Ω^2 can be solved for by using the method of false position with suitable starting values of the unknown frequency.

3.3 Approximations

When geometries become more complicated than the cylinder or sphere or when the fluid environment cannot be considered as infinite in extent then analytical solutions no longer exist.

An approximate method must then be utilised and for many years decoupling schemes based upon doubly asymptotic approximations (DAAs) have been extensively employed.

The DAA is an amalgam of the plane wave approximation (PWA) and virtual mass approximation (VWA) which approaches the exact solution at high and low frequencies. The total pressure field surrounding any point on the shell is divided into three components; due to incident, reflected and radiated pressure. The PWA providing the early-time (high frequency), non-oscillatory response of the interaction and the VMA adding the later (low frequency), oscillatory response. The advantage of this approach is its inherent simplicity and computational efficiency against which must be weighed a certain level of inaccuracy and uncertainty as to the frequency range over which that inaccuracy exists.

The first order doubly asymptotic approximation (DAA1) generally overpredicts the fluid resistance at intermediate frequencies and thus overdamps the structural vibration. Refinements DAA2c, DAA2m and an Inertial Damping Collocation Approximation (IDCA) have been proposed and produce improved results for problems for which exact solutions exist such as the response of a submerged spherical shell excited by an incident step wave.

Despite the uncertainties which surround them DAAs have received widespread support and are often used in conjunction with discrete-element representations of structures which introduces yet more inaccuracy and uncertainty. This work does not use DAA in any form but seeks instead to solve the hydrodynamic equations in toto providing that the fluid loading can be adequately expressed.

3.4 Hydroelastic analysis

The theoretical background to the general three dimensional hydroelasticity analysis adopted here has been discussed in detail elsewhere (Bishop, Price & Wu(1986)) and is therefore omitted. The equations of motion describing the responses of an arbitrary shaped, floating or submerged structure are given by

$$[m]\ddot{u} + [c]\dot{u} + [k]u = q \qquad (3.19)$$

where

m Mass matrix

c Structural (viscous) damping matrix

k Stiffness matrix

u Structural displacement vector

q External force vector describing all fluid actions, imposed forces, etc.

The analysis consists of two parts :

(i) The dry or in-vacuo analysis in which the structure vibrates freely in vacuo in the absence of any structural damping or external forces. The motion is described by the equation

$$[m]\ddot{u} + [k]u = 0 \qquad (3.20)$$

The structure is discretised using finite elements and the natural frequencies and principal mode shapes of the structure are determined. To each principal mode shape a principal coordinate can be assigned and equation(3.19) rewritten in terms of the principal coordinates of the structure, namely

$$[\tilde{m}]\ddot{p} + [\tilde{c}]\dot{p} + [\tilde{k}]p = Z(t) \qquad (3.21)$$

where

$\tilde{m}$ Generalised mass matrix

$\tilde{c}$ Generalised structural damping matrix

$\tilde{k}$ Generalised stiffness matrix

p Principal coordinate vector

Z Generalised external force vector describing the fluid actions, etc.

(ii) The wet analysis introduces the fluid actions which are applied as an external loading to the flexible structure. A three dimensional velocity potential theory is employed and the wet surface of the structure discretised by panels with a source situated at the centre of each panel (Bishop, Price & Wu (1986)). This part of the analysis produces the fluid structure interaction effects which are usually described by added mass, fluid damping, restoring force coefficients and other external excitations. Consequently it may be shown that equation(3.21) takes the form

$$[(M+\tilde{m})]\,\ddot{p} + [(C+\tilde{c})]\,\dot{p} + [(K+\tilde{k})]\,p = Q(t) \qquad (3.22)$$

where

M Generalised added mass matrix

C Generalised fluid damping matrix

K Generalised restoring matrix

Q Generalised excitation vector describing wave actions, imposed forces, etc.

These equations of motion can be solved for the principal coordinates of the structure, which are subsequently used to evaluate the loadings and stresses associated with the structure (Price, Temarel & Wu(1988)).

3.4.1 Dry analysis using finite elements

The finite element analysis of a structure under static or dynamic conditions involves replacing a

continuous structure which has an infinite number of degrees of freedom with a mathematical model having only a finite number of degrees of freedom. The structure is divided into segments, called elements, superimposed on a co-ordinate grid system and the elements are interconnected at discrete points known as "nodes". With up to six degrees of freedom at each node all but the simplest of models will contain hundreds if not thousands of degrees of freedom. Manipulation of matrices of this order involves a considerable computational effort. One of the most important aspects of the idealisation and modelling of the finite element model is, therefore, consideration of the errors induced by the dynamic condensation techniques for solving the eigenvalue problem.

Having selected an element type and produced the finite element mesh, the governing equations are determined for each element and the overall structural equations are formed using the principle of superposition (assuming the system is linear). In static structural analysis a consideration of equilibrium of forces relates external forces to displacements in the form :

$$q = [k]\, u \qquad (3.23)$$

where { q } = vector of external nodal forces (Nx1)

[k] = structural stiffness matrix (NxN)

{ u } = vector of nodal displacements (Nx1)

N = number of degrees of freedom of the structure

Thus, if [k] can be formed and the loading and restraint conditions are known, the unknown displacements can be obtained through inversion of the stiffness matrix and substitution of the known external forces.

Inversion is a time consuming, costly process and reduction of the stiffness matrix can be a useful process for large problems. Turner, Clough, Martin & Topp(1956) have shown that, when a structure has no external forces at certain nodal degrees of freedom, the equations can be rearranged so that all displacements corresponding to zero load can be kept together as follows

$$\begin{Bmatrix} q_a \\ 0 \end{Bmatrix} = \begin{bmatrix} k_{aa} & k_{ab} \\ k_{ba} & k_{bb} \end{bmatrix} \begin{Bmatrix} u_a \\ u_b \end{Bmatrix} \qquad (3.24)$$

Expanding the above

$$q_a = [k_{aa}]\, u_a + [k_{ab}]\, u_b \qquad (3.25)$$

$$0 = [k_{ba}]\, u_a + [k_{bb}]\, u_b$$

$$u_b = -[k_{bb}]^{-1}[k_{ba}]\, u_a \qquad (3.26)$$

Substituting eqn(3.26) into eqn(3.25)

$$\begin{aligned} q_a &= [k_{aa}]\, u_a - [k_{ab}][k_{bb}]^{-1}[k_{ba}]\, u_a \\ &= [k_c]\, u_a \end{aligned} \qquad (3.27)$$

where $[k_c]$ is the condensed stiffness matrix. $\{u_a\}$ can be computed from eqn(3.27) and the remaining displacements $\{u_b\}$ can subsequently be obtained by back substitution in eqn(3.26).

In dynamic studies, the inertia and damping properties within the structure must also be considered. For a viscously damped structure the governing equations are as stated above (eqn.(3.19)). The elemental mass matrix is a matrix of equivalent nodal masses that dynamically represent the actual distributed mass of the element. It can be shown that

$$[m]_e = \rho \int_{vol} [N]^T[N]\, dv \qquad (3.28)$$

where $[m]_e$ is referred to as the consistent mass matrix. An alternative approach is to use a lumped mass matrix in which the mass of the element is distributed evenly between its nodal points in the form of concentrated or lumped masses.

Transformation of the elemental mass matrix from local to global coordinates and assemblage of the mass matrix of the entire structure is carried out in a manner similar to that adopted for the stiffness matrices.

The formulation of a damping matrix is more problematical because although it is possible to derive an equation similar to that describing the consistent

mass matrix

$$[c] = \kappa \int_{vol} [N]^T[N]\, dv \qquad (3.29)$$

it is difficult to determine κ the viscous damping parameter for the element because the damping mechanism is less well defined than inertia or stiffness. It is also more convenient to resort to special types of damping that permit decoupling of the system equations to aid to the solution procedures. Two types of damping model that are often encountered in finite element studies are modal and proportional damping.

3.4.1.1 Dynamic reduction techniques

Having formed equation (3.20) the theories and techniques applicable to classical multi-degree of freedom systems may be used to obtain solutions for the finite element model. Efficient eigenvalue solution techniques are available but with systems with more than 100 degrees of freedom even these can be prohibitively expensive. In a manner similar to that adopted for the stiffness matrix in static analysis, it is possible to reduce the size of the mass matrix for the dynamic analysis.

Suppose that the mass matrix [m] is subdivided into

$$\begin{bmatrix} m_{aa} & m_{ab} \\ m_{ba} & m_{bb} \end{bmatrix}$$

so that the dynamical equation becomes,

$$\begin{Bmatrix} q_a \\ 0 \end{Bmatrix} = \left(\begin{bmatrix} k_{aa} & k_{ab} \\ k_{ba} & k_{bb} \end{bmatrix} - \omega^2 \begin{bmatrix} m_{aa} & m_{ab} \\ m_{ba} & m_{bb} \end{bmatrix} \right) \begin{Bmatrix} u_a \\ u_b \end{Bmatrix} \qquad (3.30)$$

expanding

$$(-\omega^2[m_{ba}]+[k_{ba}])\{u_a\} + (-\omega^2[m_{bb}]+[k_{bb}])\{u_b\} = 0$$

from which

$$\{u_b\} = (-\omega^2[m_{bb}]+[k_{bb}])^{-1}(-\omega^2[m_{ba}]+[k_{ba}])\{u_a\} \qquad (3.31)$$

and displacements for the reduced system can be obtained from

$$(-\omega^2[m_{aa}]+[k_{aa}])\{u_a\} - (-\omega^2[m_{ab}]+[k_{ab}])(-\omega^2[m_{bb}]+[k_{bb}])^{-1} \times (-\omega^2[m_{ba}]+[k_{ba}])\{u_a\} = \{q_a\} \qquad (3.32)$$

This is an exact formulation but it requires inversion for every value of ω because of the frequency dependance of the $(-\omega^2[m_{bb}]+[k_{bb}])^{-1}$ term. However Kidder(1975) has shown that this term can be expanded using a standard binomial function providing $\omega^2<\lambda^2$ where λ^2 is the lowest eigenvalue of $k_{bb} - \lambda^2 m_{bb} = 0$. The expansion can be truncated after the first term so that the reduction utilises eqn.(3.26) which is based upon static considerations. This is the Guyan(1965) reduction technique employed by PAFEC. Alternatively more terms from the binomial series can be accepted and a modified dynamic reduction method is obtained which still has ω^2 dependence.

There will be some loss of accuracy due to the fact that either a static relationship has been used to link the dynamic displacements { u_a } and { u_b } and the inertial forces of the system are not preserved in the reduction process or by the truncation of the series approximation.

Several dynamic condensation techniques have been developed recently (Miller(1980), O'Callaghan, Avitabile & Riemer(1989), O'Callaghan(1989)) to overcome some of the shortcomings of the Guyan reduction technique but these were not available on the FE package that was used in this investigation. The PAFEC code that was used did address the problem of inverting a large $[K_{bb}]$ matrix by following the method proposed by Irons (1965) which reduces the size of the problem by a factor of 10 or more with little further loss of accuracy.

The displacement vector u is partioned into

$$u = (\{u_m\} , \{u_s\})$$

where u_m are master degrees of freedom which will be retained in the condensation process whereas u_s are slave degrees of freedom which will be reduced out. The selection of which degrees of freedom to retain and which to reject is left to the analyst and is partly solved by judgement and partly by experience. The master degrees of freedom should be those which are

important in describing kinetic energy i.e. those which record large amplitude vibrations or those in areas of large mass concentration. The ratio k_{ii}/m_{ii}, involving the leading diagonal stiffness and mass terms for the ith. degree of freedom can be used as an indicator of which degrees of freedom are important. When k_{ii}/m_{ii} is high either the mass at the ith. degree of freedom is small or its stiffness is large signifying a nearly rigid connection within the stucture then u_i can be relegated to becoming a slave degree of freedom. Conversely when k_{ii}/m_{ii} is low there are likely to be significant inertia effects and it would be wise to keep the degree of freedom u_i as a master. The difficulty in modelling a symmetrical cylinder of uniform thickness is that the ratio k_{ii}/m_{ii} will be similar for a large number of degrees of freedom, more than can be retained. Careful selection of the master degrees of freedom is therefore important in this instance, where it is obvious that the deformed mode shapes must themselves be symmetrical.

With the master degrees of freedom selected, a continuous reduction process can be utilised using frontal solution techniques (Henshall (1975)). The mass and stiffness matrices are assembled progressively commencing at one part of the structure and working systematically through to the other end. As the degrees of freedom are incorporated into the system mass and

stiffness matrices they may be eliminated if they correspond to a slave displacement. From eqn(3.30) the kth. equation of motion at any stage may be written

$$\sum_{j-1}^{N} k_{kj}.u_j + \omega^2.m_{kj}.u_j = q_k \qquad (3.33)$$

upon elimination of the slave displacement, u_s, in the ith. equation of motion the new ij terms become

$$k'_{ij} = k_{ij} - k_{is}(k_{sj}/k_{ss}) \qquad (3.34)$$

$$m'_{ij} = m_{ij} - m_{is}(k_{sj}/k_{ss}) - m_{sj}(k_{is}/k_{ss}) + m_{ss}(k_{sj}/k_{ss})(k_{is}/k_{ss}) \qquad (3.35)$$

and the forcing term will be similarly amended. The system mass and stiffness matrices are therefore never fully formed with a commensurate saving of core space when the calculations are performed by computer. Upon solution of the master degrees of freedom the slave degrees of freedom are found by back substitution.

3.4.1.2 Selection of element type

While the analyst should be aware of the dynamic reduction techniques that are being employed there is, very often, little scope for variation within a particular FE software package. On the other hand there are a number of choices in the type of element that can be employed in modelling the structure. For the case of a thin cylindrical shell PAFEC allows the choice of three types of element: a thin shell of revolution (3

noded), a flat facet shell element (8 noded) and a semi-loof curved shell element (8 noded).

The thin shell of revolution element is based on theory due to Novozhilov (1959) and incorporates membrane as well as bending effects. This model corresponds approximately to Kirchoff plate theory and the element provides a highly efficient and accurate solution which was used as a benchmark for comparison with other predictions. The displacement assumptions are in three orthogonal directions, with the order of the displacement polynomial in the radial direction twice that for the axial and tangential directions. The element has three degrees of freedom at each of the nodes which vary sinusoidally according to the harmonic number specified. Unfortunately, applications with this element are limited to structures with simple geometries and are not entirely suitable for use with the wet analysis theory.

The facet approach to shell analysis is less exact introducing a number of factors whose effects cannot be readily quantified. The facet shell element used is one which has five degrees of freedom at each node with the extra freedom 0z introduced after the transformation to global coordinates (Fig.3.2). The first assumption of an approximate displacement (or shape function) relates displacements within the element to nodal displacements.

This produces errors in the element stiffness relationship but is one of the basic assumptions upon which all finite element analyses are based. Secondly there is the obvious approximation caused by representing the smooth curved surface by a multifaceted polyhedral surface. Finally there are other errors associated with the element itself. Plate elements assume that the effects of membrane and bending stresses are uncoupled and combine the two effects separately. The thin isotropic shell element used in this analysis combines plate bending with a constant strain membrane element. The bending element has three degrees of freedom at each node, w, dw/dx and dw/dy. The radial displacement, w, is defined by a cubic expression in terms of area coordinates and this degree of variation ensures compatability between elements. The normal slope varies quadratically on an edge and since only two

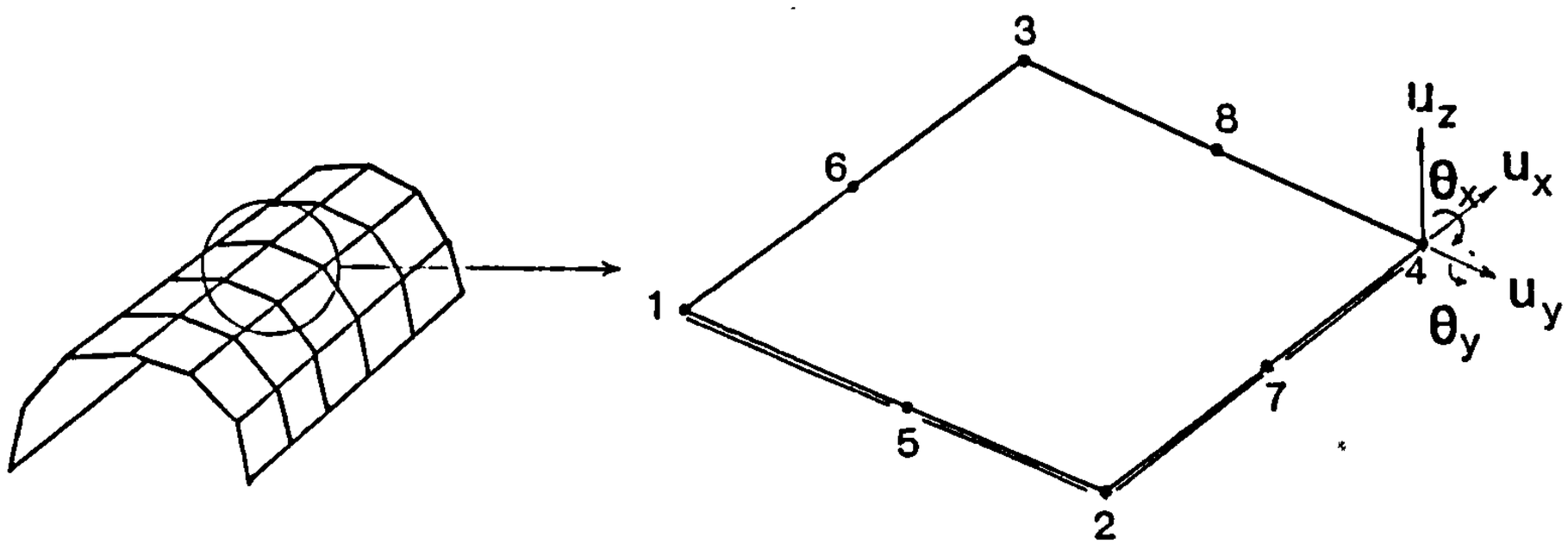

Figure 3.2 Nodal variables for rectangular plate element

end values are available to define the normal slope its variation is not uniquely specified by the end values; thus a discontinuity of normal slope will occur between adjacent elements in general. The in-plane displacements, u and v, are accounted for by an assumption of constant stress throughout the element.

Finally a curved element is .considered, the semi-Loof element was used which has a curvilinear quadrilateral shape. There are 32 degrees of freedom associated with the element in its final form and it is noted that the rotational freedoms are applied at different points to the translational freedoms. The element freedoms are displacements u_x, u_y, u_z at corner and midside points and normal rotation values at two Gauss points along each side (Fig.3.3). The 32 degrees of freedom of this element should be sufficient to define

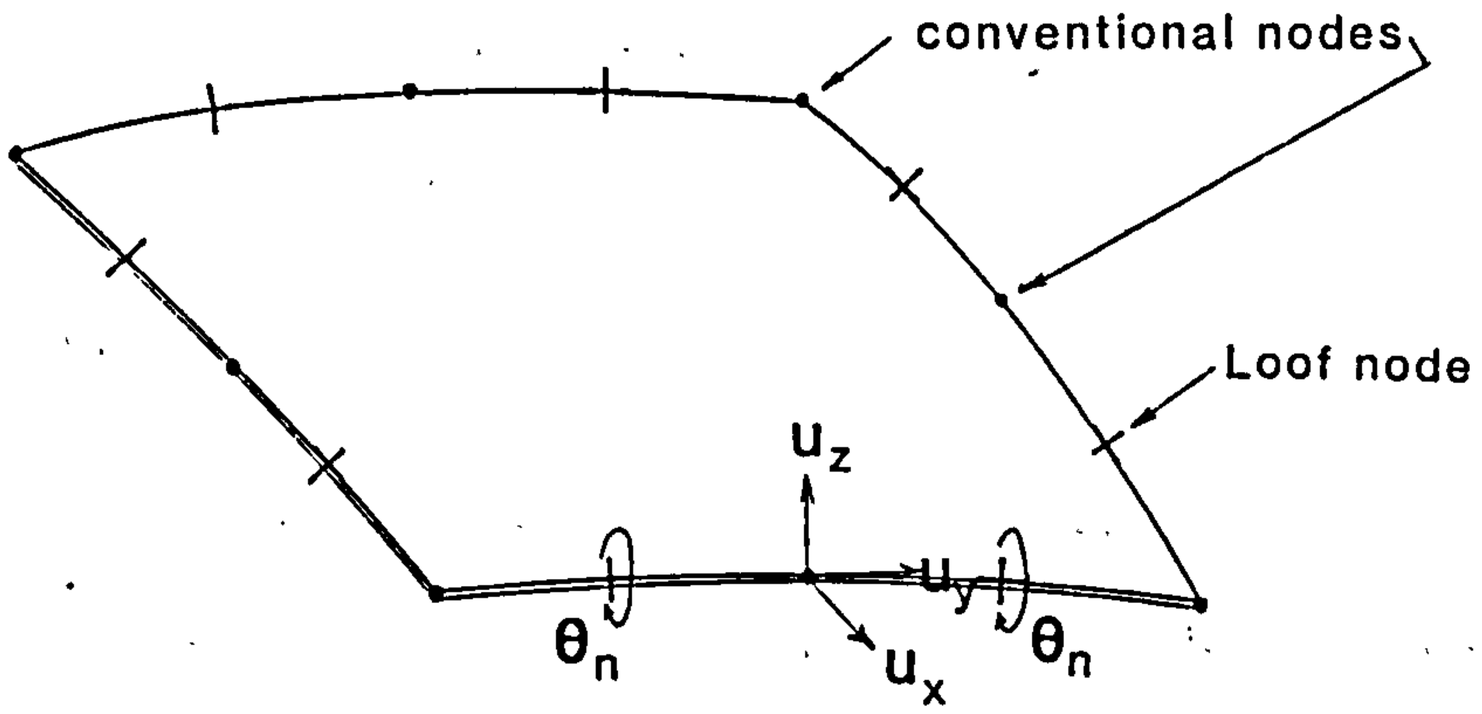

Figure 3.3 Nodal variables for quadrilateral semi-Loof element

linear stress fields for both membrane and bending behaviour. The theory and philosophy of the semi-Loof element are very complex and its application must be considered with caution.

The element can give spurious mechanisms on elements which store little or no strain energy and particular attention is paid to the order of integration used over the mid-surface of the element. There are three options; 4-point (i.e. 2*2), a special 5-point and 9-point (3*3) Gaussian integration. At each integrating point discrete Kirchoff assumptions are made so that normals to the mid-surface remain approximately normal, this is effected by imposing zero lateral strains. Due to some variance with the published results (Hellen & Irons(1987)) the benefits of using reduced integration appear to be only predictable on a trial and error basis. However flexible structures such as thin cylinders are considered suitable for reduced integration and this has been practised here.

3.4.2 Wet analysis

The fluid forces on the submerged cylinder under investigation have been calculated using a general three dimensional linear hydroelasticity theory developed by Bishop, Price and Wu (1986).

This approach accounts not only for the interaction

of the fluid with the structure but also assesses the influence of the structures forward speed and the effect of a finite depth of water.

The speed of the structure is irrelevant in this instance as all the models tested were tethered. However the tanks in which the models were tested were relatively confined and the models themselves were flexible shell-type structures. The following description of the hydroelasticity theory will concentrate on these aspects.

3.4.2.1 Co-ordinate system

Three right-handed Cartesian coordinate systems were chosen to define the hydrodynamic analysis.

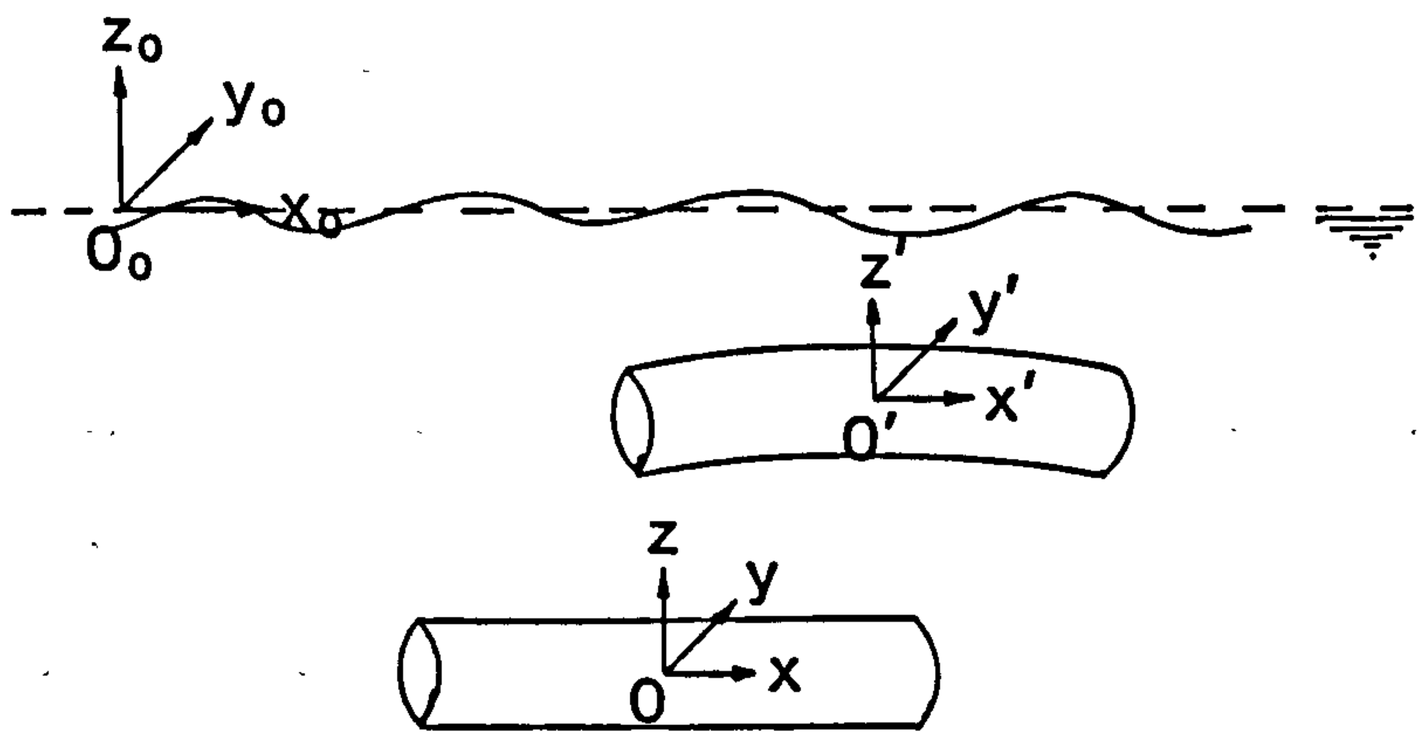

Figure 3.4 Coordinate system employed for hydrodynamic analysis

$\underline{x_o} = (x_o,y_o,z_o)$ is fixed in space with origin O_o on the mean water surface with O_ox_o parallel to the centreline of the submerged body pointing from stern to bow. $\underline{x} = (x,y,z)$ are an equilibrium set of axes parallel with x_o but moving forward at the speed of the structure. $\underline{x'} = (x',y',z')$ are fixed in the structure and in the absence of any disturbance coincide with x.

3.4.2.2 General formulation.

The fluid is assumed to be ideal, i.e. irrotational, incompressible and inviscid. Hence the fluid motion can be described by the velocity vector V (x_o,y_o,z_o,t) which is the gradient of the velocity potential Φ (x_o,y_o,z_o,t) .

i.e. $$V = \nabla\Phi \qquad (3.36)$$

where Φ is governed by Laplaces' equation throughout the fluid domain that is

$$\nabla^2\Phi = 0 \qquad (3.37)$$

The velocity potential satisfies boundary conditions (Newman (1978)).

(i) on the free surface and the seabed, ensuring no flow across these boundaries.

(ii) a radiation condition in the x and y directions such that the energy conservation laws are satisfied.

(iii) at the solid-fluid interface so that there is no cavitation.

The total velocity potential can be separated into two parts, $\overline{\Phi}$ due solely to the non-varying forward speed of the body and the residual potential Φ due to the oscillatory motion caused by waves or other external stimuli.

$$\Phi(x_o,y_o,z_o,t) = \tilde{\Phi}(x,y,z,t) = U_b\overline{\Phi}(x,y,z,t) + \phi(x,y,z,t) \quad (3.38)$$

If the oscillatory motions of the fluid are assumed small, the potential Φ can be decomposed linearly into separate components

(i) the incident wave potential Φ_o

(ii) the diffraction (or scattered) potential Φ_d

(iii) the radiation potentials Φ_r , r = 1...6 rigid body modes and r= 7...n flexible modes where n is the number of modes included in the analysis

$$\phi(x,y,z,t) = \Phi_o(x,y,z,t) + \Phi_d(x,y,z,t) + \sum_{r=1}^{n}\Phi_r(x,y,z,t) \quad (3.39)$$

All of these components of the total velocity potential must satisfy the boundary conditions and the continuity condition imposed by Laplaces' equation.

3.4.2.3 The free surface boundary condition

The elevation of the free surface is generally unknown although it can be expressed from Bernoulli's

equation as

$$\xi = -\frac{1}{g}\left(\frac{\delta\Phi}{\delta t} + \frac{1}{2}\nabla\Phi.\nabla\Phi\right)_{z_o=\xi} \qquad (3.40)$$

using $\frac{D\xi}{Dt} = \left(\frac{\delta\Phi}{\delta z_o}\right)_{z_o=\xi}$, where $\frac{D}{Dt} = \frac{\delta}{\delta t} + V.\nabla$

it is possible to derive the kinematic boundary condition, namely

$$\Phi_{tt} + 2\nabla\Phi.\nabla\Phi_t + \frac{1}{2}\nabla\Phi.\nabla(\nabla\Phi.\nabla\Phi) + g\Phi_{z_o} = 0 \quad \text{on } z_o=\xi \qquad (3.41)$$

subscripts (t, z_o) refer to partial differentiation.

If the amplitude of surface waves is small or if the forward speed is small then equation (3.41) can be linearized to

$$\Phi_{tt} + g\Phi_{z_o} = 0 \quad \text{on } z_o=0 \qquad (3.42)$$

This equation applies equally to the total potential or the potential due to oscillatory motion Φ; if this motion is assumed sinusoidal then

$$\Phi(x,y,z,t) = \Phi(x,y,z).e^{i\omega t}$$

and (3.42) becomes

$$\frac{\delta\Phi}{\delta z} - \frac{\omega^2}{g}\Phi = 0 \quad \text{on } z_o=0 \qquad (3.43)$$

3.4.2.4 The seabed condition

The seabed is assumed flat, impervious and rigid such that

$$\Phi_z = 0 \quad \text{on } z_o=-d \qquad (3.44)$$

where d is the depth of water which may be infinite.

3.4.2.5 The radiation condition

The radiation condition ensures that the energy flux of waves associated with the disturbance of the moving body is directed away from the body and decays to zero at infinity.

For zero forward speed, two forms of the radiation condition are considered, due to Sommerfeld (1949)

$$\lim_{R\to\infty} R^{(n-1)/2}\left(\frac{\partial}{\partial R} + \frac{\partial}{\partial t}\right)\left(\tilde{\Phi} - \Phi_0\right) = 0 \qquad (3.45)$$

where $R = \sqrt{x^2 + y^2}$ the distance from the body and

n is the number of spatial dimensions.

Newman(1977) derived a simpler form for rigid body radiation and diffraction potentials

$$\Phi_r \text{ or } \Phi_d \propto e^{\pm ikx} \text{ as } x\to\pm\infty \qquad (3.46)$$

Alternative forms of (3.46) may be found in John(1950) and Rellick(1953).

3.4.2.6 The body surface boundary condition

The condition that the body and the fluid move together at their interface (i.e. no cavitation) can be expressed as

$$(V_s - V).n = 0 \text{ on } S \qquad (3.47)$$

where V_s represents the body's velocity and n the unit normal vector of the body wetted surface, S. S can also represent the wetted surface on the body in the equilibrium position as the difference between the instantaneous and equilibrium wetted surfaces is a second order quantity.

Using the simplification made in section 3.4.2.2,

$$\Phi = \Phi_o + \Phi_d + \Phi_r$$

this boundary condition can be stated in two parts.

The incident and diffraction potentials satisfy the relationship

$$\frac{\partial \Phi_d}{\partial n} = - \frac{\partial \Phi_o}{\partial n} \text{ on } S \qquad (3.48)$$

and the components of the radiation potentials due to the motion of the body in the six rigid body degrees of freedom can also be obtained (Wu(1984)).

3.4.2.7 Solution of boundary value problem

Having posed the boundary value problem in terms of velocity potentials now consider its solution.

Exact solutions only exist for a few simple cases under restricted conditions (Havelock(1931), MacCamy & Fuchs(1954)), so numerical techniques such as finite elements or boundary integral methods must be employed.

Fluid finite elements exist and have been extensively reviewed by Shen(1977), Mei(1978) and Baar &

Price(1983a,b). This work uses boundary integral or singularity distribution techniques in which the velocity potential is obtained through an arrangement of sources (and/or dipoles) on the body surface. The form of the velocity potential associated with the singularities satisfies all the boundary conditions described in previous sections with the exception of the body surface boundary condition which is then used to determine the strength of the singularities.

First, consider a fluid domain V enclosed by a surface, So. If Φ and G are any two functions which, together with their first and second derivatives, are finite and single valued within V. Then Green's second identity (or divergence theorem) shows that

$$\iint_{S_o} \left[\Phi \frac{\partial G}{\partial n} - G \frac{\partial \Phi}{\partial n} \right] ds = - \iiint_{vol} \left[\Phi \nabla^2 G - G \nabla^2 \Phi \right] dv \quad (3.49)$$

where n is the normal vector of the surface S_o pointing inwards.

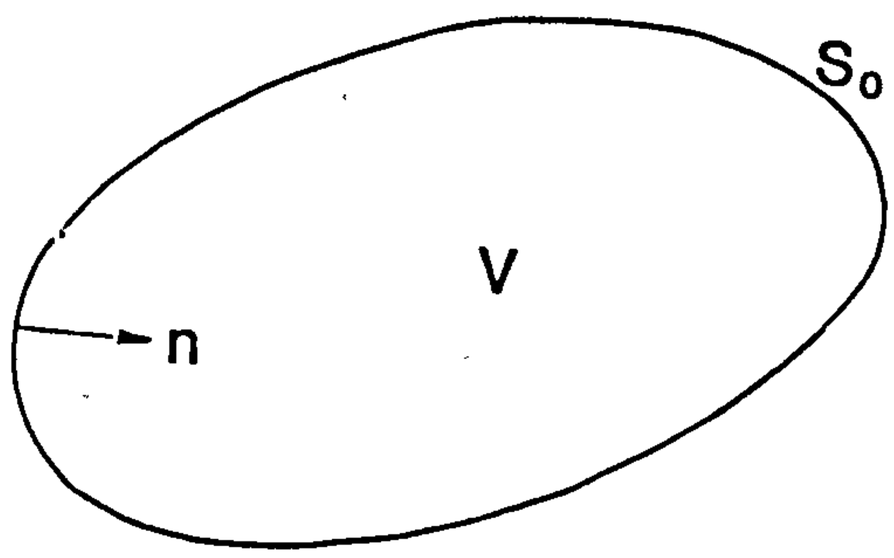

Figure 3.5 Fluid domain

Let Φ be the unknown velocity potential which satisfies Laplaces' equation in V and let G be a combination of a singular function and a harmonic function.

$$G(r,r_1) = \frac{1}{r - r_1} + f(r,r_1) \qquad (3.50)$$

where $\nabla^2 f(r,r_1) = 0$ in v

$$r = (x,y,z) \quad r_1 = (x_1,y_1,z_1)$$

$$r-r_1 = \sqrt{((x-x_1)^2 + (y-y_1)^2 + (z-z_1)^2)} = R .$$

There is, by definition, a singularity point at $r = r_1$; but if it is enclosed by a sphere of small radius δ and surface S_1 (when r is in V) or a hemisphere of small radius δ (when r is on S_0), see fig. 3.6, then the

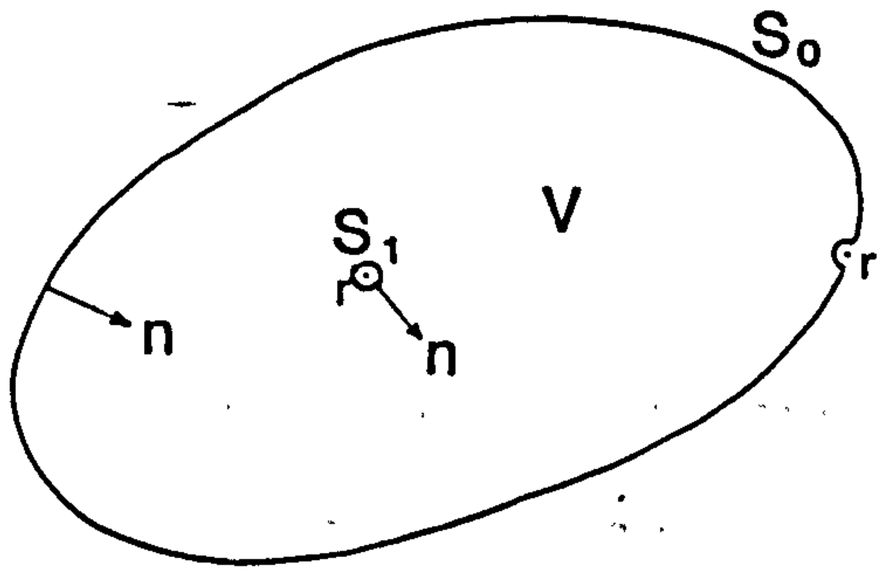

Figure 3.6 Singularity points

volume integral of $\Phi\nabla^2 G$ can be evaluated and applying $\nabla^2\phi = 0$ eqn.(3.50) simplifies to

$$\iint_{S_o} \left[G(r,r_1)\frac{\delta\phi(r_1)}{\delta n(r_1)} - \phi(r_1)\frac{\delta G}{\delta n} \right] ds = \begin{cases} -4\pi\phi(r) & \text{for r in V} \\ -2\pi\phi(r) & \text{for r on } S_o \\ 0 & \text{for r outside V and } S_o \end{cases} \tag{3.51}$$

since ϕ and G are complex functions the surface integral in eqn.(3.51) is a principal value integral.

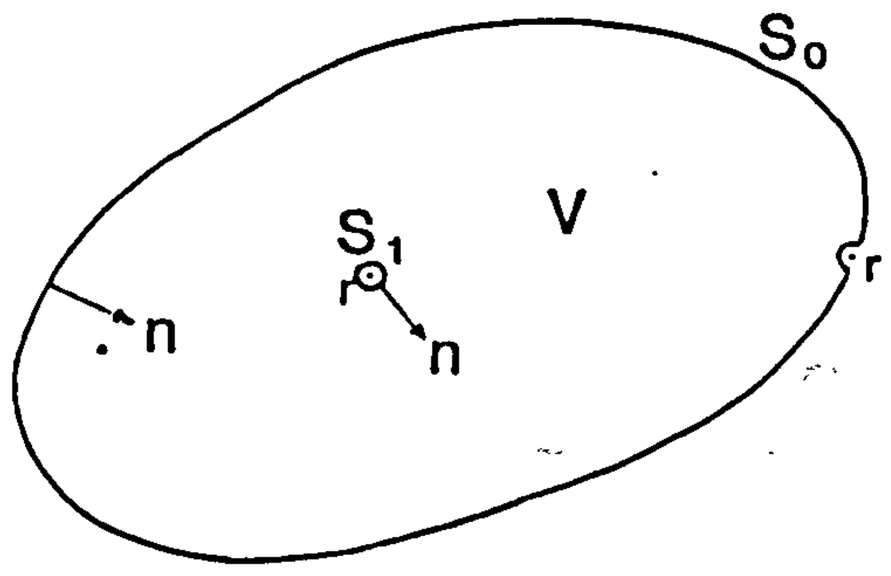

Figure 3.6 Singularity points

G is a potential function at any point r due to a source situated at point r_1 and different boundary conditions on S_o can be satisfied by selection of suitable functions of $f(r,r_1)$ in eqn.(3.50), (Wehausen & Laitone(1960)). In addition, $\delta G/\delta n$ can represent a velocity potential at any point r due to a dipole at r_1 and having its axis in the direction n. Therefore the

velocity potential can be stated as the sum of a distribution of sources with density $\partial\Phi/\partial n$ and a distribution of dipoles with density $-\Phi$. The distributions are over S_0 and the dipoles are oriented normal to S_0.

The external boundary can be used to represent a finite depth of water by including a free surface, S_e and a rigid seabed, S_b. The inclusion of a body moving in the fluid can also be incorporated by use of a moving boundary dividing the fluid into interior and exterior regions, this boundary will pierce the free surface if the body is floating (fig 3.7).

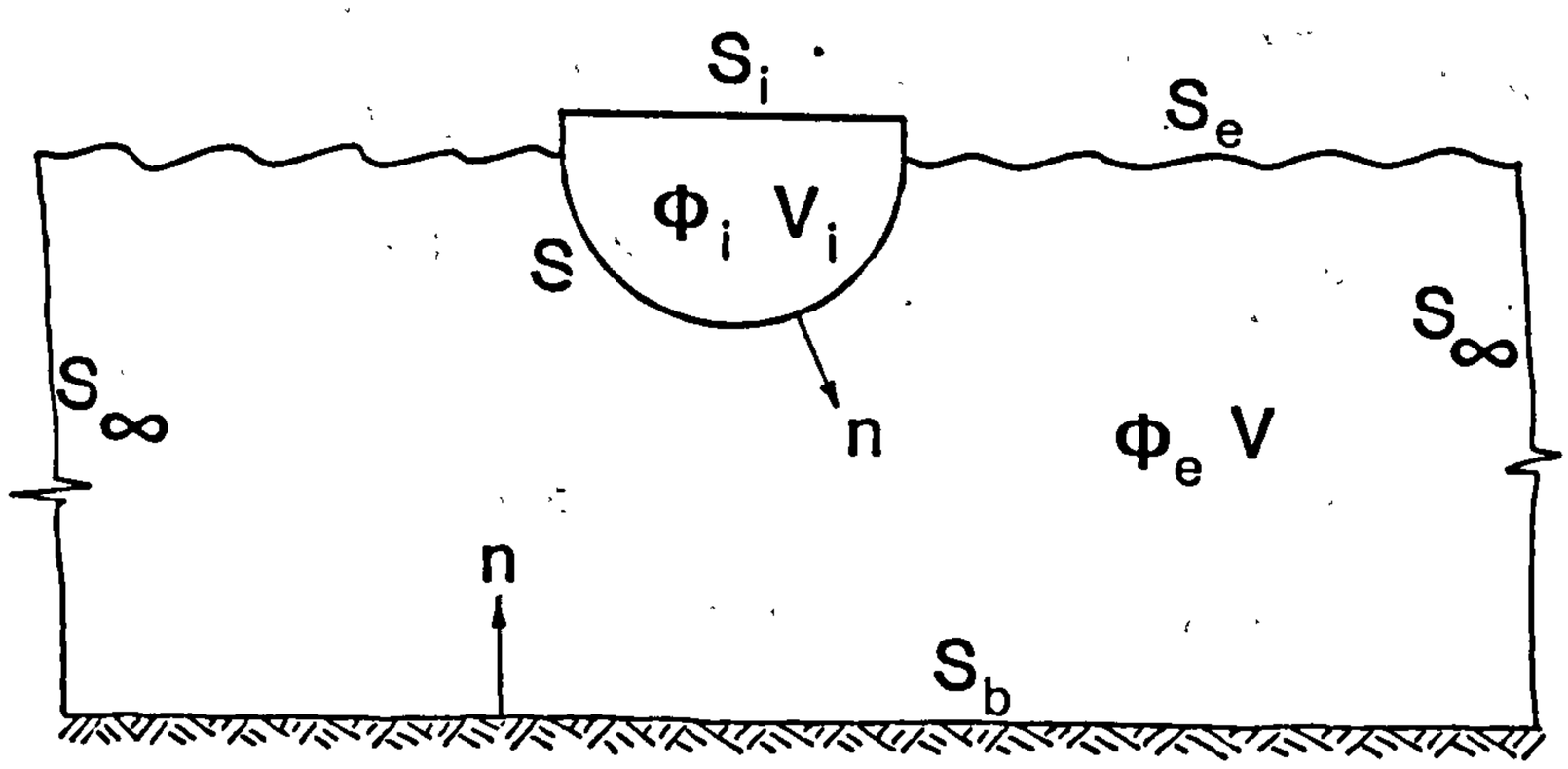

Figure 3.7 Interior and exterior regions

The two velocity potentials Φ_e and Φ describe the flow in the separate regions and although Φ_i exists

mathematically there may be no fluid within the body and its solution has no physical meaning except to assist in the solution of Φ_e.

If the source point r_1 is in the exterior region then the velocity potential at r also in the exterior region is

$$\Phi_e(r) = \frac{1}{4\pi} \iint_{S\text{-}S_e\text{-}S_\infty\text{-}S_b} [\, \Phi_e(r_1)\frac{\delta G(r,r_1)}{\delta n(r_1)} - G(r,r_1)\frac{\delta \Phi_e(r_1)}{\delta n(r_1)} \,]ds \quad (3.52)$$

The potential at r outside the body can also be stated in terms of Φi when r_1 is in the interior region.

$$\iint_{S\text{-}S_i} [\, G(r,r_1)\frac{\delta \Phi_i(r_1)}{\delta n(r_1)} - \Phi_i(r,r_1)\frac{\delta G(r,r_1)}{\delta n(r_1)} \,]ds = 0 \quad (3.53)$$

Adding

$$\Phi_e(r) = \frac{1}{4\pi} \iint_S [\Phi_e - \Phi_i]\frac{\delta G}{\delta n} - [\, \frac{\delta \Phi_e}{\delta n} - \frac{\delta \Phi_i}{\delta n} \,]G.ds \quad (3.54)$$

$$+ \frac{1}{4\pi} \iint_{S_e\text{-}S_b\text{-}S_\infty} [\, \Phi_e\frac{\delta G}{\delta n} - G\frac{\delta \Phi_e}{\delta n} \,]ds - \frac{1}{4\pi} \iint_{S_i} [\, \Phi_i\frac{\delta G}{\delta n} - G\frac{\delta \Phi_i}{\delta n} \,]ds.$$

It is well known (Fung (1987)) that the Greens function $G(r,r_1)$ can be defined to reduce the whole boundary integral problem (eqn.(3.54)) to a boundary problem over the body wetted surface S and its waterline C. This reduction is accomplished by selection of a suitable Greens function to satisfy one or all of the boundary conditions in equations (3.43-45). For example, the Greens function 1/R descibes a source at rest in an infinite fluid domain and will only satisfy the Sommerfeld radiation condition (eqn.(3.45)) whereas

a more complicated formulation may describe a pulsating and translating source which satisfies all of the boundary conditions (Wu (1984)).

Finally the potential Φi and the body surface boundary condition are used to determine the source strength. Assuming $\Phi_i(r)_S = \Phi_e(r)_S$ and denoting the source strength $Q(r) = \left(\frac{\partial \Phi_i}{\partial n} - \frac{\partial \Phi_e}{\partial n}\right)_S$ the velocity potential is given by

$$\Phi_e(r) = \frac{1}{4\pi}\int\int_S Q(r_1)G(r,r_1)ds + \frac{V^2}{4\pi g}\oint_C Q(r_1)G(r,r_1)n_1^2(r_1)dC \qquad (3.55)$$

$\oint_C$ denotes contour integration over the line of intersection between the body and the calm free surface. For submerged bodies or situations where there is zero forward speed this term vanishes. The unknown source strength in eqn.(3.55) can be found by imposing the body boundary conditions to give

$$\frac{1}{4\pi}\int\int_S Q(r_1)\frac{\partial G(r,r_1)}{\partial n(r)}ds + \frac{V^2}{4\pi g}\oint_C Q(r_1)\frac{\partial G(r,r_1)}{\partial n(r)}n_1^2(r_1)dC = V_s.n \qquad (3.56)$$

Unique solutions for the velocity potential on certain floating bodies with zero forward speed have been proved (John (1950)) and the uniqueness theorem has been extended by Lenoir & Martin(1981), removing geometrical restrictions so that it is applicable to any arbitarily shaped floating body. Further extension to situations in which the forward speed of the body is significant has not been proved but has been assumed intuitively. This remains an area of uncertainty but it

is noted that velocity potential has been used in linearised three-dimensional hydrodynamic analyses on many occasions. (Garrison & Chow(1972), van Oortmerssen(1972), Faltinsen & Michelsen(1975), Brown, Eatock-Taylor & Patel(1983), Chang(1977) and Inglis & Price(1980,1982a,b)).

A further difficulty which has been experienced by many investigators is irregular behaviour at frequencies which are eigenfrequencies of the interior eigenvalue problem. These eigenfrequencies do not have any physical significance merely being a feature of the boundary integral formulation but they do cause the system to be ill-conditioned over a finite bandwidth. Fortunately, it can be shown that when the body is totally submerged these irregular frequencies do not exist.

If the flexible body has port-starboard symmetry, then certain symmetrical and reciprocal properties of the employed Green's function can be used to obtain an efficient singularity distribution method. The composite singularity distribution method described by Price & Wu(1985) has been used in this investigation. Briefly, the body surface is represented by a large number of small plane elements on which the source strength, Q is assumed constant. The continuous variation of Q over the body surface is thus approximated by a large number of discrete values of Q.

3.4.2.8 Hydrodynamic coefficients

In the remainder of this chapter determination of hydrodynamic coefficients from the established velocity potential values and their inclusion into the generalised equations of motion will be discussed.

The generalised fluid force (eqn(3.21)) which includes all the prescribed and induced fluid actions, can be expressed in terms of pressure p(x,y,z,t) acting on the body surface, from

$$Z_r = -\iint_S n\, u_r\, p.ds \qquad (3.57)$$

where only the normal force is considered since, in general, the tangential force exerted by the fluid is negligible. Using Bernoulli's equation the pressure can be expressed as

$$\frac{p}{\rho} = -\left(\frac{\delta\Phi}{\delta t} + \frac{1}{2}V^2 + gz_o\right) + \frac{p_a}{\rho} \qquad (3.58)$$

p_a is atmospheric pressure which is ignored hereafter. The remainder of equation (3.58) can be simplified significantly by considering a body in calm water with zero forward speed and using the equilibrium coordinate system.

$$p = -\rho\frac{\delta\Phi}{\delta t} \qquad (3.59)$$

Assuming that the temporal variation of the velocity potential is sinusoidal and noting that the total

velocity potential can be subdivided, the total fluid action force has the following components

$$Z = \left(F_R + \Theta_R\right) e^{i\omega t} \tag{3.60}$$

where $F_R = F_{OR} + F_{DR}$

(3.61)

$$F_{OR} = \rho \iint_S n\, u_r\, i\omega\Phi_o .ds$$

accounting for the action of the incident wave is referred to as the Frode-Krylov force.

$$F_{DR} = \rho \iint_S n\, u_r\, i\omega\Phi_d .ds \tag{3.62}$$

accounting for the action of the scattered wave is referred to as the diffraction force.

$$\Theta_r = \rho \iint_S n\, u_r \left[\frac{\delta}{\delta t}\right] \sum_{k=1}^{n} p_k(t)\Phi_k ds \qquad \text{for } k=1,2\ldots n \tag{3.63}$$

is the generalised radiation force, where n modes have been included into the analysis. The radiation potential is a complex variable which can be separated into real and imaginary components, thus

$$\Theta_r = \sum_{k-1}^{n} p_k T_{rk}\, e^{i\omega t} \qquad \text{for } k=1,2,\ldots,n \tag{3.64}$$

where $T_{rk} = \omega^2 M_{rk} - i\omega C_{rk}$ (3.65)

and $$M_{rk} = \frac{\rho}{\omega^2} \mathrm{Re} \iint_S n\, u_r\, i\omega\Phi_k ds \tag{3.66}$$

$$C_{rk} = -\frac{\rho}{\omega} \mathrm{Im} \iint_S n\, u_r\, i\omega\Phi_k ds \tag{3.67}$$

The terms M_{rk} and C_{rk} relate to added mass and damping coefficients and describe fluid actions in phase with the bodies acceleration and velocity respectively.

3.4.2.9 Generalised equations of motion.

Ignoring any other external loads such as tethering forces etc. the equation of motion for the rth. mode of the submerged body will be given by

$$m_{rr}\,\ddot{p}_r + c_{rr}\,\dot{p}_r + k_{rr}\,p_r = Z_r \qquad (3.68)$$

$$= (F_r + \Theta_r)$$

$$= F_r - \sum_{k=1}^{n} M_{rk}\ddot{p}_k + C_{rk}\dot{p}_k$$

In general there will be a generalised hydrodynamic restoring force and the generalised equations of motion in matrix form are

$$[\,-\omega^2(m+M) + i\omega(c+C) + (k+K)\,]\,p = F \qquad (3.69)$$

which can be solved to obtain principal coordinates.

CHAPTER 4 - MEASUREMENT TECHNIQUES

4.1 Introduction

This chapter is not intended as a step-by-step guide to one particular test on a submerged cylinder but rather as an overview of the measurement methods used in this investigation. The rationale behind decisions on types of equipment and analyses used and practices followed will be explained.

The first section is applicable to all types of vibration testing not solely to underwater structures and deals with the terminology and definitions to be used later in the text. The philosophy of vibration testing and the various types of excitation that can be used are also discussed.

The next section details the types of equipment used in the measurement process and is also of a general nature. The specific details relating to vibration testing in a fluid environment are explained in Section 4.3 together with details of the cylindrical test structures.

Finally modal analysis techniques are examined and a method appropriate to this investigation is described in detail in Section 4.4.

4.1.1 Terminology

Modal testing is the term which has been "coined" for vibration measurement which is undertaken with a view to obtaining a mathematical description of the dynamic behaviour of a structure.

A simple spring-mass system has only one mode of vibration which occurs at a **resonance frequency** determined by the magnitude of the mass M, stiffness K and viscous damping C. Further resonances can only be obtained by the addition of further discrete masses and springs. For the purposes of obtaining a mathematical model a continuous structure can be considered to be made up of a combination of these springs and masses. In this crude representation of the continuous structure the "masses" are subdivisions of the total structural mass and the nature of the "springs" will depend on the geometrical, material properties and the fixity of the structure. There is no limit on the number of modes of vibration for a continuum but if they are to be modelled correctly each will have mass, stiffness and damping levels associated with it. The **modal analysis** which is performed after the measurement stage can attempt to asssign values to these parameters for every mode within the analysis bandwidth. The minimum requirement of an analysis will be to determine the natural frequency and mode shape and possibly modal damping factor which together form the **modal parameters** and represent the response model.

From the above it can be seen that it is necessary to be able to differentiate between the various modes of vibration that occur during a test and this will limit the frequency range over which modal testing can satisfactorily operate. Figure 4.1 shows the response of a typical engineering structure as a function of the excitation frequency. The behaviour is divided into four zones and experimental modal analysis can only be applied in the first two of them. The low frequency

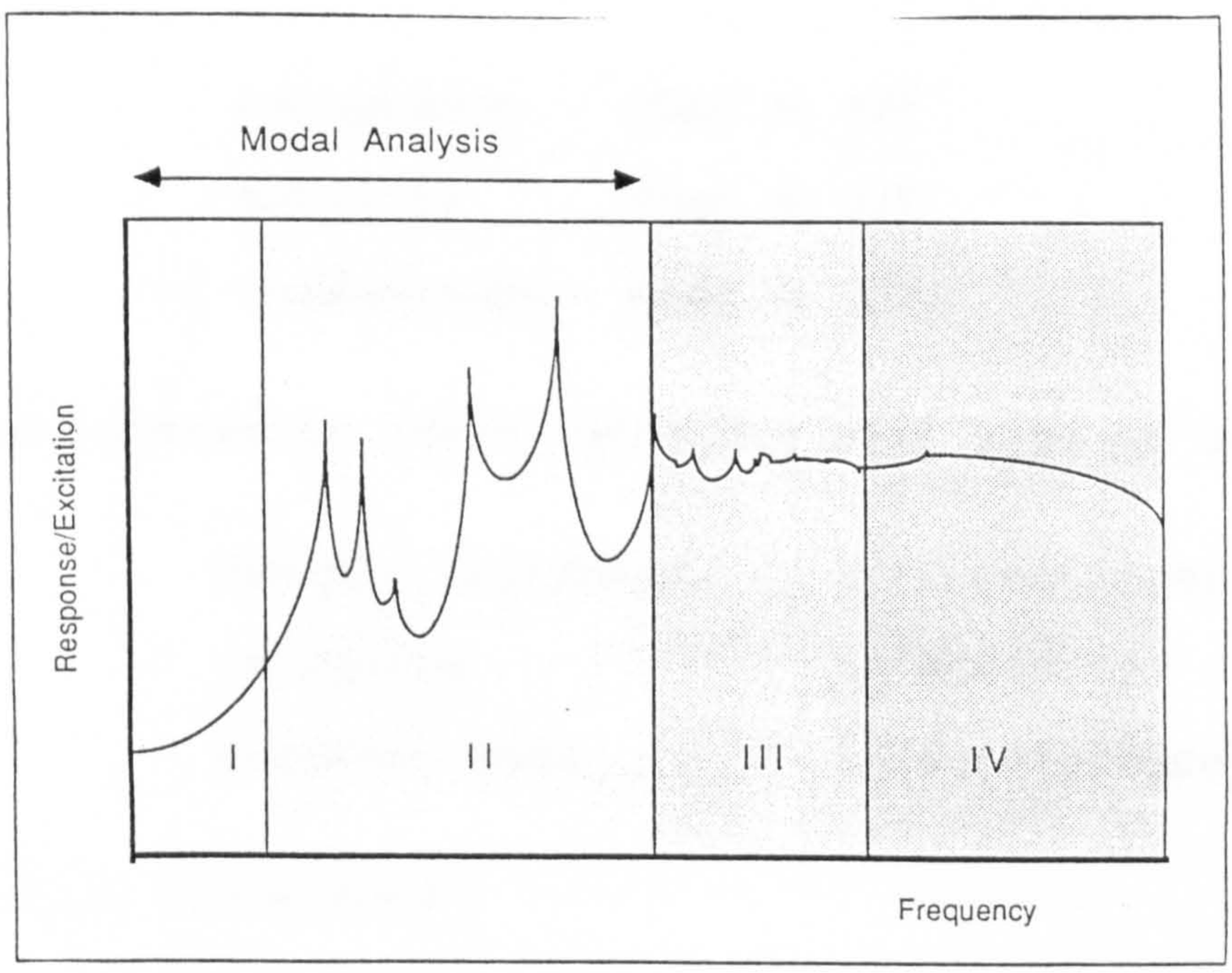

Figure 4.1 Frequency range of modal analysis

response is determined by the fixity of the structure. In the second zone the behaviour can be described as "modal" with clearly defined resonance peaks, but beyond

this region the detail becomes more confused as the modal density increases. Finally the local structure starts to dominate the response and the transducers that measure the response begin to reach the limit of their dynamic range.

The measured responses of a structure undergoing forced vibration will be determined in terms of displacement, velocity or acceleration. The frequency response function (FRF) will therefore be expressed as either;

$$\text{receptance} \quad \alpha(\omega) = x/F$$

$$\text{mobility} \quad Y(\omega) = \dot{x}/F$$

$$\text{or accelerance} \quad A(\omega) = \ddot{x}/F$$

The inverse of these functions will also be used

$$\text{dynamic stiffness} = 1/(\text{receptance})$$

$$\text{impedance} = 1/(\text{mobility})$$

$$\text{apparent mass} = 1/(\text{accelerance})$$

4.1.2. Coherence

The objective of testing is to obtain a FRF for the structure over the required frequency range. The time-varying response o(t) may be either acceleration, velocity or displacement but if it is non-zero and Fourier transformable (i.e. periodic) the FRF, $H(\omega)$, can be defined as the ratio of the Fourier transforms of

the response to the input i(t).

$$H(\omega) = O(\omega)/I(\omega) \tag{4.1}$$

In practice the signals i(t) and o(t) will be corrupted to some extent by measurement noise, such that

$$H'(\omega) = Y(\omega)/X(\omega) = (O(\omega) + M(\omega))/(I(\omega) + N(\omega)) \tag{4.2}$$

and the measured FRF, H' will only be a good approximation of the true frequency response if the noise levels are small compared with the response signals.

An alternative approach is to multiply equation (4.1) by the complex conjugate of the input Fourier transform to obtain the FRF as the ratio of the cross spectrum between input and response and the power spectrum of the input.

$$H'(\omega) = \frac{I^*(\omega).O(\omega)}{I^*(\omega).I(\omega)} = \frac{S_{io}(\omega)}{S_{ii}(\omega)} \tag{4.3}$$

in the same way the measured FRF becomes

$$H_1(\omega) = \frac{Sxy}{Sxx} = \frac{Sio + Sin + Smo + Smn}{Sii + Sim + Smi + Smm} \tag{4.4}$$

If the noise signals m(t) and n(t) that have been picked up are purely random, i.e. uncorrelated with each other or with the system input and output, the expected value of their cross-spectra will be zero.

Therefore

$$H_1(\omega) = \frac{S_{io}}{S_{ii} + S_{mm}} = \frac{H(\omega)}{(\,1 + (S_{mm}/S_{ii})\,)} \qquad (4.5)$$

Therefore $H_1(\omega)$ will duplicate the true frequency response $H(\omega)$ when the denominator in eqn (4.5) is unity (i.e. $S_{mm}/S_{ii} \rightarrow 0$). The magnitude of noise ,m(t) on the input signal will be generally independant of frequency. Therefore the ratio S_{mm}/S_{ii} will only become significant when the input signal itself is low. This will occur at resonance as only a small disturbing force is required to produce measureable response levels. It follows therefore, that the measured FRF, $H_1(\omega)$, is less accurate in the regions around resonance.

An alternative measured FRF, $H_2(\omega)$, can be computed by multiplying equation (4.2) by the complex conjugate of the measured output fourier transform.

$$H_2(\omega) = \frac{S_{yy}}{S_{yx}} = \frac{S_{oo} + S_{on} + S_{\bar{n}o} + S_{\bar{n}n}}{S_{oi} + S_{om} + S_{ni} + S_{nm}} \qquad (4.6)$$

and if the noise is uncorrelated

$$= \frac{S_{oo} + S_{nn}}{S_{oi}}$$

$$= H(\omega) + (\,S_{nn}/S_{oi})$$

So that $H_2(\omega)$ will be less precise as an

approximation of $H(\omega)$ when there is noise on the output signal. This will be proportionately largest at antiresonance (i.e. when response is small although force may be large).

The ratio

$$\frac{H_1(\omega)}{H_2(\omega)} = \frac{S_{xy}}{S_{xx}} \times \frac{S_{yx}}{S_{yy}}$$

$$= \frac{S_{xy}.S^*_{xy}}{S_{xx}.S_{yy}}$$

$$= \frac{S_{xy}{}^2}{S_{xx}.S_{yy}}$$

$$= \gamma^2 \qquad (4.7)$$

where γ^2 is termed coherence.

Coherence is often taken as an indication of the quality of the measurement signals as in the absence of extraneous noise it will be unity. If the total input and output signals are uncorrelated, coherence will be zero. While aiming to achieve a coherence of unity during testing it is worthwhile considering the causes for a less than ideal state of affairs. As shown above significant noise levels on either the input or the output signal will have a direct bearing on the coherence, this is particular true when the noise levels are correlated with each other, e.g. if both are due to mains supply at 50 Hz., as the cross-spectra Smn will be non-zero.

If the response is not caused solely by the measured excitation, i.e. it is due to multiple excitations or non-linear behaviour of the structure, this is equivalent to additional "noise" on the output signal but this will be "noise" that is related to the measured input ($S_{mn} \neq 0$). Finally there will be a systematic or "bias" error due the fourier transformations being performed at discrete intervals rather than continuously, which will be more marked in regions of rapidly varying FRF i.e. at resonance and antiresonance. The magnitude of this error is proportional to the inverse of the number of averages and can ,unlike the other causes of low coherence, be reduced by accumulating a running average of the FRF estimates and coherence.

4.1.3. Testing philosophy

The study of vibration is of paramount importance in engineering where vibration reduction (and isolation) has become an integral part of machinery and structural design. A large industry exists to cater for the demands of improved instrumentation and better methods of analysis. However, state of the art assessments of vibration testing both in the USA (Remmers, Belshem (1964)) and more recently in this country (Ewins(1981)) have shown that however sophisticated the instrumentation, fundamental errors in experimentally based studies can, do and will occur.

Therefore it is appropriate to adopt a strategy when conducting vibration testing in which a two stage test procedure is followed. The first stage is exploratory and is intended to establish the essential nature of the structures dynamic properties including modal density, level and type of damping, degree of non-linearity and repeatability of data. The second stage constitutes the data acquisition process in which all the data required are measured according to the most appropriate method.

Quite what that method should be depends to a large extent upon the use to which the data will be put afterwards. These uses may include:

i. Coupling of the experimental FRF with data obtained from other sources to develop a frequency domain model of an installation.

ii. The extraction of a modal model defined in terms of natural frequency, mode shapes and damping.

iii. The measurement of physical properties (in particular damping levels) that may be used in the construction of spatial models defined in terms of mass, stiffness and damping.

This study concentrates upon the second application in which modal data are extracted from experimental FRFs. These modal parameters can be used for:

i. Correlation with data from finite element or other theoretical models.

ii. Compiling a data base for use in monitoring or diagnostic applications.

iii. Reproducing the response of the structure with a mathematical model so that different excitation conditions or structural modifications can be examined.

iv. Force determination whereby measurements of responses are combined with transfer functions of the structure to deduce the excitation forces.

The experimental study did not attempt to develop a complete modal model of the cylindrical models under investigation. However, it was found possible to identify individual natural frequencies of modes with similar shapes. (It should be noted that cylindrical shells can possess many closely spaced modes because of structural symmetry.)

4.1.4 Excitation techniques.

There are numerous choices for the type of excitation to be used during the structural testing process. The testing may be by discrete frequency methods or it may use broadband excitation. The exciting force may be applied at one site or by multi-point excitation and be driven continuously or applied at one instant as an impact.

Each method has its advantages and disadvantages and it is not intended to go into full details of their

development and use in this text but brief notes on their respective features and merits are included.

The various methods divide into the following broad categories

i. sinusoidal (stepped-sine,swept-sine)

ii. periodic (multi-sine,pseudo-random)

iii. random (periodic random,shaped random)

iv. transient (chirp,impact)

Not all of the methods listed above have been used in this investigation and only those that were used will be described.

4.1.4.1 Sinusoidal testing

Steady state harmonic testing is conceptually the simplest of all excitation techniques. If a structure behaves linearly the response will be a sine wave at the same frequency. By directly comparing the two responses (input and output) the transfer function can be computed in terms of gain and phase shift. There is no statistical manipulation necessary as the signals are deterministic and averaging is only required to eliminate random noise . This amounts to an element of filtering as the effect of noise becomes proportionally large compared with the force and response signals at resonance and anti-resonance respectively.

The filtering is performed digitally by a

multiplication and averaging process so that the output is correlated with two different forms of the input (Wellstead (1983)). An integration over one cycle removes any dc offset and higher harmonics of the fundamental signal and noise are progressively eliminated by continuing the integration over further cycles to effectively produce a narrow band-pass filter.

By incrementing the excitation through the analysis bandwidth, a complete frequency response function can be identified. This abrupt stepping between frequencies will induce a transient into the system, the response from which must have decayed before further measurement can take place. In practice this can never be achieved since the amplitude of a transient vibration decay obeys an exponential law and will never theoretically decay to zero. However providing the amplitude of any transient response created as a result of the frequency step is below the noise threshold of the instrumentation in use, it can be assumed that a steady state has been achieved.

The rate at which a vibration decays after a transient depends on the magnitude of the impulse and on the proximity and damping levels of other structural modes and it will be necessary to dwell a pause between measurements until the steady state is resumed. The length of the delay should be measured in number of cycles rather than seconds and therefore measurements at

low frequencies will take longer than those at high frequencies. However the delay will only be comparable with the integration time in the regions around resonance.

It is possible to obtain very accurate measurements using sinusoidal excitation. The main advantages being that near resonance a single mode will tend to dominate the response of the structure. Therefore, modal separation (which is the aim of the subsequent analysis) is provided mechanically. The energy that is to be input at each frequency can be predetermined thereby enhancing the signal to noise ratio and allowing large structures to be tested with smaller shakers and amplifiers than a broadband excitation method would allow. Flexibility in harmonic testing can be achieved by adjusting the frequency increments within the analysis bandwidth; larger spacings are used where there is little variation in the amplitude of the frequency response curve and finer intervals taken around resonance and anti-resonance.

4.1.4.2. Random excitation

The biggest single drawback with sinusoidal testing is the amount of time that the measurement process takes. Broadband excitation techniques are able to overcome this disadvantage and have come to prominence since digital signal processing has been developed to

use FFT techniques on a commercial scale. Random excitation is a favoured method of broadband analysis as it has complete compatability with FFT processing bearing in mind that the spectra shown in equations (4.4) - (4.7) will be power or cross spectral densities which are Fourier transforms of correlation functions rather than Fourier transforms of time series.

A wide range of properties of the incoming signals (auto power, cross power spectra, transfer function, coherence, auto/cross correlation, impulse response) can be swiftly calculated and displayed. There are some penalties to be paid for the speed of calculation of this approach due to the derivation of frequency response functions being based on statistical information and therefore being inherently less precise. The main sources of error are aliasing, leakage, and

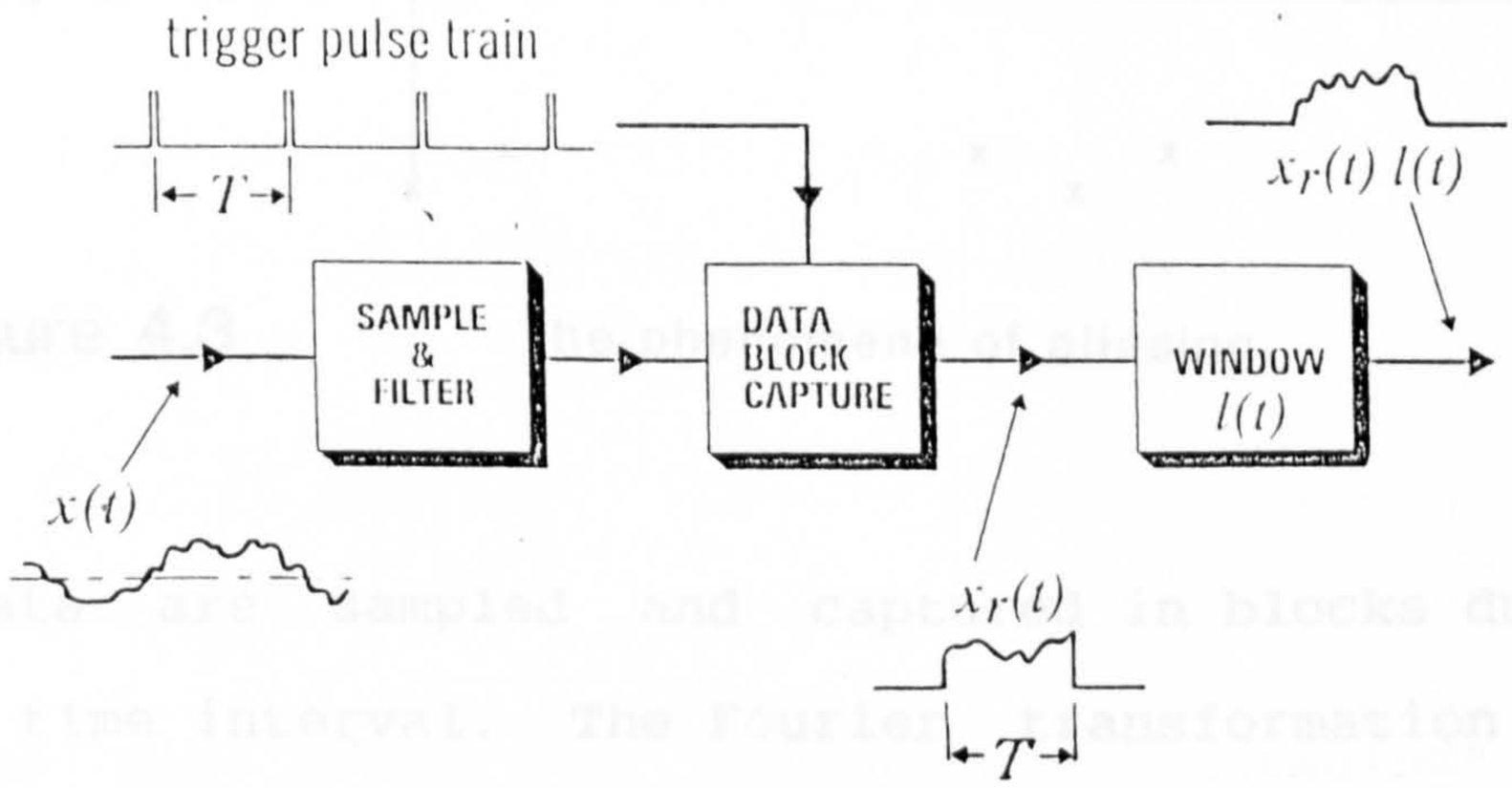

Figure 4.2 Digital measurement procedure

windowing which enter the analysis at the points indicated in Figure 4.2 and must be avoided or limited in their effect.

Aliasing, which is the misinterpretation of a high frequency signal as a lower frequency occurs when the sampling is not being carried out quickly enough. However, it is not generally a problem as most analysers have built-in low pass frequency filters set at half of the sampling frequency.

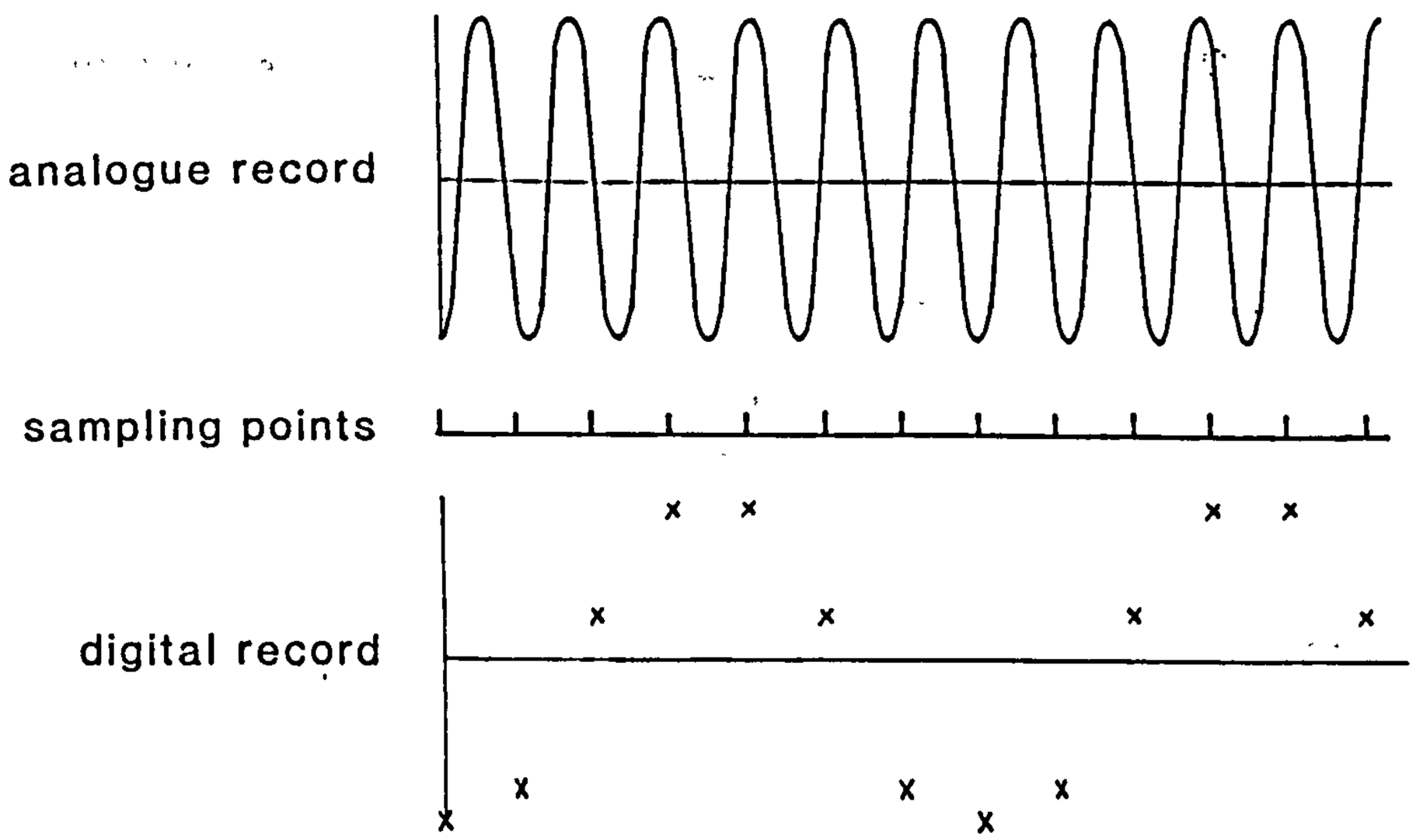

Figure 4.3 The phenomena of aliasing

Data are sampled and captured in blocks during a short time interval. The Fourier transformation which is the next stage of the measurement process will assume that data outside the block is zero and that data within the block is periodic over that time period. This

periodicity may not occur, even for a sinusoidal signal, depending on when the sampling occurs and introduces certain systematic errors, termed leakage, into the analysis. The effects of leakage may be reduced by the use of a window function which tapers the data at the beginning and end of the block so that the transition from zero outside to non-zero inside the block is smoothed.

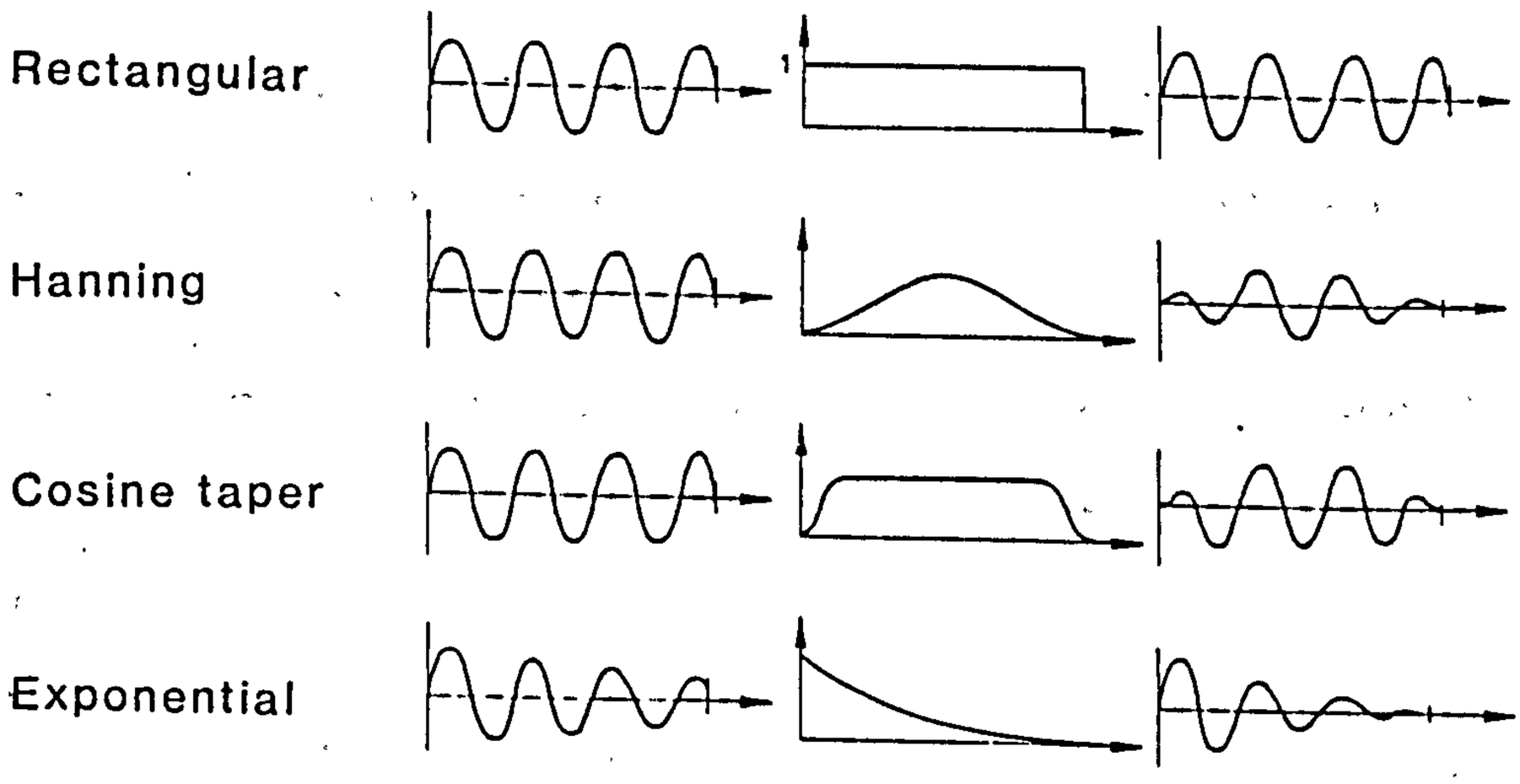

Figure 4.4 Different types of window

The net effect of all of this "massaging" of the measured data is to "smear" the resultant FRF and yet it retains much of the information contained in the true FRF.

4.1.4.3 Impulse testing

Attaching a shaker to the structure, however carefully it is done, alters the boundary conditions of the system. The alternative is to carry out an impact test using a hammer incorporating a force gauge.

A discrete Fourier series description of the force and response signal can be obtained and the frequency response function determined directly as their ratio

$$H(\omega) = O(\omega)/I(\omega) \qquad (4.1)$$

Alternatively $H_1(\omega)$ can be calculated from the ratio of the cross-spectrum between the input and output to the power spectrum of the input. Whichever approach is taken the prime advantage of this method is speed and therefore only a small number of averages is normally taken.

There are several problems with the transient excitation technique. Firstly there is the practical difficulty in obtaining a repeatable impulsive input which is applied at the same position and orientation every time. The input must be monitored for overloads and multiple hits when ,for example, a lightly damped structure recoils against the impactor. The structure may be subjected to high local peak stresses which will induce material non-linearities and the high crest-factor in the data, i.e. the difference between

peak and rms values places a heavy burden on the entire measurement system.

All of the above methods of excitation were used in this investigation, and their benefits and drawbacks have been discussed. Using the testing strategy that was discussed in Section 4.1.3, preliminary measurements were taken over a wide frequency range using random or transient excitation and this was followed by more detailed sinusoidal testing concentrated at frequencies near resonance.

4.2 Instrumentation

The prime requirement of a measuring system is that it records responses without altering the characteristics of the structure that is under investigation. This ideal state of affairs could be achieved using a non-contacting transducer which converts the required quantity (force, motion etc.) into an electrical signal which is measured and then stored.

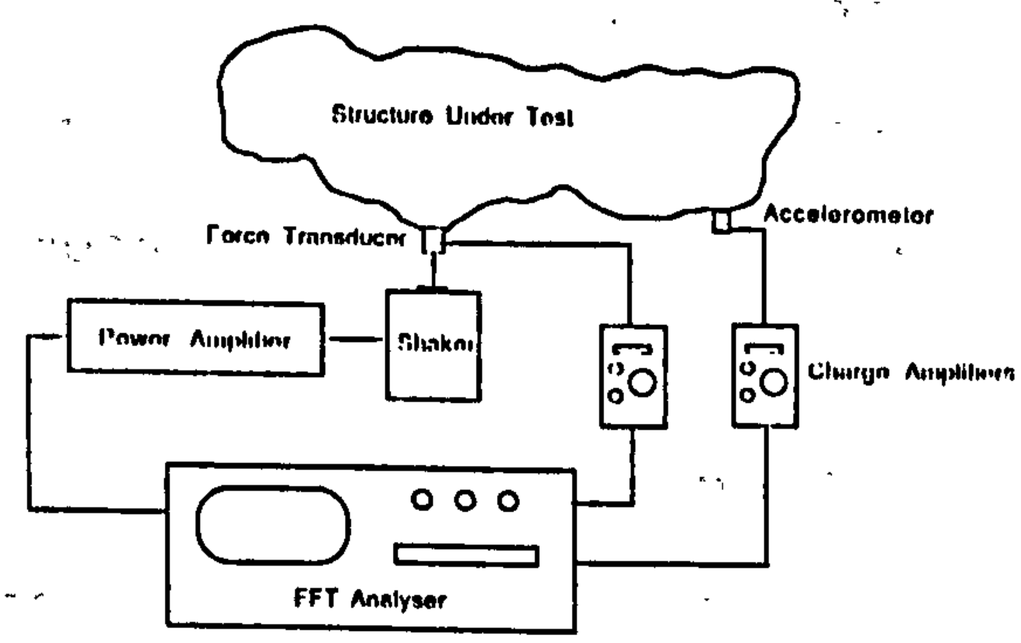

Figure 4.5 Experimental set-up

Non-contacting transducers measuring changes in displacement due to changes in capacitance or inductance across a gap between the measuring instrument and the vibrating structure have been commercially available for many years (Harris, Crede (1976)). One terminal of the instrument acts as the datum and its position in space must be known. Effectively this means that it is fixed in space and in certain circumstances, e.g. if the transducers are to be placed within a small flexible structure, there may be installation difficulties. Further problems may arise because the instrument will record rigid body as well as distortion modes. The main disadvantage however is their attenuation at the high frequency end of the spectrum where amplitude of vibrations become very small and indistinguishable from ambient electrical noise levels.

Reflected wave transducer systems using microwave or optical interferometry are based on ideas conceived around the same time but the instruments that have been produced have not been widely used. The fundamental advantages of monitoring vibrating surfaces which are undisturbed by the measuring device together with the capability of examining large regions in rapid succession and over a wide frequency bandwidth make these techniques potentially very powerful. The advent of improved laser technology has introduced the possibility of a new approach. There are now

commerically available compact laser vibrometers offering interferometric line of sight, 0-1 MHz responsivity and sub-nanometre sensitivity.

4.2.1 Transducers

The majority of vibration tests which are performed nowadays employ either strain gauges or accelerometers. Both types of transducer will produce results of comparable accuracy. Strain gauges exhibit linear characteristics over a wide frequency range, are lightweight and are relatively easily fitted. However they are used less often than accelerometers because they are not so robust and because it is not always convenient to develop a model in terms of strain rather than displacement.

Accelerometers contain a piezoelectric material usually in the form of an artifically polarised ferroelectric ceramic element which generates an electrical charge when stressed. The accelerometer is a seismic (spring-mass) instrument where the spring is replaced by the piezoeletric element and when the assembly vibrates the mass exerts a varying force on the element which is directly proportional to the vibratory acceleration. For frequencies well below the resonance frequency of the assembly the acceleration of the mass will be extremely close to the acceleration of the base and the output signal level will be proportional to the

acceleration to which the accelerometer is subjected (Broch (1980)). The design of the accelerometer should always ensure that the stiffness of the ceramic element gives a high resonance frequency of the assembly as this will extend the frequency range over which the accelerometer can be used. Frequency response, sensitivity, mass and dynamic range are the principal factors that should be considered when assessing an accelerometers suitability.

The sensitivity of the "general-purpose" accelerometers used in this investigation was between 1 to 10 pC per ms-2, which was not critical as modern pre-amplifiers are designed to accept low level signals. A higher output level, up to 10000 pC per ms^{-2}, could have been obtained but only by using larger piezoelectric assemblies enclosed in heavier units which would have been unacceptable for the thin-walled shell structures tested. Inertia forces and moments will be caused by the additional mass of any accelerometer and this can only be minimised by using the smallest accelerometers possible. Accelerometers weighing only 0.4 gram were used at one stage of this investigation; they had the added attraction of built-in hybrid amplifiers with a low output impedance. The unit cost of each of these accelerometers is considerably more than for comparable accelerometers without the built-in electronics and is the main reason why they were not

used elsewhere.

In all other aspects the "general-purpose" type of accelerometer were satisfactory, the dynamic range started from 0.1 ms-2 and was determined by electrical noise from connecting cables and amplifier circuitry rather than the accelerometer directly. The upper limit was determined by the accelerometers structural strength and they remained linear to above 50000 ms-2 due to their rigid construction.

Selecting the correct type of accelerometer is less liable to present a problem than choosing the right locations for the accelerometers within the model and then securing them in position. The locations were determined by the modes of vibration of the cylindrical structures that were being tested (see Section 4.3.2). Circumferential distortions of the shell were measured using a complete ring of accelerometers at one cross-section.

Various methods of mounting the accelerometers were employed which included; clamping magnets, adhesives and threaded studs. The frequency limits for each type of attachment can be obtained from the manufacturers literature (Broch (1980)) but for the methods mentioned there is no significant response due to the fixing below 2 kHz. The reliability of the fixing was therefore the prime concern and because of the need to attach the

accelerometers to a curved surface it was found necessary to develop a specialised fitting. This consisted of a shaped washer adhered to the cylinder using cyanoacetate adhesive. A central stud was used to attach the accelerometers. Care was necessary when fitting the transducers to avoid the introduction of base strain.

4.2.2 Cable connections

Flexible coaxial cables were used for the connection between accelerometer and pre-amplifier. The cables were screened to reduce the effect of electrostatic interference, they were anti-microphonic and treated to reduce the tribo-electric effect caused by dynamic bending. Extra precautions such as preventing the cable from slapping against the structure by taping it down as close to the transducer as possible further reduced this effect.

The connecting cables were handled with care as they were very flexible and fatigue cracks were experienced particularly at the connections, due to excessive handling. New cables were made up and used whenever possible as it was noticed that signals did not completely break down due to partial or even total severance of the inner core if the ends butted together. This partial breakdown was most problematical as it inevitably lead to progressive signal degradation which

could not always be detected in its early stages.

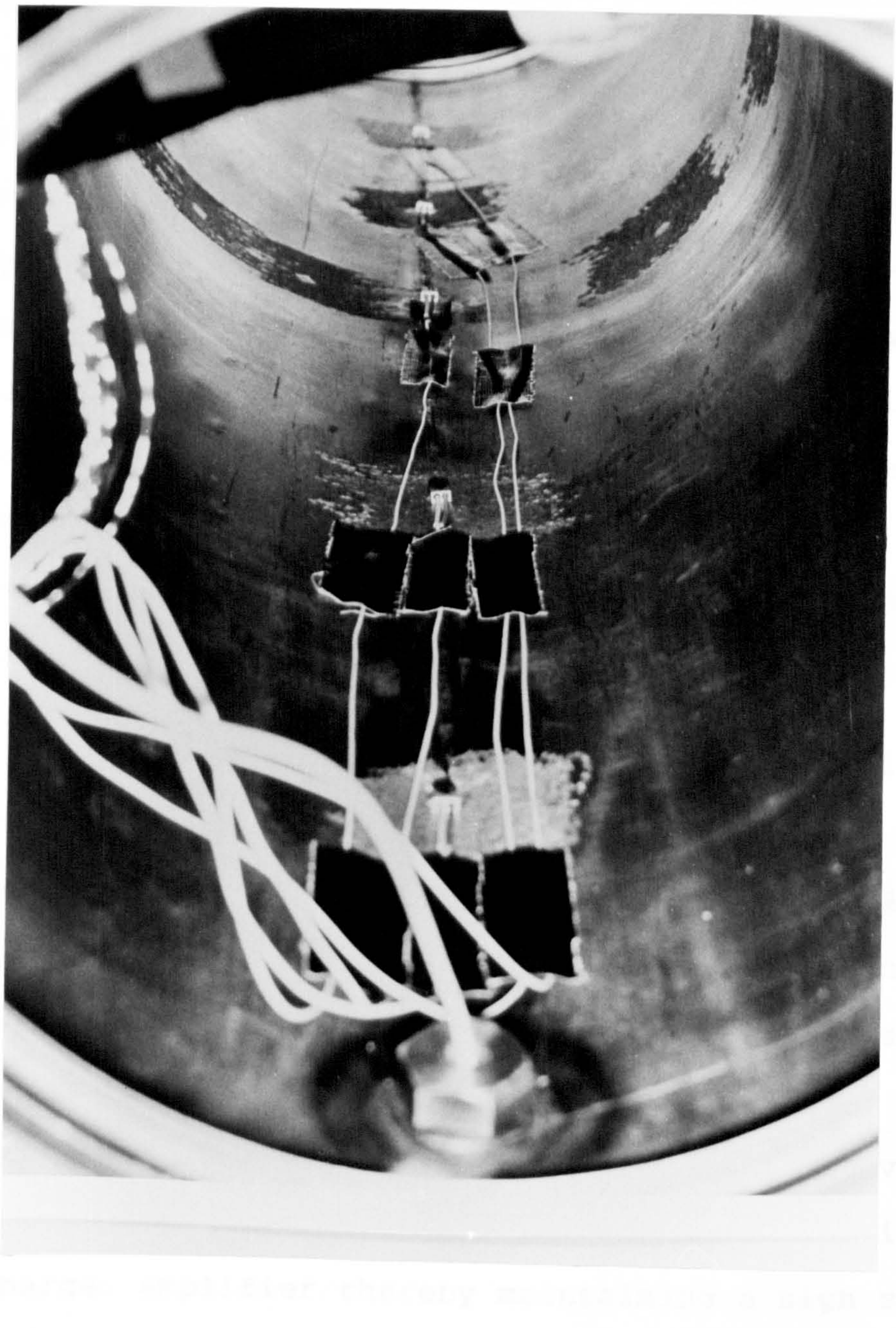

Figure 4.6

Accelerometer cables taped to prevent slapping

4.2.3 Signal Processing

A pre-amplifier is included in the measuring system to amplify the relatively weak electrical charge generated by the accelerometer and to reduce the impedance to a level suitable for connection to the measuring and analyzing instrumentation. The type of pre-amplifier used was a charge amplifier which works on the change in the input signal. One of its main advantages is that a relatively high capacitance feedback across a condenser effectively reduces the capacitance of the connecting cables so that long lengths may be used without altering the sensitivity of the measuring system.

In addition to the low and high frequency filters (3dB at 0.3Hz and 30kHz respectively) the most useful features of the instruments were overload and 20dB from overload indicator lights. The maximum output signal is 10V (10mA) peak with less than 1% distortion, so the -20dB indicator, signals a level greater than 1V. It is normally good practice to ensure that this level is maintained throughout testing by adjusting the gain on the charge amplifier thereby maintaining a high signal to noise ratio.

4.2.4 Analyser

The final link in the measurement chain is the data logging/analysis system. This will monitor the conditioned signals and may perform selected analysis functions or store data for later analysis. Two types of analyser were used in this investigation, a frequency response analyser (FRA) was used with sinusoidal excitation and a spectrum analyser for broadband measurement. Both machines were digital devices. The FRA measured the signals from force and response transducers and correlated them with the generated sinewave so that an accurate measurement of impedance was obtained at each discrete frequency. The spectrum analyser, on the other hand, sought to measure all the frequency components in the complex time-varying signal. The machine used operated with 501 spectral lines, the equivalent of that number of FRAs, each tuned to a separate frequency and working simultaneously. The spectrum analyser was then capable of computing a wide range of properties based on the Discrete Fourier Transform.

The dual channels of the spectrum analyser and the 12 channels of the FRA had a dynamic range of between 10 microvolts to 300 volts which could be fixed at a set level or allowed to 'auto-range'. For a good signal to noise ratio the smallest possible input range that did

not cause overloading was used. Measuring a small signal with an unnecessarily large range can seriously degrade portions of the signal and reduce it to the same proportions as analogue noise or digital noise introduced by the micro-processors. The use of the 'auto-ranging' facility was not always the optimum solution as it was assessed that this facility would attenuate data in broadband random testing but not stepped-sine testing due to the in-built conservative estimation of the required range and the inability to react instantaneously at each frequency level being tested.

4.2.5 Force Input.

A controlled experiment differs from the majority of situations in which a structure is caused to vibrate. Usually the vibrations within a system are self-induced due to sliding or rotating components of machinery or if the system is very lightly damped it may be excited by acoustical noise. In modal testing it is necessary for all of the forcing input or inputs to be directed through force gauge transducers at the point or points of excitation, so that the force measured is the only external force applied to the system.

Force transducers, like accelerometers, use a piezoelectric element which, when compressed produce an electrical output proportional to the force transmitted

through it.

Force excitation can be applied in a number of ways. Shock testing using non-contacting underwater explosions was one possibility but the incident pressure pulse would have to have been measured using an array of pressure transducers. The total forcing input would have been difficult to quantify and therefore accelerance, mobility and receptance would not have been accurately determined. It is more usual for the force to be applied via an instrumented "hammer" (for impact loading) or through some form of "shaker" attached to the structure. The practical difficulties, such as repeatability, of impact testing have already been dealt with, therefore this section will concentrate on the use of mechanical shakers.

The shakers used in this work were of the electromagnetic type in which the input signal is converted to an alternating magnetic field in which is placed a moving coil assembly. The size of this assembly determines the magnitude of the force that can be applied to the structure. Shakers of this type are manufactured so that they move freely in one direction only; the direction in which the force is applied. However there is no such restraint on the behaviour of the structure at the point where it is attached to the shaker. If the attachment were made rigid it could have

generated resisting forces and moments in either of the other two transverse directions or in any of the three rotational directions. It was therefore necessary to try to eliminate any but the intended axial driving force by the use of a flexible pushrod which was stiff in that direction but relatively flexible in the other five.

Generally when testing in air a short, (typically 2-5 cm. of 1mm. diameter wire), push-rod was used. This was unsatisfactory for testing underwater structures as it would be very difficult to waterproof an external shaker and there will be non-linear interactive effects if the structure is very close to the free surface. Consequently a longer push-rod, sometimes with a non-flexible extension rod, was used; the penalty for this is that the resonance frequency (axial or flexural) of the push-rod may come within the range of interest. Separate testing of the pushrod was therefore necessary to eliminate these modes from the mobility measurements of the structure. These extraneous modes may not always influence the test results if the force gauge is sited correctly. However very little energy will be transmitted through the push-rod when it is approaching resonance and excessive transverse deflections may induce forces in any of the 5 degrees of freedom that are not being measured at the point of attachment.

The use of long pushrods, up to 2 metres long, has been accomplished quite successfully during the course of this research. It was necessary to include a short

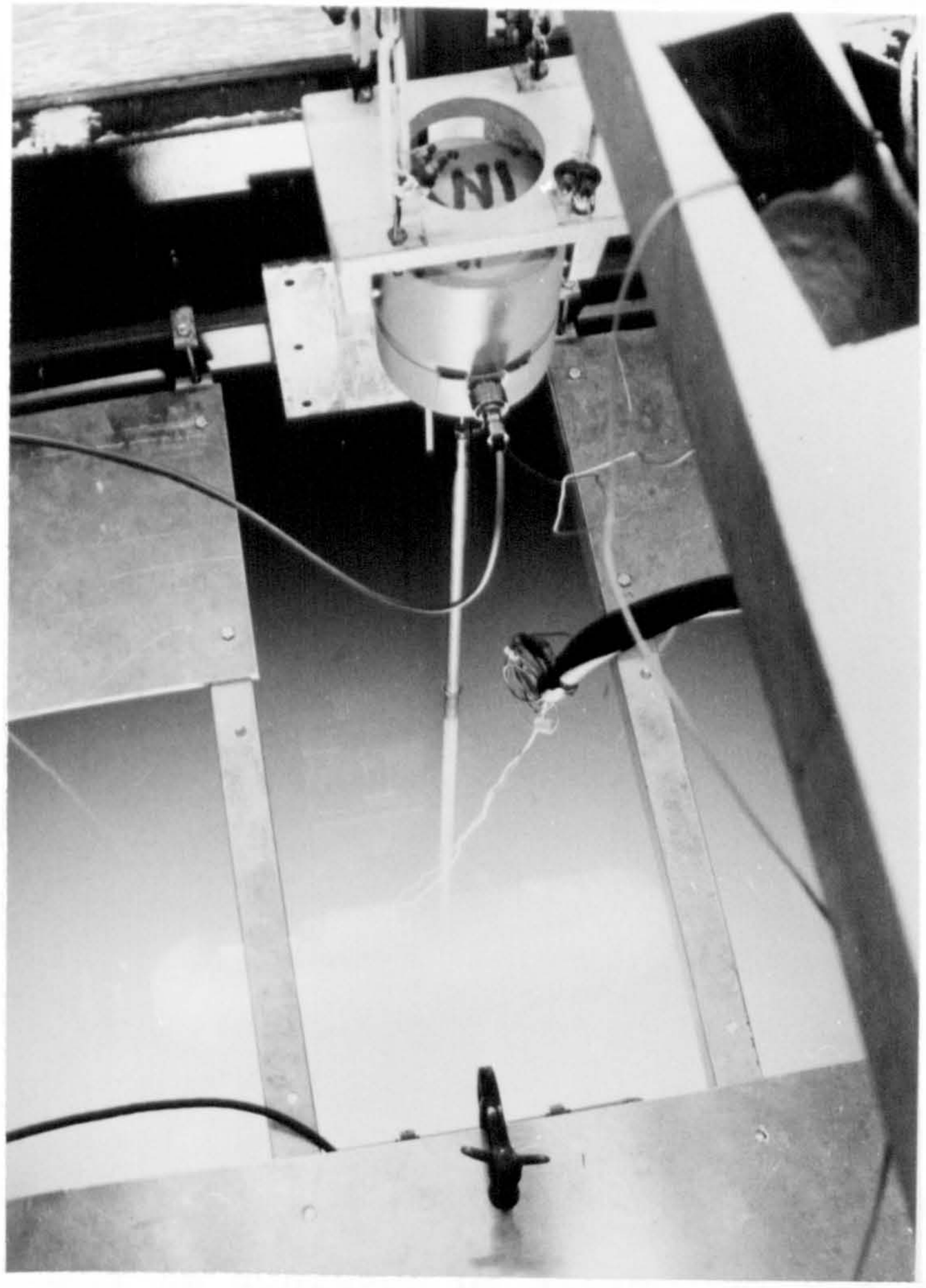

Figure 4.7

Push-rod extension for external shaker

flexible piece next to the structure but the remainder of the pushrod was made from relatively large diameter, hollow tube for strength and lightness. Obviously with a pushrod of this length there were practical difficulties in attaching it to the structure and ensuring that the flexible piece did not become damaged during the setting up of the trial. Besides these problems, posed by the cumbersome nature of a very long pushrod, there was a further limitation that had to be resolved. The limited draught of the water tanks in which the cylinders were submerged precluded the cylinders from being tested in any orientation other than the horizontal. The shaker was therefore attached near the centre of the cylinder and primarily excited the "cylindrical" modes with much less energy being transmitted to the ends where the displacements were orthogonal to the direction of the exciting force.

For further investigation of the behaviour of the ends it became necessary to devise a method of providing a horizontal forcing input to the submerged structure. This could only be achieved by siting the shaker within the cylinder. The problem which then had to be overcome was to ensure that the reaction forces from the shaker, which were equal and opposite to those applied to the pushrod, were not transmitted to the structure. This could have been achieved if the shaker were supported on soft springs as the suspension resonance would have been

well below the driving frequency. Unfortunately any uneven handling of the structure would have placed considerable strain on the flexible connection at the stinger and it was deemed that this was not a practical solution. Instead a "bridge" was constructed that attached to the cylinder near its outer edges and on which the shaker was located. It was important that resonances of this support structure should not affect the measured data therefore the bridge was made as stiff

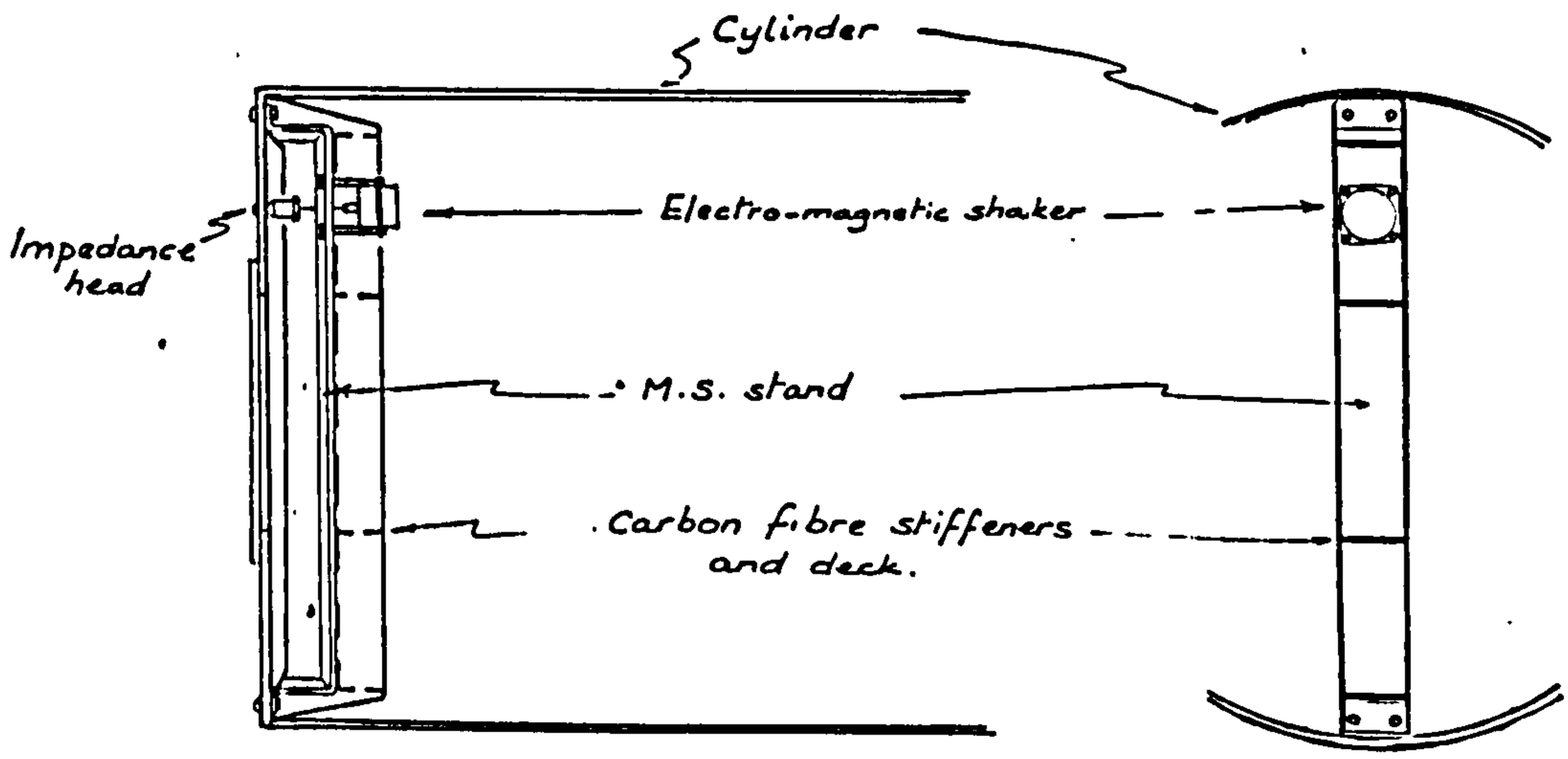

Figure 4.8 Support structure for internal shaker

as possible so that its resonance frequencies were above the frequency range of interest. This was accomplished by stiffening the side plates and the deck of the bridge with laminated sheets of carbon fibre. The stiffened support structure was no barrier to the reaction forces and the isolation of the shaker from the cylinder was

never achieved. This method of mounting the shaker was only successful because the bridge was attached at positions where the cylinder was very stiff and where there was minimal motion even at resonance.

4.3.1 Physical model

This work is intended to have practical significance and therefore the models that were examined were designed as scale models of prototype submarine structures. Conversely the geometric intricacies and details of real structures make analysis of their overall dynamic behaviour extremely difficult. Consequently a thin-walled cylinder was selected for testing as this is a simple geometrical shape which could, nevertheless, be considered as representative of a class of typical submarine structures.

In the course of this investigation four physical models were tested, each possessing different characteristics. They were also tested in a number of different ways. All the models had radius/thickness aspect ratios greater than 18 and can thus be considered as thin-walled shells.

The tests which were performed on the first model (Randall, Squire (1984)) highlighted the effect of non-uniform wall thickness and lack of circularity on the frequency response characteristics of the model. If

Table 4.1 Physical model dimensions

Length	External diameter	Wall Thickness	Remarks
1.145	c.0.1335	c.0.0036	Unstiffened,open ends. Non-uniform circularity +0.5% Non-uniform wall thickness +7%.
1.284	0.357	0.003	Unstiffened,flat ends. Non-uniform circularity +0.4%
0.892	0.242	0.0025	Unstiffened,hemi-spherical ends.
0.397	0.305	0.0014	14 evenly spaced ring stiffeners. Flat ends.

cf. Upholder (Type 2400) Class Submarine

Overall dimensions : Length 70.26(47.5 pressure hull)

Width 7.60

Depth 5.50

(Couhat (1984),Wrobel (1985))

geometrical irregularities had to be modelled it would complicate the analysis procedure considerably. Therefore an early decision was taken to expend effort on producing a physical model manufactured to the most stringent tolerances, aiming for less than 1% variation in wall thickness and no more than 0.2 mm. linear variation in length and external diameter for models 2 and 3. Nevertheless the finished product would never be perfect, particularly as the cylinders were manufactured from flat plate, which was rolled and then seam welded.

Table 4.2 - Inspection Details

Model#1 Internal Diameter (mm.)

Axial co-ordinate	0.02	1.45
Radial co-ordinate		
0	126.5	126.5
45	125.8	125.6
90	126.6	126.7
135	127.0	125.9

Wall Thickness (mm.)

Radial co-ordinate	
0	3.49	3.53
45	3.57	3.58
90	3.78	3.58
135	3.84	3.66
180	3.73	3.71
225	3.63	3.95
270	3.51	3.79
315	3.44	3.67

Model#2 - External Diameter (mm.)

Axial co-ord.	0.04	0.34	0.64	0.94	1.24
Radial co-ord.					
-45		357.1	356.8	356.7	
0		357.5	358.2	357.6	357.9
45	356.8			357.4	356.8
90			355.1	355.1	

Model#3 - Wall Thickness (mm.)

Axial co-ord.	0.05	0.30	0.45	0.60	0.85
Radial co-ord.					
-120	2.37	2.50		2.50	2.43
0	2.40	2.50	2.52	2.45	2.49
120	2.41	2.45		2.45	2.59

Where deviations from circularity were significant, the deformed (oval) cross-section produces closely spaced modes of vibration operating at resonance frequencies determined by the major and minor axes of the elliptical cross-section but which are typically separated by less than 5Hz.

4.3.2 Modes of Cylindrical Shell

Consider a cylindrical shell of thickness h, radius a, and length L. Let the cylinder be referred to an x, θ, z coordinate system where z is taken in the direction of a generator, θ measures the angle in the circumferential direction and the x axis is directed outward along the normal to the shell middle surface. The displacements of the shell middle surface in these three directions are u, v and w respectively.

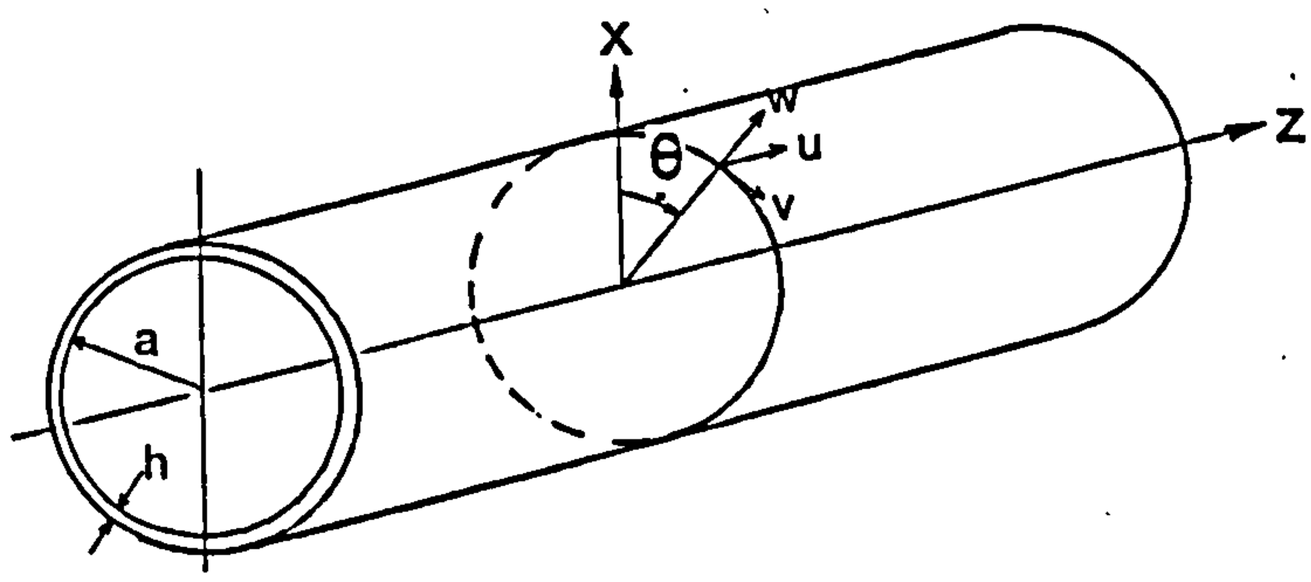

Figure 4.9

Geometry of cylindrical shell showing direction of displacement components

The basic deformations involved in the vibration of the cylinder are bending and stretching of the cylinder walls. Associated with these actions the displacements u, v and w will be such that there will be nodal lines on the cylinder running longitudinally and

circumferentially. The number and location of these lines will depend on the particular mode of vibration.

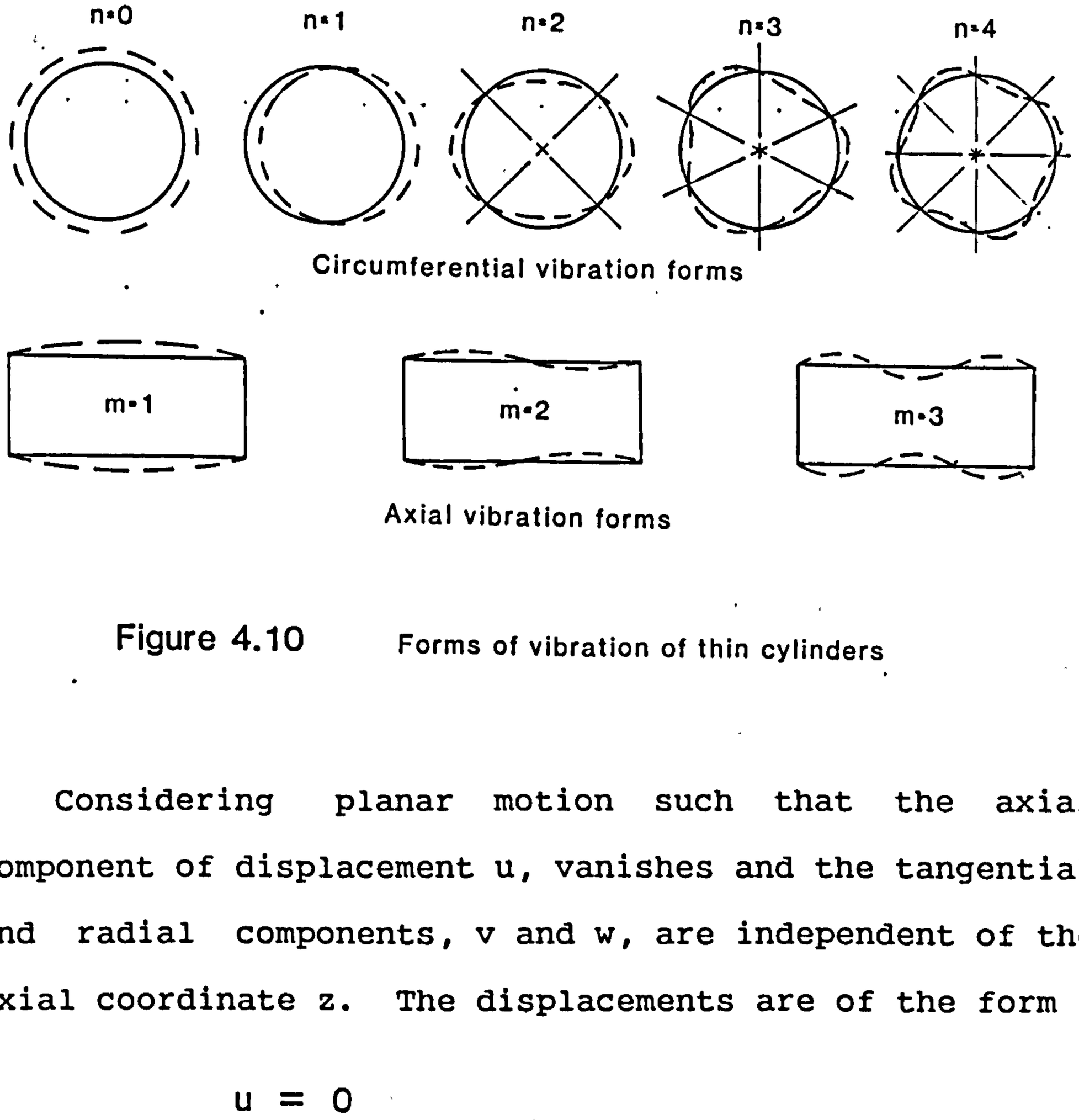

Figure 4.10 Forms of vibration of thin cylinders

Considering planar motion such that the axial component of displacement u, vanishes and the tangential and radial components, v and w, are independent of the axial coordinate z. The displacements are of the form

$$u = 0$$
$$v = V_n.\sin n\theta.e^{-i\omega t} \qquad (4.8)$$
$$w = W_n.\cos n\theta.e^{-i\omega t}$$

For n=0 all points on the cross-section move radially outwards and inwards together so that the cylinder walls are undergoing stretching only. Conversely when n=1 the cross-section translates but

does not deform which corresponds to pure bending. For integers of n>2 the displacements will be caused by a combination of bending and stretching and the circumferential vibration modes consist of periodic movement of standing waves distributed around the circumference. The simplest case (n=2) will have four positons at which radial motion is zero. These positions are called circumferential nodes but they are not positions of absolute rest due to tangential movement. Theoretically, this type of vibration is possible for any value of n greater than 2.

We now consider the situation in which the axial dependence of the response is accounted for. It can be shown that the motion of the cylindrical shell consists of standing waves in both the circumferential and axial directions. The number of half-waves that occur in the cylinder length are denoted by the letter m and will vary according to the complexity of the vibration and the type of restraint at the ends of the cylinder.

Since any number of circumferential waves may combine with any number of axial waves to form a nodal pattern the wide range of possibilities can be appreciated. Flugge (1973) obtained a frequency equation for a cylinder with freely supported ends, the roots of which defined three natural frequencies for any given nodal pattern. The modes associated with each of

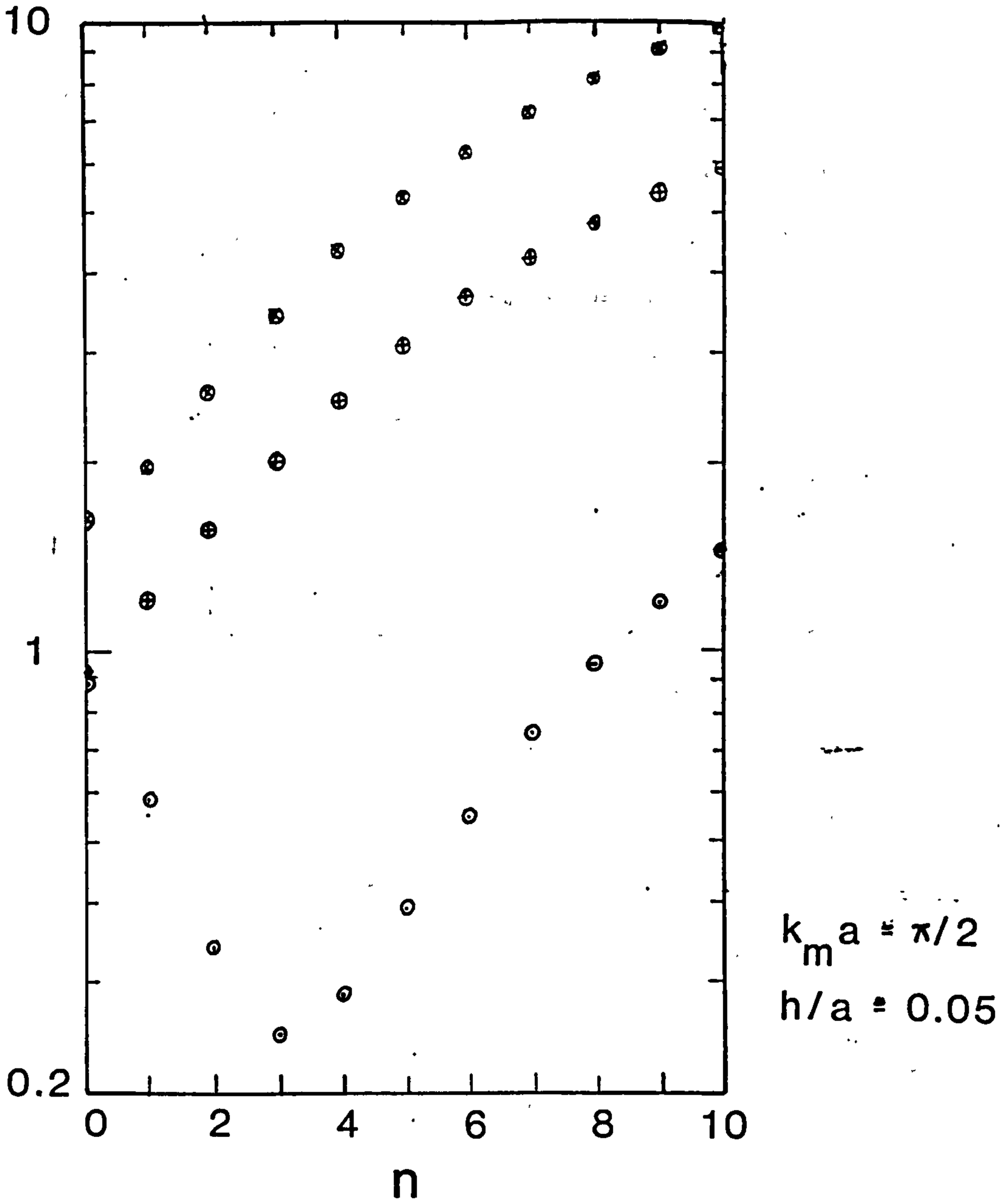

Figure 4.11

Resonance frequencies of a finite cylindrical shell with simply supported ends

these frequencies correspond to motion which is primarily radial, axial or circumferential. Fortunately, only the lowest natural frequency associated with motion that is primarily radial is

normally of interest. The hierarchy of modes in terms of frequency bears little relation to the complexity of the nodal pattern but depends on the geometry of the cylinder and the proportion of strain energy contributed by bending and stretching. A knowledge of the nodal patterns of the modes to be investigated is essential if tranducers recording the motion are to be sited effectively.

4.3.3 Fluid environment

An essential feature of this investigation is that the modal testing was performed with the structure either freely supported in air or submerged in water. If the surrounding medium is ignored in a theoretical formulation, it is equivalent to assuming that the system is vibrating in-vacuo. If the responses of the system are then measured in air the discrepancies will be negligible due to the low density of air. However when the structure is submerged in water it is not possible to ignore the surrounding medium and a suitable body of water has to be located in which to perform the tests. Even then it is not sufficient merely to immerse the structure without being aware of the implications of the water tanks' finite dimensions which will determine the proximity of rigid and free surface boundaries. The radiated pressure field from the vibrating structure will be reflected positively from solid boundaries and as a wave of rarefaction from the surface and there is

the possibility of standing waves being established. Only if the distances involved are sufficiently large will the reflected pressures decay to a level which is insignificant compared with the radiated pressure field.

It was fortunate that the towing-tank facilities at ARE Haslar and RNEC Manadon were available for this investigation. Nevertheless some of the experiments were performed in tanks where side and end clearances were in the order of one or two diameters of the model so that the boundaries were definitely in the near-field environment.

4.3.4 Tethering arrangements.

Another significant effect of submerging the test cylinders was that they were all positively buoyant, the upthrust varying from 20 to 900 N. Tethering arrangements had to be devised to hold the models in position whilst not affecting the dynamic behaviour of the structure. The mooring lines were attached at the ends of the cylinders. Under this arrangement bending stresses were induced because of the buoyancy forces. These stresses were superimposed on the compressive effects caused by the action of hydrostatic pressure and defined a set of initial conditions about which the structure oscillated. In addition the cylinders could no longer be considered as freely supported as the freedoms of pitch and heave were partially restrained.

Figure 4.12a

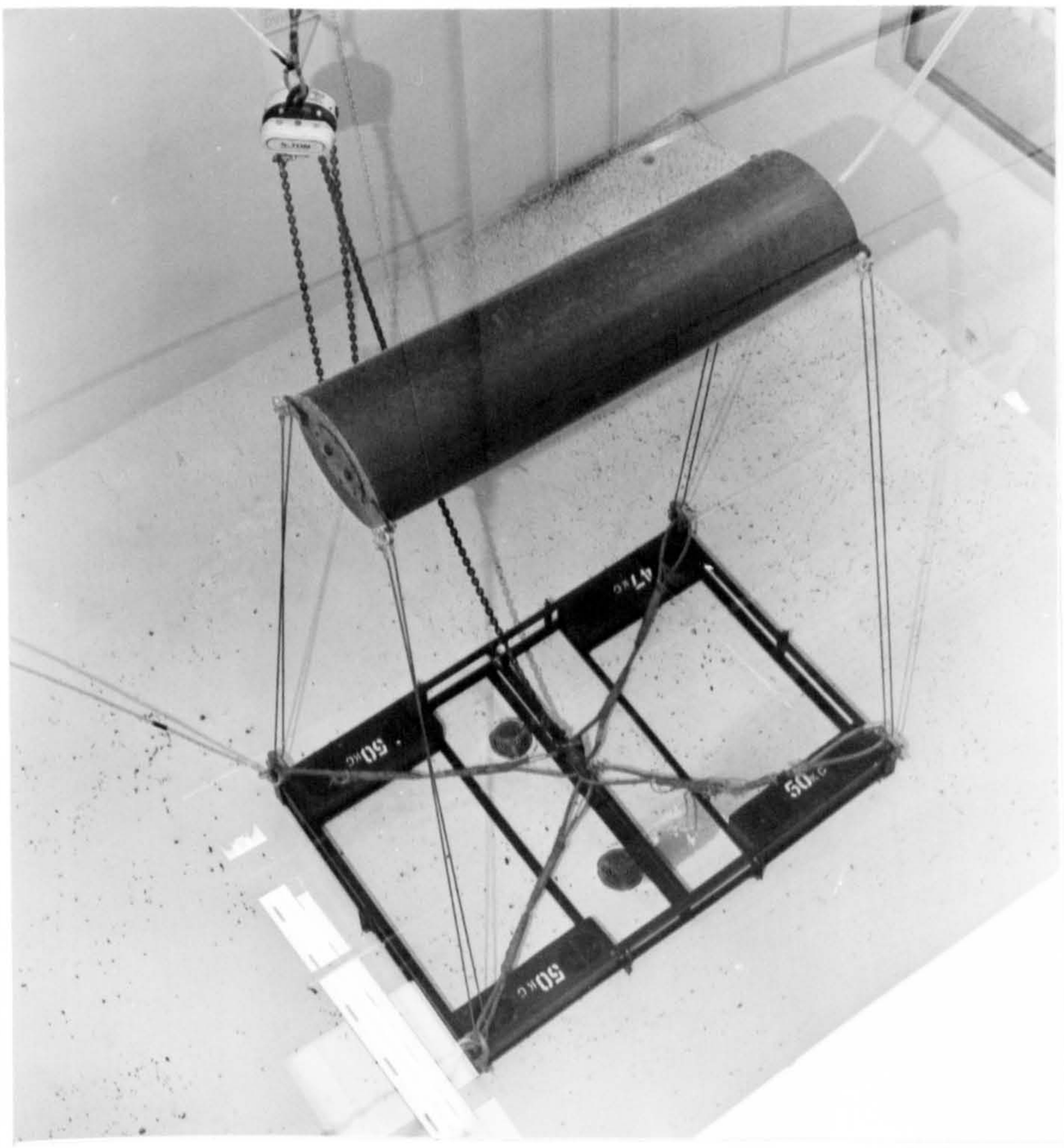

Figure 4.12b

Means of tethering model No.2 (a) shallow (b) deep

4.4. Modal Analysis

Once all the data had been acquired the next step was to extract the modal parameters using one of the many curve-fitting routines that are available. The various methods have been reviewed by Ewins (1984) and Rades (1985) and fall into two main categories. In one group the analysis concentrates on individual modes as they occur witin the frequency range of interest. If the required accuracy warrants it, the influence of other modes on the single degree of freedom model can be included. The alternative is to curve-fit a multi-degree of freedom model to the measured data, which is spread throughout the analysis bandwidth. This latter approach was not really suitable for this investigation, as only a limited number of the modes would be admitted into the subsequent analysis to calculate the hydrodynamic properties of the structure.

The equations of motion for an N degree of freedom model exhibiting hysteretic damping may be expressed in the form

$$[\,m\,]\{\ddot{u}\} + i\,[\,h\,]\{\dot{u}\} + [\,k\,]\{u\} = \{P\} \qquad (4.9)$$

where [m] = N x N mass matrix

[h] = N x N hysteretic damping matrix

[k] = N x N stiffness matrix

{u} = N x 1 vector of time dependent displacements at each degree of freedom.

{P} = N x 1 vector of applied time dependent forces at each degree of freedom.

It may be shown (Ewins (1979)) that the receptance between two degrees of freedom j and k can be computed from:

$$\alpha_{jk}(\omega) = \frac{\text{displacement response at j}}{\text{force excitation at k}}$$

$$= \frac{u_j}{f_k} = \sum_{r-1}^{N} \frac{{}_rA_{jk}}{\omega_r^2 - \omega^2 + i\eta_r\omega_r^2} \qquad (4.10)$$

where ω_r = undamped resonance frequency of the rth mode (rad/sec)

ω = harmonic excitation frequency (rad/sec)

η_r = loss factor of rth mode

${}_rA_{jk}$ = modal constant between points j and k of rth mode

The modal constant in equation (4.10) is defined as

$${}_rA_{jk} = {}_r\Phi_j \, {}_r\Phi_k \qquad (4.11)$$

where Φ are elements of the mass normalised modal matrix, defined by

$$[\Phi]^T[m][\Phi] = [I] \qquad (4.12)$$

where $[\Phi]$ are the mode shapes in an N x N matrix written column by column

[I] is an identity matrix

As the excitation frequency (ω) approaches the natural frequency of the rth mode (ω_r), the influence of

the other N-1 modes decreases. So that, particularly if the modes are well-spaced, the effect of the remaining modes can be expressed as a constant residual term.

$$(\underline{a}_{jk})_r = \frac{{}_rA_{jk}}{\omega_r^2 - \omega^2 + i\eta_r\omega_r^2} + \text{residual term} \qquad (4.13)$$

If the real and imaginary components of receptance given by equation (4.13) are plotted against frequency in the vicinity of the resonance frequency, ω_r, they will describe a circular locus.

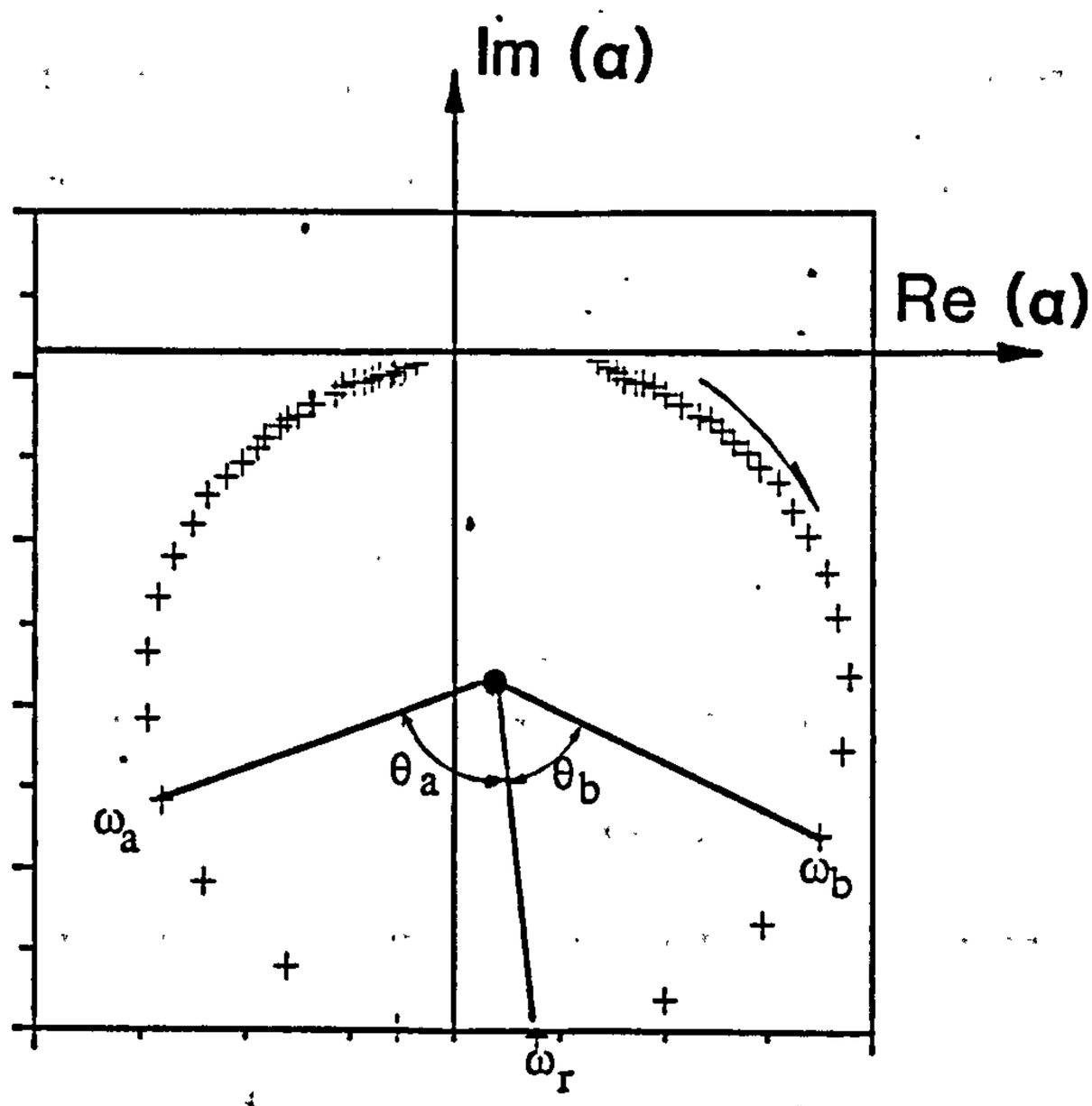

Figure 4.13

Argand diagram of receptance

The modal parameters can be extracted from the information given in this plot in the following sequence. The natural frequency is computed by determining the maximum rate of change of arc length. Then the loss factor can be determined from

$$\eta_r = (\omega_a^2 - \omega_b^2)/(\omega_r^2(\tan(\theta_a/2)+\tan(\theta_b/2)) \qquad (4.14)$$

Finally the modal constant can be calculated from the diameter of the circle

$$_rA_{jk} = \omega_r^2.\eta_r.\text{diameter of circle} \qquad (4.15)$$

Each step of this analysis is dependant on the previous stage with the modal constant being calculated after the loss factor which is based on the theoretical concept of hysteretic damping.

4.4.1 Dobson Technique

An alternative approach referred to as dynamic stiffness uses the inverse of receptance. In this case and neglecting the residual effects of other modes

$$(1/\alpha_{jk})_r = \frac{f_k}{u_j} = \frac{\omega_r^2 - \omega^2 + i\eta_r\omega_r^2}{_rA_{jk}} \qquad (4.16)$$

Plotting real and imaginary components of equation (4.16) against ω^2 will yield straight lines. The intercept of the real part with the ω^2 axis will give

the resonance frequency ω_r and the modal constant can be found directly from the slope

$$ {}_rA_{jk} = -1/\text{slope} \qquad (4.17) $$

The advantage of finding the modal constant in this way is that the estimate is independent of any estimates of loss factor. Loss factor is found separately; from the offset of the imaginary part from the ω^2 axis using the estimates of modal constant and resonance frequency alreay obtained.

The drawback with the method so far described is that modal constants will only be real for proportionally damped systems and it was assumed that the effects of residual modes could be assessed. The method used here (Dobson (1987)) retains many of the advantages of the inverse method but also provides a direct measurement of complex residuals.

This is achieved by selecting an analysis bandwidth of frequencies near resonance, so that

$$ (\alpha(\Omega)_{jk})_r = \frac{{}_r(A + iB)_{jk}}{\omega_r^2 - \Omega^2 + i\eta_r\omega_r^2} + \text{residual term} \qquad (4.18) $$

Residual effects are assumed not to vary over the analysis bandwidth and are eliminated by subtracting eqn(4.13) from eqn(4.18). The difference so formed is then inverted and by considering different frequencies

within the analysis bandwidth a family of curves is produced.

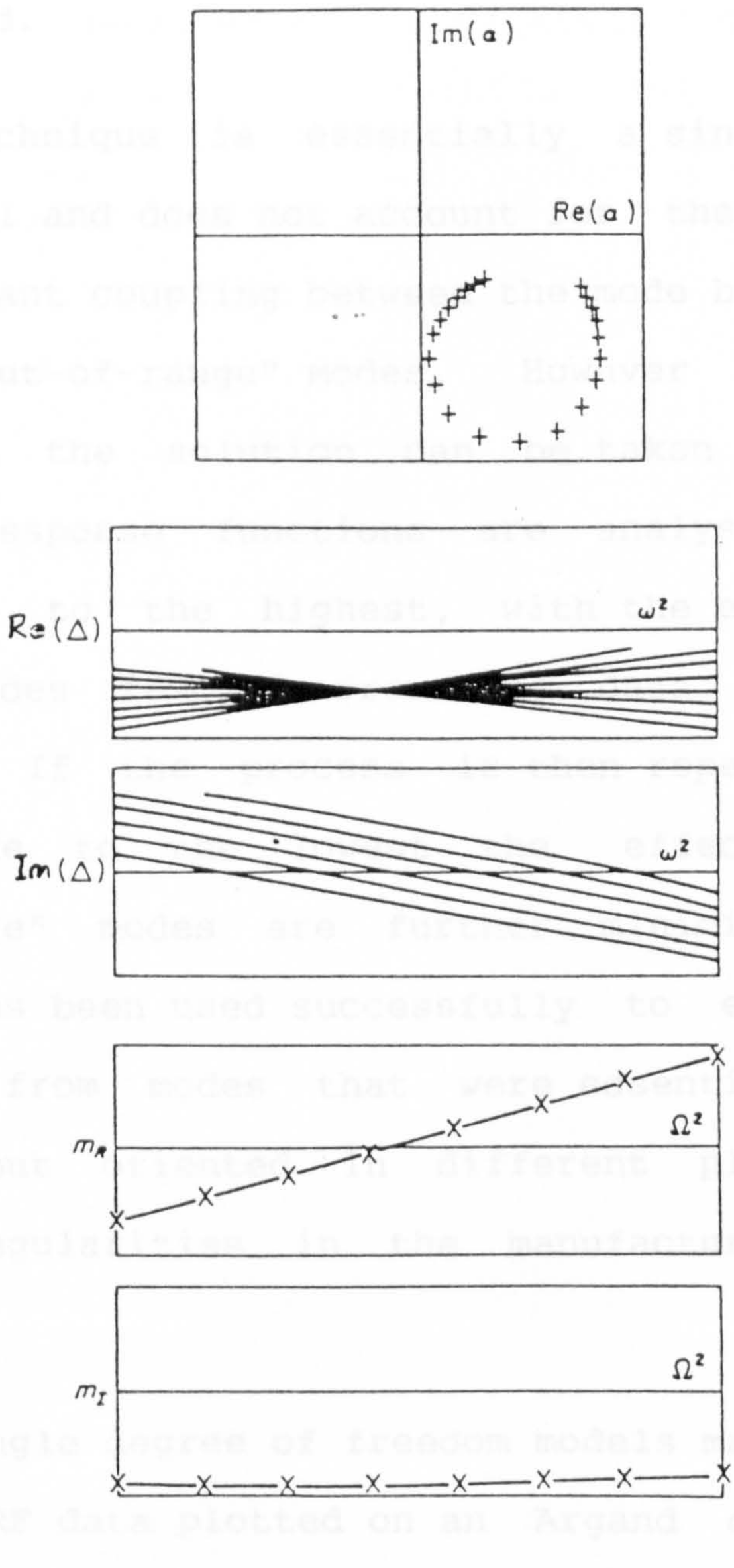

Figure 4.14
Dynamic stiffness plots to obtain modal parameters

The slopes and intercepts of these curves (real and imaginary) are linear functions of Ω^2 in terms of the four modal parameters A,B, ω_r and η_r which can therefore be determined.

This technique is essentially a single degree of freedom model and does not account for the possibility of significant coupling between the mode being examined and other "out-of-range" modes. However an iterative approach to the solution can be taken such that the frequency response functions are analysed from the lowest mode to the highest, with the effects of the analysed modes removed from the data after each analysis. If the process is then repeated from the highest mode to the lowest the effects of the "out-of-range" modes are further minimised and the technique has been used successfully to extract modal parameters from modes that were essentially the same mode shape but oriented in different planes due to slight irregularities in the manufacture of the test cylinders.

Most single degree of freedom models make use of the fact that FRF data plotted on an Argand diagram (i.e. real vs. imaginary) generates a circular (or almost circular) locus. In fact, for hysteretic damping the receptance is circular and for viscous damping, the mobility is circular. However the Argand diagram of the

inverse of receptance is linear and the method used here (Dobson (1987)) capitalises on the greater simplicity and computational efficiency that is obtainable when fitting experimental data to a straight line.

CHAPTER 5 - RESULTS

5.1 Physical Model

In section 4.3.1 four models were described which have been used during the course of this investigation. The first model was simply a length of large diameter mild steel pipe which was supplied from stock. The large variations in wall thickness and the lack of cross-sectional circularity meant that it was satisfactory only for some fairly rudimentary early investigations (Randall & Squire(1984)). The other models were all manufactured specifically for the purpose of vibration testing. Model No.2 was the largest model and essentially the simplest in form, being unreinforced with flat ends. Model No.3 was used in validation trials of FE software for PAFEC Ltd at ARE Portland (Randall (1986b). Hemispherical domed end-caps were screwed onto the cylindrical central section producing an improved outline (Figure 5.1). However the end connections proved to be very difficult to model satisfactorily and although useful information was obtained from the central section, the modelling difficulties plus the enhanced stiffness of the ends prevented further experimentation with this model. The final model which was ring stiffened was produced by ARE Dunfermline and was used for studying pressure loading effects (Figures 5.2 & 5.3). The model collapsed catastrophically at about 70% of the predicted failure

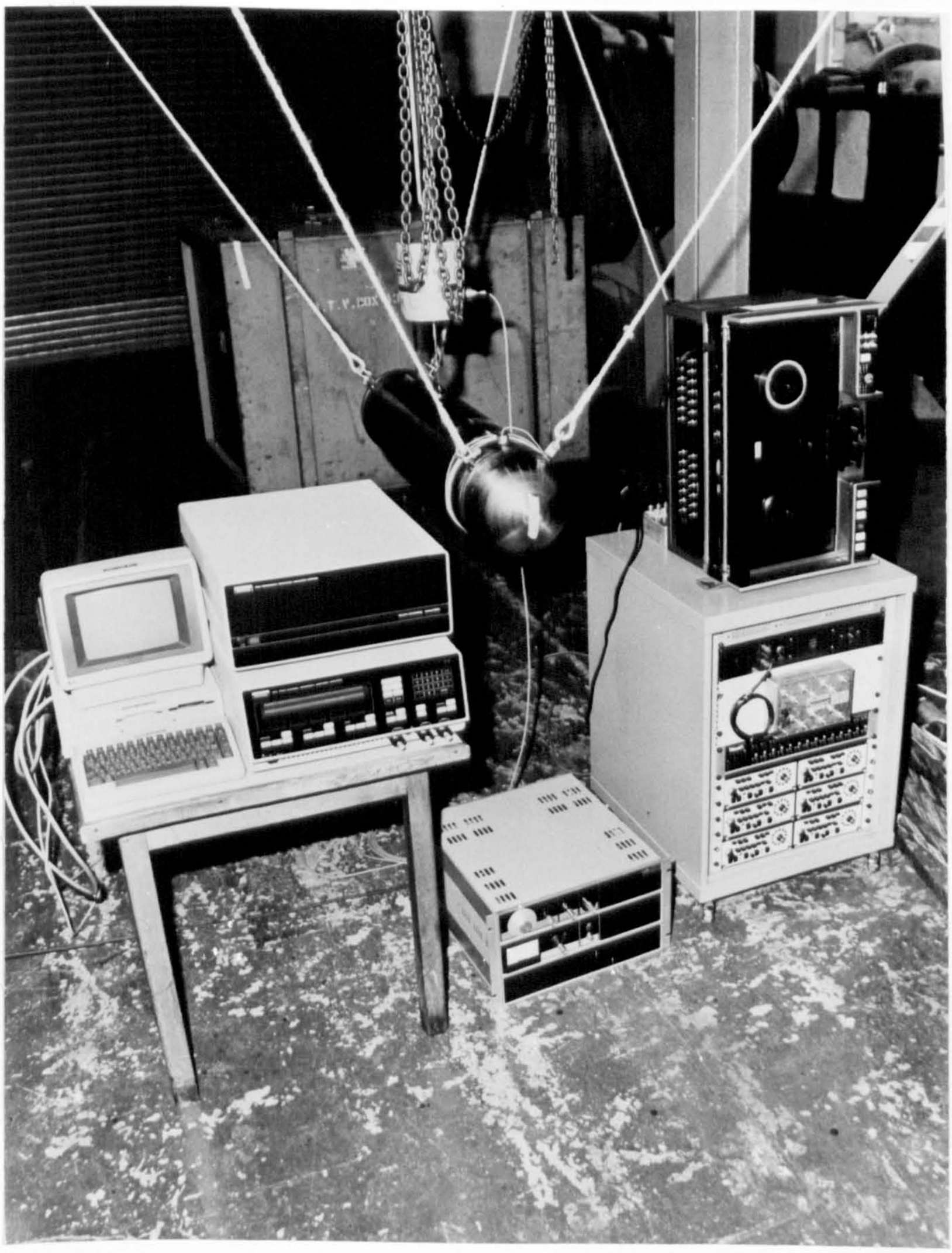

Figure 5.1

Model No.3 prior to testing

Figure 5.2

Pressure testing chamber at Rosyth Naval Base

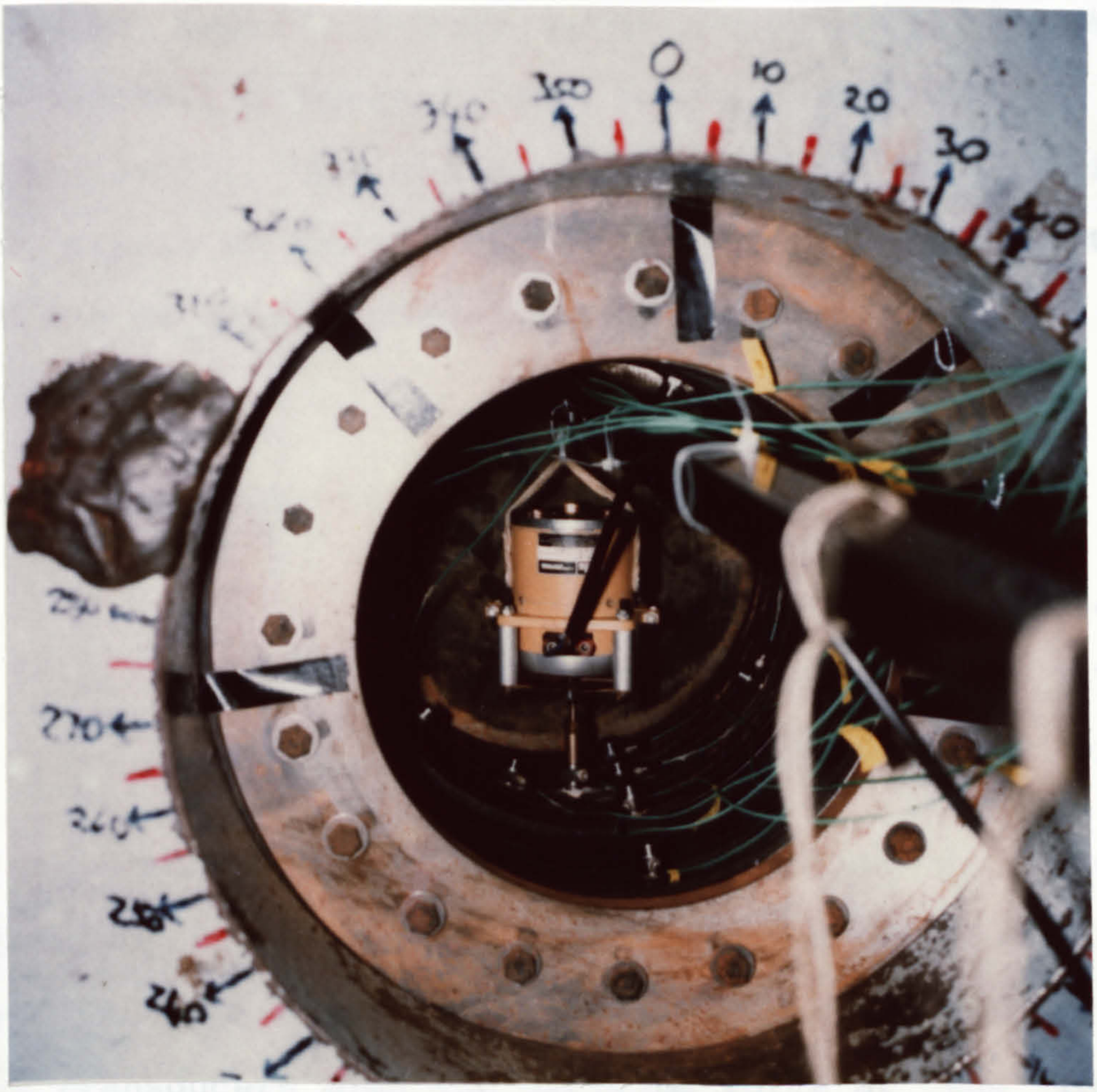

Figure 5.3

Rib-stiffened cylinder (model No.4)

with shaker attached

pressure but after sufficient data had been collected to conclude the study (Okpe (1988)).

In this chapter results obtained from model No.2 will be presented even though some of these findings have also been published elsewhere (Randall (1985), Price, Randall & Temarel(1988), Ergin, Price, Randall & Temarel(1990)). All the essential information relating to the trials on the other cylinders has been presented elsewhere as already indicated and further repetition is unnecessary.

The dimensions of model No.2 are :-

Length	1.284m.
Ext. Diameter	0.357m.
Thickness	0.003m.

The accelerometer positions selected to record distortions in both axial and circumferential planes are shown in figure 5.4. The acceleration response for up to 15 transducers plus the exciting force at the input point were recorded digitally. These data were then converted to receptance before being downloaded onto disc for storage and subsequent analysis.

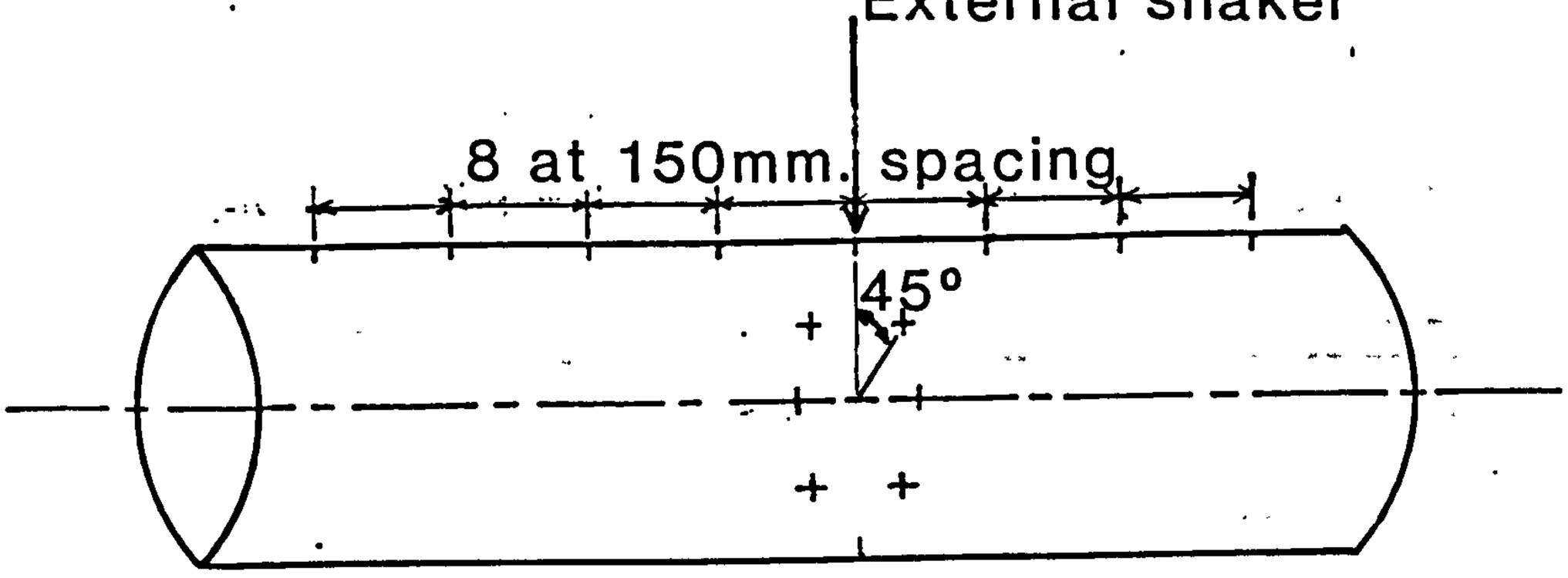

General Arrangement

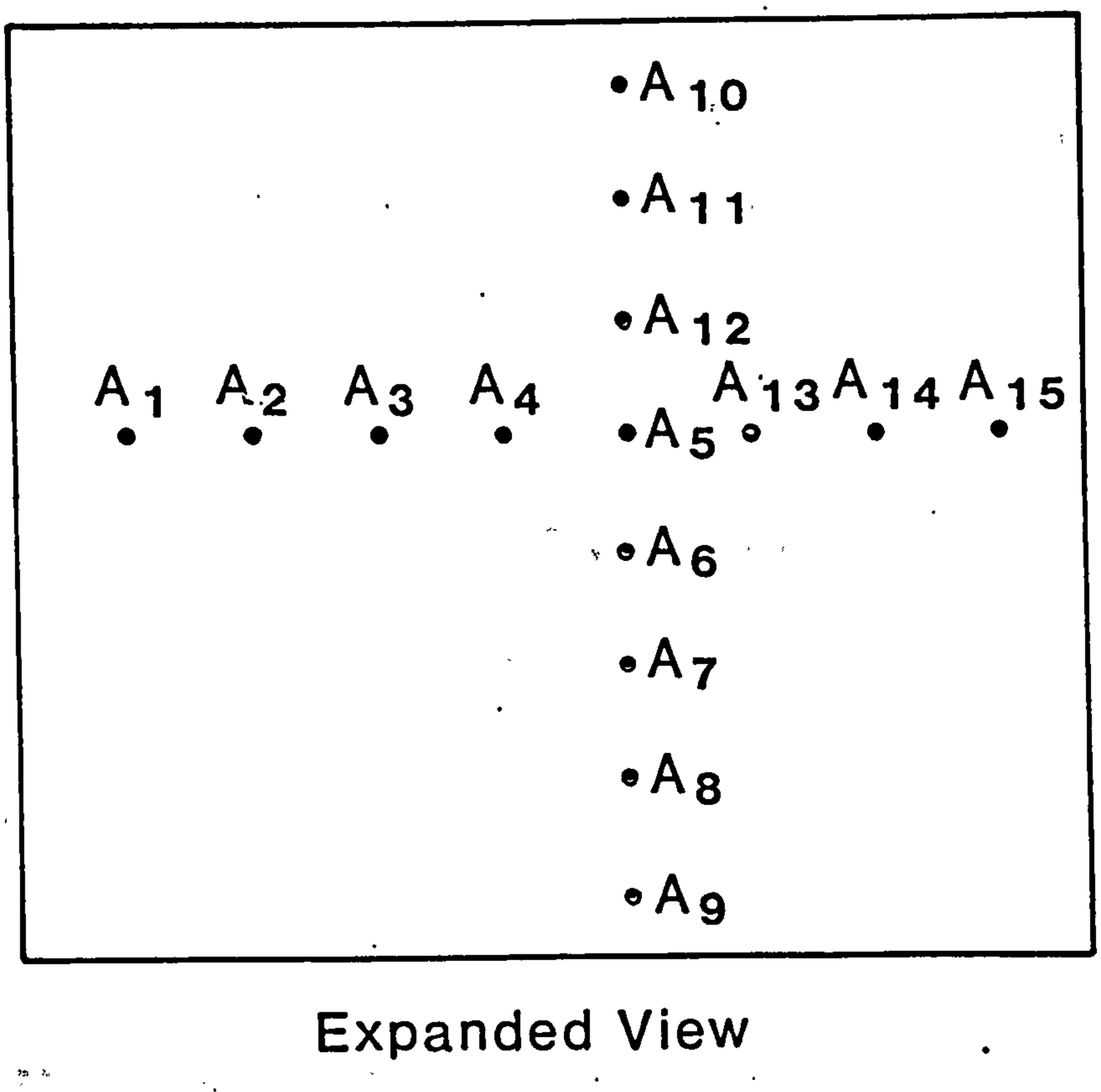

Expanded View

Figure 5.4a

Accelerometer positions.

Layout A

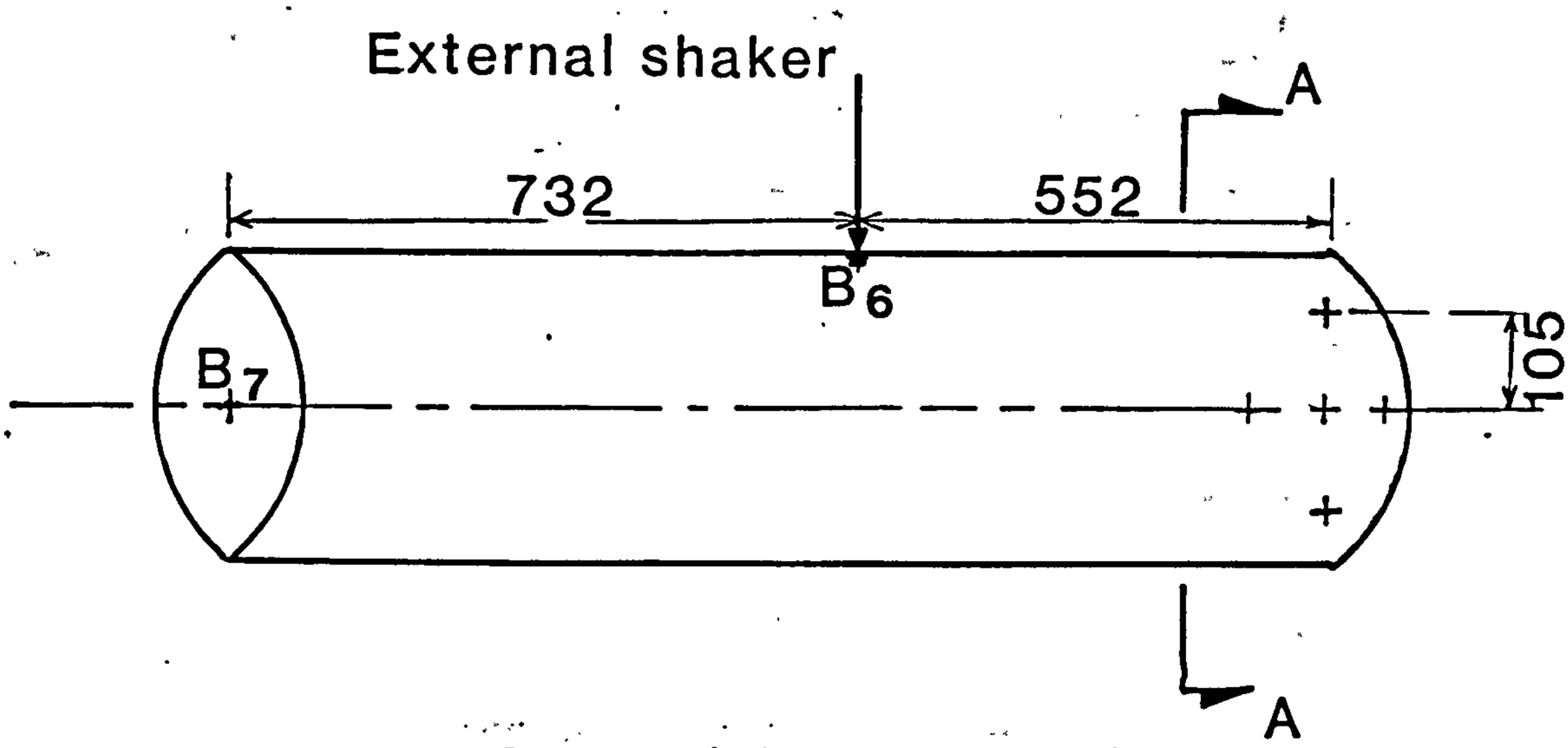

General Arrangement

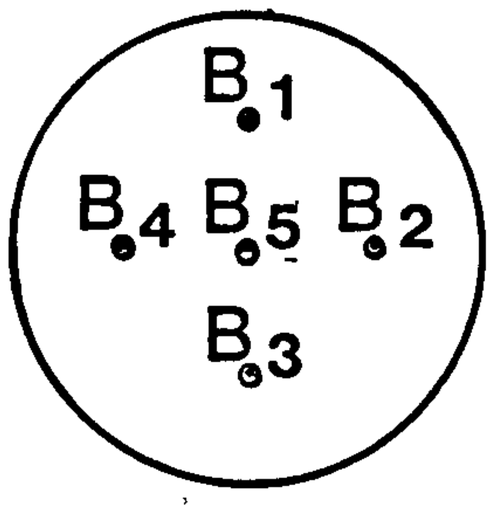

View AA

Figure 5.4b

Accelerolmeter positions

Layout B

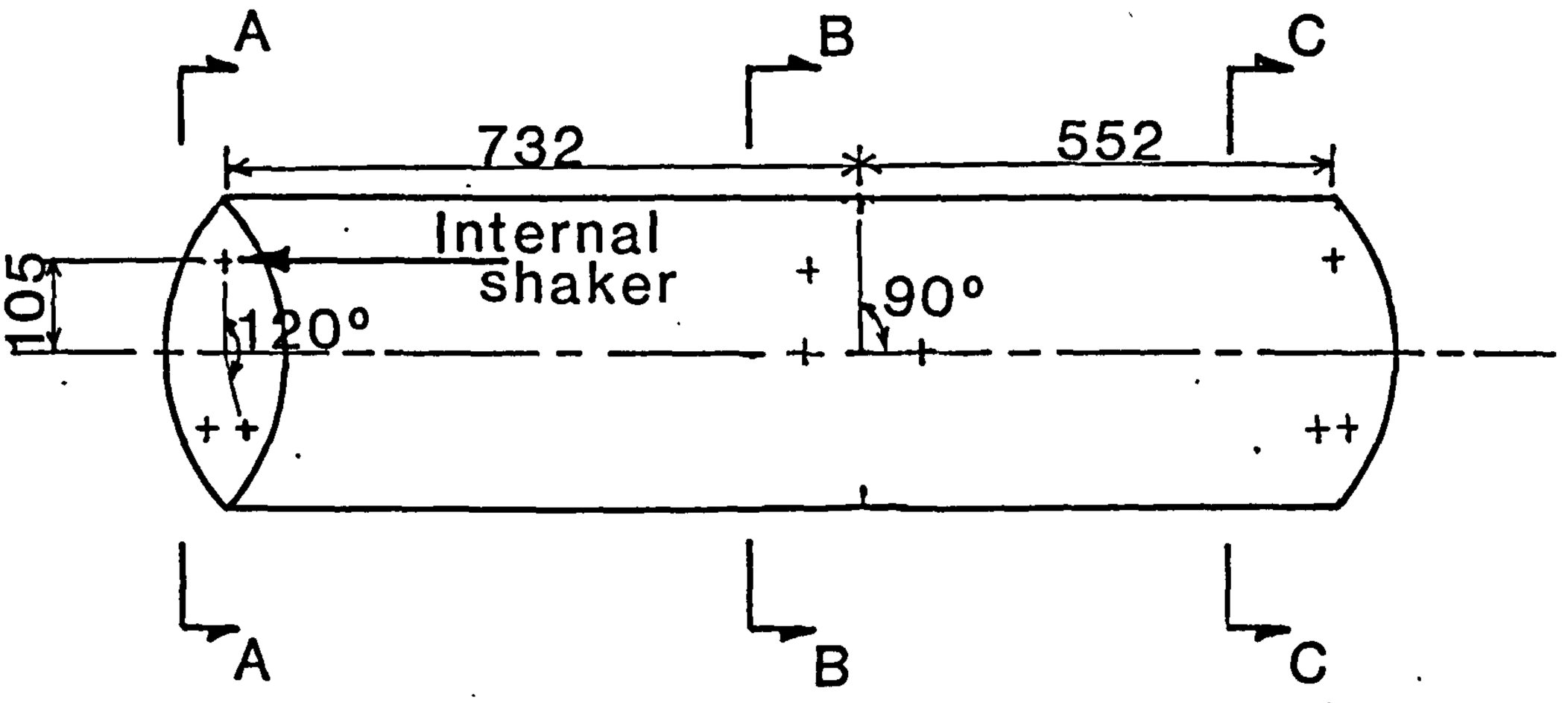

General Arrangement

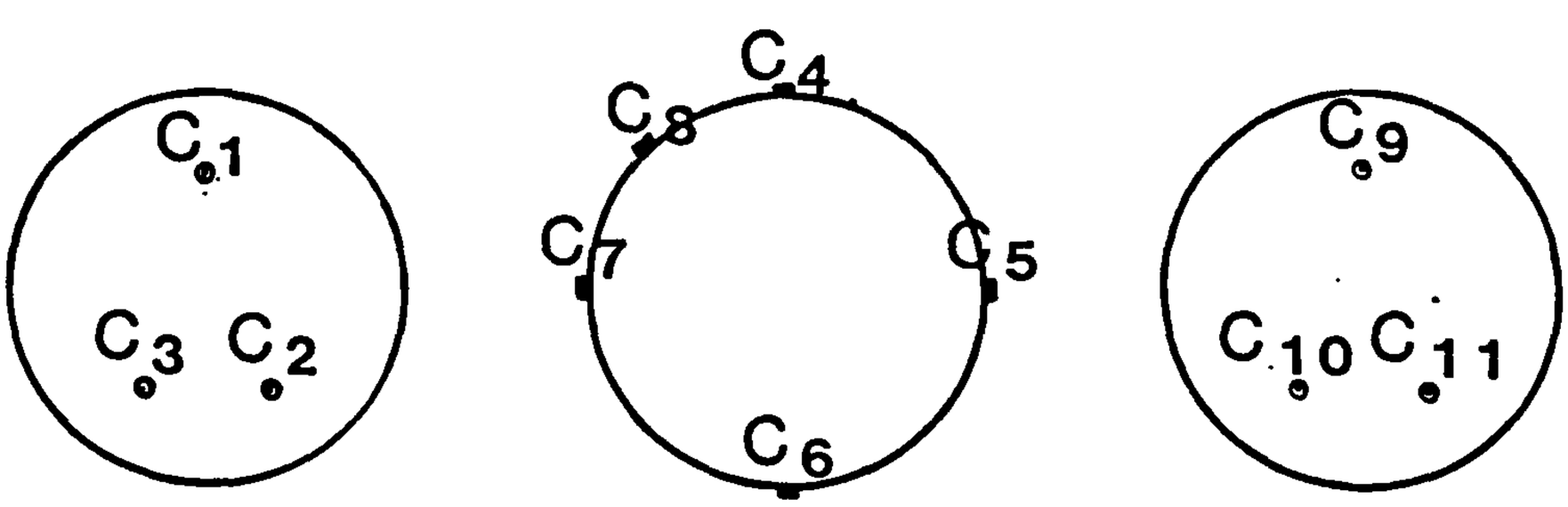

View AA View BB View CC

Figure 5.4c

Accelerometer positions

Layout C

Figure 5.5 Towing tank at RNEC Manadon

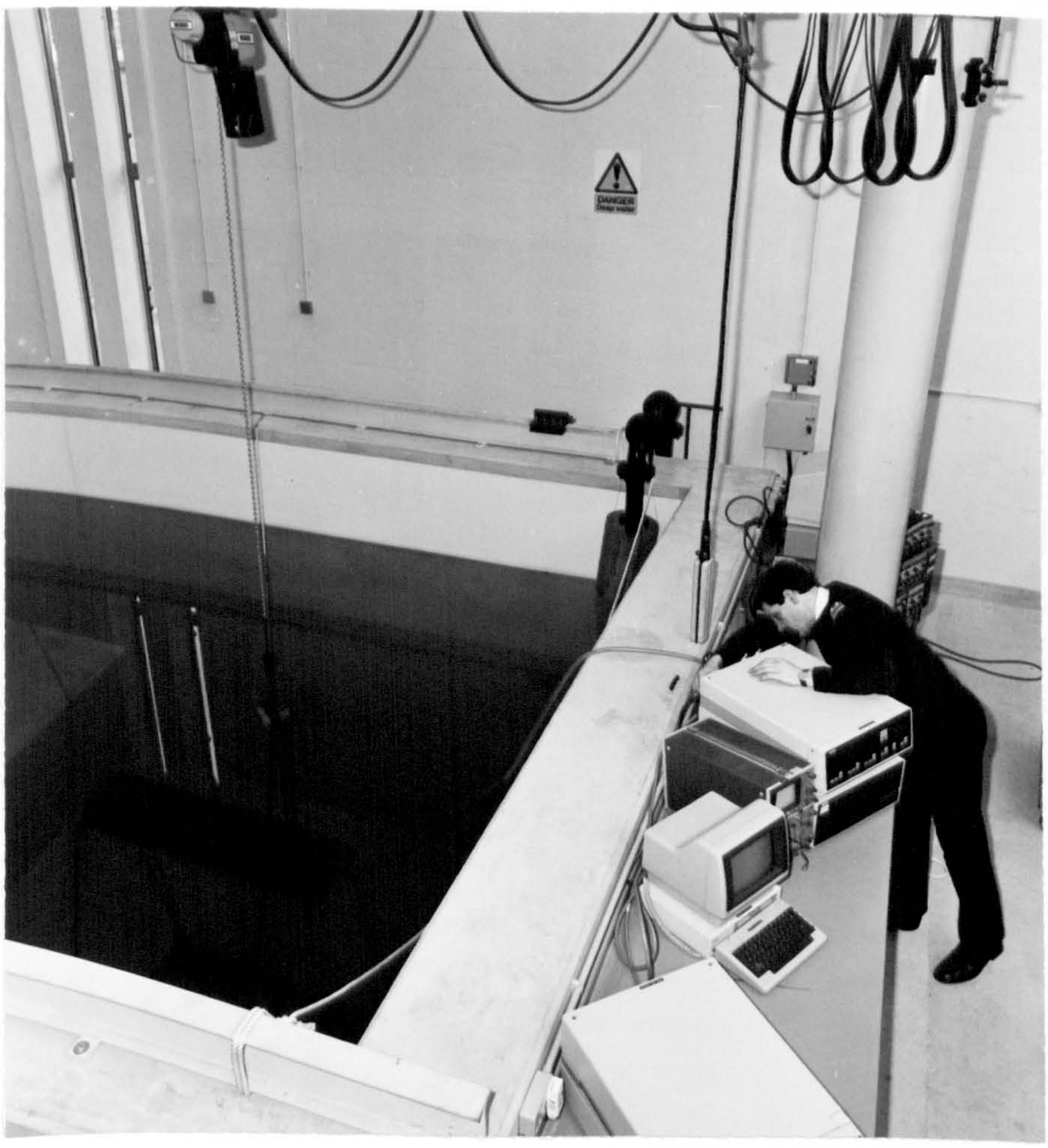

Figure 5.6

Underwater testing of model No.2

5.2 Testing facility

Two water tanks, both at RNEC Manadon, were used for testing this cylinder underwater. The first tank (Figure 4.12a) was relatively confined, measuring 7.5m. long by 1.7m. wide and contained water to a depth of 1.6m. It was lined with ceramic tiles and the position of the cylinder could be varied by means of the tethering ropes. The second tank was considerably larger being a towing tank measuring 32m. long by 4m. wide and 2.5m. deep (Figure 5.5). The experiments on the cylinder were carried out at one end where there was a 4m. depth of water over an area measuring 4m. by 4m. (Figure 5.6). In this tank the buoyancy of the test structure was counteracted by securing it with wire ropes to a ballast frame placed on the bottom of the tank (Figure 4.12b). The wire ropes were of equal length ensuring not only that the cylinder was at the required depth but also that it was on an even keel.

5.3 Vibration testing in air

The first set of tests was performed in air to provide a comparison for all later testing when the structure was in contact with water and to validate the finite element analysis of the dry structure. Testing in air is essentially the same as testing in-vacuo and there was no restriction on the orientation or situation of the structure, provided it was physically isolated

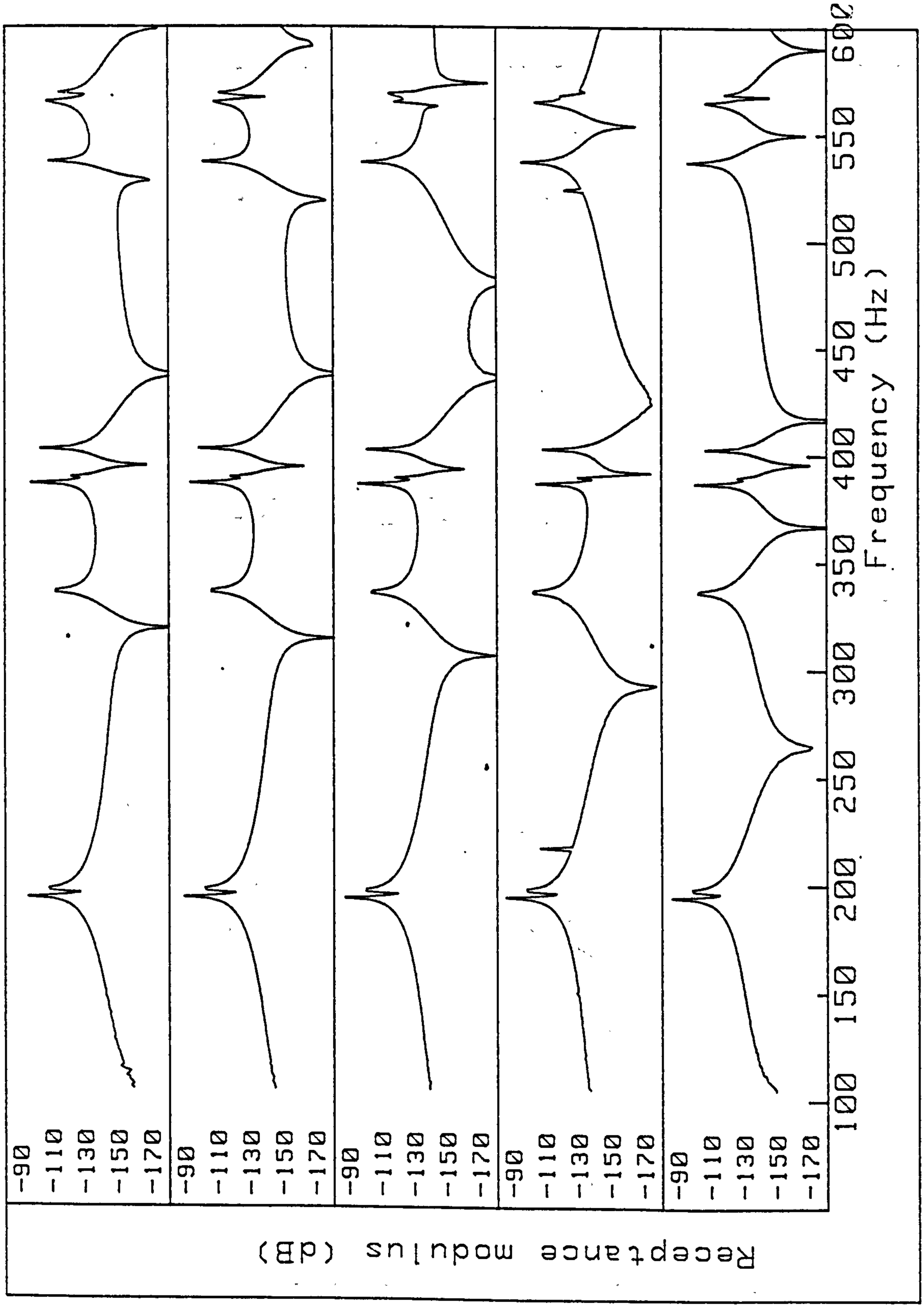

Figure 5.7a. In-air. External shaker. Channels A1-A5

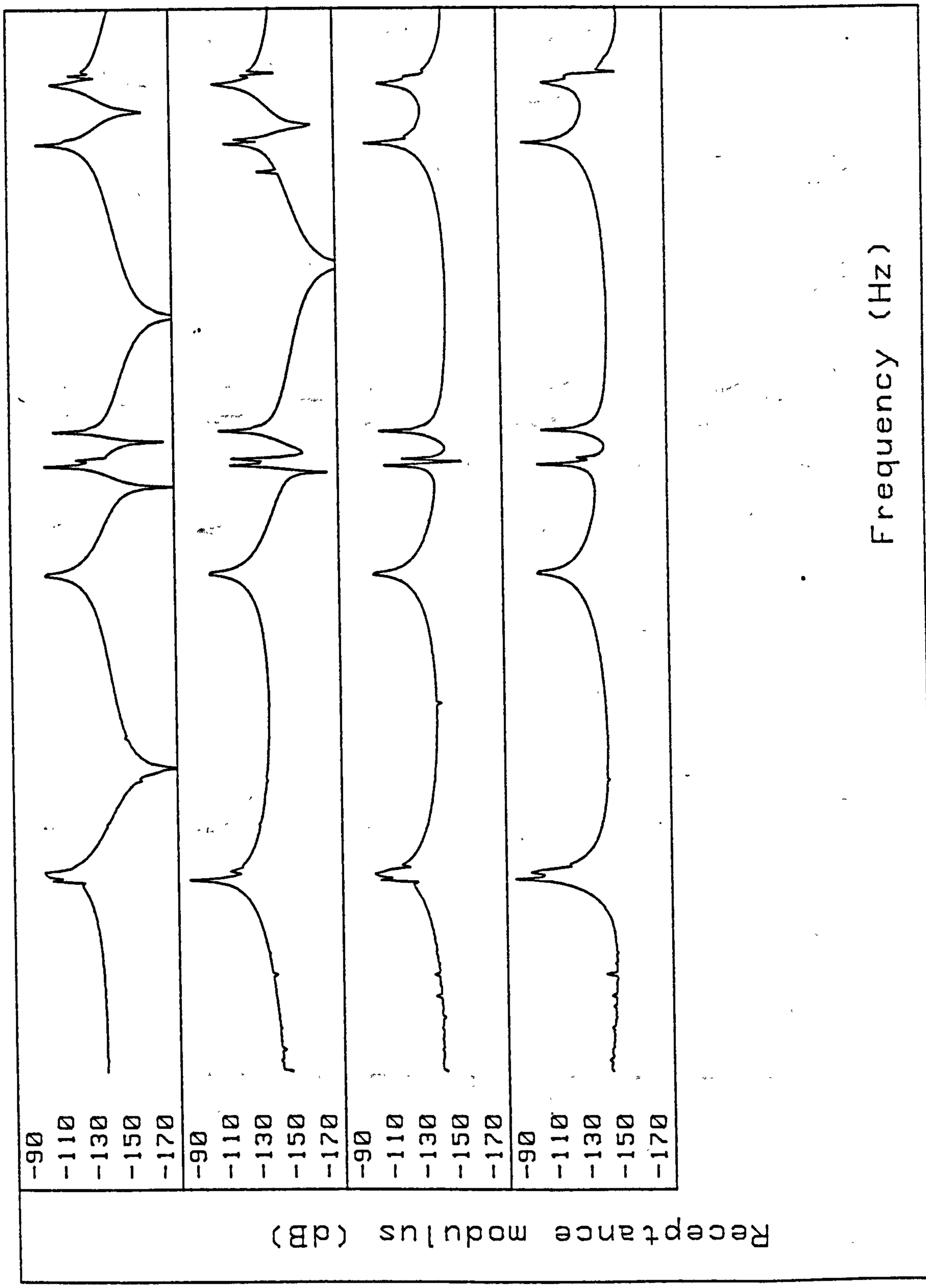
Channels A6-A9
Frequency (Hz)
Receptance modulus (dB)
-90
-110
-130
-150
-170

Figure 5.7b.

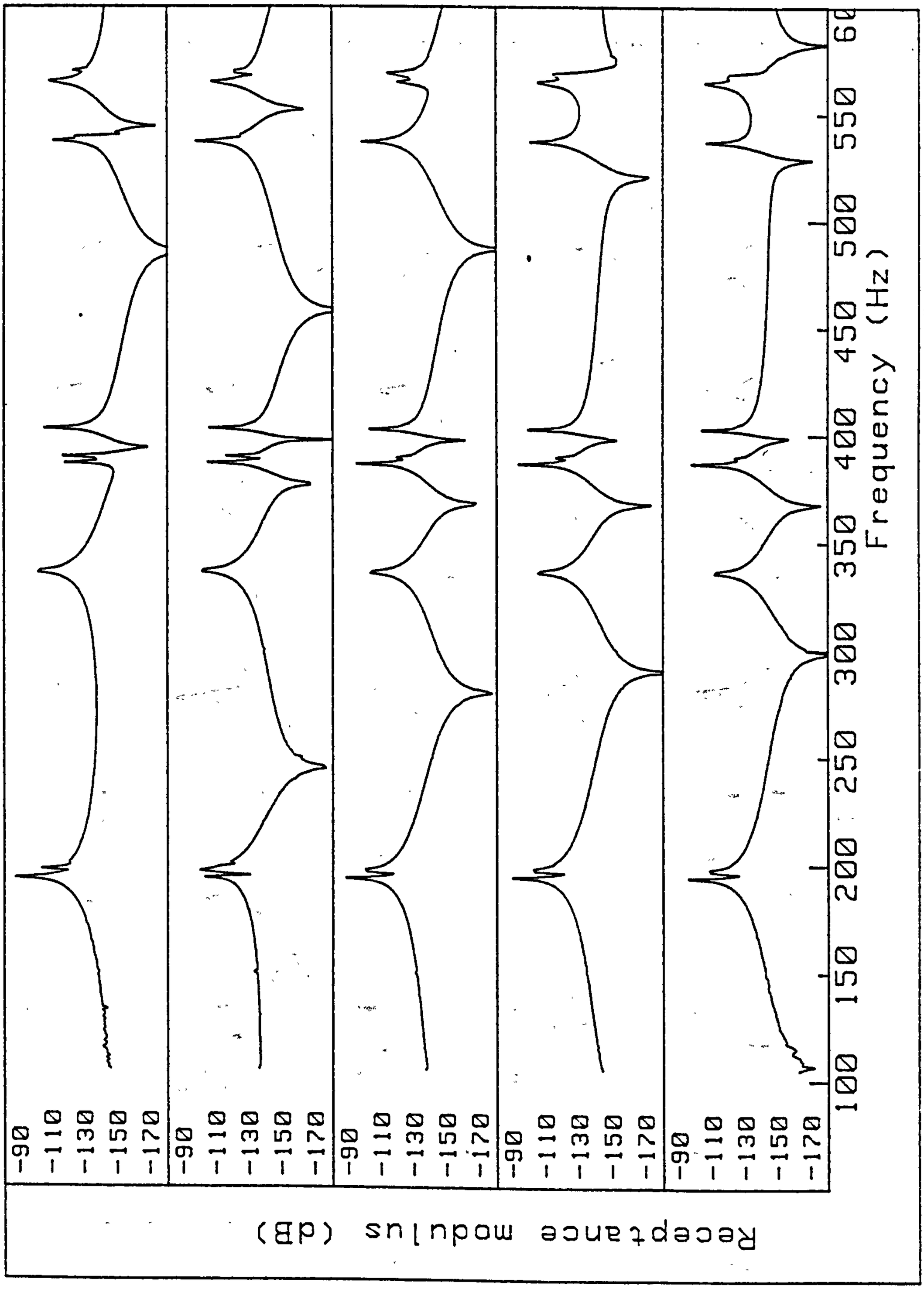
Receptance modulus (dB)
-90
-110
-130
-150
-170
100
150
200
250
300
350
400
450
500
550
600
Frequency (Hz)
Channels A10-A15

Figure 5.7c.

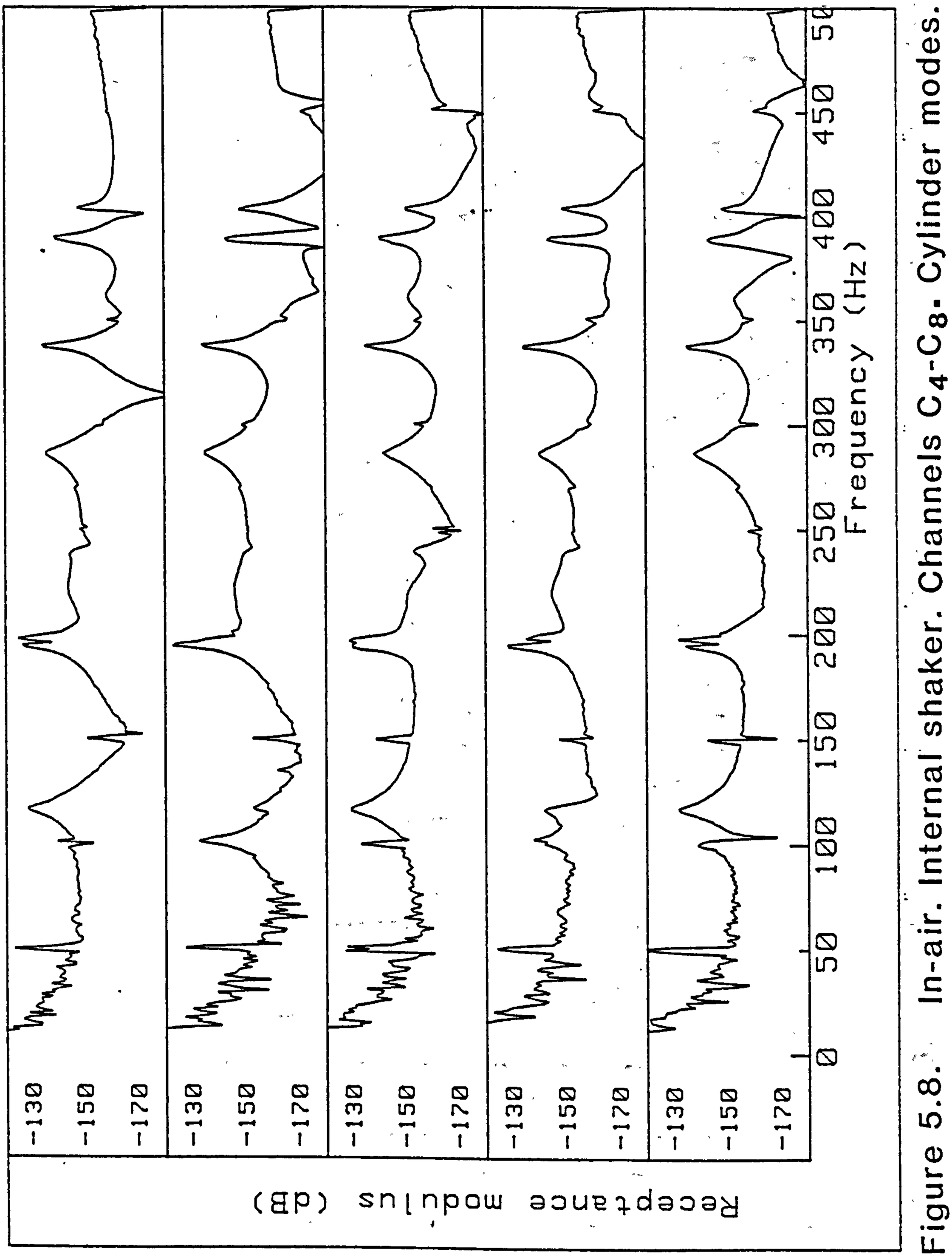
Receptance modulus (dB)
-130
-150
-170
0
50
100
150
200
250
300
350
400
450
500
Frequency (Hz)
In-air. Internal shaker. Channels C4-C8. Cylinder modes.

Figure 5.8.

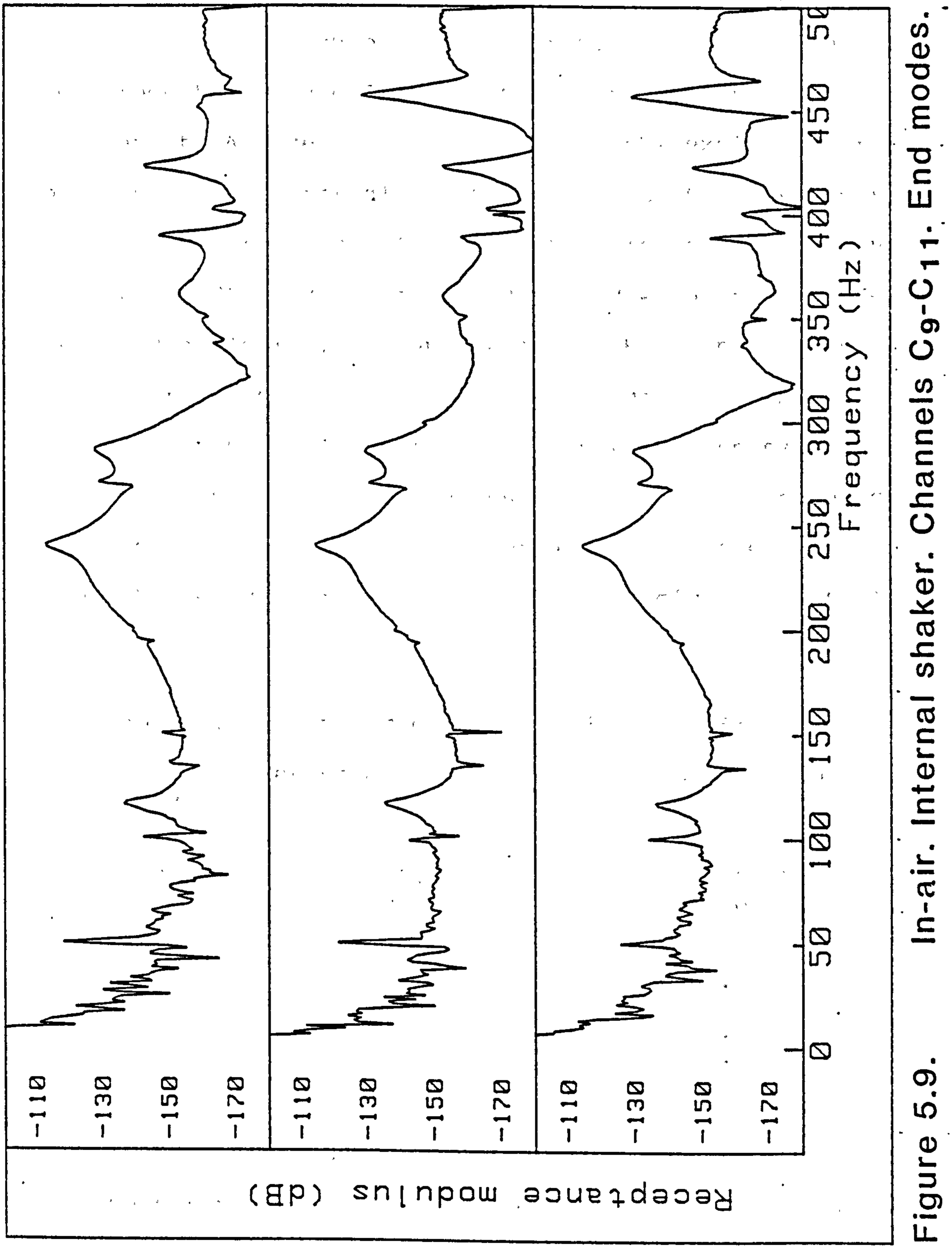
Receptance modulus (dB)
-110
-130
-150
-170
-110
-130
-150
-170
-110
-130
-150
-170
0
50
100
150
200
250
300
350
400
450
500
Frequency (Hz)
In-air. Internal shaker. Channels C9-C11. End modes.

Figure 5.9.

from the surroundings. This was achieved by slinging the cylinder from an overhead gantry using soft rubber bungees. The results from two series of in-air tests are shown in Figures 5.7 - 5.9. The first set of measurements (Figure 5.7) was taken from the transducers in layout A (see Fig. 5.4) with the exciting force provided by an external shaker coupled to the structure using a short flexible push-rod. The quality of the receptance data is generally very good with only a few faulty signals (cf. channel 4 at 217 Hz. and 524 Hz.). The major resonances are easily identified and each channel only differs from the others by the existence and position of anti-resonances and minima. Resonance frequencies, damping loss factor and mode shape obtained from the measured modal constants are given in table 5.1.

Table 5.1 In-air cylinder modes (29605)

Mode (m,n)	Resonance frequency (Hz)	Loss factor
1,2	193.9	0.00051
1,3	197.4	0.00060
1,4	336.5	0.00045
2,3	387.0	0.00041
	389.9	0.00010
2,4	403.1	0.00025
1,5	537.1	0.00062
3,4	564.7	0.00037
2,5	568.6	0.00035

In the first series of tests there was no provision for measuring the motion of the ends and this problem

was addressed in a second series. The ends could have been excited in the same manner as before using an external shaker or alternatively impacted with a calibrated hammer; however a different method had to be devised for the underwater trials, so for consistency the in-air tests were performed using the internal shaker described in section 4.2.5. Transducers were attached in the 11 locations comprising layout C. Figure 5.8 shows the results from transducers c4-c8 which are directly comparable with transducers a5-a12 from the first series.

The resonances which were identified as being modes of vibration of the ends are shown in Figure 5.9 and are tabulated below (Table 5.2).

Table 5.2 In-air end modes (22389C1-3)

Mode (r,s)	Resonance frequency (Hz)	Loss factor
0,0	240.7	0.020
0,0	270.5	0.0064
0,1	389.3	0.023
0,1	402.2	0.0032
0,1	422.6	0.0034
0,1	457.0	0.0030

5.4 Vibration testing underwater

When the cylinder is tested underwater the frequency response charateristics cannot be assessed without consideration of the position of the model within the testing tank (Fig. 5.10). The proximity of

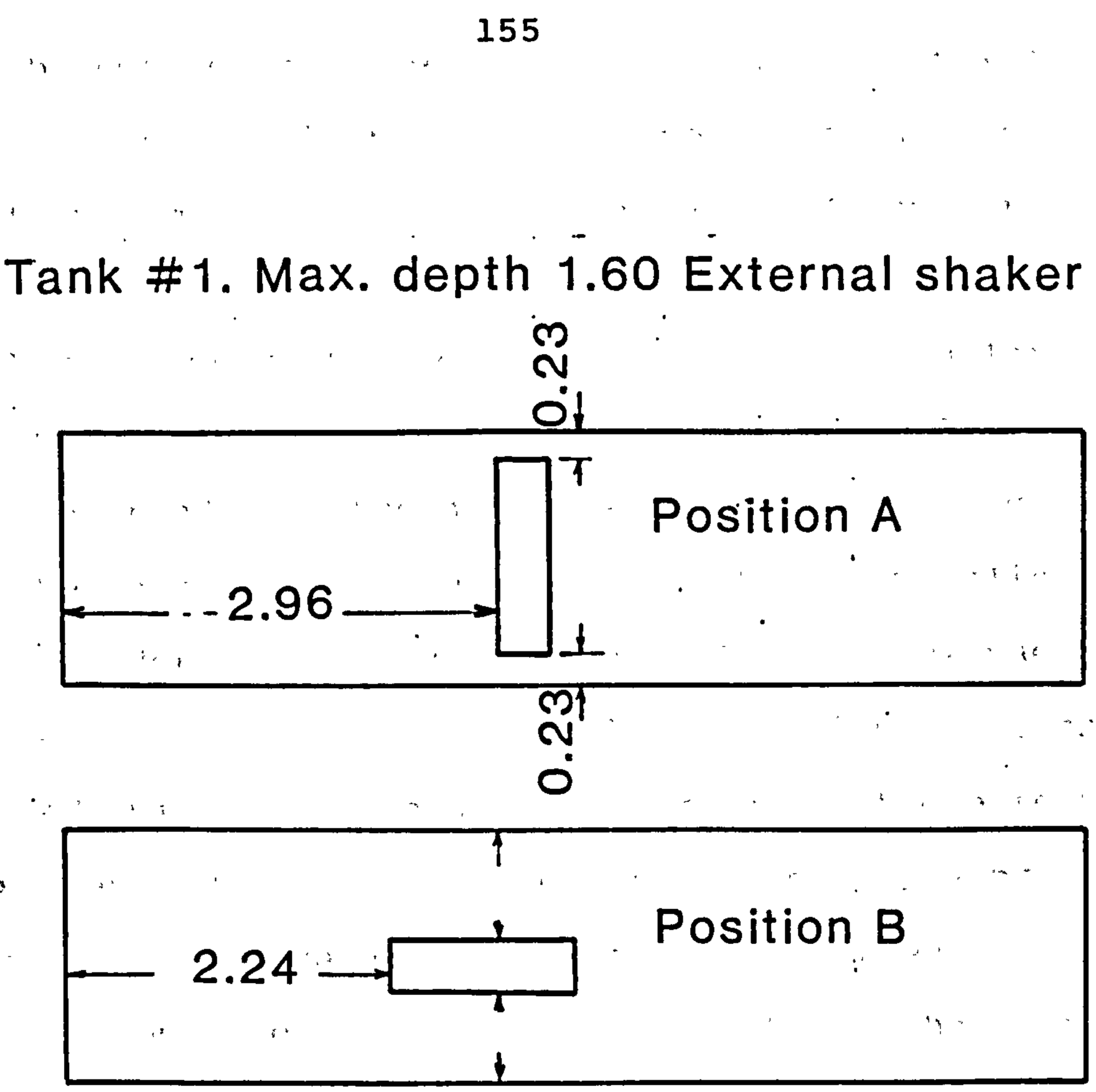

Figure 5.10

Underwater test locations

solid boundaries and the free surface must be taken into account. In the first underwater tests an attempt was made to minimise the influence of external boundaries by situating the model as near to the centre of the tank as possible. Owing to the dimensions of the smaller tank this could only have limited success. Figure 5.11 shows data recorded by the same transducers as in fig. 5.7 with the same method of excitation, the centreline of the cylinder was horizontal and 0.68m. below the free surface. There is a reduction in signal strength compared with the in air testing due to the effect of hydrodynamic damping on the amplitude of vibration. There is a discernible difference between channel 5 which is opposite the forcing point, where there is a relatively strong response signal and other channels corresponding to sites further away from the source of excitation.

The first objective of the underwater tests was to establish the resonance frequencies of the structure under the influence of the fluid actions. These tests took place before the larger tank was available and had the complication of limited clearance to the external boundaries; but there was one advantage in that an external shaker could be used so that all modes and in particular end modes could be recorded before the internal shaker was fitted. This was particularly useful as the resonance frequency of the first end mode is close to the first support structure resonance.

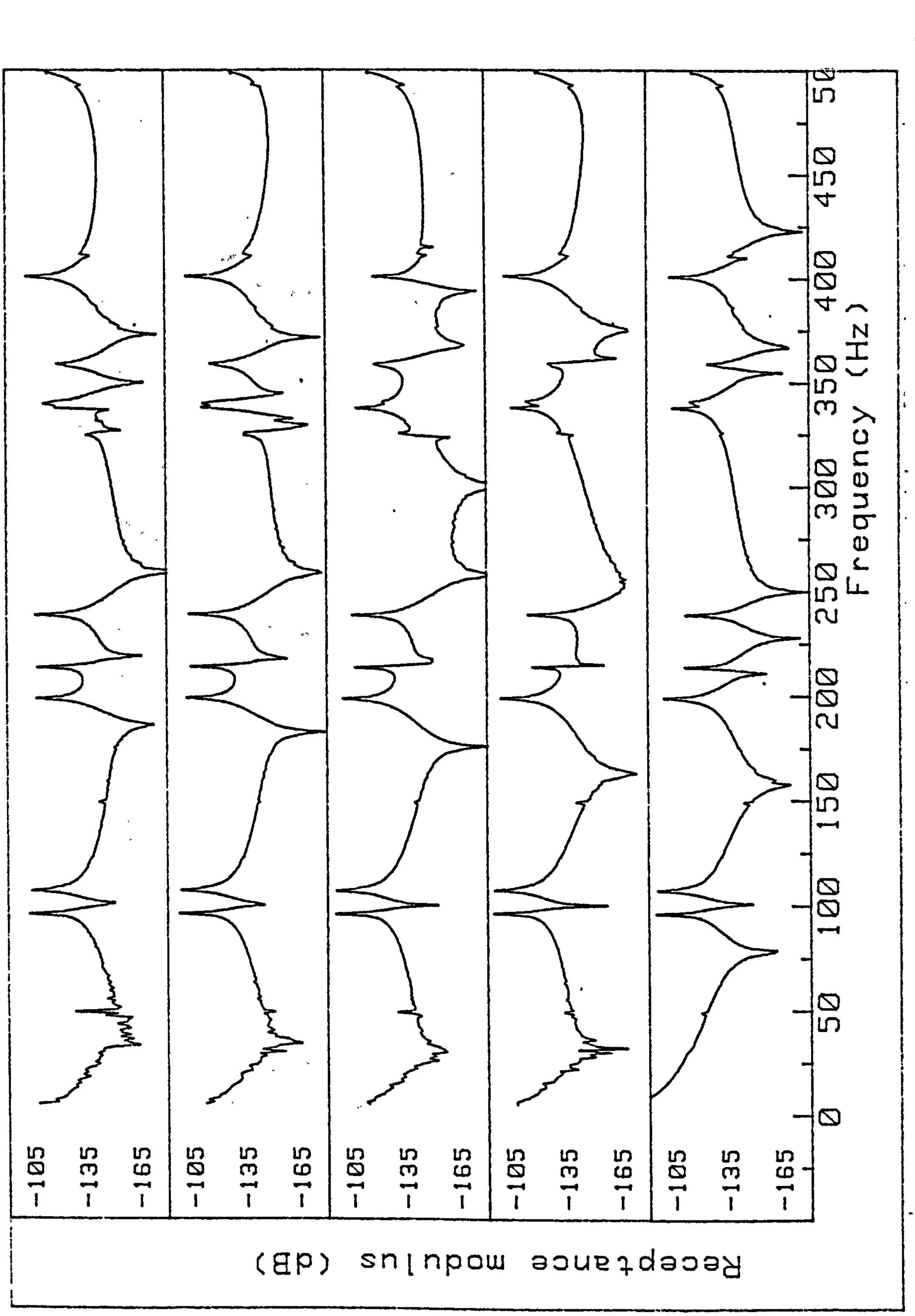

Figure 5.11a. Underwater. Position A. Depth to ℄ 0.68m.

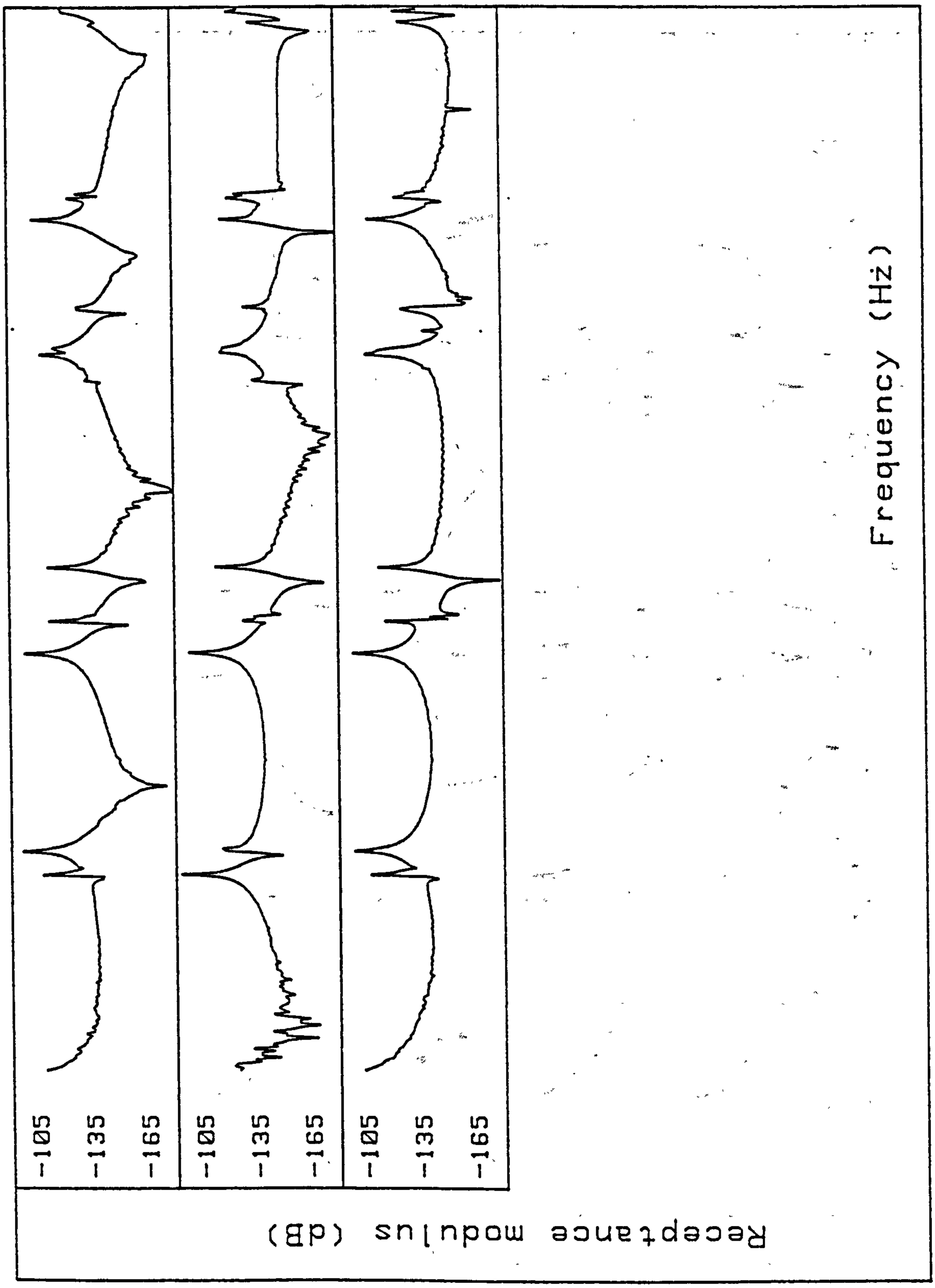
Channels A6-A8
Frequency (Hz)
-105
-135
-165
-105
-135
-165
-105
-135
-165
Receptance modulus (dB)

Figure 5.11b.

PAGE NUMBERING AS ORIGINAL

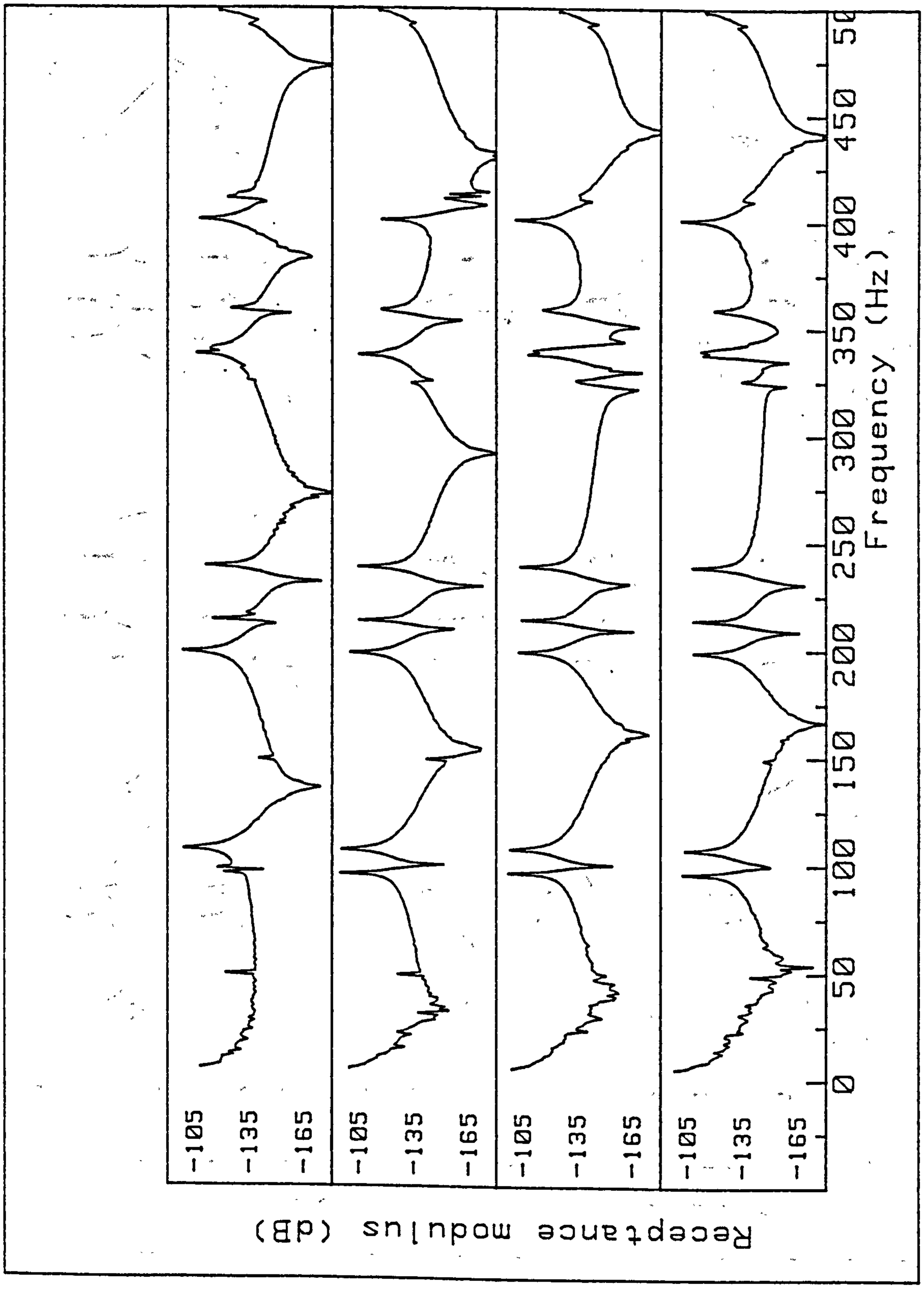
Receptance modulus (dB)
-105
-135
-165
Frequency (Hz)
100 150 200 250 300 350 400 450 500
0 50
Channels A12-A15

Figure 5.11c.

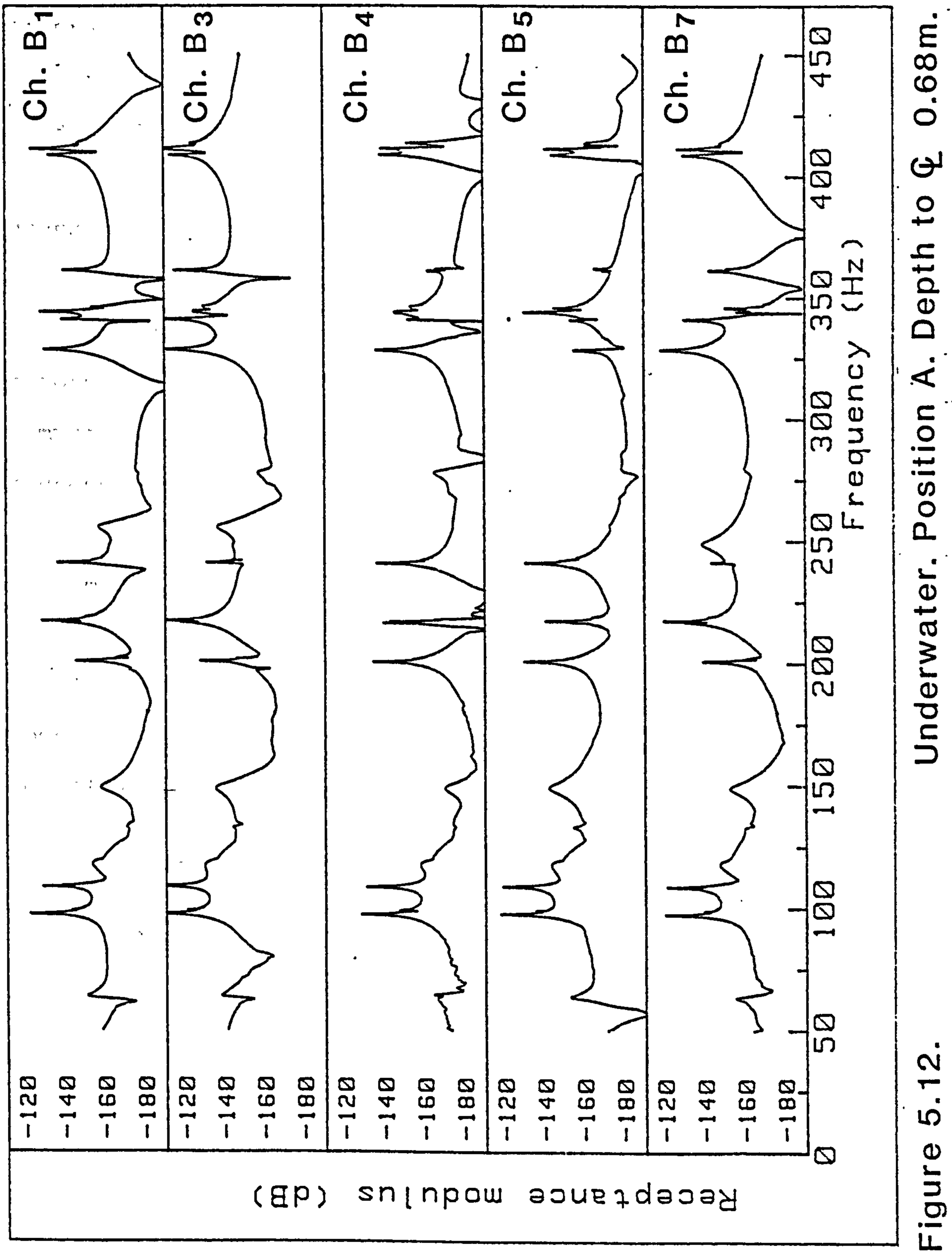
Ch. B1
Ch. B3
Ch. B4
Ch. B5
Ch. B7
250
300
350
400
450
Frequency (Hz)
Underwater. Position A. Depth to ℄ 0.68m.
0
50
100
150
200
-120
-140
-160
-180
Receptance modulus (dB)

Figure 5.12.

Modes of vibration of the cylindrical central portion of the tube are essentially due to radial motion of this section, but these deformations will cause some lateral motion at the ends, which was recorded. The converse is not true however as lateral motion of the ends at resonance will only cause axial movement in the central section which will only be picked up if the cross-sensitivity of the accelerometers is poor. Figure 5.12 shows receptance data from accelerometers on the ends of the cylinder with both cylindrical and end modes recorded. The increased damping of the end modes compared with the cylinder modes is evident by the rounded shape of the peaks. Further tests were performed to measure both cylinder and end modes with the model across the tank and at various depths below the free surface (Figs. 5.13-5.16).

Table 5.3 Underwater modes. Tank #1 (6_50,7_50)

Model position:	Across CL (A)				Along CL (B)			
Depth(m)	0.21	0.23	0.66	0.68	0.21	0.29	0.68	0.72
Mode								
1,2	101.6	98.9	97.2	97.5	101.6	97.7	97.4	97.2
1,3	114.8	109.4	108.3	108.7	113.4	109.2	108.6	108.5
		109.8			114.4			
e1	122.4	120.6	119.0	118.3	116.9	113.6	115.1	115.3
e2	153.6	149.5	151.3	149.1	149.2	148.7	147.1	149.2
1,4		201.5	200.9		203.0		200.4	
2,3		218.6	216.9		220.5		216.7	
			217.4				217.2	
2,4		242.0	241.3		243.6		240.9	
e3		248.7	249.1		248.3		248.4	
2,2		332.2	328.6				328.1	
3,4		341.4	341.0		341.0		340.3	
1,5		346.7			346.9		343.5	
2,5		362.1	361.1		363.4		360.4	
3,3		409.4	408.8		411.1		407.9	
					412.7			
3,5		412.2	411.3		418.1		410.5	

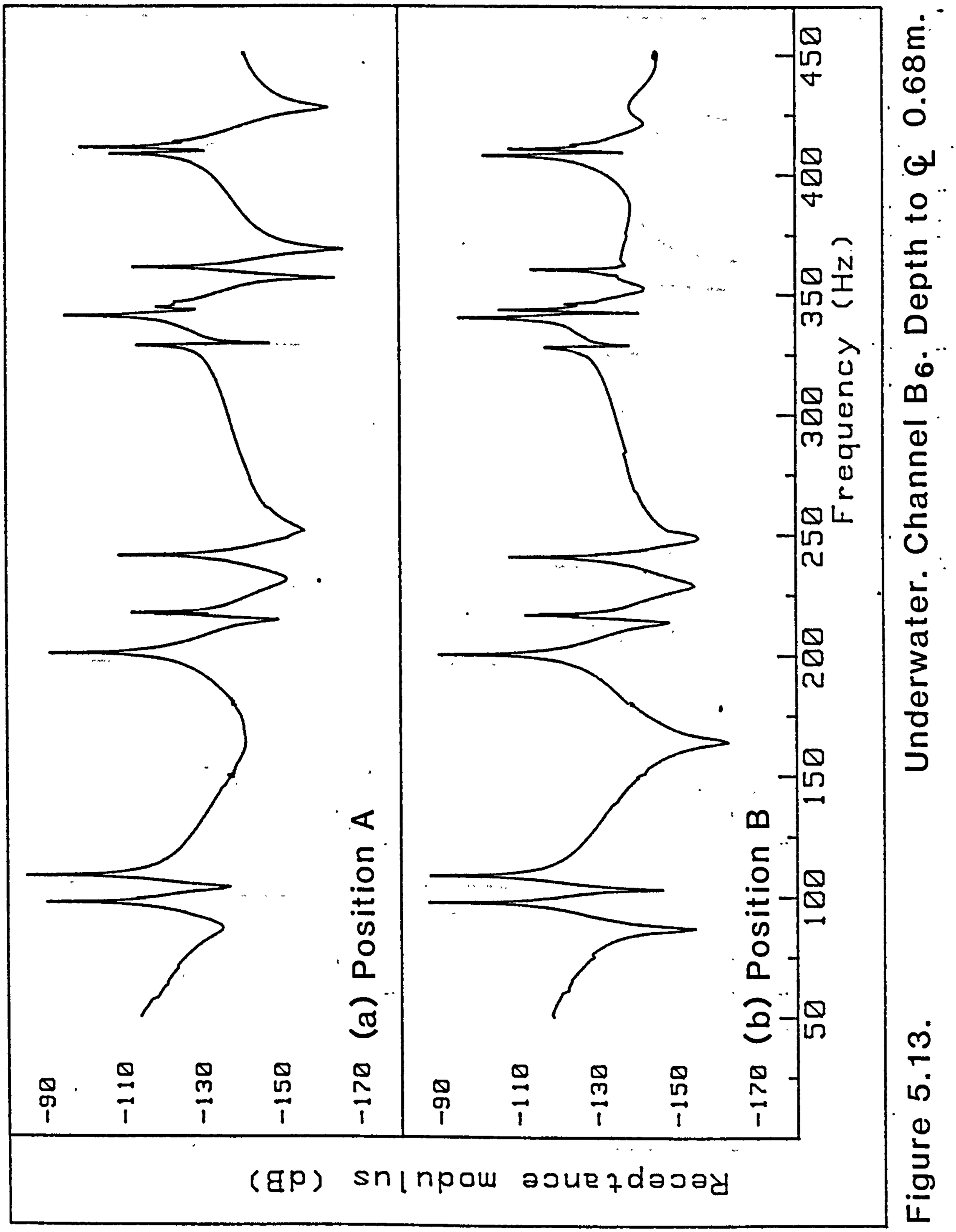
Receptance modulus (dB)
-90
-110
-130
-150
-170 (a) Position A
-90
-110
-130
-150
-170 (b) Position B
50
100
150
200
250
300
350
400
450
Frequency (Hz)
Underwater. Channel B6. Depth to C 0.68m.

Figure 5.13.

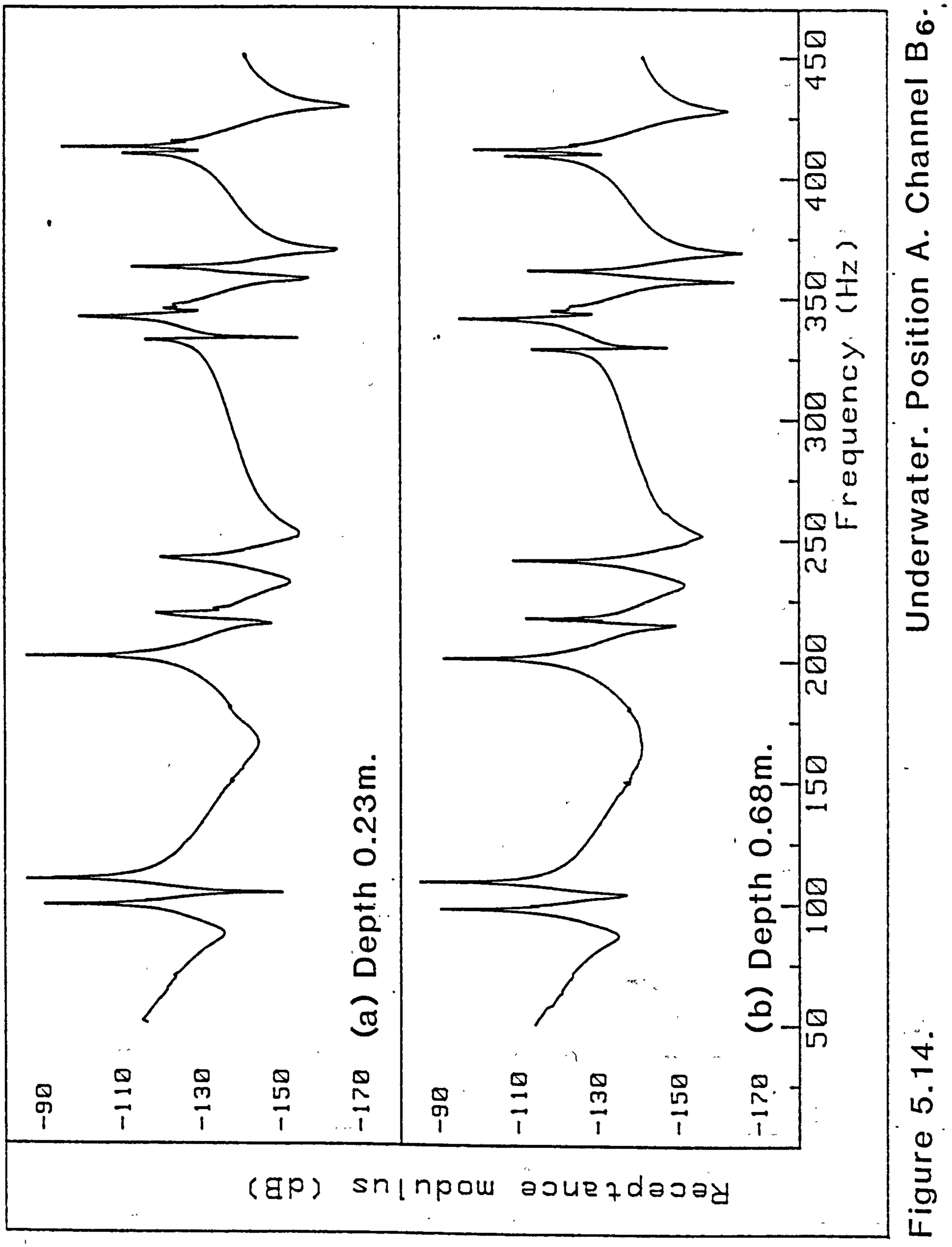
Receptance modulus (dB)
-90
-110
-130
-150
-170
(a) Depth 0.23m.
(b) Depth 0.68m.
100
150
200
250
300
350
400
450
Frequency (Hz)
Underwater. Position A. Channel B6.

Figure 5.14.

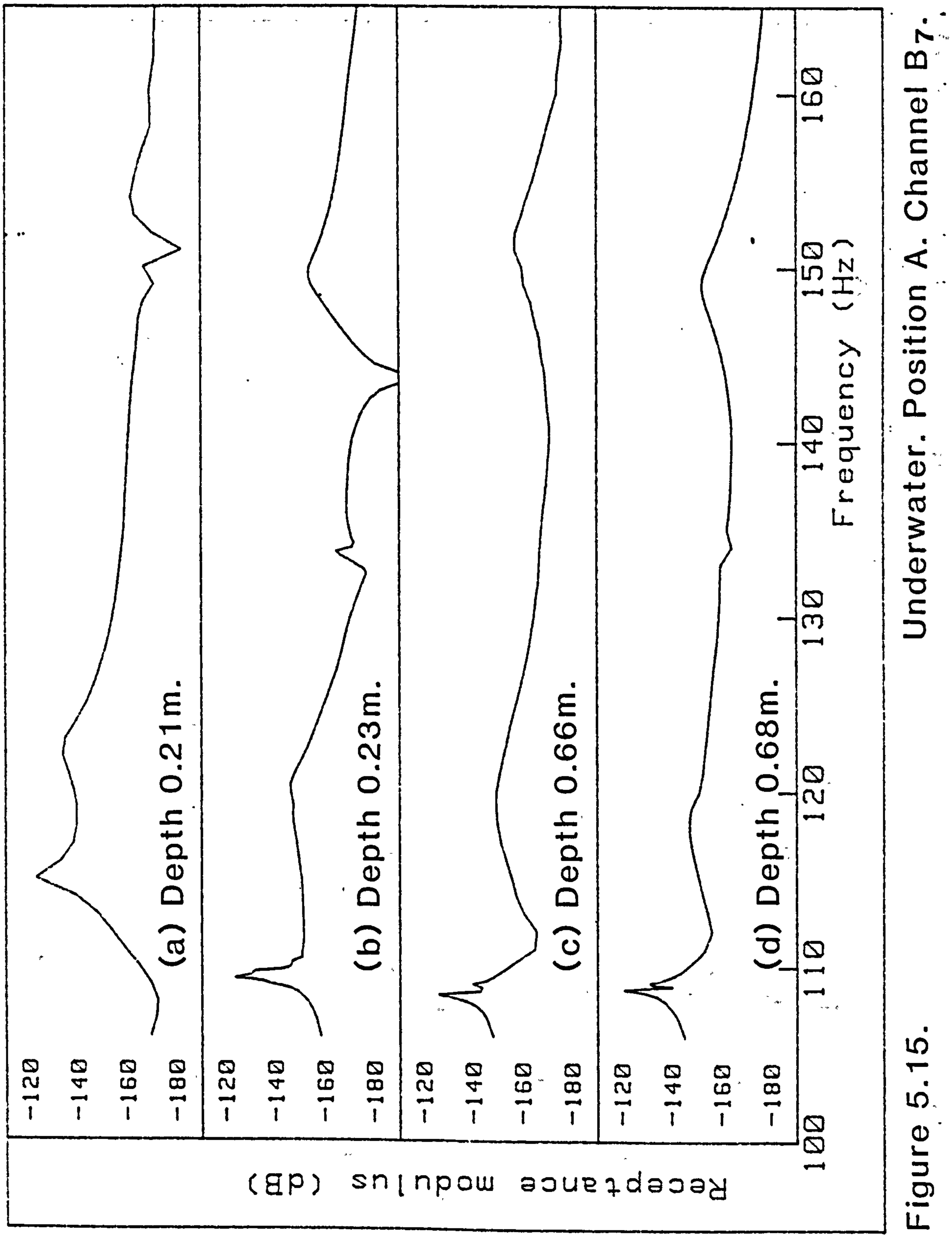
Underwater. Position A. Channel B7.
(a) Depth 0.21m.
(b) Depth 0.23m.
(c) Depth 0.66m.
(d) Depth 0.68m.
Frequency (Hz)
100
110
120
130
140
150
160
Receptance modulus (dB)
-120
-140
-160
-180

Figure 5.15

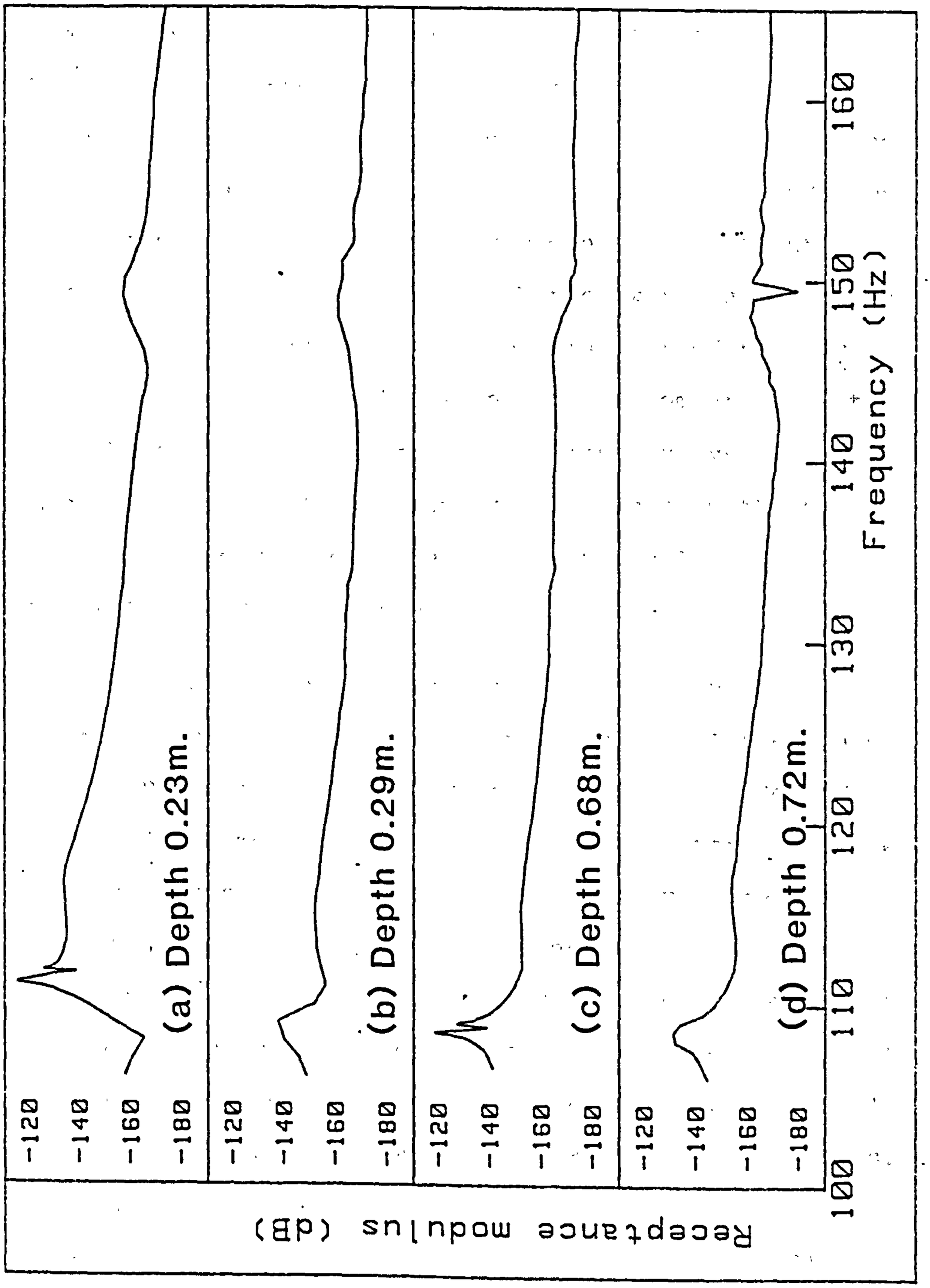
Receptance modulus (dB)
-120
-140
-160
-180
(a) Depth 0.23m.
(b) Depth 0.29m.
(c) Depth 0.68m.
(d) Depth 0.72m.
100
110
120
130
140
150
160
Frequency (Hz)
Underwater. Position B. Channel B7.

Figure 5.16.

PAGE NUMBERING AS ORIGINAL

Although the vibration of the ends of this model were of particular interest during this measurement programme it should be noted that the design of the model was not prepared with this specifically in mind. There was a hatch plate at each end and the transducer connection cables fed in through a central gland at one end. The hatches were screwed on to the ends and then glued with a rubber sealing compound to prevent the ingress of water. So, although they were manufactured from the same gauge steel as the remainder of the model, the ends were not uniform and do not compare directly with the plain ends assumed in the dry analysis. The relatively high loss factors associated with the end modes has already been noted and is probably due to the rubber compound around the sealing hatches.

The internal shaker was then fitted to the model and a further series of tests performed in the large water tank. Receptance data were obtained for cylinder (Fig. 5.17) and end modes (Fig. 5.18) with a better response from the ends albeit with the shaker support resonances superimposed on the overall signal. A further improvement was achieved by the use of stepped-sine excitation which could be applied at the frequencies of interest thus avoiding areas were spurious results could occur. The model was tested at various depths (Figs. 5.19-5.20), next to the tank wall (Fig. 5.21) and floating in the free surface (Figs. 5.22-5.23) and again the results have been tabulated (Table 5.4).

Table 5.4 Underwater modes. Tank #2 (44_70,303_85,9289)

Depth(m) Mode	0.25	1.50	3.50	1.50(Posn D)
1,2	99.4	97.1	96.4	
1,3	109.9	107.9	106.7	
e1	122.1	118.9	114.4	114.7
e2	141.1	139.7	128.6	139.6
1,4	199.4	198.9	195.9	
2,3	214.1	215.4	216.3	
2,4	240.1	238.9	239.2	
e3	242.9	248.0	252.9	247.7

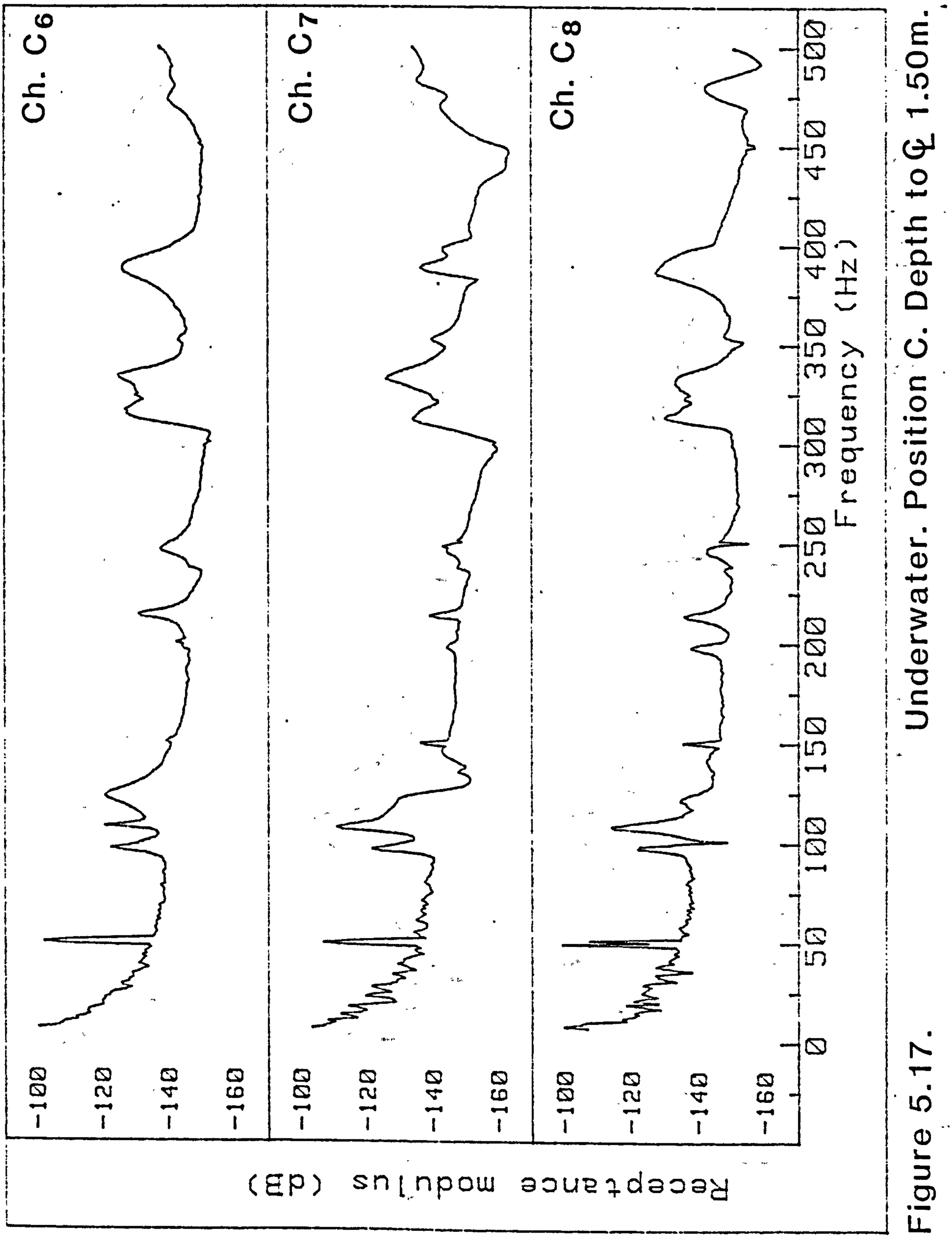
Ch. C6
Ch. C7
Ch. C8
-100
-120
-140
-160
0
50
100
150
200
250
300
350
400
450
500
Frequency (Hz)
Underwater. Position C. Depth to Q 1.50m.
Receptance modulus (dB)

Figure 5.17.

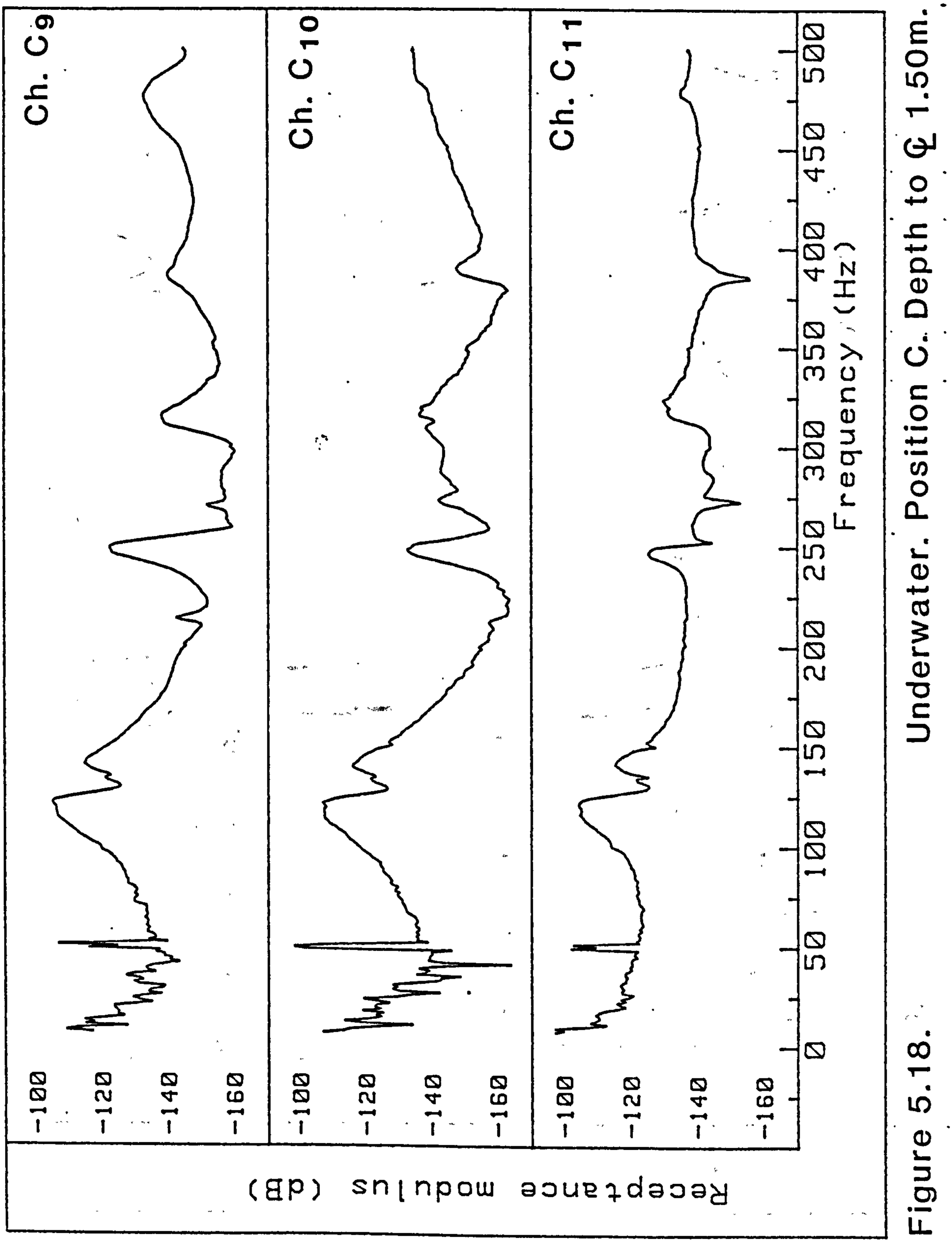
Ch. C9
Ch. C10
Ch. C11
-100
-120
-140
-160
-100
-120
-140
-160
-100
-120
-140
-160
0
50
100
150
200
250
300
350
400
450
500
Frequency (Hz)
Underwater. Position C. Depth to ℄ 1.50m.
Receptance modulus (dB)

Figure 5.18.

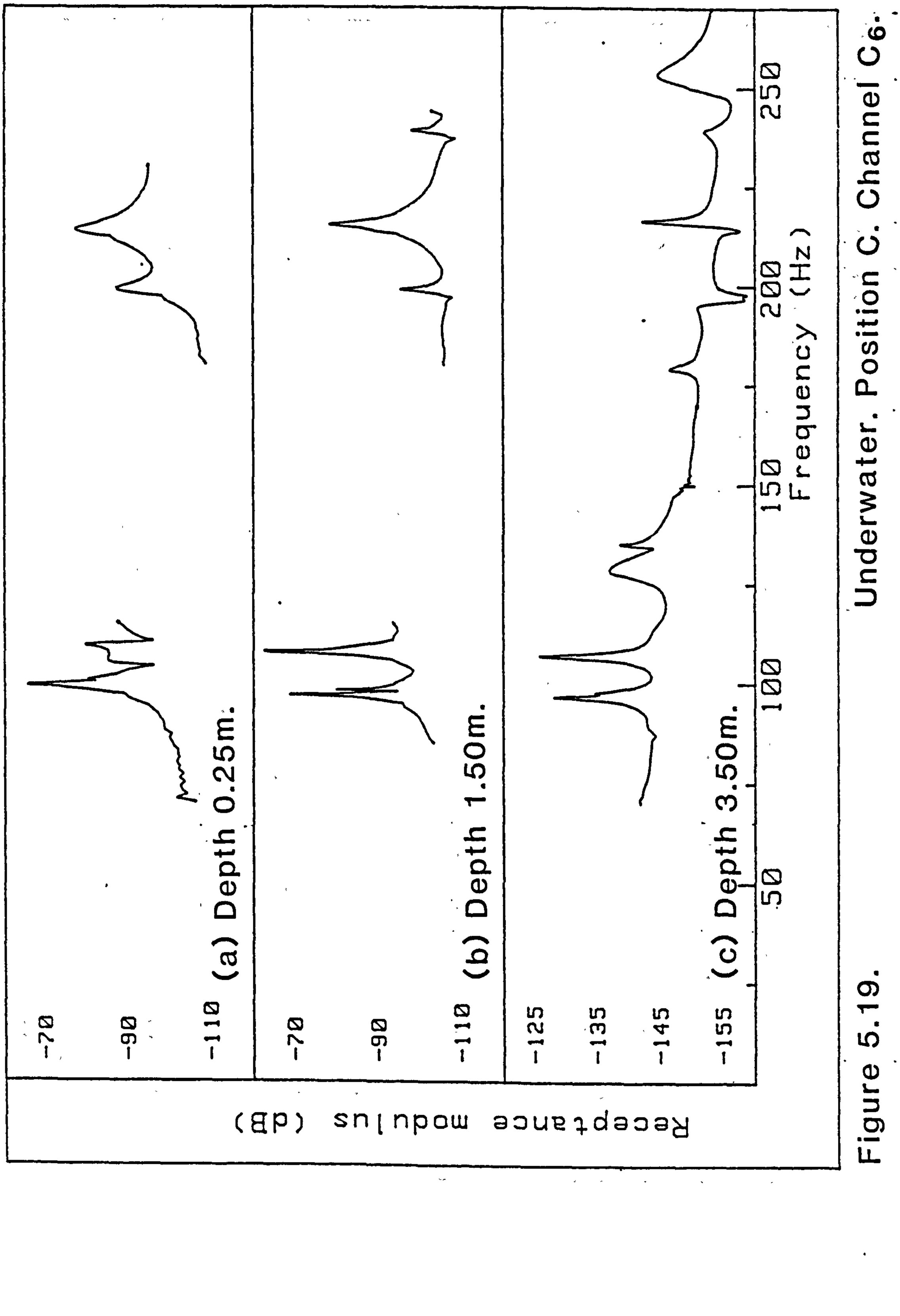
Underwater. Position C. Channel C6.
250
200
150
Frequency (Hz)
(a) Depth 0.25m.
(b) Depth 1.50m.
(c) Depth 3.50m.
100
50
-70
-90
-110
-125
-135
-145
-155
Receptance modulus (dB)

Figure 5.19.

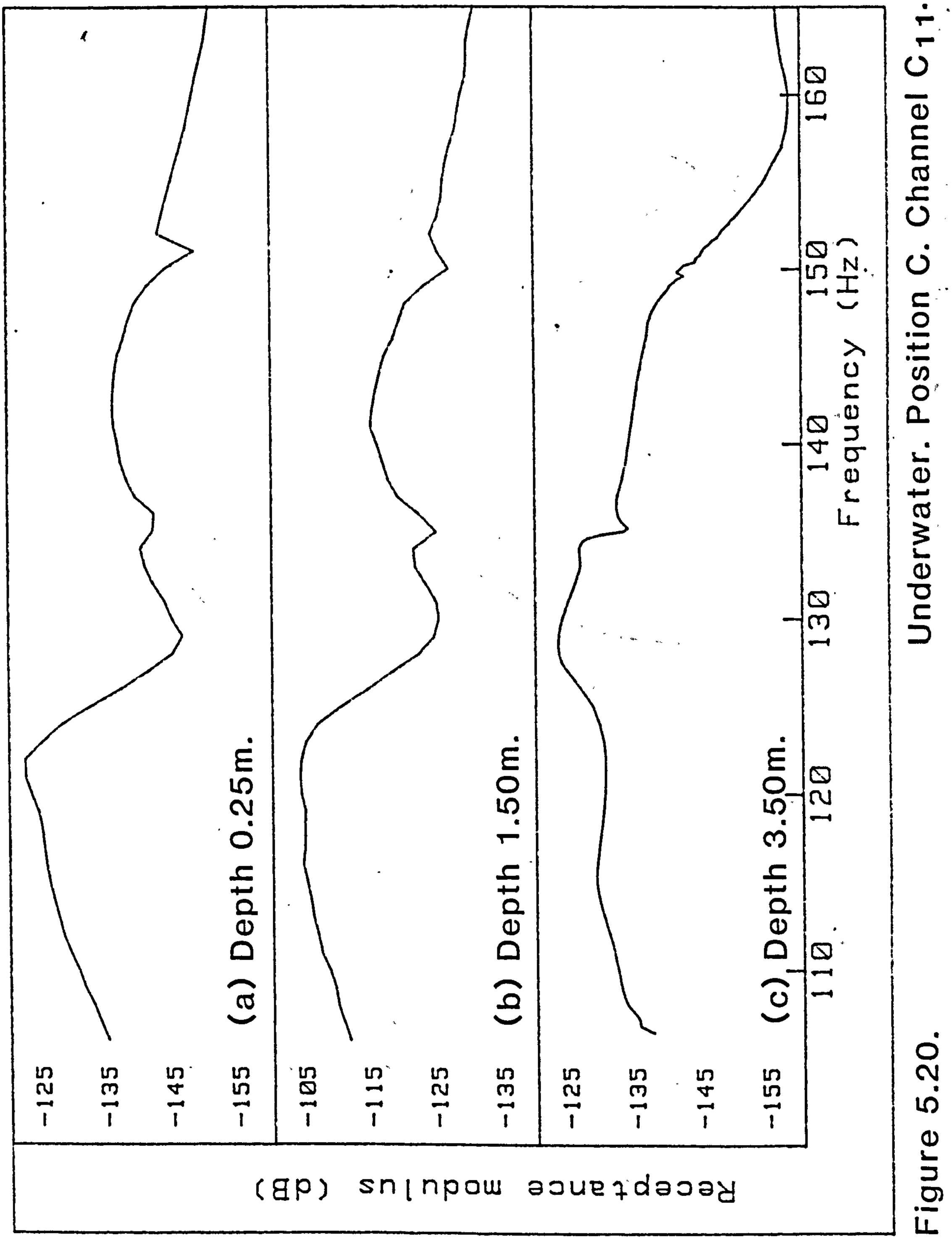

Figure 5.20. Underwater. Position C. Channel C_{11}.

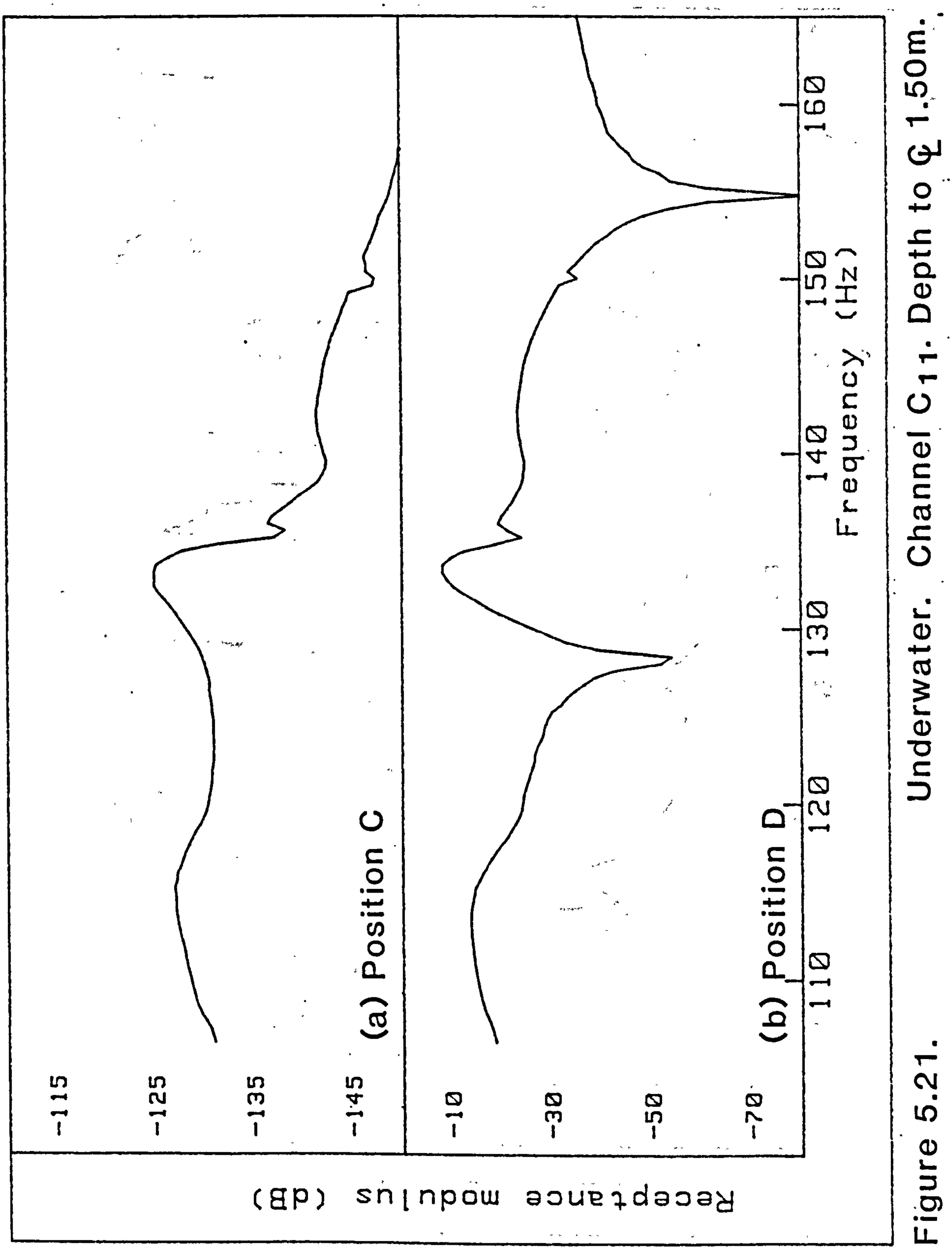
Receptance modulus (dB)
-115
-125
-135
-145
(a) Position C
-10
-30
-50
-70
(b) Position D
110
120
130
140
150
160
Frequency (Hz)
Underwater. Channel C11. Depth to ℄ 1.50m.

Figure 5.21.

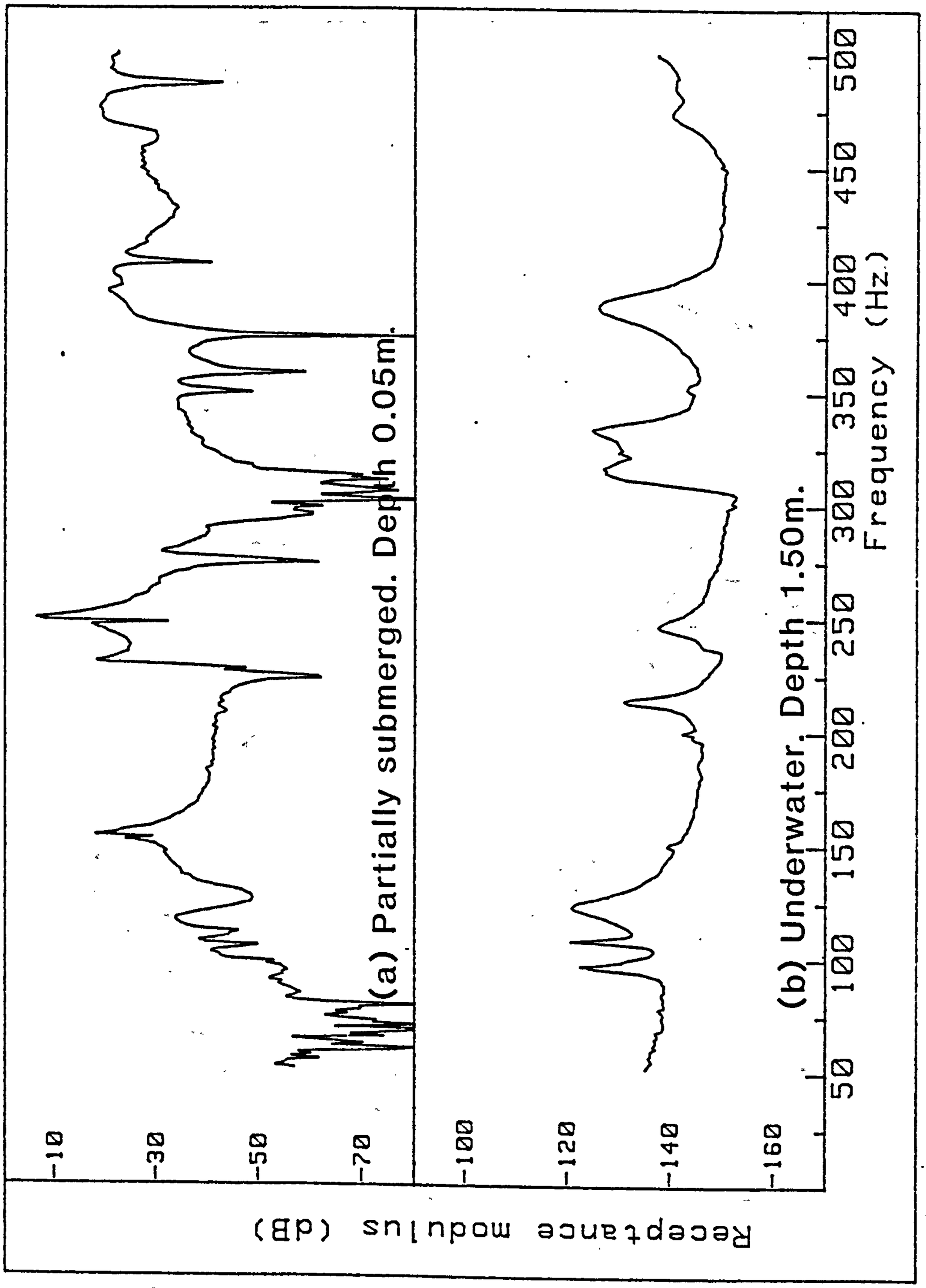
Receptance modulus (dB)
-10
-30
-50
-70
(a) Partially submerged. Depth 0.05m.
-100
-120
-140
-160
(b) Underwater. Depth 1.50m.
300
350
400
450
500
50
100
150
200
250
Frequency (Hz)
Position C. Channel C6.

Figure 5.22.

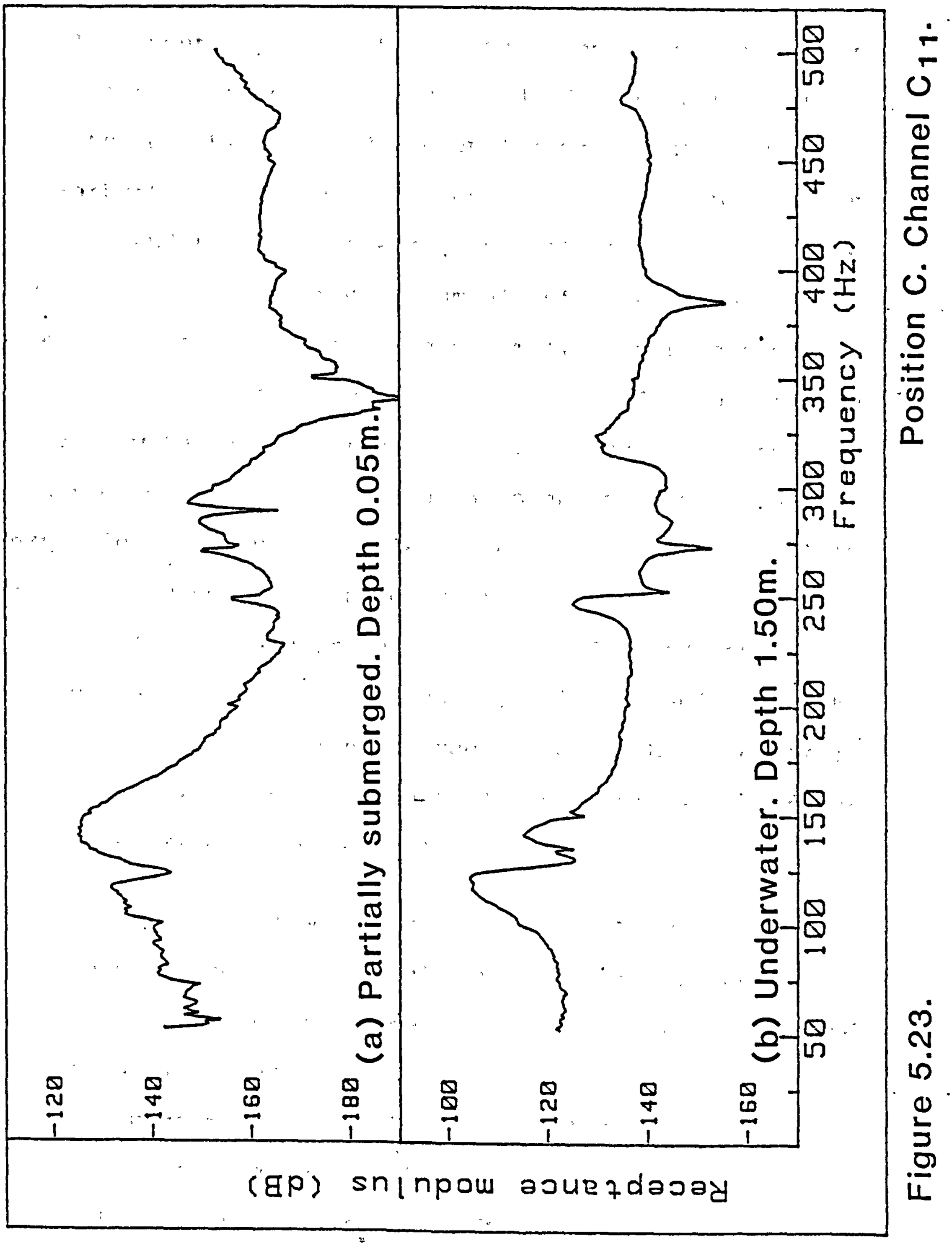
Receptance modulus (dB)
(a) Partially submerged. Depth 0.05m.
(b) Underwater. Depth 1.50m.
Frequency (Hz)
Position C. Channel C11.

Figure 5.23.

5.5 Theoretical predictions

5.5.1 Analytical

In contrast to the almost endless number of different situations from which differing experimental results can be obtained the analytical solution derived by Warburton(1961) and presented in section 3.2 is unique and refers to the response of an infinitely long cylinder in an acoustic medium of infinite extent. If the ends of the shell are simply supported then the analysis can also be used for a cylinder of finite length with an internal fluid. The supports are positioned at nodes of the axial standing wave. Further extension to situations where there is an external fluid must acknowledge that no correction is applied for the finite fluid domain or the influence of fluid actions on the closed ends, Additionally, simple end supports implies a restriction on radial motion but freedom to move in axial or tangential directions; further deviating from the practical case.

Using the dimensions of model No.2, resonance frequencies predicted by this analysis are presented in

Table 5.5. Material properties of steel and water used in the analysis are

Youngs modulus, E - $2.07*10^{11}$ N/m^2

Poissons ratio, ν - 0.29

Mass density, ρ_s - 7750 kg/m3

Fluid density, ρ - 1000 kg/m3

Table 5.5 Cylinder modes predicted by Warburtons'(1961) method.

In-vacuo		External fluid	
Mode (m,n)	Natural frequency (Hz.)	Mode (m,n)	Natural frequency (Hz.)
1,2	196.6	1,2	98.3
1,3	204.6	1,3	113.2
1,4	353.5	1,4	212.0
2,3	389.9	2,3	216.0
2,4	413.8	2,4	248.2
1,5	564.2	2,2	327.8
3,4	574.1	3,4	344.5
2,5	590.6	1,5	360.4
2,2	653.2	2,5	376.9
3,5	662.0	3,3	401.7
3,3	724.6	3,5	422.4

5.5.2 Finite element analysis

A finite element approach has been adopted for the three dimensional hydroelasticity analysis detailed in chapter 3 and commences with a dry or in-vacuo analysis in which the structure vibrates freely in the absence of any structural damping or external forces. This section will concentrate on the modelling of the dry structure using PAFEC and NASTRAN finite element codes.

Most of the work performed during this investigation was undertaken using PAFEC code on the CDC Cyber 180/840 at RNEC Manadon. The NASTRAN programme only became available at a comparatively late stage when alternative choices were being sought owing to the difficulties which had been encountered using PAFEC. Within the PAFEC code four element types were selected to determine

modes and natural frequencies of a circular cylindrical shell.

i. Three noded thin shell of revolution element -42130

ii. Eight noded semi-Loof curved shell element -43210

iii. Four noded facet shell element -44200

iv. eight noded facet shell element -44210

Any finite element analysis will be a compromise between the accuracy of the solution and the amount of effort and cost involved in producing that result. These two conflicting requirements are linked by the selection of a suitable size of finite element, the assumption being that progressively more refined meshes will produce more accurate results. In the dynamic analysis of a cylindrical shell the mesh employed must be capable of reproducing all the required axial and circumferential motions. One of the advantages of using thin shell of revolution elements is that there is no restriction on circumferential distortion as the harmonic number is part of the input data. The only considerations therefore, are the number of modes to be analysed and the number of axial elements to reproduce the corresponding motions. Computer resources were not unlimited and it was reasonable to restrict attention to the first five modes of vibration. Inspection of Table 5.1 shows that the axial wavelength number will not exceed 2 until mode 7 and there was very rapid

convergence of the solution starting from the very crudest idealisation using 4 longitudinal elements. The converged solution shown in Table 5.7 uses 16 elements with a total of 33 nodes and 132 degrees of freedom. The default of 60 automatic master degrees of freedom was used.

Table 5.7 Natural frequencies of model No.2 using PAFEC 42130 elements.

Mode No. / Harmonic No.	1	2	3	4
0	216.5*	224.2*	845.1	859.7
1	448.0*	449.1*	877.3	1293.0
2	197.6	641.2	736.6	738.3
3	201.3	391.3	724.1	1067.5
4	344.4	408.7	574.8	824.9

(* denotes end mode.)

There is a limited application for thin shell of revolution elements and for more general use alternative shell elements must be examined. Semi-Loof curved shell elements would appear to be well-suited for this type of analysis, however notable difficulties were encountered during their use for models Nos.2 and 3 (Randall (1988)). Using the derived natural frequencies as the assessment criteria it appeared that convergence was very rapid even for relatively coarse meshes but examination of the mode shapes revealed several anomalies. Excessive deflections of mid-side nodes, shown greatly exagerated in Figure 5.24 produces distorted mode shapes. Contrary to the published

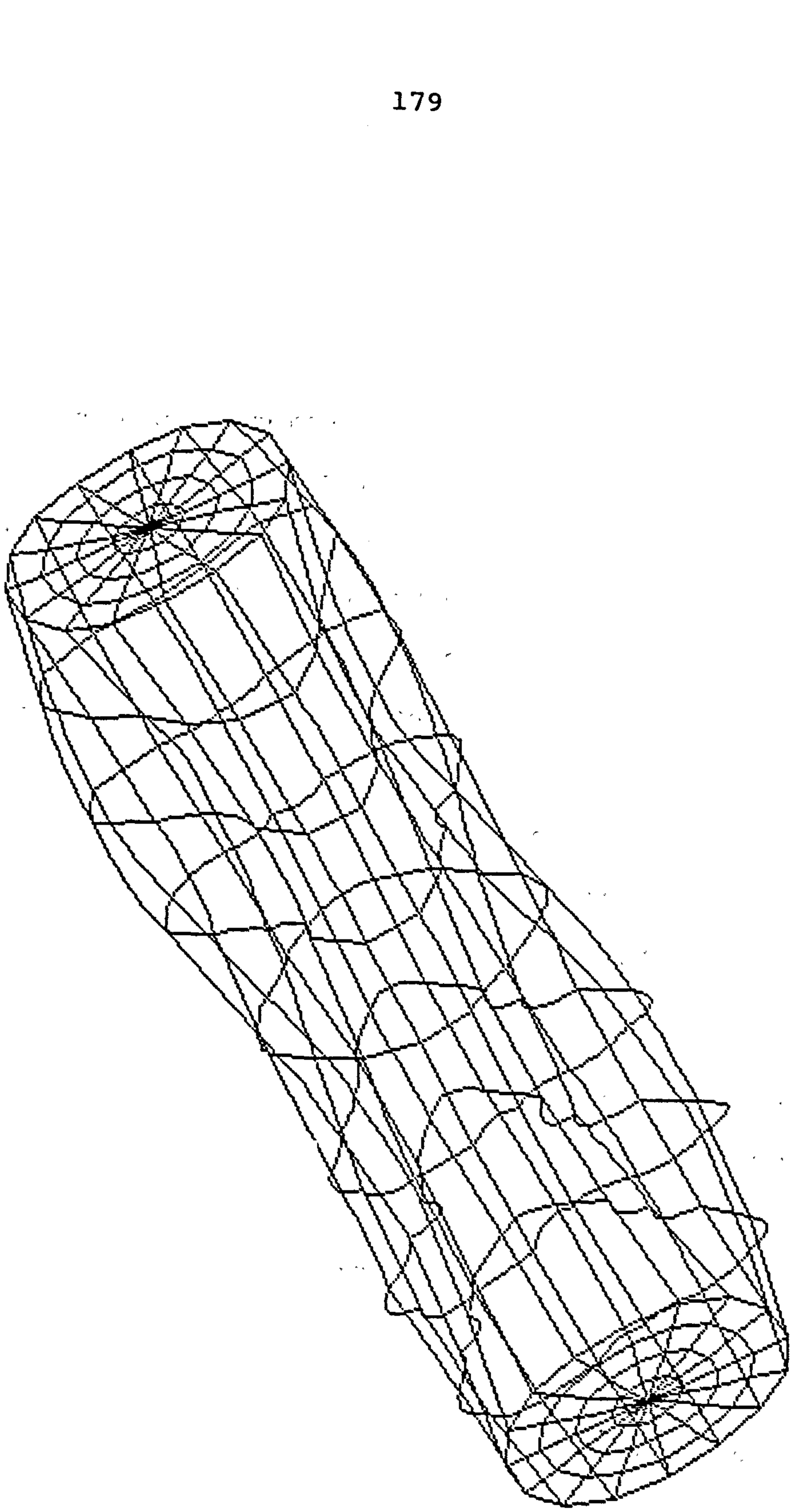

Figure 5.24 PAFEC 42100 (semi-Loof) elements.
Distortion mode 11 (m=2,n=3) using Gaussian integration 2x2.

recommendations (Henshall (1984)) this could be improved by increasing the number of Gaussian integration points (Fig.5.25). As the mesh size was reduced further there was evidence of divergence, especially at higher modes, and asymmetry of axial mode shapes (Fig.5.26). Automatic master degrees of freedom were used throughout this stage of the dry structure analysis and the solution is obviously highly dependant on the position and number of master degrees of freedom selected. This uncertainty lead to the conclusion that semi-Loof elements could give good results but must be used with caution both regarding order of integration and shell geometry. In both instances a prior knowledge of the solution although not essential greatly enhances the degree of certainty with which the results can be viewed.

Although less sophisticated than semi-Loof elements more acceptable results were obtained using facet shell elements. Convergence was obtained rather slowly, at the expense of a large number of elements but importantly the derived mode shapes had a smooth outline and were generally symmetric (Fig. 5.27). Two element types (PAFEC 44200 and 44210) were examined and convergence assessed in relation to mesh size and number and position of master degrees of freedom. These parameters were examined separately despite the fact that mesh size directly affects the total number of

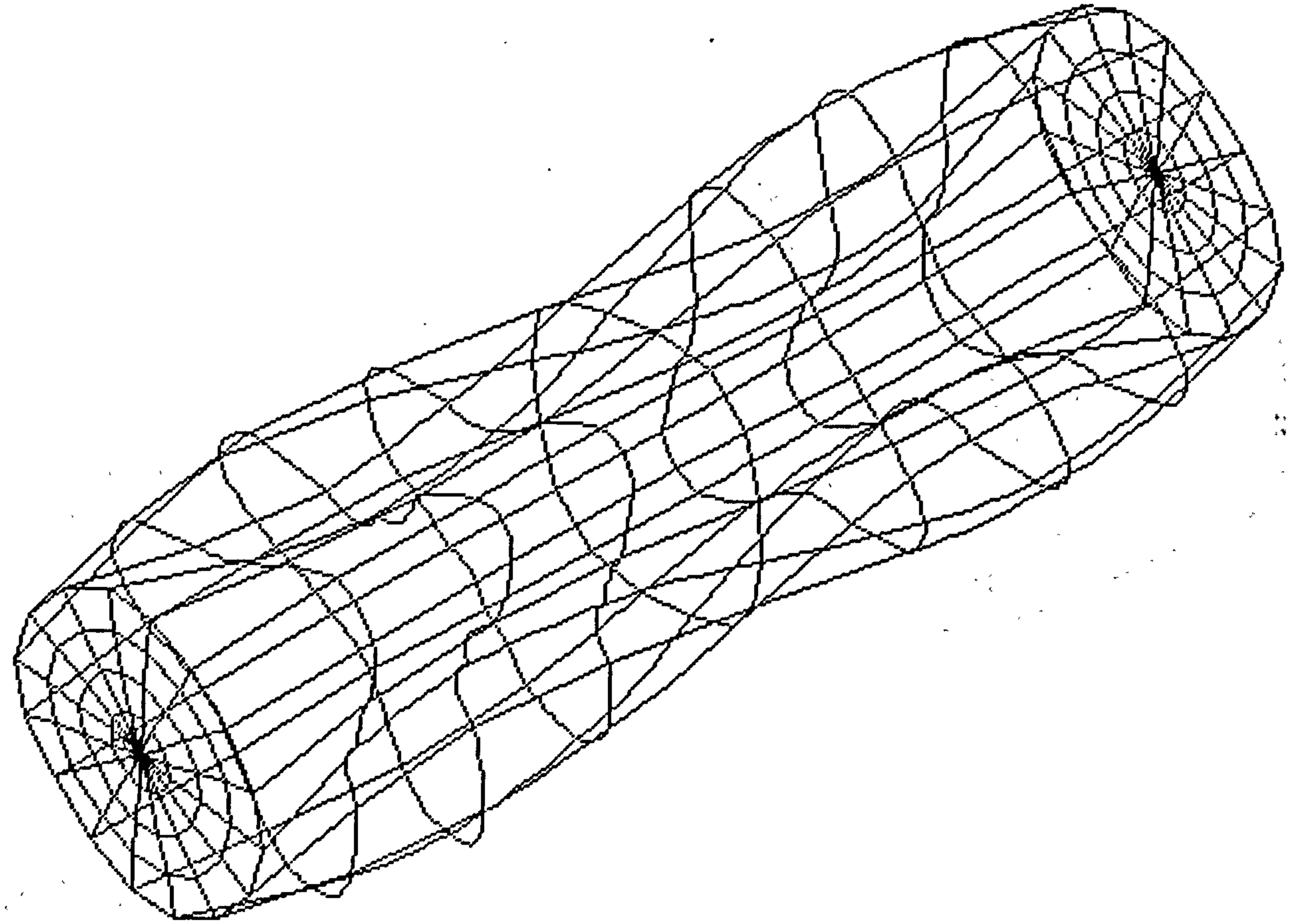

Figure 5.25

Distortion mode 11 (m-2,n-3) using PAFEC 42100 (semi-Loof) elements.

Gaussian integration 3x3.

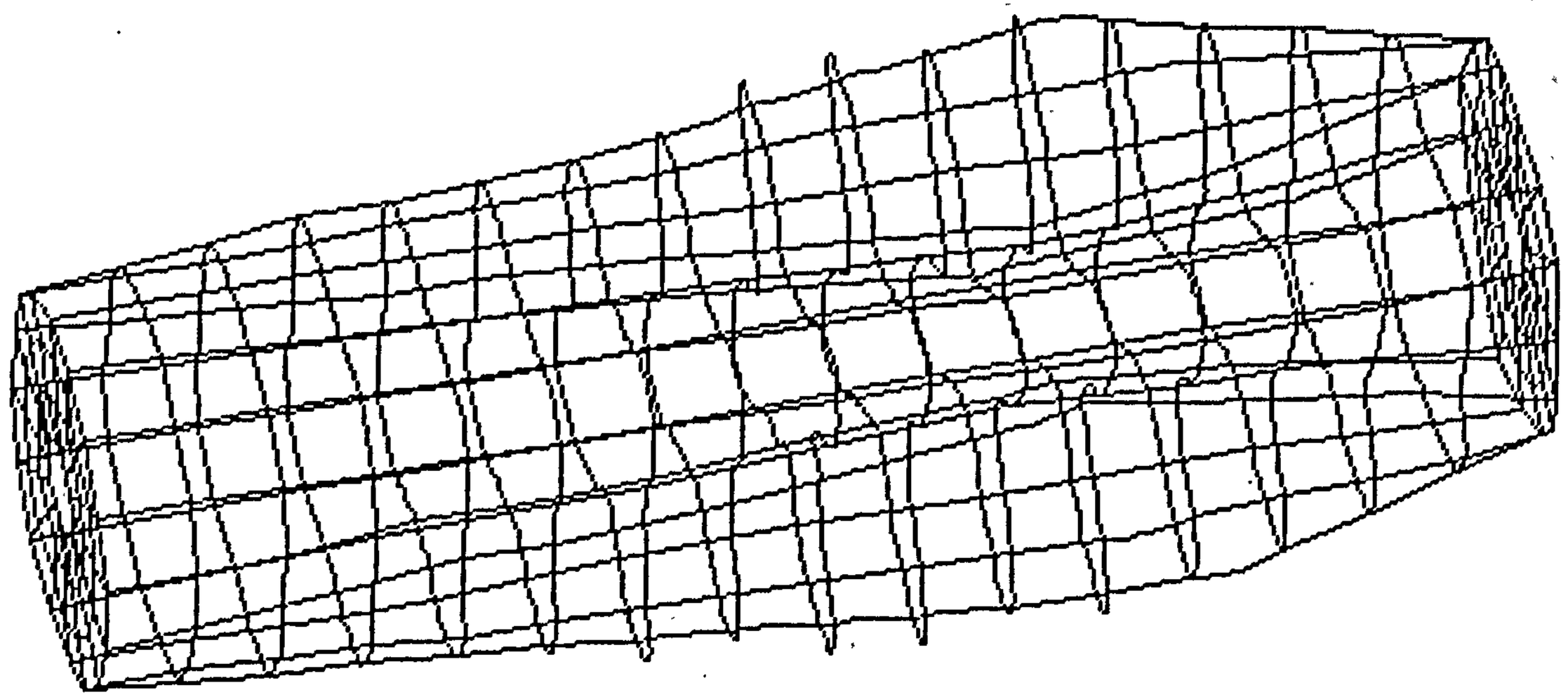

Figure 5.26

Distortion mode 15 (m=1,n=4) using PAFEC 42100 (semi-Loof) elements.
Gaussian integration 2x2.

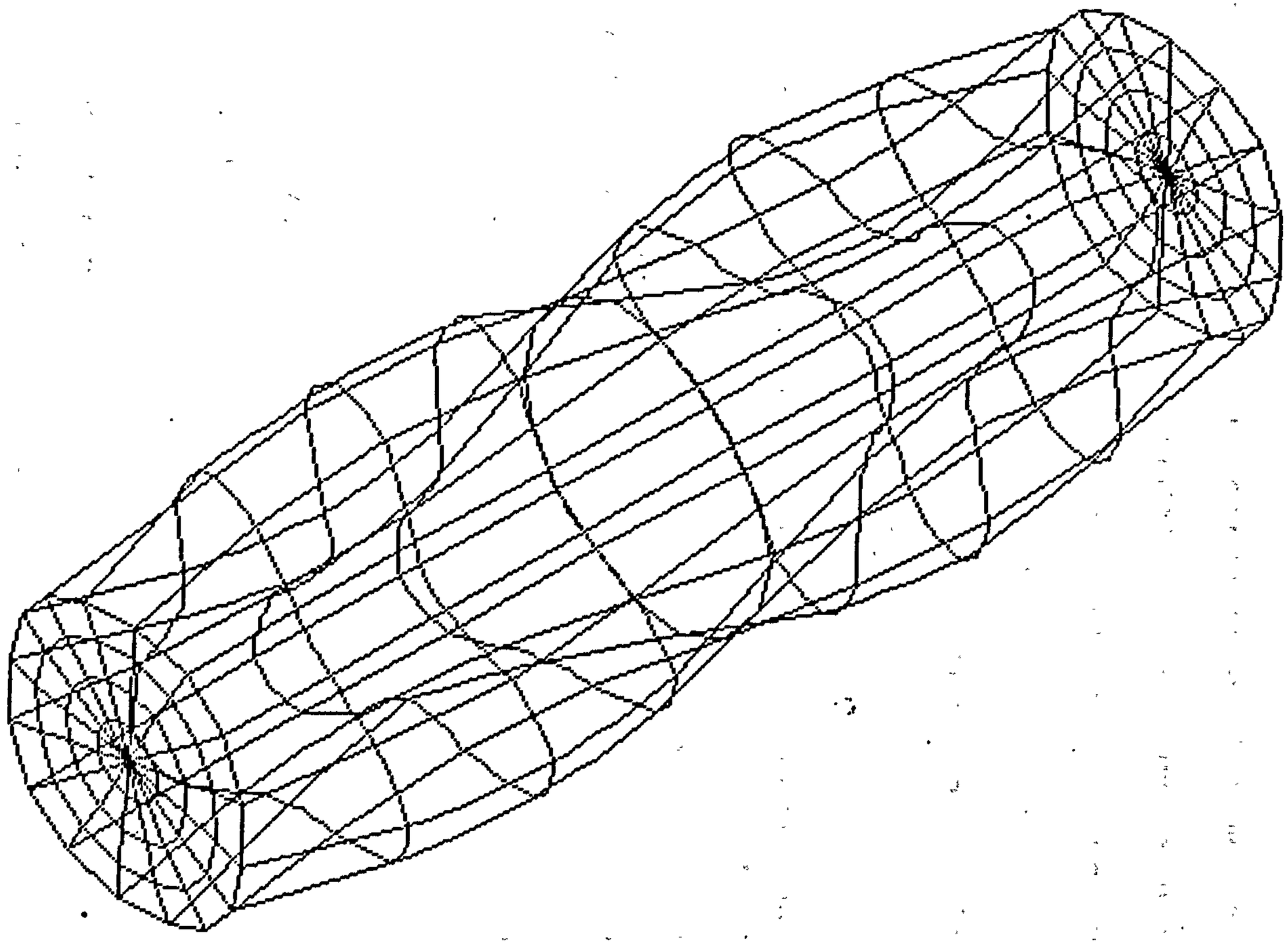

Figure 5.27

Distortion mode 11 (m=2,n=3) using PAFEC 44210 (facet) elements.

degrees of freedom of the structure and the ratio of slave to master degrees of freedom will affect the final accuracy of the solution. Nevertheless an estimate of the validity of the solution was obtained.

All cylindrical structures vibrate with a combination of axial and circumferential motion but for the aspect ratios of model No.2 circumferential motion was more critical than axial motion. The model was divided into 8 sections longitudinally and the number of elements around the circumference varied. The results are given in Table 5.8.

Table 5.8 Natural frequencies of model No.2 using PAFEC 44200 elements. 100 automatic dof.

	Mesh	8x12	8x18	8x24
	Elements	192	288	576
Mode (m,n)	DoF	1258	1882	3562
e1	(216.5)	171.36	175.02	189.13
e2	(224.2)	178.90	186.03	203.07
1,2	(197.6)	211.70	215.72	209.71
1,2		213.05	217.65	215.72
1,3	(201.3)	215.55	219.30	217.95
1,3		217.72	222.92	227.24
1,4	(344.4)	377.32	383.89	395.19
1,4		378.94	384.75	409.34
e3	(448.0)	373.77	381.62	408.39
e4	(449.1)	374.46	384.44	410.44

From these results it was concluded that the four noded facet shell element (44200) was not sufficiently accurate. This assessment was based on the magnitude of the two natural frequencies given for each mode rather than the divergence exhibited by both frequencies in

relation to the thin shell of revolution benchmark and between themselves. This divergence was more likely caused by the increase in slave to master degrees of freedom ratio.

The problem of two values for the natural frequency for each mode is not confined to this particular element type. For a circular cross-section there are theoretically, an infinite number of modes occuring simultaneously on any plane between 0 and 360 degrees. This infinite variation can be obtained by a linear combination of the two orthogonal mode shapes given. Numerically these natural frequencies should be equal and the difference shown above highlights errors caused by the dynamic reduction technique used in PAFEC.

The procedure described above for the 44200 element was repeated for the eight noded facet shell element (44210) with the improved accuracy shown in Table 5.9.

Table 5.9 Natural frequencies of model No.2 using PAFEC 44210 elements.

Mesh	10x8	8x12	8x16	8x18	12x24
Elements	144	192	256	288	576
DoF	2280	2998	3994	4492	9058
Masters	37+50	102+20	0+100	0+100	0+100
Mode (m,n)					
1,2	195.0	196.5	197.7	198.3	199.3
1,2	204.7	201.3	198.4	198.7	200.1
1,3	226.1	208.3	206.1	205.5	205.1
1,3	230.0	208.9	206.3	206.1	205.8
e1	234.1	212.6	203.0	201.7	211.6
e2	248.6	224.8	211.9	210.5	227.0
1,4	390.7	370.1	361.8	360.6	360.5
1,4	454.1	372.4	363.4	362.6	362.9
2,3	409.6	401.1	406.2	406.9	412.6
2,3	422.1	406.8	408.1	411.2	413.7

To assess the influence of the number of master degrees of freedom on the overall accuracy of the solution it was varied for two mesh sizes.

Table 5.10 Natural frequencies of model No.2 using PAFEC 44210 elements with differing master degrees of freedom.

Mesh		8x18			12x24	
Elements		288			576	
DoF		4492			9058	
Masters	100	150	200	100	150	200
Mode (m,n)						
1,2	198.3	197.0	198.2	199.3	199.8	199.1
1,2	198.7	198.4	199.5	200.1	202.4	200.7
1,3	205.5	204.5	204.4	205.1	204.4	203.6
1,3	206.1	205.3	205.6	205.8	206.1	205.5
e1	201.7	201.4	201.7	211.6	209.6	208.5
e2	210.5	209.9	210.6	227.0	218.8	217.6
1,4	360.6	356.4	355.1	360.5	356.1	353.0
1,4	362.5	359.8	358.2	362.9	361.9	358.0
2,3	406.9	404.6	399.3	412.6	405.2	401.0
2,3	411.2	407.9	407.7	413.7	408.7	404.9

Two problems remained at this stage, the numerical

difference between the natural frequencies of the two orthogonal mode shapes and the orientation of these mode shapes which were not generally port-starboard symmetric. This symmetry was necessary to take advantage of economies offered by the composite source distribution method used and could be corrected by careful selection of manual master degrees of freedom in a symmetric pattern. The other problem of two numerically different natural frequencies for essentially the same mode shape was not overcome until the programmes were re-run using eight noded quadrilateral elements in the NASTRAN package on a Cray computer at ULCC.

Table 5.11 Natural frequencies of model No.2 using NASTRAN 8 noded quad. shell elements.

Mode (m,n)	Mesh Elements	8x16 256	16x32 768
1,2	(197.6)	197.44	197.21
1,2		197.44	197.21
1,3	(201.3)	203.81	203.55
1,3		203.81	203.55
e1	(216.5)	198.60	212.39
e2	(224.2)	206.61	220.61
1,4	(344.4)	350.84	349.56
1,4		350.84	349.56
2,3	(391.3)	393.85	391.18
2,3		393.85	391.18
2,4	(408.7)	416.15	412.21
2,4		416.15	412.21

5.5.3 Wet Analysis

To complete this chapter results of wet analyses for some of the finite element solutions from the previous section are presented. The method of evaluating the

hydrodynamic properties has been described in section 3.4.2 and will depend upon the position of the structure and depth of water, the number of fluid panels used in the analysis and the accuracy of the finite element analysis.

The results in Table 5.12 are for an analysis which uses data from a finite element model using semi-Loof elements. The derived mode shapes have already been identified as erroneous with regard to the relative displacements between corner and mid-side nodes and the mode shapes do not have the port-starboard symmetry required by the composite source method (Fig. 5.28). No attempt has been made to revolve the mode shapes into a better orientation, the one most nearly satisfying the symmetry condition having been selected. These results are included to indicate the sensitivity of the wet analysis to a relatively poor choice of dry structural modes. The wet surface of the cylinder was discretised into 384 elements using a one-to-one correspondence between fluid and structural elements.

Table 5.12 Resonance frequencies of model No.2 using PAFEC 43210 elements.

Depth to CL of model - 0.68m

Mode (m,n)	Depth of water	1.6m	
e1		74.0	90.6
e2		83.1	101.4
1,2		93.8	109.2
1,3		110.3	120.1
1,4		241.3	237.5
2,3		246.4	264.6

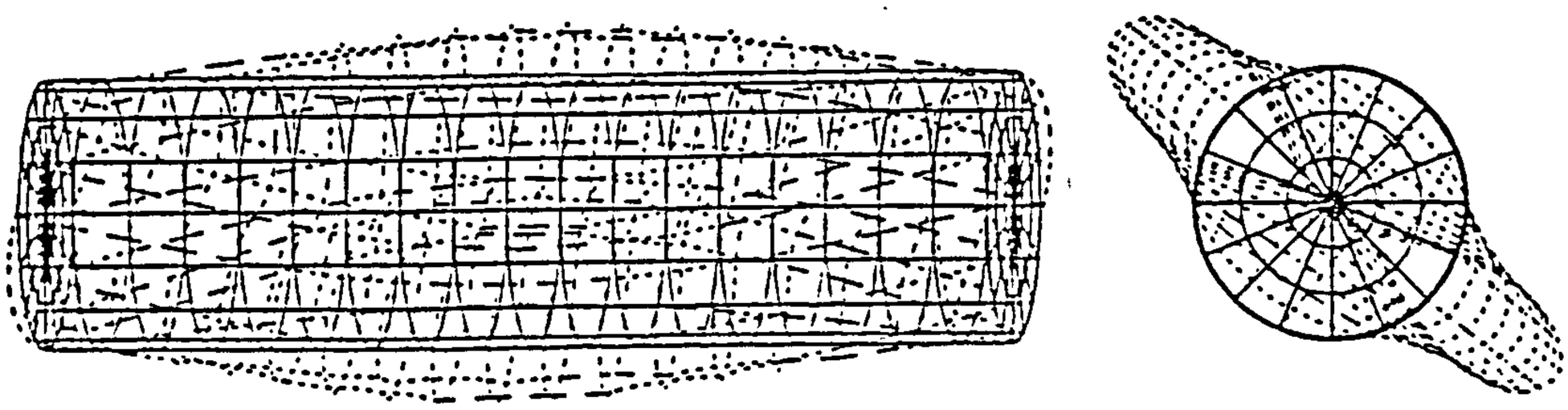

m=1, n=2 199.1 Hz

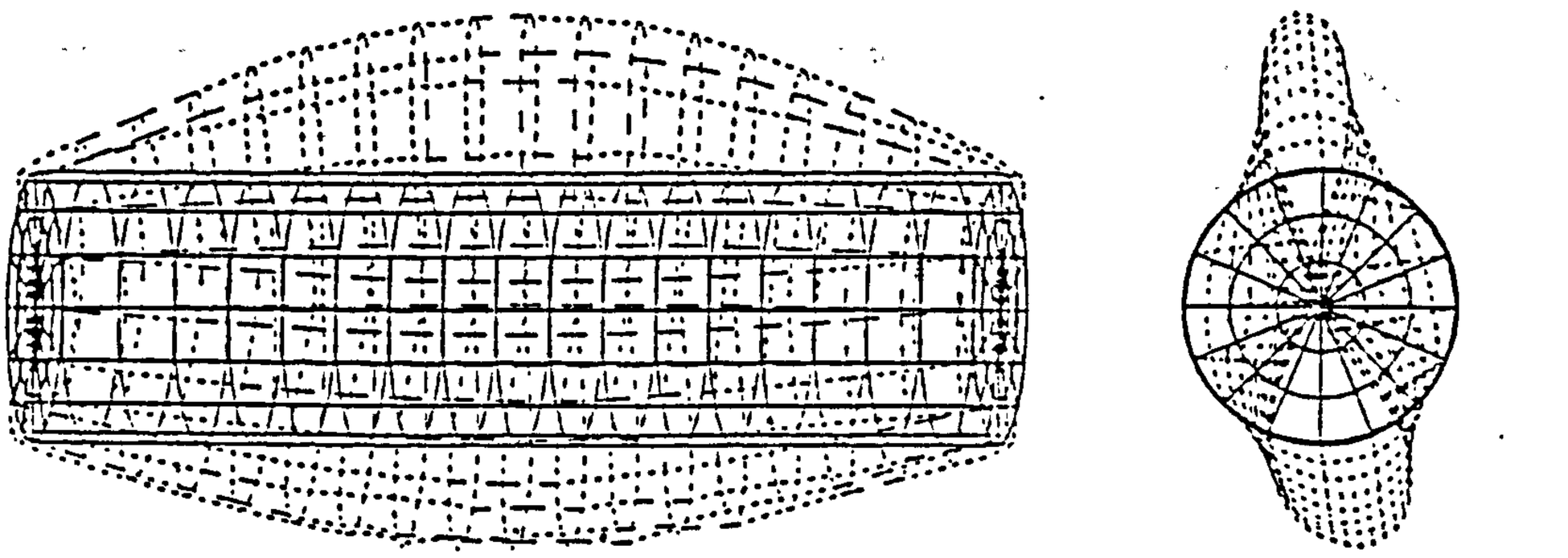

m=1, n=2 200.1 Hz

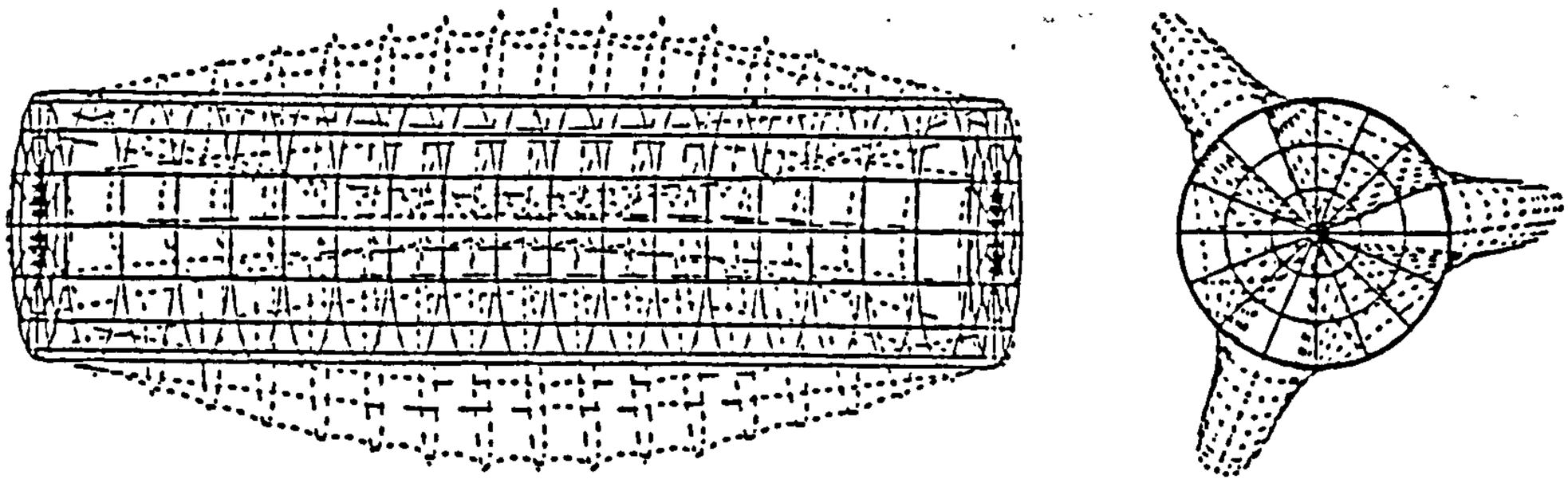

m=1, n=3 202.9 Hz

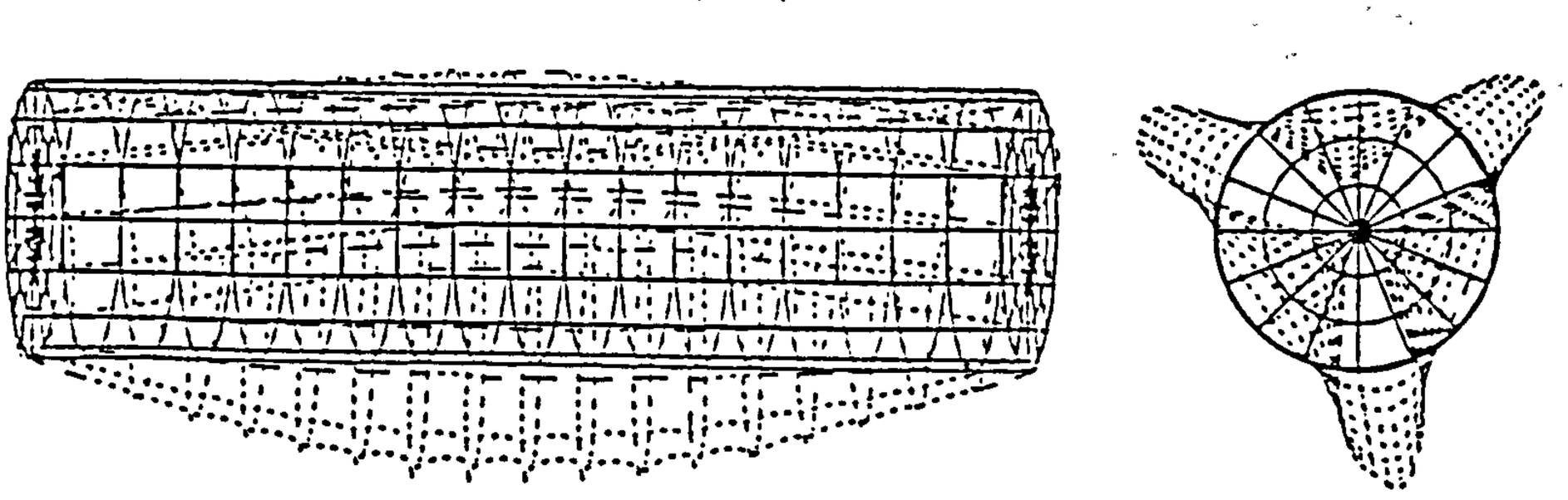

m=1, n=3 203.3 Hz

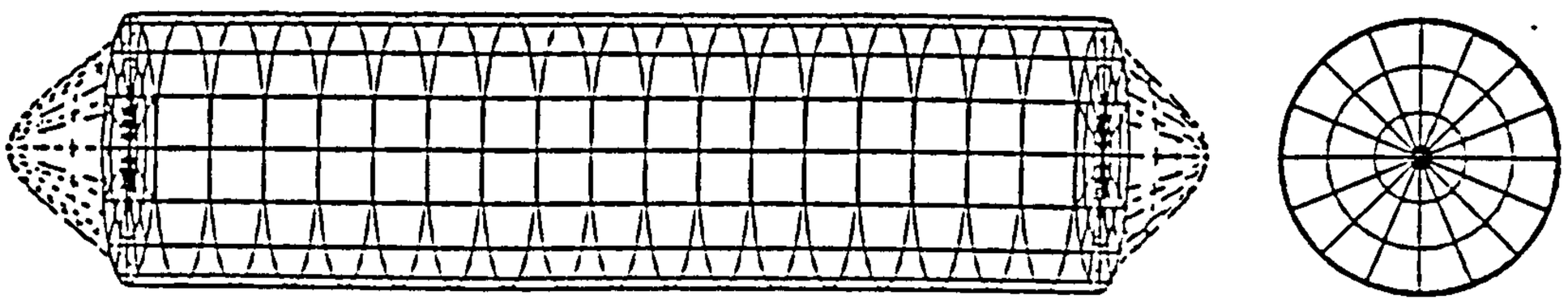

209.2 Hz

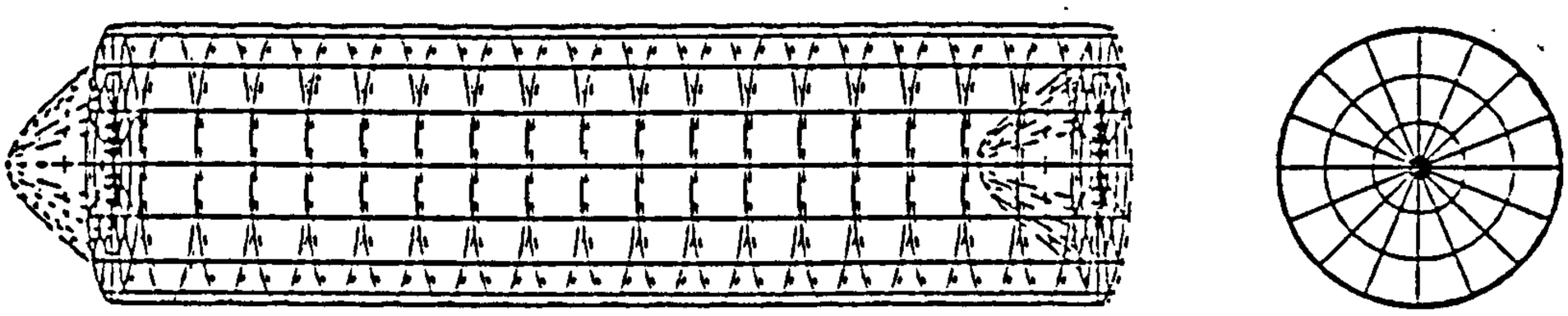

218.0 Hz

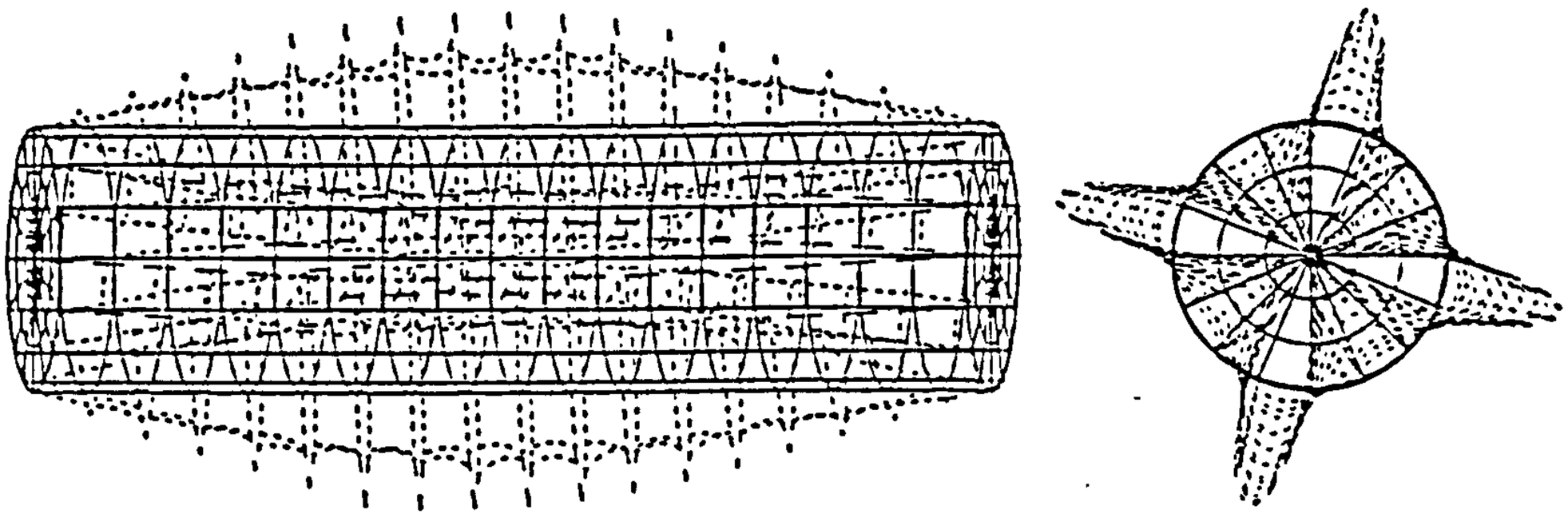

m=1, n=4 352.5 Hz

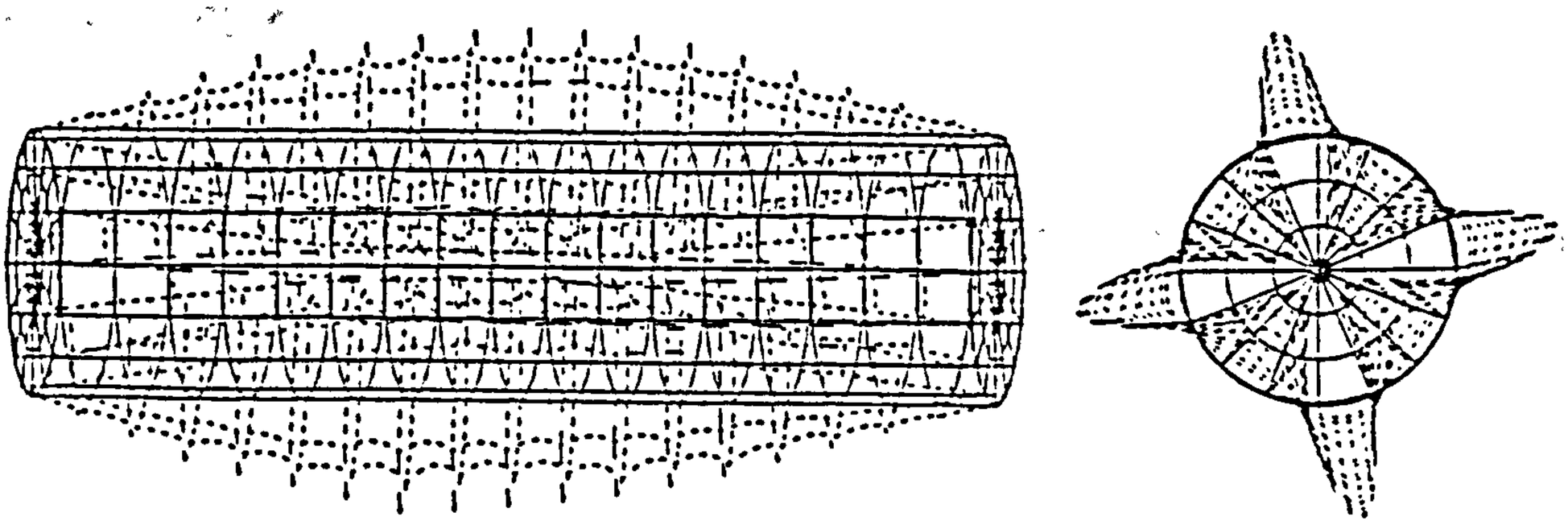

m=1, n=4 353.7 Hz

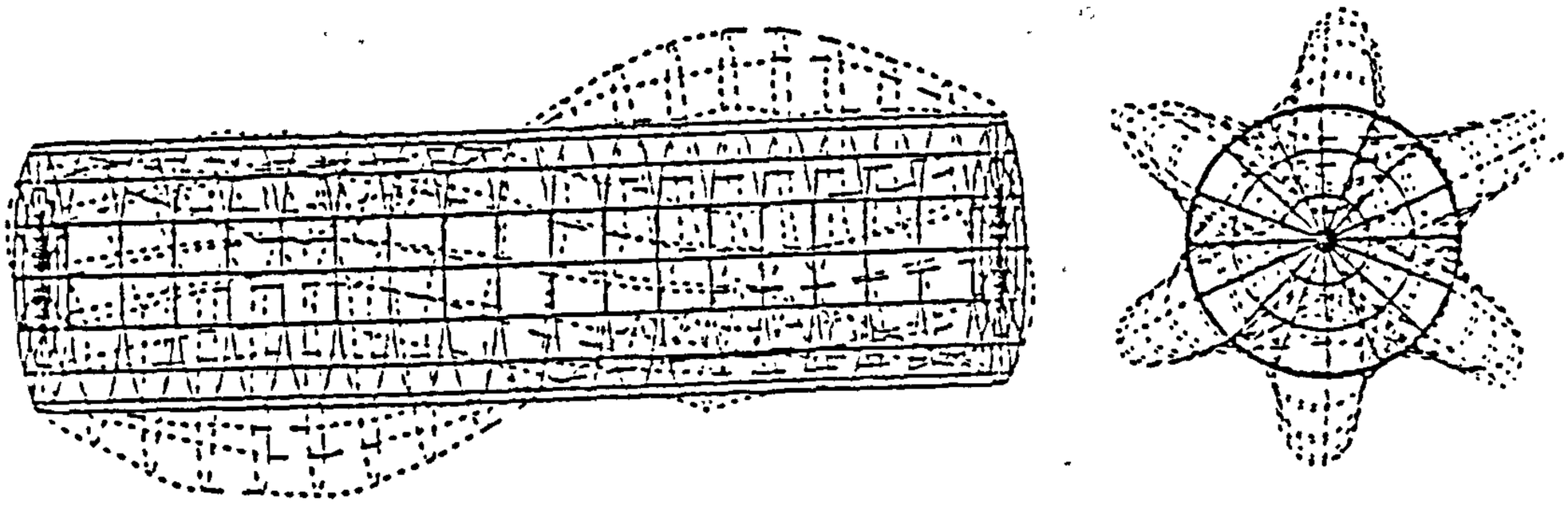

Figure 5.28

Mode shapes and natural frequencies obtained with PAFEC semi-Loof elements used in wet analysis.

An improved dry analysis was obtained for the same model with 384 elements by using facet shell elements, the wet modes calculated from this analysis are shown below.

Table 5.13 Resonance frequencies of model No.2 using PAFEC 44210 elements.

Depth of water / Depth of CL of model	% 0.68	1.6 0.68	1.6 1.18	1.6 1.305
Mode (m,n)				
e1	96.0	79.4	77.7	76.9
1,2	102.4	87.6	87.3	85.7
e2	106.8	88.8	87.4	86.4
1,3	126.8	119.6	119.3	118.4
2,3	250.0	237.7	237.2	235.5
1,4	262.6	288.9	289.4	289.6

The analysis of dry modes computed from the NASTRAN code was used from this point on (Fig 5.29). The results from both models detailed in table 5.11 were used. The model with the coarser mesh (256 elements) formed the basis of a convergence test to assess the effect of increasing the number of panels in the model, the other model (768 elements) was used to determine resonance frequencies over a range of depths comparable to Table 5.13 above.

The convergence test was performed for a finite (1.6m.) and infinite depth of water and the number of panels on the curved portion of the cylinder was progressively refined. A one to one correspondence

between panels and finite elements, which was the starting point for the analysis, was retained throughout for the end plates.

Table 5.14 Convergence test for NASTRAN model. 256 structural elements.

Depth to CL of model - 0.68m

Depth	∞			1.6		
Mesh	8x16	16x16	16x32	8x16	16x16	16x32
No of panels	256	384	768	256	384	768
Mode (m,n)						
e1	87.0	85.0	87.0	72.7	70.5	72.4
e2	96.0	93.5	96.0	80.4	78.0	80.0
1,2	103.0	102.0	100.0	102.0	87.6	84.4
1,3	117.0	116.0	109.0	119.0	106.8	93.5
2,3	248.0	239.0	226.0	251.0	226.0	194.0
1,4	252.0	250.0	223.0	290.0	276.0	213.0
2,4	284.0	275.0	247.0	272.0	268.0	223.0

It is anticipated that an increase in the number of panels on the model will enhance the accuracy of the solution. As it has been shown that the dry analysis is a critical factor in obtaining accurate results, the more refined model (768 elements) was then used in a wet analysis; the same mesh was used for the panel discretisation.

Table 5.15 Resonance frequencies of model No.2 using NASTRAN model (768 elements).

Depth of water	∞	1.6	1.6	1.6	1.6
Depth of CL of model	0.68	0.68	0.93	1.18	1.38
Mode (m,n)					
e1	93.4	78.0	77.0	76.0	74.0
1,2	99.2	83.6	83.5	83.1	78.1
e2	102.5	86.0	84.8	84.0	82.0
1,3	114.6	98.1	98.1	98.0	95.0
2,3	225.6	194.0	193.6	193.5	187.0
1,4	218.0	208.2	208.2	208.3	205.3
2,4	260.9	250.2	250.3	250.4	246.9

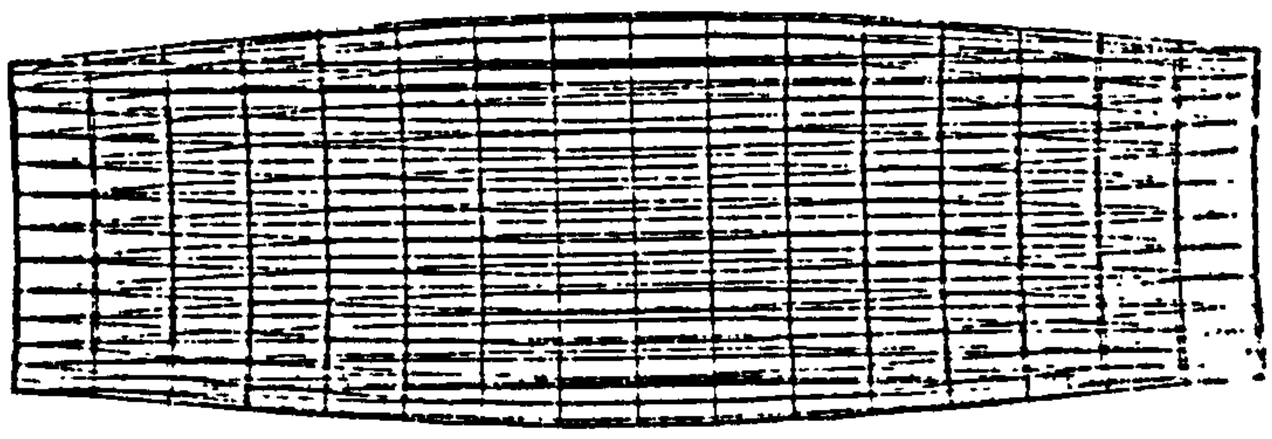

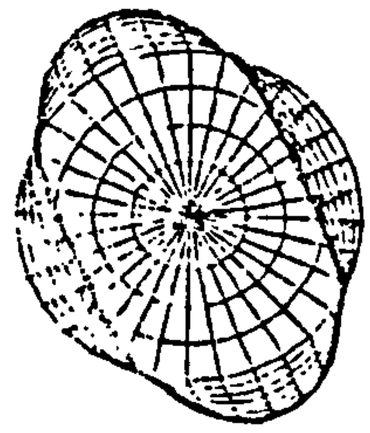

VIBRATION OF THE CYLINDER IN VACUO
LANCHOS METHOD

MODAL DEFOR. SUBCASE 1 MODE 1 FREQ. 197.2162

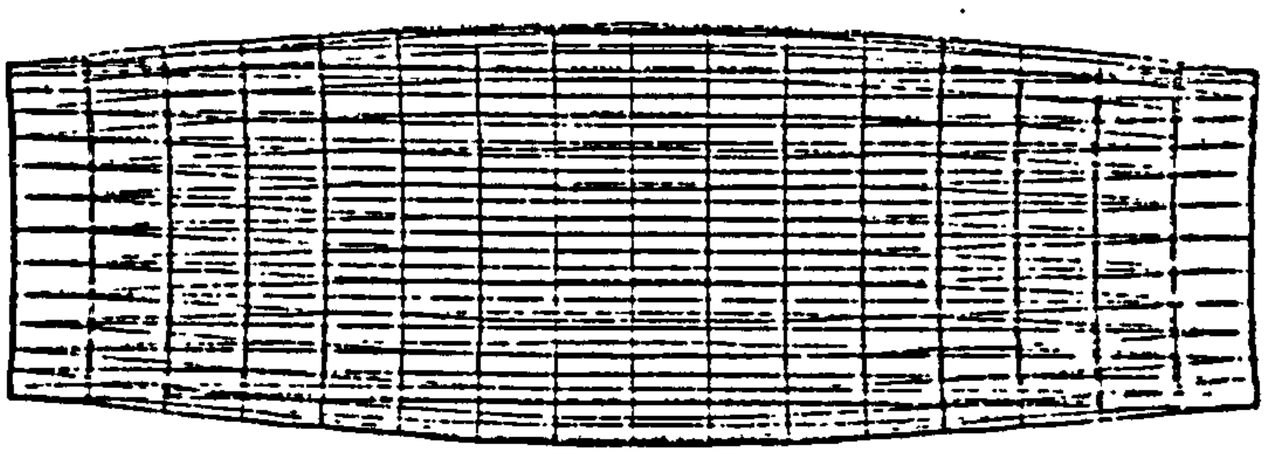

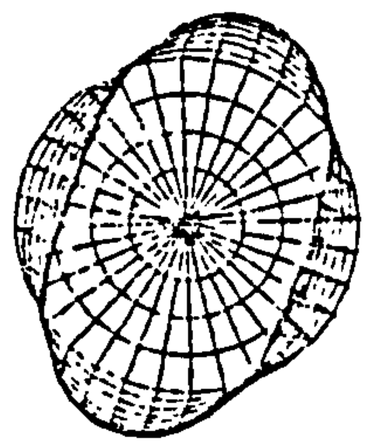

VIBRATION OF THE CYLINDER IN VACUO
LANCHOS METHOD

MODAL DEFOR. SUBCASE 2 MODE 2 FREQ. 197.2166

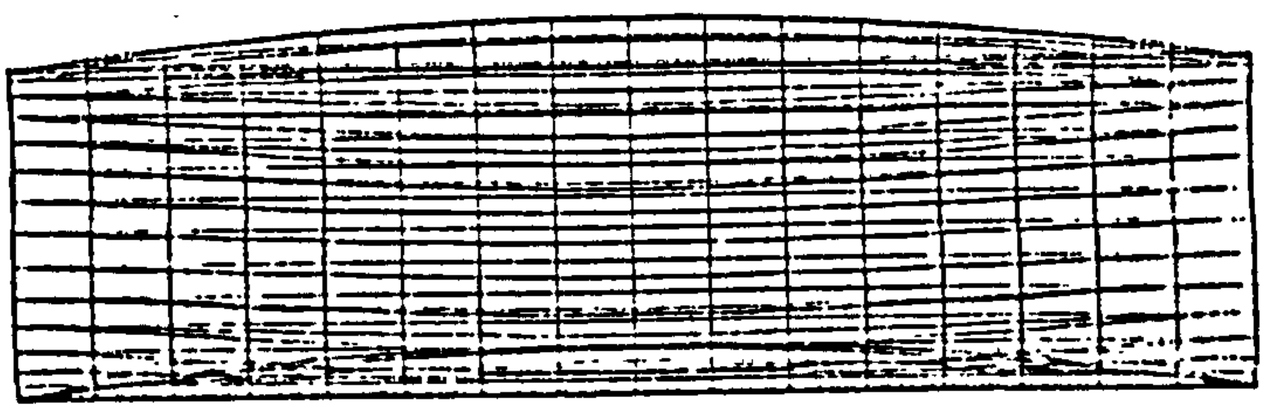

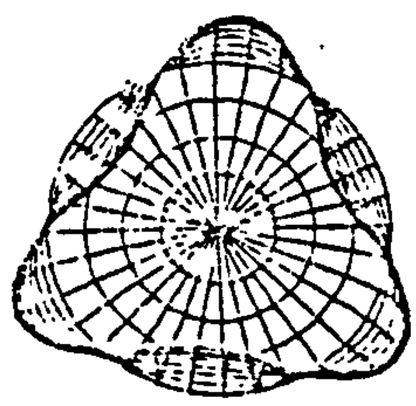

VIBRATION OF THE CYLINDER IN VACUO
LANCHOS METHOD

MODAL DEFOR. SUBCASE 3 MODE 3 FREQ. 203.5523

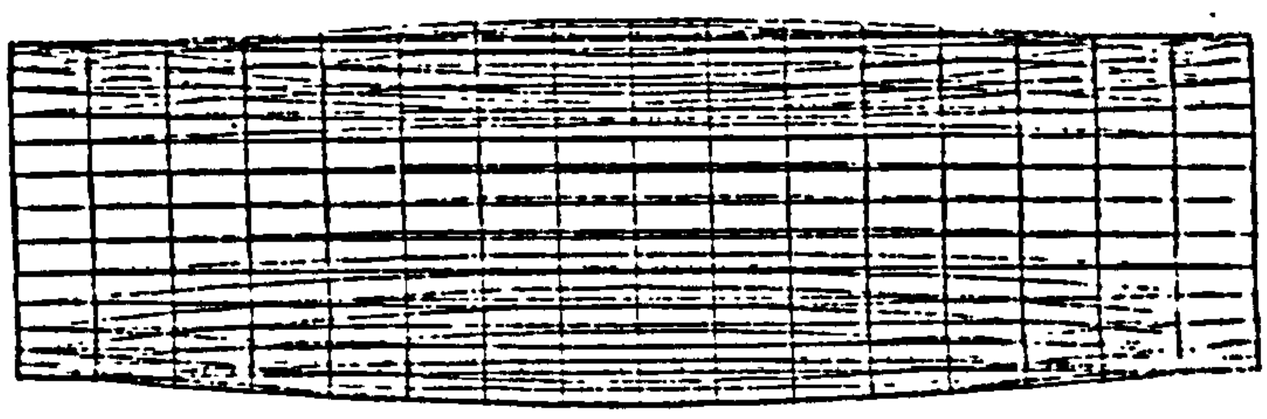

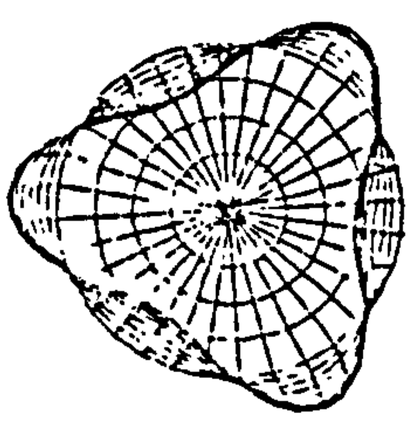

VIBRATION OF THE CYLINDER IN VACUO
LANCHOS METHOD

MODAL DEFOR. SUBCASE 4 MODE 4 FREQ. 203.5523

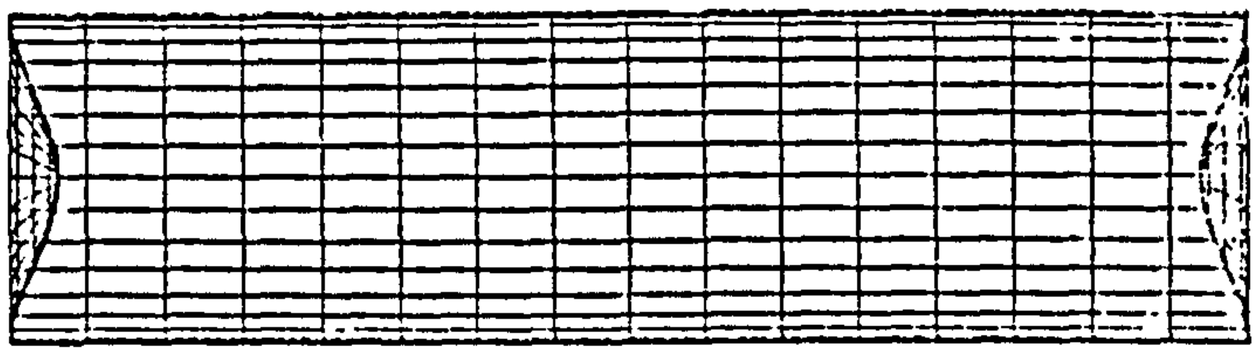

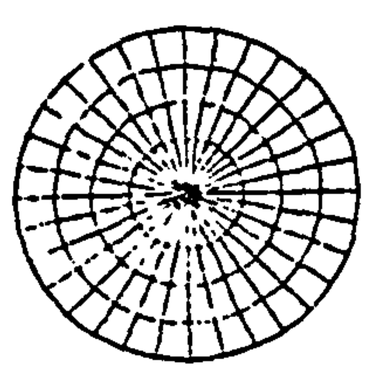

VIBRATION OF THE CYLINDER IN VACUO
LANCHOS METHOD

MODAL DEFOR. SUBCASE 5 MODE 5 FREQ. 212.3961

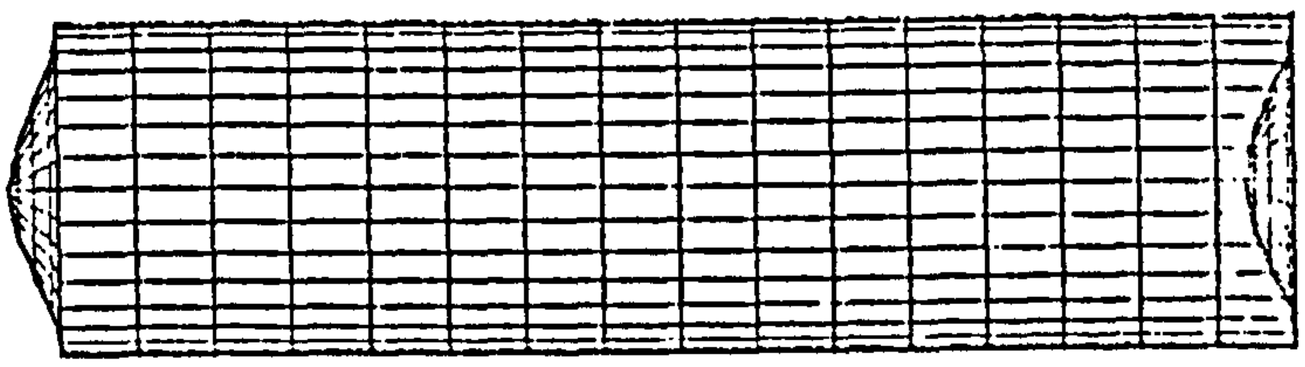

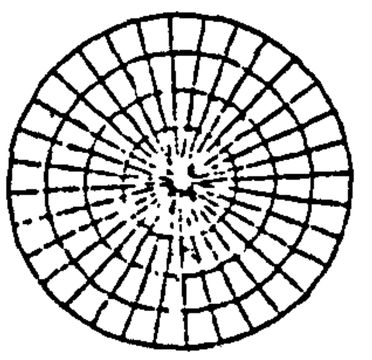

VIBRATION OF THE CYLINDER IN VACUO
LANCHOS METHOD

MODAL DEFOR. SUBCASE 6 MODE 6 FREQ. 220.6156

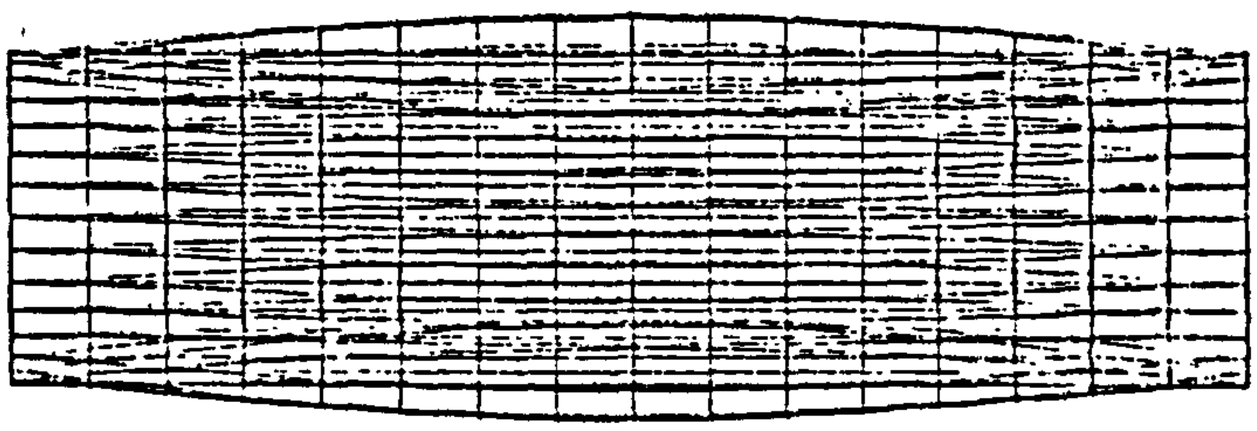

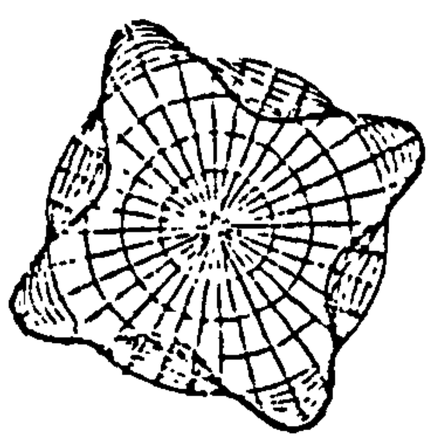

VIBRATION OF THE CYLINDER IN VACUO
LANCHOS METHOD

MODAL DEFOR. SUBCASE 7 MODE 7 FREQ. 349.5635

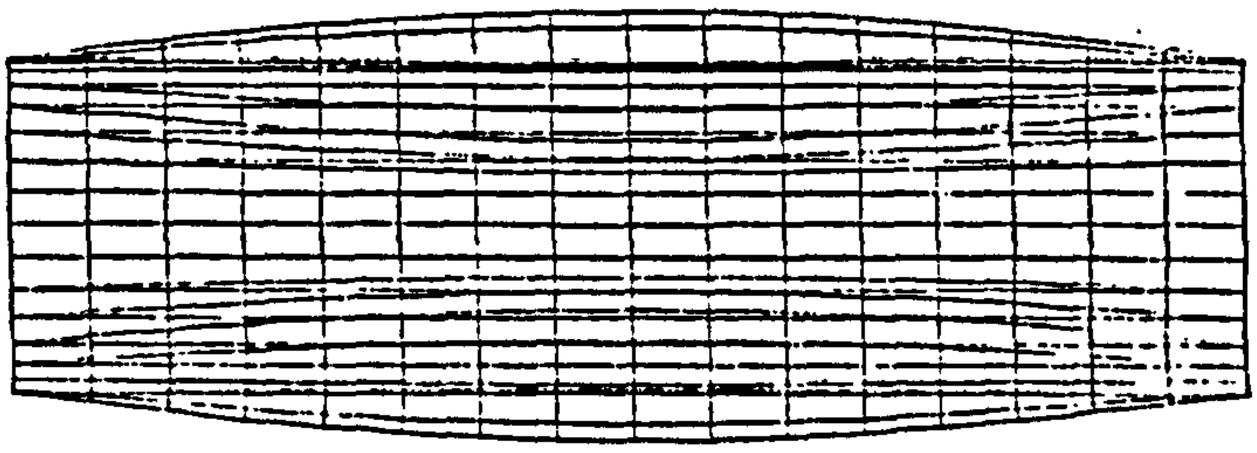

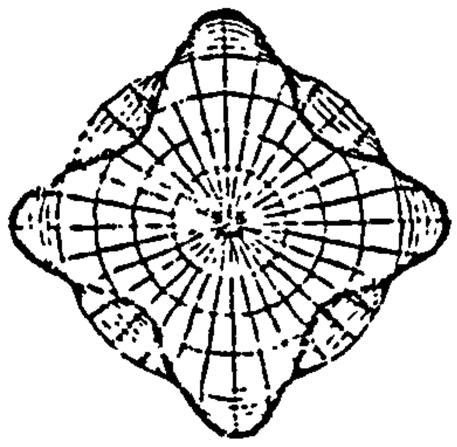

VIBRATION OF THE CYLINDER IN VACUO
LANCHOS METHOD

MODAL DEFOR. SUBCASE 8 MODE 8 FREQ. 349.5639

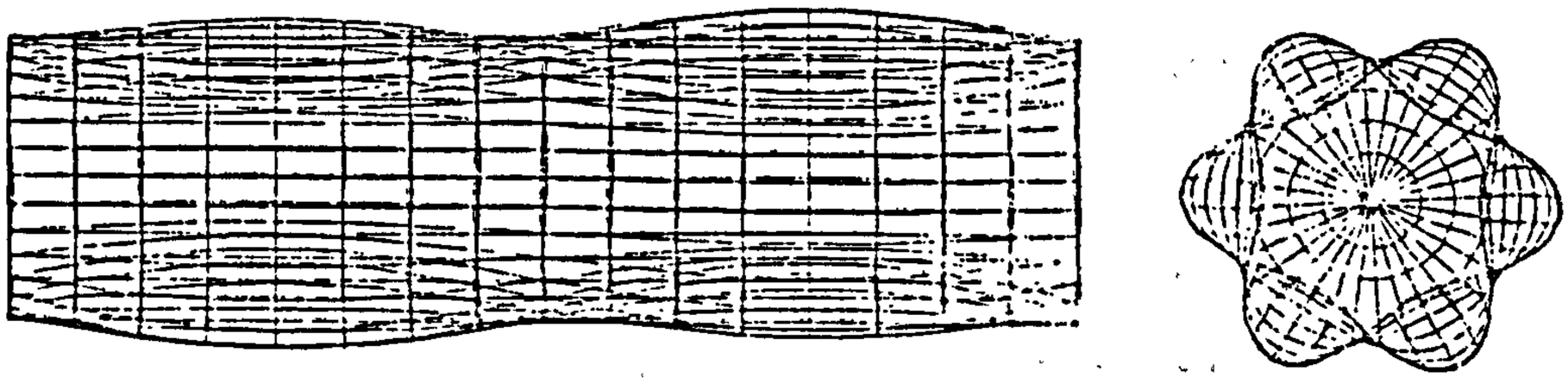

VIBRATION OF THE CYLINDER IN VACUO
LANCHOS METHOD
MODAL DEFOR. SUBCASE 9 MODE 9 FREQ. 391.1868

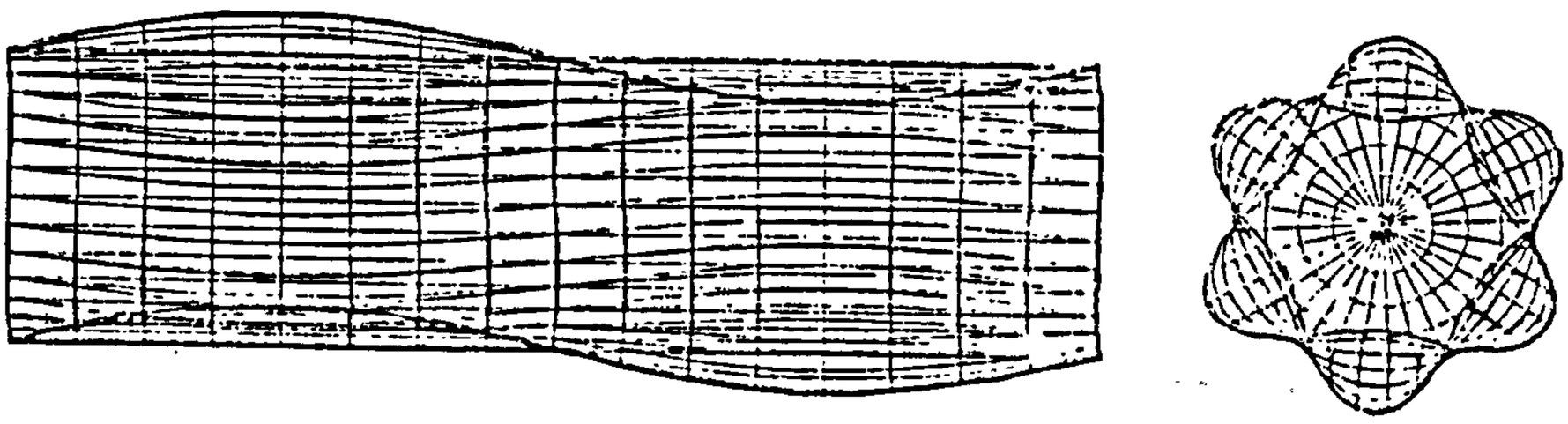

VIBRATION OF THE CYLINDER IN VACUO
LANCHOS METHOD
MODAL DEFOR. SUBCASE 10 MODE 10 FREQ. 391.1868

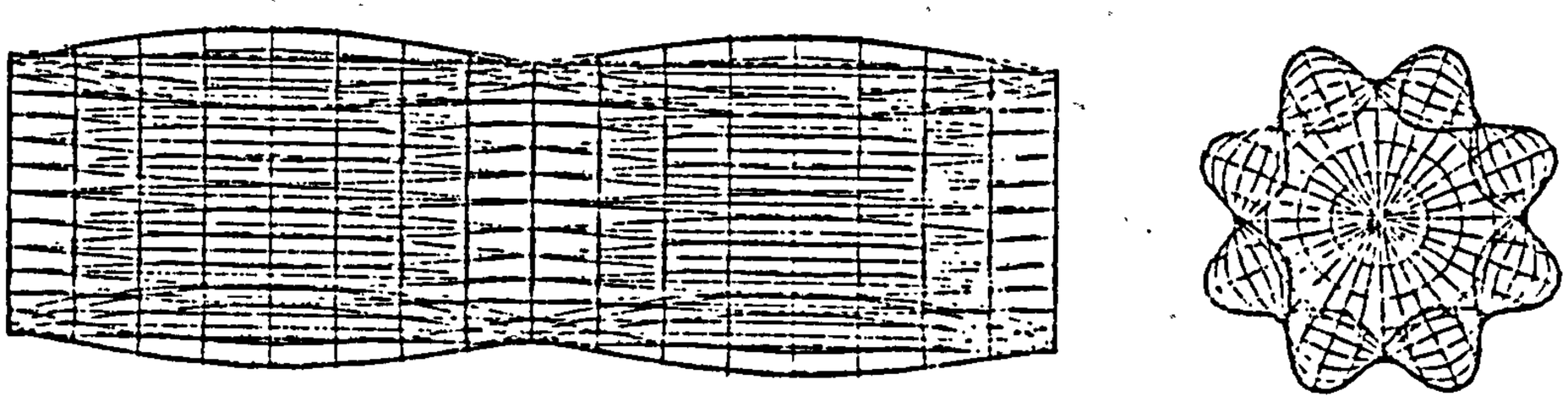

VIBRATION OF THE CYLINDER IN VACUO
LANCHOS METHOD
MODAL DEFOR. SUBCASE 11 MODE 11 FREQ. 412.2143

Figure 5.29

Mode shapes and natural frequencies obtained with NASTRAN facet elements used in wet analysis.

CHAPTER 6 - DISCUSSION

6.1 Introduction

In this section the numerous experimental results presented in the previous chapter will be compared with predictions obtained from the hydroelastic analysis. Comparison with the resonance frequencies for the various modes of vibration given by Warburtons' method is included and the accuracy of the experimental results and theoretical predictions is also discussed.

6.2 Error assessment

6.2.1 Accuracy of experimental results

Each accelerometer used in the measurement trials was calibrated, by measuring the apparent mass of a rigid body of known weight, before installation in the test cylinder. The calibration procedure included the cabling and charge amplifier associated with each individual accelerometer so that possible anomalies in the amplifying circuit were eliminated.

Signal failures did occur at some measurement sites during the trials but these failures tended to be permanent and instantaneous rather than progressive deterioration. The number of transducers employed and the knowledge of the vibration modes of the cylindrical shell which had been built up ensured that these failures were inconvenient but did not compromise the

validity of the remainder of the testing programme.

The likely errors in the measurement process have been listed in Chapter 4 but they will invariably produce spurious modes rather than corruption of existing modes of vibration. One of the major difficulties was the installation of an internal shaker and the errors that this caused can be observed in Figures 5.7 and 5.8. Firstly the overall signal strength has declined in Figure 5.8 where the excitation is from the internal shaker, due to the measured modes not being directly excited. The reduction in signal to noise ratio is most marked below 100 Hz. where the acceleration signal is relatively low and there is noticeable interference at the fundamental (50 Hz.) and higher harmonic frequencies of the electrical mains supply. The receptance data obtained with an internal shaker (Fig. 5.8) is well defined with only one region requiring any further explanation. There is a "split" peak or twin resonances for the fourth mode (m=2,n=3) of vibration, however this is a feature of the test cylinder rather than the measurement system. The less well defined receptance data in Figure 5.8 also includes additional resonances at 117, 287 and 361 Hz. These are due to the resonance of the internal shaker support structure and were highlighted so that they could be eliminated in the subsequent analysis. These resonances reappear as fairly major features in Figure 5.9

recording the receptance data from the ends.

As the frequencies of resonance rather than the absolute magnitude of the response was of primary interest in this study, the accuracy of the experimental results was only limited by the resolution of the analysers. The greatest range employed when testing using broadband excitation was 500 Hz. With a spectrum analyser operating over 501 spectral lines this corresponds to a frequency increment of 1 Hz. This was also the largest increment set on the frequency response analyser during swept-sine excitation and the setting was reduced to 0.1 Hz. near resonance.

In addition to frequency, damping loss factors have also been presented in Chapter 5 but due to the uncertainties that exist in the modelling of damping generally, the same level of confidence is not attached to these figures. It was noted during the extraction of modal parameters that slight variations in the selection of data points could produce differences of up to 10% in the damping loss factor.

6.2.2 Warburtons method

Results derived by Warburtons' method have been presented in Table 5.5 using the given physical properties. Changes in any of these properties will have a proportionate change on the predicted

frequencies. The hierarchy of the modes cannot be easily forecast but is a function of the geometry of the cylinder and is altered when the external fluid is introduced. Similarly, the sensitivity of the analysis to changes in any of the key dimensions is not regular and changes in radius and thickness affect modes with a large number of circumferential nodes whereas changes in length has a greater effect on modes with lower n values.

Table 5.6 Sensitivity of Warburtons' method to changes in key parameters.

In-vacuo

Mode (m,n)	Nat. freq (Hz)	10% increase in Leng.	Rad.	Thick
1,2	196.6	-14.8%	+6.2%	+1.2%
2,2	653.2	-14.8%	+6.2%	+0.2%
3,2	1231.1	-13.1%	+3.9%	+0.1%
1,3	204.6	-3.4%	-11.2%	+8.1%
2,3	389.9	-12.2%	+2.7%	+2.6%
3,3	724.6	-13.9%	+4.8%	+0.9%
1,4	353.5	-0.6%	-16.5%	+9.8%
2,4	413.8	-4.3%	-9.9%	+7.7%
3,4	574.1	-9.4%	-1.9%	+4.5%

External fluid (water)

Mode (m,n)	Nat. freq (Hz)	10% increase in Leng.	Rad.	Thick.
1,2	98.3	-15.3%	+2.6%	+4.9%
2,2	327.8	-14.9%	+2.5%	+3.7%
3,2	614.8	-12.9%	-0.1%	+3.7%
1,3	113.2	-3.5%	-14.2%	+11.7%
2,3	216.0	-12.1%	-0.1%	+6.0%
3,3	401.7	-14.0%	-1.4%	+4.2%
1,4	212.0	-0.5%	-19.0%	+13.1%
2,4	248.2	-4.4%	-12.6%	+11.0%
3,4	344.5	-9.3%	-4.9%	+7.8%

The length of the cylinder was not difficult to measure and presented few problems. Conversely, the radius and thickness were not only difficult to measure but these were the parameters most difficult to control during the manufacture and fabrication process (cf. Table 4.2). Variations in the order of 10% may be excessive but anything less than 1-2% was very difficult to achieve and gives an appreciation of the accuracy of the predicted results.

6.2.3 Finite element analysis

As the hydroelastic analysis analysis which has been used here is dependant upon an accurate representation of the "dry" modes, considerable time and effort was expended trying to get this right. An acceptable finite element solution was deemed to be one that satisfied two criteria

i. accurate prediction of the natural frequencies for all modes to be included in the wet analysis.

ii. symmetrical and uniform mode shapes

Alternative mesh sizes and element types were investigated over a long period to try to meet these conditions; the majority of this work being unreported because it was unproductive (Appendix C.). Semi-Loof elements were eventually discarded , despite the good agreement with predicted natural frequencies, because

the mode shapes produced were irregular (Fig. 5.26). Facet shell elements produced acceptable mode shapes but convergence of the numerical process was difficult to achieve because of the dynamic reduction technique employed by PAFEC and the relationship between master and slave degrees of freedom. The convergence of four and eight noded quadrilateral facet shell elements from Tables 5.8 and 5.9 is shown in Figures 6.1 and 6.2 but the number of master degrees of freedom is decreasing as the total degrees of freedom increases and this will affect the convergence.

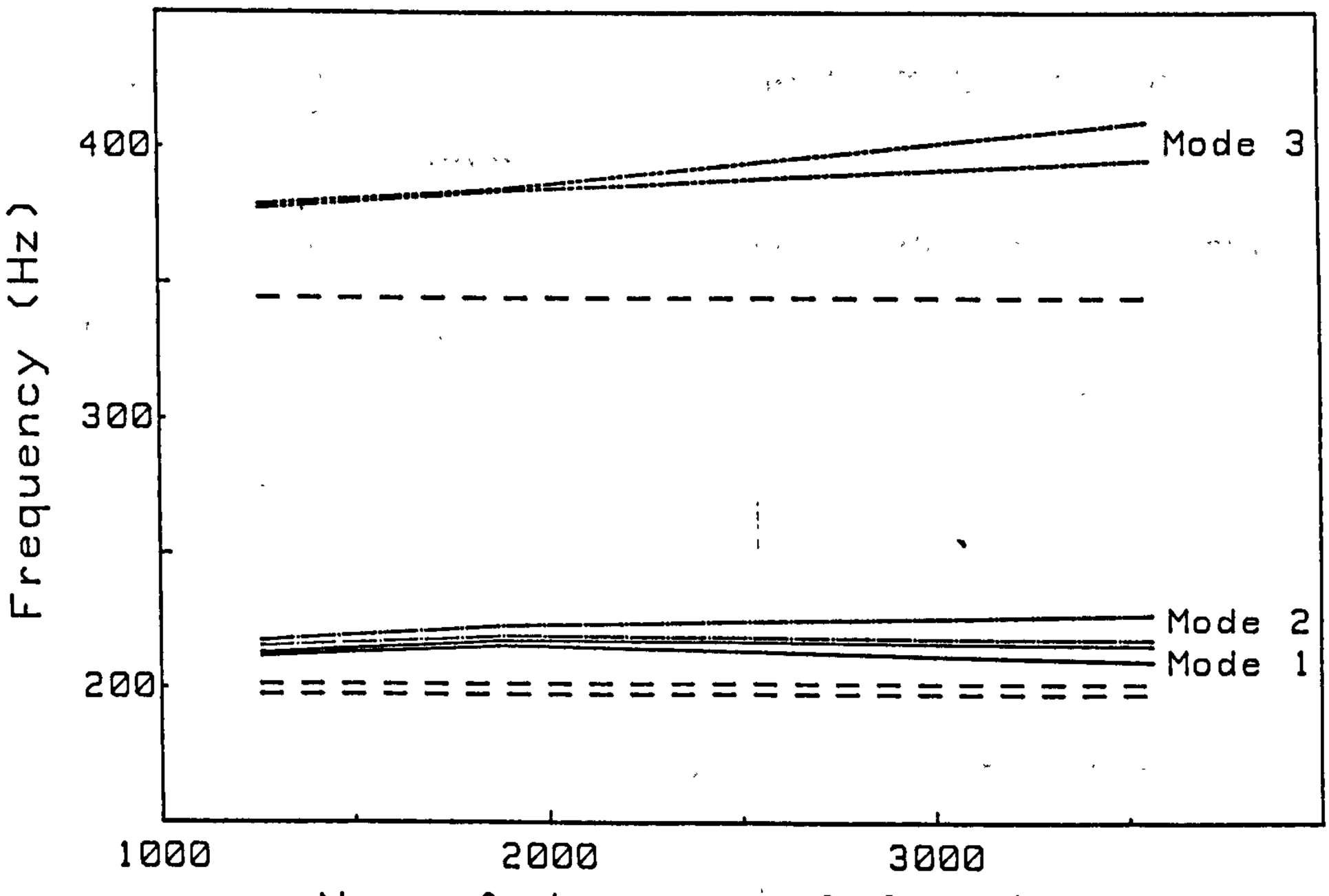

Figure 6.1 Convergence of PAFEC 44200 elements

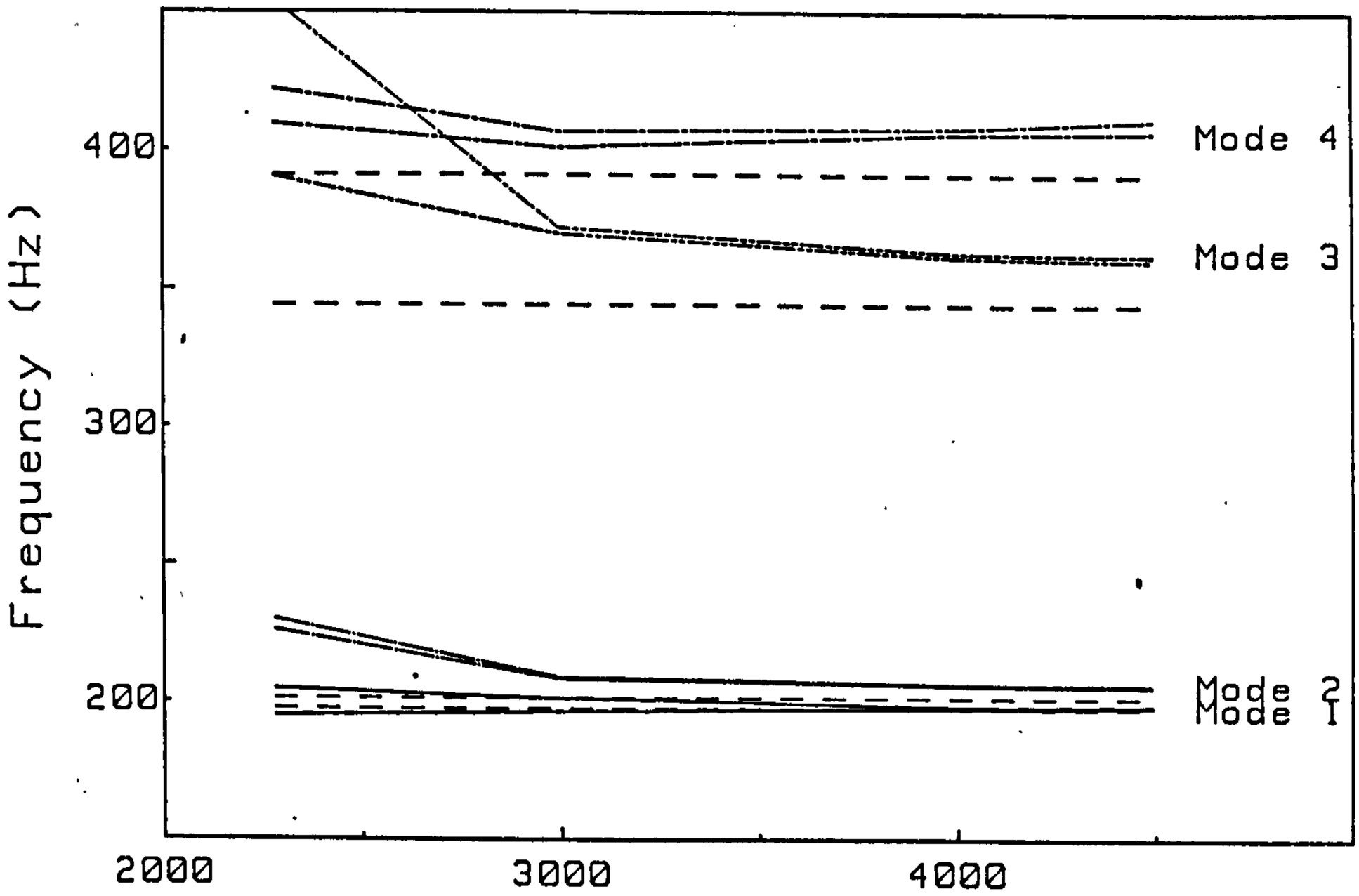

Figure 6.2 Convergence of PAFEC 44210 elements

Eventually the use of the NASTRAN finite element package on a Cray computer enabled eigenvalues to be calculated without reduction and produced much improved solutions (Fig. 6.3).

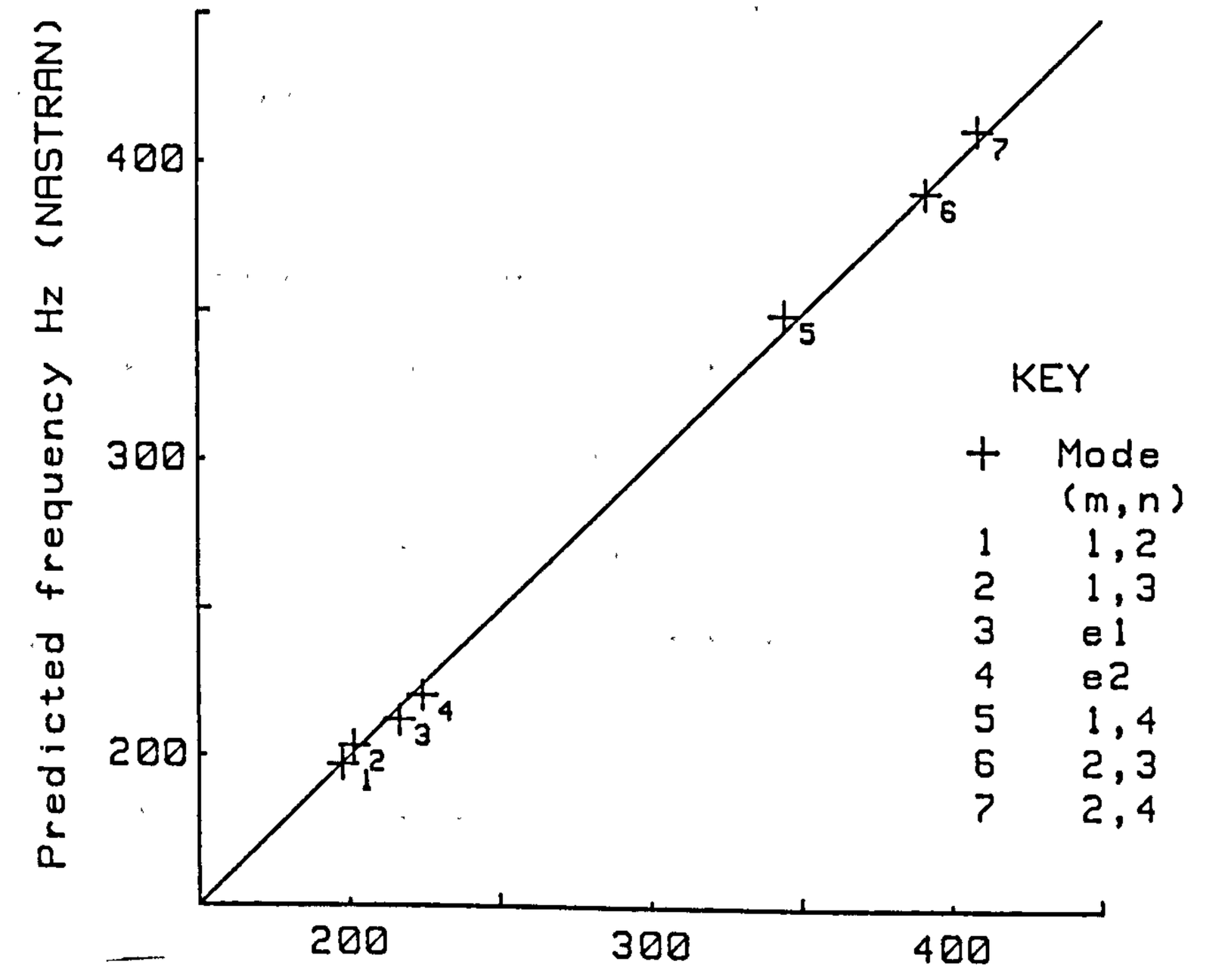

Figure 6.3 Comparison of FE solutions

6.3 Comparison of in-air results

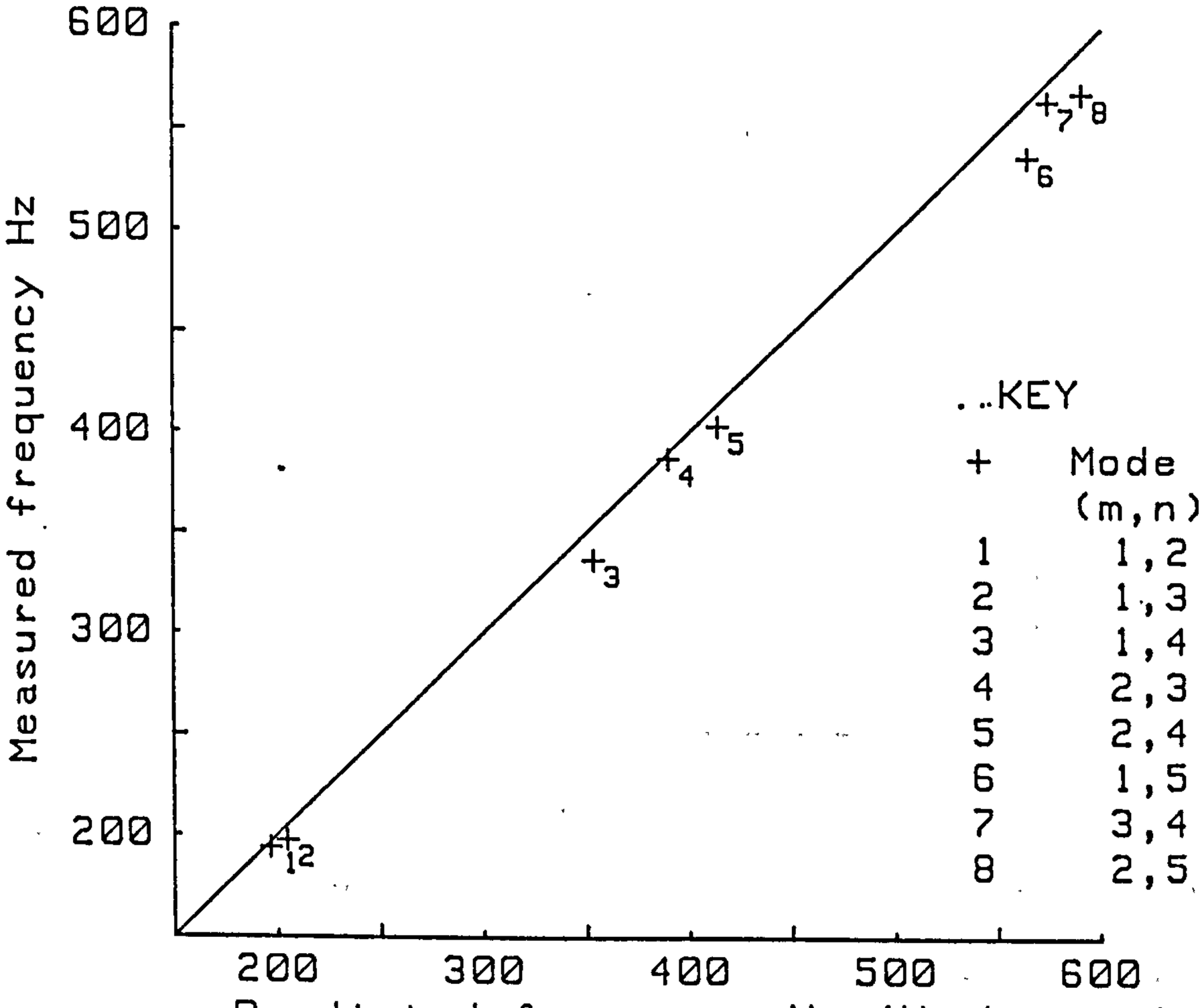

Figure 6.4 Comparison of in-air results

The first comparison (Fig. 6.4) is between experimental results in air (Table 5.1) and the theoretical predictions from Warburtons' method (Table 5.5). This shows a slight over-estimate (up to 5%) by the theory but generally deviating by only 3%, which considering the geometrical imperfections is not excessive. The finite element solution produced by NASTRAN (Table 5.11) also compares favourably with the experimental results (Fig. 6.5) and creates confidence for its adoption for the wet analysis.

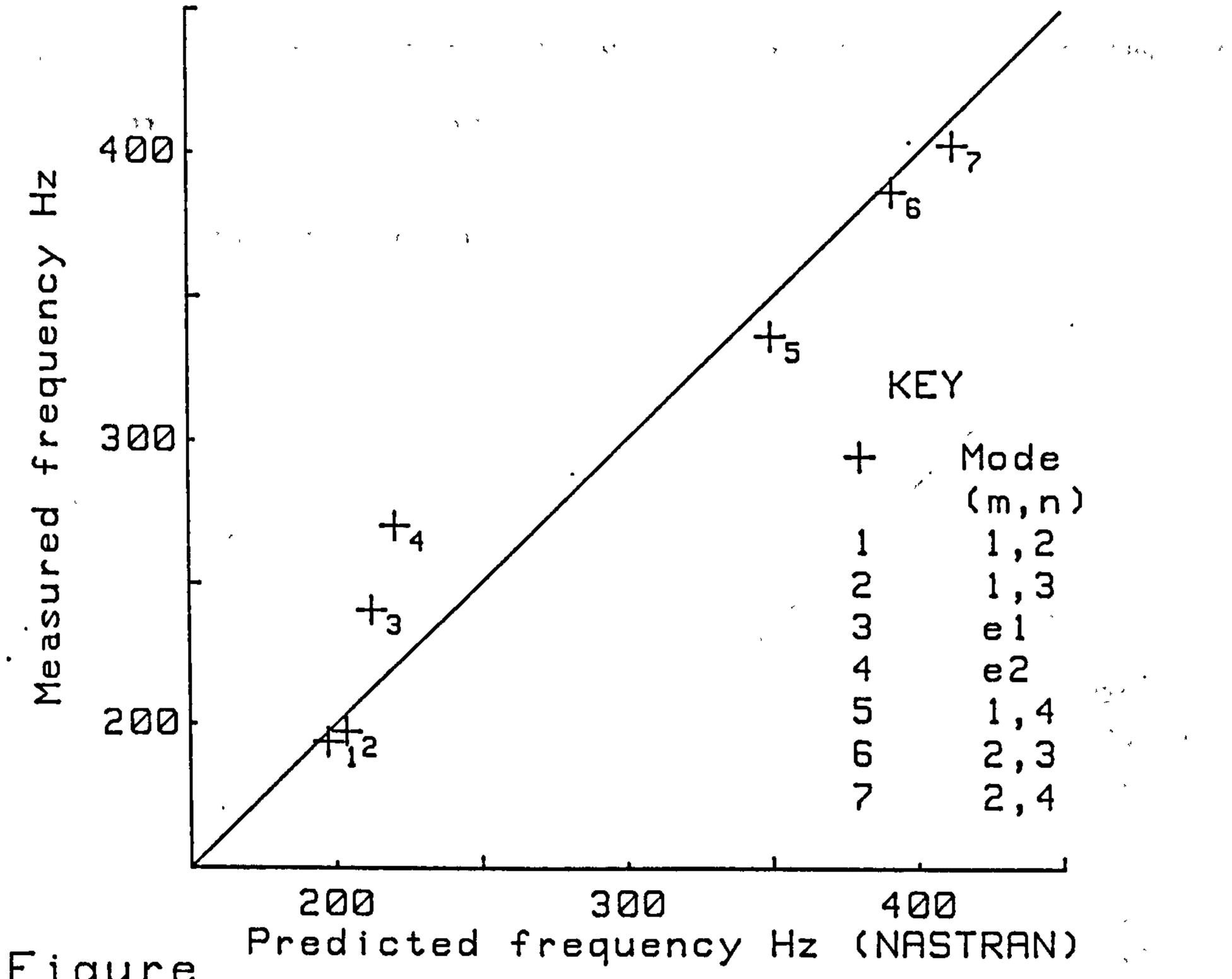

Figure 6.5 Comparison of in-air results

So far only the cylinder modes have been considered. Warburtons' solution was derived for an infinitely long cylinder therefore excluding end conditions and the finite element solution although three dimensional did not attempt to accurately reproduce the physical model at the ends. To seal the ends, the hatch plates needed to be wider than the end openings; the hatches were then fixed by rubber sealant and screws. Glands for transducer cabling added further weight and provided some restriction for free motion. These practical considerations affecting the free response of the ends were one of the reasons why the finite element solution assumed plain closed ends. Consequently the finite

element solution for the ends typically under-estimated the natural frequencies.

6.4 Comparison of underwater results

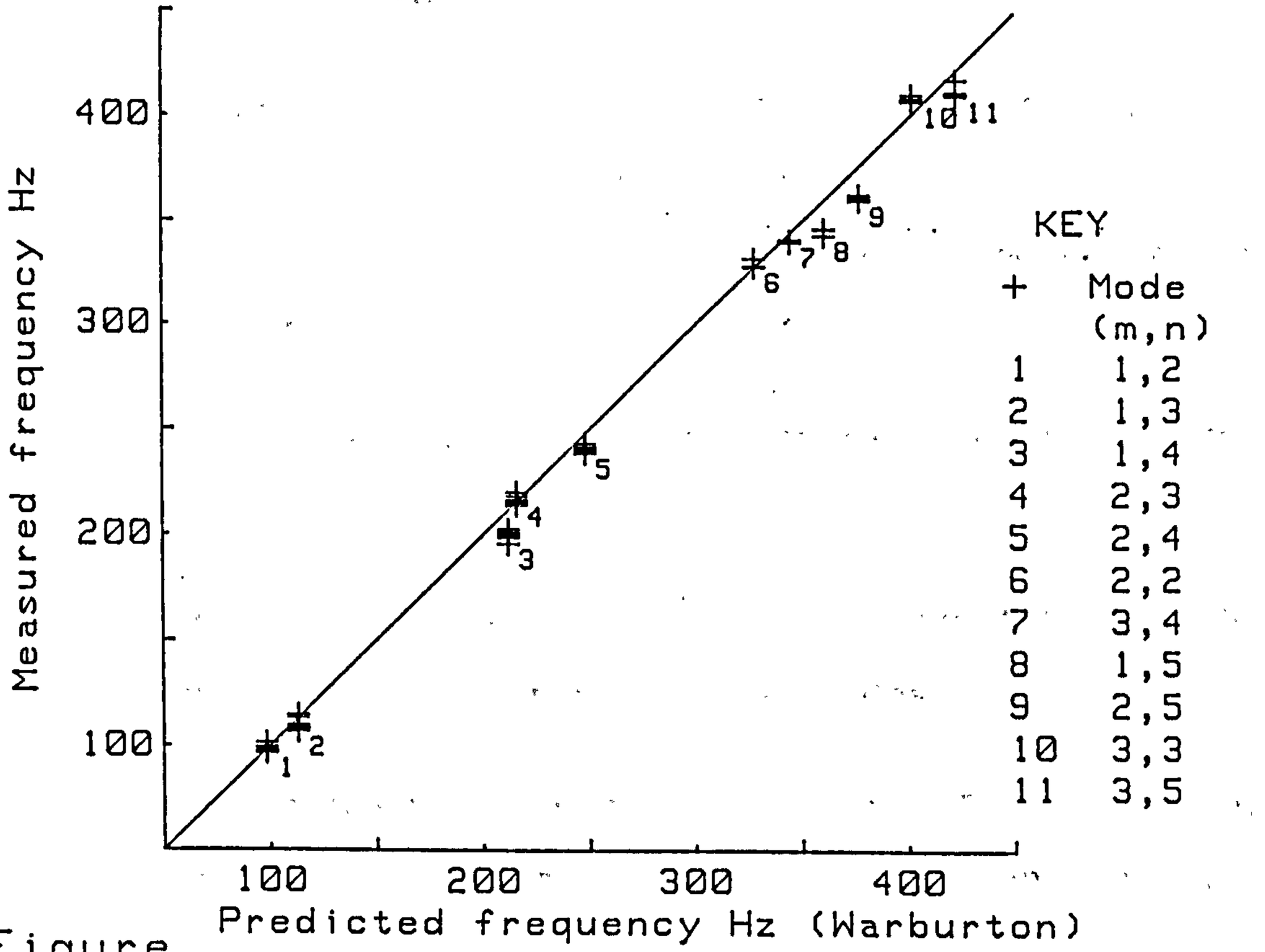

Figure 6.6 Comparison of underwater results

6.4.1 Warburtons' method

Attempts at reconciliation between measured data and theoretical predictions for the submerged cylinder are not as straightforward as in the in-air case. Comparison with the solution given by Warburtons' method (Fig. 6.6) clearly demonstrates the differences. There is no longer one unique resonance frequency for each

mode shape and although the predicted solution is a reasonable approximation it cannot account for the changes that occur due the proximity of rigid or free surfaces or for the modes of the ends.

6.4.2. Measured data

The changes in the measured resonance frequencies were observed to follow certain trends

i. there is a decrease in resonance frequencies at increased depth

ii. the rate of change is most rapid near the free surface

iii. changes in orientation (e.g. Posn.A to Posn.B) affect end modes more than cylinder modes.

iv. differences in measured data from Tank #1 (1.6m. depth) and Tank #2 (4.0m. depth) are not significant.

The experimental data can be reduced to five categories, namely

Tank #1 (1.6m. depth)	shallow	0.21m.
	medium	0.68m.
Tank #2 (4.0m. depth)	shallow	0.25m.
	medium	1.50m.
	deep	3.50m.

6.4.3 Hydroelastic "wet" analysis

The hydroelastic analysis is capable of calculating the differences due to changes in surroudings and position and the various cases will now be evaluated.

Initially an inaccurate dry analysis solution employing semi-Loof elements was used to obtain resonance frequencies for cylinder #2 at 0.68m. depth in 1.6m. of water (Fig. 6.7). There was reasonable agreement for the first two cylinder modes but in view of the dry analysis this was rather more unexpected than the poor correlation of the ends modes 3 & 4. It was also observed but could not be verified experimentally that results for an infinite depth of water differed by up to 15% from solutions in the limited depth.

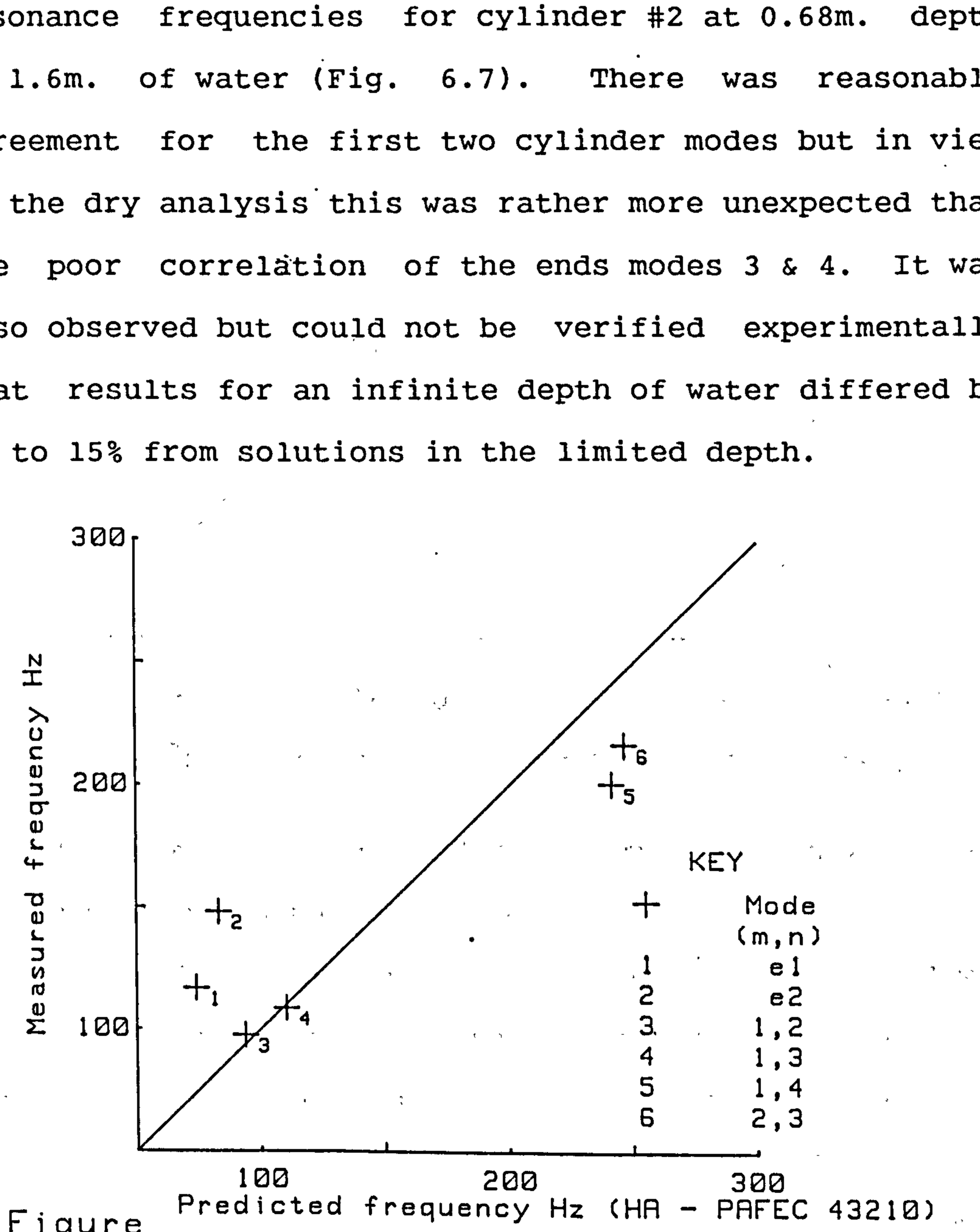

Figure 6.7 Comparison of underwater results

Repeating the analysis using an improved dry analysis (PAFEC 44210 elements), perversely resulted in decreased accuracy (Fig. 6.8) but confirmed the experimentally observed trend of decreasing resonance frequency at increased depths.

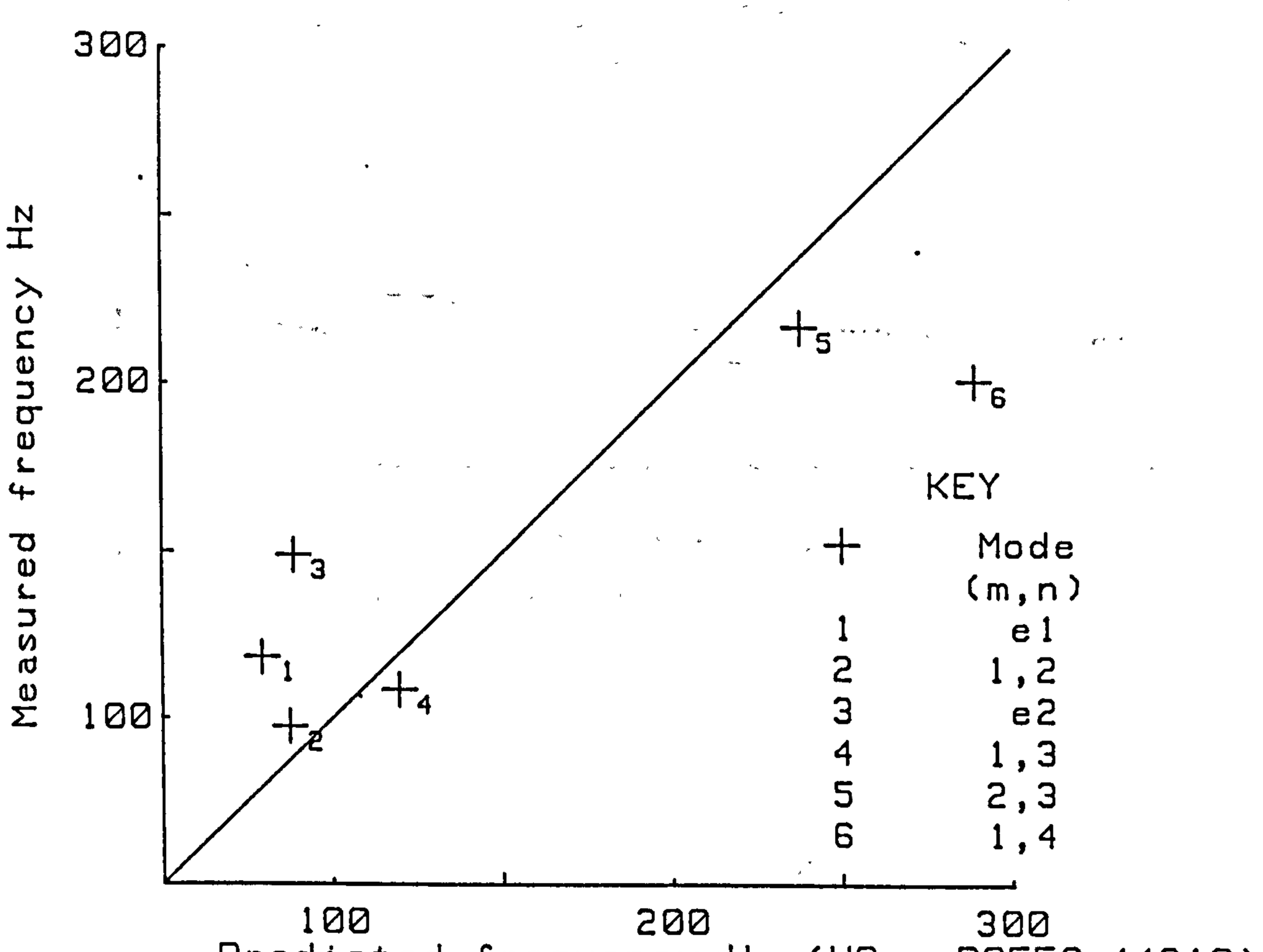

Figure 6.8 Comparison of underwater results

At this stage the NASTRAN dry analysis was used. Convergence was assessed using a 256 structural element model with differing numbers of panels (Fig.6.9) and wet analyses were performed using an improved 768 element model. This improved the correlation with the measured data, particularly at higher modes (Fig.6.10), but at the lower end it tended to confirm the PAFEC 44210 model

rather than approaching the experimental results.

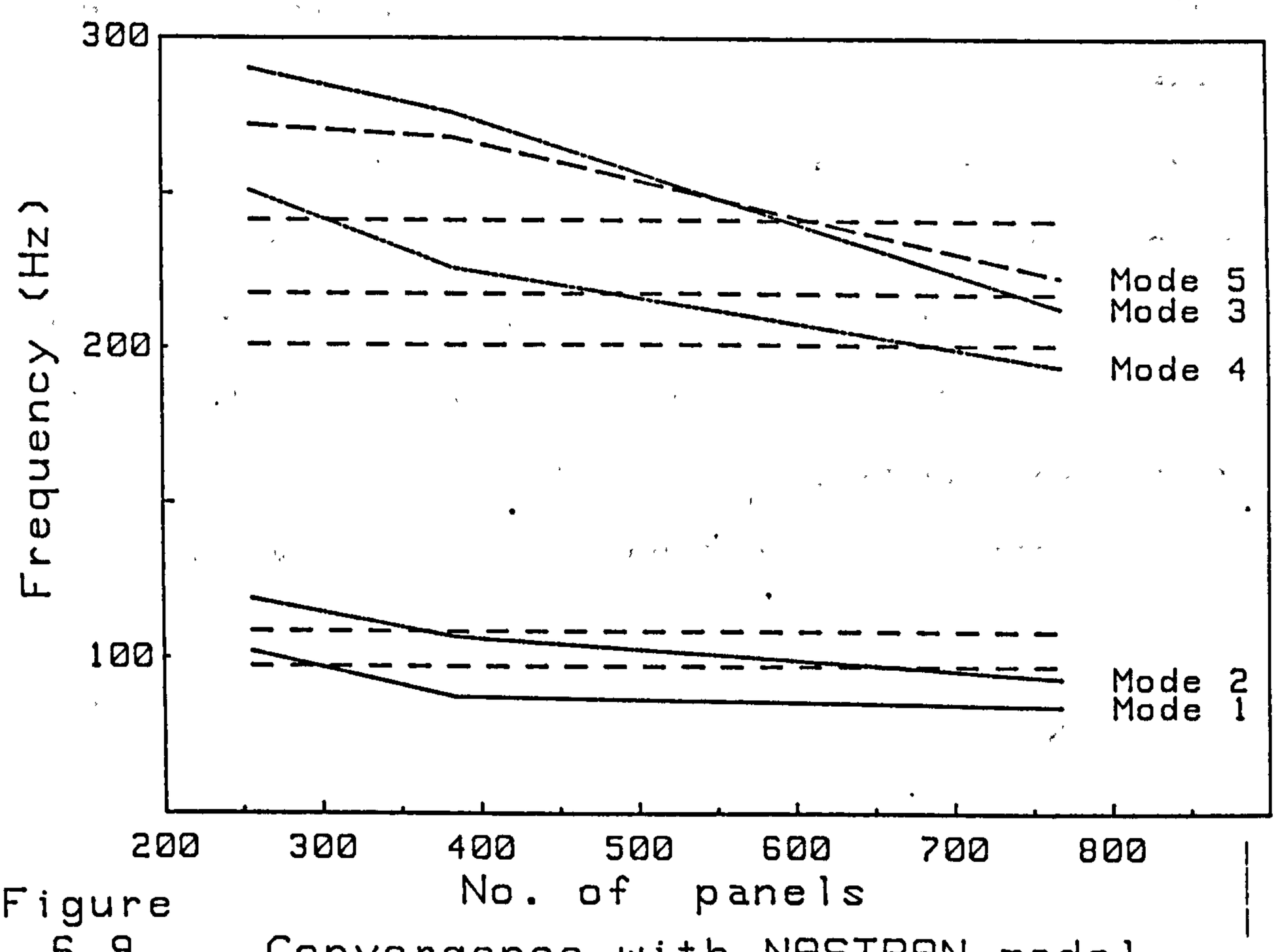

Figure 6.9 Convergence with NASTRAN model

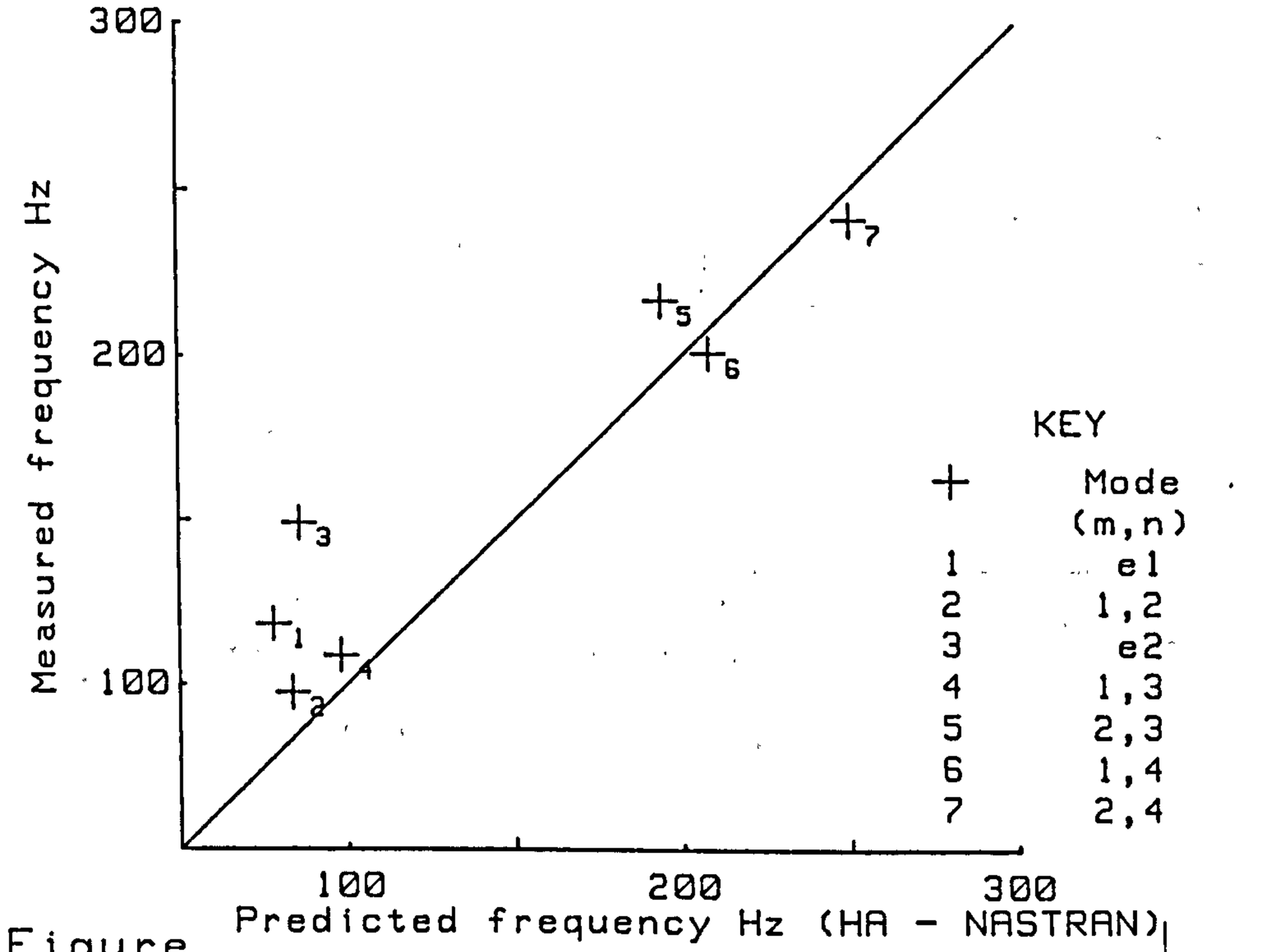

Figure 6.10 Comparison of underwater results

A further modification was then introduced which enabled the tethering forces to be included in the analysis. The securing points on the cylinder were positions of minimal, but not zero, motion and the inclusion of these forces changes the nature of the model from an idealised neutrally buoyant structure to a more realistic representation of the positively buoyant structure and brought about the improved prediction of the first two cylinder modes shown in Figure 6.11.

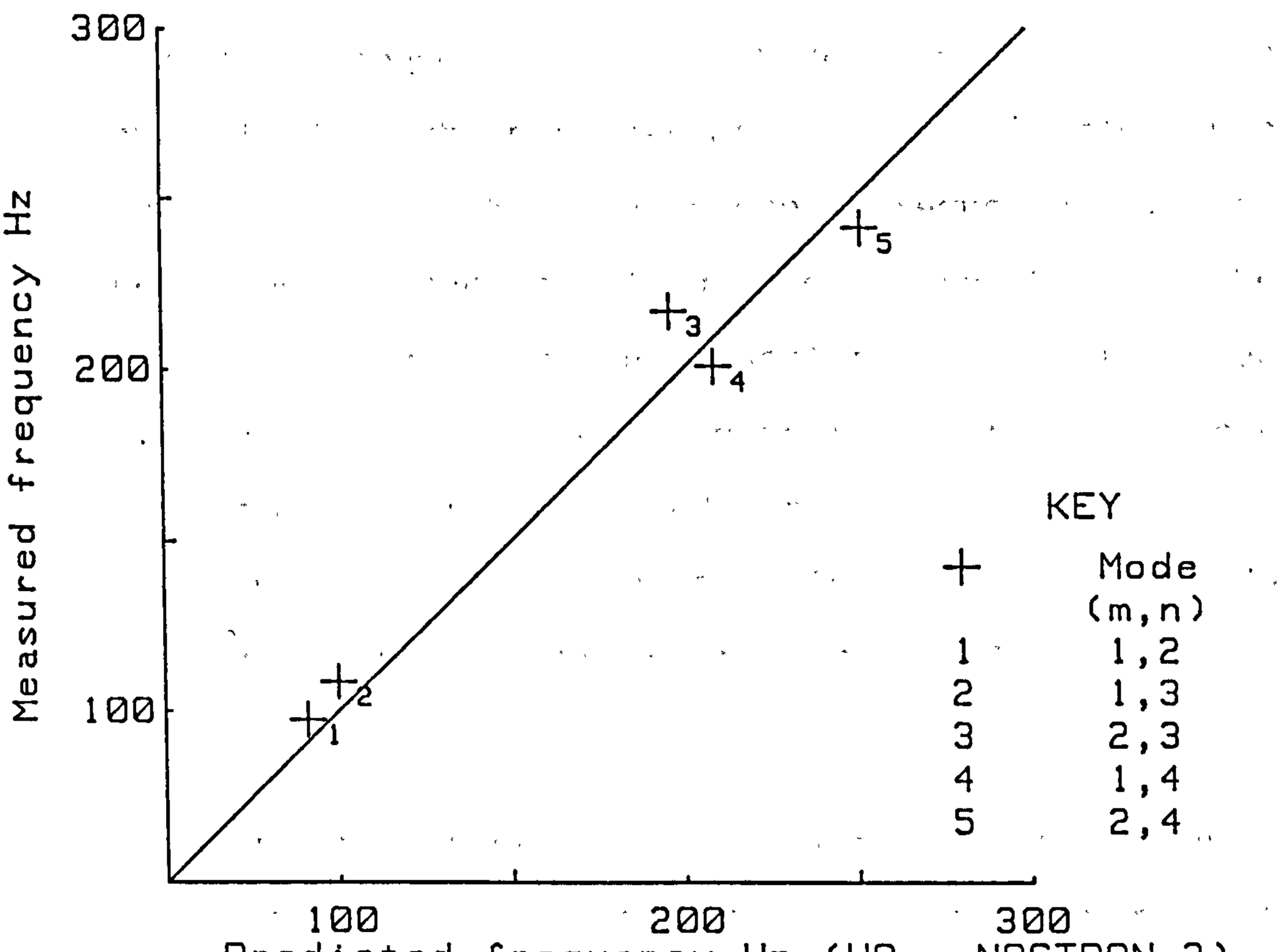

Figure 6.11 Comparison of underwater results

CHAPTER 7 - CONCLUSIONS

Two separate hydrodynamic effects have been investigated in this text. A modified hydroelasticity theory and hydroelastic analysis were presented accounting for the effect of viscosity on the forced vibration characteristics of a cylindrical beam enclosed within a rigid tube. The influence of viscosity and annular clearance were clearly demonstrated by reference to their effects on resonance frequency values and on the characteristics of the principal coordinates. These were shown to depend on the magnitude of the generalised external fluid which increases as the annular clearance decreases. Thus, the resonance frequency values decrease and stronger coupling is exhibited between the principal coordinates as the annular clearance value reduces. Only minor downward shifts in the resonance frequency values were observed when a viscous fluid (water) replaced the idealised inviscid fluid, but a decrease in the peak values of the principal coordinate occured.

Although this problem was set with the intention of evaluating the effect of viscosity in a system with straightforward, idealised, geometry, there are implications for some practical problems in naval architecture. The dynamic behaviour of a long flexible pipe or structural member or a propeller rotating in a shroud are two instances where the omission of viscosity

will influence the accuracy of resonance frequency values and responses.

The major portion of this work deals with the modelling of thin cylindrical shells and analysing the effect of submersion in water and the influence of external boundaries on their hydrodynamic characteristics. The general three-dimensional hydroelasticity theory (Wu(1984), Bishop, Price & Wu(1986)) has been extended to account for the particular distortion modes exhibited by thin shell structures. The theory has been validated in a series of experiments which were performed on scale models in air and underwater. Unlike the vibration testing performed in air the results obtained from the submerged tests displayed large variation in resonance frequency values for the various modes of vibration. The most marked changes were caused by alterations in the depth of the model below the free surface. There was also a consistently greater decrease in submerged resonance frequency values compared with in-vacuo values for end modes as opposed to cylinder modes. Approximations which concentrate on the fluid forces on the surface of the structure or analytical methods which assume an infinite extent of surrounding fluid cannot predict any variation due to external boundaries. The radiation and boundary conditions incorporated in the source distribution method overcome this limitation and hence

the method used gives a far greater insight into the physical behaviour of the interaction phenomena.

The use of finite elements in conjunction with the source distribution techniques permits a high level of flexibility in the separate modelling of the structural and hydrodynamic components. However practical difficulties and pitfalls are likely to befall the investigator in any analysis and these have not been overlooked. Some of the inaccuracies that were encountered during the course of the finite element study have been included to demonstrate the weaknesses as well as the strengths of the method and to emphasise the importance of careful selection of key parameters. Nevertheless the analysis of realistically shaped models is not possible without some form of discretisation and although the correlation between measured and predicted results in this study is less than ideal there is agreement in the behaviour of the trends. The correlation was enhanced by the inclusion of tethering forces, which reinforces the findings that the hydroelastic theory can predict the behaviour of real structures with all their practical peculiarities.

Future work may wish to investigate full-size structures which would introduce many changes but would be less stiff than the small scale models used in this investigation. A comparison with the widely used DAA is

also recommended as it is believed that the present method is greatly superior and it may be possible to highlight areas of inaccuracy.

This work does not stand in isolation it is a continuation of preceding studies on the behaviour of floating bodies (Wu (1984)), jack-up structures in waves (Fu (1987)), SWATHs (Price, Temarel & Wu(1985)) and others. Further advances are already in the process of development and include the dynamic response of marine structures to transient excitation due to slamming or an explosive pressure pulse. The efficacy and reasoning behind adopting a hydroelastic approach has been presented and it is hoped that this work has contributed towards its continued improvement.

REFERENCES

Abramowitz, M & Stegun, I.A. (1965) "Handbook of mathematical functions", Dover Publications, Inc., New York

Akkas, N., Akay, H.U. & Yilmaz, C. (1979) "Applicability of general purpose finite element programs in solid-fluid interaction problems", Computers & Structures, 10( ), pp 773-783

Baar, J.J.M. & Price, W.G. (1983a) "A proposal for an optimal coupling between a finite element and boundary integral method in fluid-structure problems", Marine Research Group, Rept. No. BME83-2, Dept. Mech. Eng., Brunel Univ.

Baar, J.J.M. & Price, W.G. (1983b) "On the use of Greens functions in marine hydrodynamics, Part 1: Singularity distributions", Marine Research Group, Rept. No. BME83-3a, Dept. Mech. Eng., Brunel Univ.

Baar, J.J.M. & Price, W.G. (1983c) "On the use of Greens functions in marine hydrodynamics, Part 2: Translating and pulsating sources in uniform water depth", Marine Research Group, Rept. No. BME83-3b, Dept. Mech. Eng., Brunel Univ.

Babu, P.V.T. & Reddy, D.V. (1981) "A numerical integration scheme for solving coupled equations of fluid-structure interaction systems", Proceedings of International Conference on Numerical Methods for Coupled Problems, Univ. of Swansea, 1981

Baker, B.B. & Copson, E.T. (1950) "The mathematical theory of Huygens' principle", Clarendon Press, Oxford

Bedrosian, B. & DiMaggio, F.L. (1972) "Acoustic approximations in fluid-shell interactions", J. Eng. Mech. Div., Proc. ASCE, 98(EM3), pp 731-742

Belik, O, Bishop, R.E.D. & Price, W.G. (1980) "On the slamming response of ships to regular head waves", Trans. RINA, 122, pp 325-337

Berger, B.S. (1969) "Vibration of the hollow sphere in an acoustic medium", J. Appl. Mech., 36(2), pp 330-333

Berglund, J.W. & Klosner, J.M. (1968) "Interaction of a ring-reinforced shell and a fluid medium", J. Appl. Mech., Trans. ASME, 35(1), pp 139-147

Bettes, P. (1980) "Infinite finite elements", Int. J. num. meth. Engng., 15( ), pp 1613-1626

Betts, C.V., Bishop, R.E.D. & Price, W.G. (1977) "The symmetric generalised fluid forces applied to a ship in a seaway", Trans. RINA, 119, pp 265-278

Bishop, R.E.D., Clarke, J.D. & Price, W.G. (1984) "Comparison of full scale and predicted responses of two frigates in a severe weather trial", Trans. RINA, 126, pp 153-166

Bishop, R.E.D. & Johnson, D.C. (1960) "The mechanics of vibration", Cambridge University Press, Cambridge

Bishop, R.E.D. & Price, W.G. (1976) "On the relationship between "dry modes" and "wet modes" in the theory of ship response", J. Sound Vib., 45(2), pp 157-164

Bishop, R.E.D. & Price, W.G. (1979) "Hydroelasticity of ships", Cambridge University Press

Bishop, R.E.D., Price, W.G. & Tam P.K.Y. (1977) "A unified dynamic analysis of ship response to waves", Trans. RINA, 119, pp 363-390

Bishop, R.E.D., Price, W.G. & Tam P.K.Y. (1978) "On the dynamics of slamming", Trans. RINA, 120, pp 259-280

Bishop, R.E.D., Price, W.G. & Temarel P. (1980) "A unified dynamic analysis of antisymmetric ship response to waves", Trans. RINA, 122, pp 349-365

Bishop, R.E.D., Price, W.G. & Temarel P. (1984) "A study of mode shapes in hull vibration of low frequency", CETENA, Genoa, Paper 20

Bishop, R.E.D., Price, W.G. & Yousheng Wu (1986) "A general linear hydroelasticity theory of floating structures moving in a seaway", Phil. Trans. R. Soc. Lond., A 316, pp 375-426

Bishop, R.E.D., Price, W.G. & Zhang Xicheng (1983) "On the structural dynamics of a Vlasov beam", Trans. R. Soc. Lond., A 388, pp 49-73

Bleich, H.H. & Baron, M.L. (1954) "Free and forced vibrations of an infinitely long cylindrical shell in an infinite acoustic medium", J. Appl. Mech., Trans. ASME, 21, pp 167-177

Broch, J.T. (1976) "The application of the Bruel & Kjaer measuring systems to mechanical vibration and shock measurements", Bruel & Kjaer, Naerum, Denmark

Brown, D.T., Eatock-Taylor, R. & Patel, M.H. (1983) "Barge motions in random seas - a comparison of theory and experiment", Jrnl. Fluid Mech., 129, pp 385-407

Carrier, G.F. (1951) "The interaction of an acoustical wave and an elastic , cylindrical shell", Tech. Rpt. No.4, Contract N7onr-35810, Brown University' Providence, R.I.

Chang, M.S. (1977) "Computations of three-dimensional ship motions with forward speed", Proc. 2nd. Int. Conf. on Num. Ship Hydrodynamics, pp 124-135

Chen, L.H. & Pierucci, M. (1977) "Underwater fluid-structure interaction. Parts 1-4", Shock Vib. Digest, 9(4).

Chen, L.H. & Schweikert, D.G. (1963) "Sound radiation from an arbitary body", J. Acoust. Soc. Am., 35(10), pp 1626-1632

Chen, S.S., Wambsganss, M.W. & Jendrzejczyk J.A. (1976) "Added mass and damping of a vibrating rod in confined viscous fluids", Jrnl. Appl. Mech., Series E, Trans. ASCE, 43(2), pp 325-329

Chertock, G. (1970) "Transient flexural vibrations of ship-like structures to underwater explosions", J. Acoust. Soc. Am., 48(1), pp 170-180

Conceicao, C.A.L., Price, W.G. and Temarel, P. (1984) "The influence of heel on the hydrodynamic coefficients of ship like sections and a trawler form", Int. Shipbldg. Progr., 31 , pp 56-66

Copley, L.G. (1968) "Fundamental results concerning integral representations in acoustic radiation", J. Acoust. Soc. Am., 44(1), pp 28-32

Couhat, J.L. (Ed.) (1984) "Combat Fleets of the World 1984/85", Publ Arms & Armour Press, N.Y.

DeRuntz, J.A., Geers, T.L. & Felippa, C.A. (1980) "The underwater shock analysis code (USA - Version 3), A reference manual", DNA Rept. 5615, Washington, DC, Sep 1980

Deshpande, S.S., Belkune, R.M. & Ramesh, C.K. (1981) "Dynamic analysis of coupled fluid-structure interaction problems", Proceedings of International Conference on Numerical Methods for Coupled Problems, Univ. of Swansea, 1981

DiMaggio, F., Ranlet, D., Bleich, H.H. & Baron, M.L. (1978) "The inertial damping collocation approximation (IDCA) for uncoupling fluid-structure interaction problems", Mech. Res. Comm., 5(4), pp 207-210

Dobson, B.J. (1987) "A Straight-line technique for extracting modal properties from frequency response data", Mech Sys & Signal Processing (1987), 1(1), pp29-40

Ewins, D.J.A. (1981) "State-of-the-art assessment of mobility measurement techniques (SAMM)- Summary of results", Jrnl. Soc. Environmental Engs, March 1981, 20(1), (Issue 88)

Ewins, D.J.A (1984) "Modal Testing: Theory and Practice", Research Studies Press Ltd. Letchworth 1984

Faltinsen, O.M. (1974) "A numerical investigation of the Ogilvie-Tuck formulas for added mass and damping coefficients", J. Ship Res., 18, pp 73-84

Faltinsen, O.M. & Michelsen, F.C. "Motions of large structures in waves at zero Froude number", Int. Symp. Dynamics Marine Veh. & Struct. in Waves, Univ. College, London, pp 99-114

Firth, D. (1975) "Acoustic vibration of structures in liquids", Shock Vib. Digest, 7(4), pp 4-7

Felippa, C.A. & Geers, T.L. (1980) "Axisymmetric free vibration of a submerged spherical shell", J. Acoust. Soc. Am., 67(5), pp 1427-1431

Felippa, C.A. (1985) "Symmetrization of the contained compressible fluid vibration eigenproblem", Comm. Appl. Num. Meth., 1, pp 241-247

Flugge, W. (1962) "Stresses in shells", Springer-Verlag

Forrestal, M.J. (1968) "Response of an elastic cylindrical shell to a transverse acoustic pulse", J. Appl. Mech., Trans. ASME, 35(3), pp 614-616

Forrestal, M.J. & Alzheimer, W.E. (1968) "Transient motion of a rigid cylinder produced by elastic and acoustic waves", J. Appl. Mech., Trans. ASME, 35(1), pp 134-138

Fu, Y., Price, W.G. & Temarel, P. (1986) "The dynamics of a flexible jack-up transported in a seaway", 18th. Annual Offshore Tech. Conf., Houston, paper 5284, pp 513-524

Fung, Y.C. (1965) "Foundations of solid mechanics", Prentice-Hall, Englewood Cliffs, N.J.

Garrison, C.J. & Chow, P.Y. (1972) "Wave forces on submerged bodies", Jnrl. of Waterways & Harbours Div., ASCE, 98, pp 375-392

Geers, T.L. (1969) "Excitation of an elastic cylindrical shell by a transient acoustic wave", J. Appl. Mech., Trans. ASME, 36(3), pp 459-469

Geers, T.L. (1975) "Transient response analysis of submerged structures", Finite Element Analysis of Transient Nonlinear Structural Behaviour, ASME, AMD-Vol.14, NY, pp 59-84

Geers, T.L. (1978) "Doubly asymptotic approximations for transient motions of submerged structures", J. Acoust. Soc. Am., 64(5), pp 1500-1508

Geradin, R., Robert, G. & Huck, A. (1984) "Eigenvalue analysis and transient response of fluid-structure interaction problems", Eng. Comput., 1, pp 151-160

Gerritsma, J. & Beukelman, W. (1964) "The distribution of the hydrodynamic forces on a heaving and pitching ship model in still water", 5th. Symp. on Naval Hyrodynamics, pp 219-251

Goransson, J.P.E. & Davidsson, C.F. (1987) "A three-dimensional infinite element for wave propagation", J. Sound Vib., 115(3), pp 556-559

Grigoliuk, E.I. & Gorshkov, A.G. (1974) "Nonstationary hydroelasticity of shells", Sudostroenie, Leninigrad, USSR

Guyan, R.J. (1965) "Reduction of stiffness and mass matrices", J. AIAA, (3), p 380

Hamdi, M.A., Ousset, Y. & Verchery, G. (1978) "A displacement method for the analysis of vibrations of coupled fluid-structure systems", Int. J. num. Meth. Engng., 13(1), pp 139-150

Harris, C.M. & Crede, C.E. (1976) "Shock and Vibration Handbook 2nd Edition", McGraw-Hill N.Y.

Havelock, T.H. (1931) "The wave resistance of a spheroid", Proc. Roy. Soc. (Lond), A131, pp 275-285

Haywood, J.H. (1958) "Response of an elastic cylindrical shell to a pressure pulse", Quart. J. Mech. & Appl. Math., 11(2), pp 129-141

Hellen, T.K. & Irons, B.M.R. (1971) "On reduced integration in solid isoparametric elements when used in shells with membrane modes", Int. J. Num. Meth. Engng., 3, p.275

Henshell, R.D. (Ed.) (1975) "PAFEC 75 Theory, Results", PAFEC Ltd., Strelley Hall, Nottingham

Henshell, R.D. (Ed.) (1984) "Data Preparation. User Manual Level 5.1", PAFEC Ltd., Strelley Hall, Nottingham

Herrmann, G. & Russell, J.E. (1967) "Forced motions of shells and plates surrounded by an acoustic fluid", Proceedings of a symposium on the theory of shells, ed. Muster, D., University of Houston, Texas, pp 313-342

Huang, H. (1970) "An exact analysis of the transient interaction of acoustic plane waves with a cylindrical elastic shell", J. Appl. Mech., Trans. ASME, 37(4), pp 1091-1106

Huang, H. & Wang, Y.F. (1970) "Transient interaction of spherical acoustic waves and a cylindrical elastic shell", J. Acoust. Soc. Am., 56(1), pp 228-235

Hunt, J.T., Knittel, M.R. & Barach, D. (1974) "Finite element approach to acoustic radiation from elastic structures", J. Acoust. Soc. Am., 55(2), pp 269-280

Hunt, J.T., Knittel, M.R., Nichols, C.S. & Barach, D. (1975) "Finite element approach to acoustic scattering from elastic structures", J. Acoust. Soc. Am., 57(2), pp 287-299

Inglis, R.B. & Price, W.G. (1980) "The hydrodynamic coefficients of an oscillating ellipsoid moving in a free surface", Jrnl. Hydronautics, 14(4), pp 105-110

Inglis, R.B. & Price, W.G. (1982a) "A three dimensional ship motion theory. Comparison between theoretical predictions and experimental data of the hydrodynamic coefficients with forward speed, Trans. RINA, 124, pp 141-157

Inglis, R.B. & Price, W.G. (1982b) "A three dimensional ship motion theory. Calculation of wave loading and responses with forward speed, Trans. RINA, 124, pp 183-192

Irons, B.M. (1965) "Structural eigenvalue problems: Elimination of unwanted variables", J. AIAA, (3), p 961

Irons, B.M. (1970) "Role of part inversion in fluid-structure problems with mixed variables", J. AIAA, 7, p 568

John, F. (1950) "On the motion of floating bodies: part 2", Comm. Pure Appl. Math., 3, pp 45-101

Jones, D.S. (1974) "Integral equations for the exterior acoustic problem", Quart. J. Mech. Appl. Math., 27(1), pp 129-142

Junger, M.C. (1952) "Vibrations of elastic shells in a fluid medium and the associated radiation of sound", J. Appl. Mech., Trans. ASME, 19(1), Mar 1952

Junger, M.C. & Feit, D. (1972) "Sound, structures and their interaction", MIT Press, Cambridge, Massachusetts

Kalinowski, A.J. (1975) "Fluid-structure interaction", Shock and Vibration Computer Programs - Reviews and Summaries, (W. & B. Pilkey, Eds.), Naval Research Lab., Washington, pp 405-452

Klosner, J.M. (1976) "Response of shells to acoustic shock", Shock Vib. Dig., 8(5), pp 3-13

Korvin-Kroukovsky, B.V. (1961) "Theory of seakeeping", New York: SNAME

Krajcinovic, D. (1975) "Some transient problems of structures interacting with fluid", Shock Vib. Digest, 7(6), pp 9-16

Kupradze, V.D. (1952) "Fundamental problems in the mathematical theory of diffraction", NBS rept. No 2008, Oct 1952

Lax, J.A., Sette, W.J. & Gooding, R.C. (1953) "Additional calculations on the response of a uniform cylindrical shell to a pressure pulse", Proceedings of the 6th. Conference on Progress in Underwater Explosions Research, NAVSHIPS 250-423-26, Rpt. 1955-1, Nov 1953

Lewis, E.V. (1967) "The motion of ships in waves", in 'Principles of Naval Architecture', ed. Comstock, J.P., pp 607-715, New York: SNAME

Lou, Y.K. & Su, T.U. (1976) "Free oscillations of submerged spherical shells", J. Acoust. Soc. Am., 63(5), pp 1402-1408

MacCamy, R.C. & Fuchs, R.A. (1954) "Wave forces on piles - a diffraction theory", Beach Erosion Board Tech. Memo 69

Mei,C.C. (1978) "Numerical methods in water-wave diffraction and radiation", Ann. Rev. Fluid Mech., 10, pp 393-416

Menton, R.T. & Magrab, E.B. (1973) "Interaction of acoustic pulses with fluid-loaded shell structures", Shock Vib. Digest, 5(12), pp 2-12.

Miller, C.A. (1980) "Dynamic reduction of structural models", J. Struct. Div., ASCE

Miller, C.A., Constantino, C.J. & Fey, E.H. (1967) "Stress wave impingement on underwater structures", Final rpt. for IITRI Project M1090, IIT Research Institute, Chicago, Ill., Sep 1967

Mindlin, R.D. & Bleich, H.H. (1953) "Response of an elastic cylindrical shell to a transverse step shock wave", J. Appl. Mech., Trans. ASME, 20(2), pp 189-195

Morand, H. & Ohayon, R. (1979) "Substructure variation analysis of the vibrations of coupled fluid-structure systems. Finite element results", Int. J. Num. Meth. Eng., 14( ), pp 741-755

Murray, J.M. (1965) "Further notes on the strength of tankers", Trans. NECIES, 81, pp 261-280

Murray, W.W. (1955) "Interaction of a spherical acoustic wave with a beam of circular cross-section", UERD-DTMB Rpt. 1-55, David Taylor Model Basin, Washington, DC, Jan 1955

Newman, J.N. (1978) "The theory of ship motions", Advances in Appl. Mech., 18, pp 221-283

Noor, A.K. & Dwoyer, D.L. (1989) "Computational structural mechanics and fluid dynamics: Advances and trends", Proceedings of the symposium, Washington, DC, Oct 1988

Novozhilov, V.V. (1959) "Theory of shells", Nordhoff

O'Callahan, J. (1989) "A procedure for an improved reduced system (IRS) model", 7th. Int. Modal Analysis Conf., Las Vegas, Nevada, Feb 1989

O'Callahan, J., Avitabile, P. & Riemer, R. (1989) "System equivalent reduction expansion process (SEREP)", 7th. Int. Modal Analysis Conf., Las Vegas, Nevada, Feb 1989

Ogilvie, T.F. & Tuck, E.O. (1969) "A rational strip theory of ship motions, Part 1", Interim Technical Report No. 013, Dept. of Naval Arch. and Marine Eng., Univ. of Michigan

Okpe, P.P.O. (1988) "Pressure loading effects on the dynamic behaviour of a stiffened cylinder", RNEC-RP-88022

Olsen, L.G. & Bathe, K.J. (1985) "Analysis of fluid-structure interactions. A direct symmetric coupled formulation based on the fluid velocity potential", Computers & Structures, 21(1), pp 21-32

Park, K.C., Felippa, C.A. & DeRuntz, J.A. (1977) "Stabilisation of staggered solution procedures for fluid-structure interaction analysis", Computational Methods for Fluid-Structure Interaction Problems, ASME, AMD-Vol.26, NY, pp

Petyt, M. (Ed.) (1980) "Recent advances in structural dynamics", Proceedings of International Conference, University of Southampton, Jul 1980

Price, W.G., Temarel, P. & Yousheng Wu (1985) "Structural responses of a SWATH or multi-hull travelling in waves", Int. Conference on SWATH ships and advanced multi-hull vessels, RINA, paper 13

Price, W.G., Randall, R.J. & Temarel, P. (1988) "Fluid-structure interaction of submerged shells", Proc. Conf. on Stress Determination and Strain Measurement in Aeronautics, Naval Architecture and Offshore Engineering, Univ. of Surrey, Guildford, Sep 1988

Rades, M. (1982) "Analysis of measured structural response data", Shock Vib. Dig., 14(4), pp 21-32

Randall, R.J. & Squire, J.J. (1984) "Measurement of the dynamic response of a plain round cylinder in air and underwater", Mecanique Materiaux Electricite, Actes des Journees Vibrations Chocs, No 404, Mar-Apr 1984, pp 59-67

Randall, R.J. (1985) "Modal analysis of a cylindrical structure immersed in water", Proc. 3rd. Int. Modal Analysis Conf., Orlando, Florida, 2, pp 738-744

Randall, R.J. (1986a) "Underwater shock trials on a plain unreinforced cylinder", SVB, 56(1), Aug 1986, pp 107-120

Randall, R.J. (1986b) "Frequency domain validation trial for the PAFEC fluid structure interaction codes. Volume 1 - Measurement", ARE DN(UJI) 86179, Dec 1986

Randall, R.J. (1988) "Problems of modelling shell type structures for fluid-structure interaction problems", RNEC-RR-88001

Ranlet, D., DiMaggio, F.L., Bleich, H.H. & Baron, M.L. (1977) "Elastic response of submerged shells with internally attached structures to shock loading", Computers & Structures, 7(3), pp 355-364

Rayleigh, Lord (1851) "Theory of sound", 2nd. Edition, Dover Publications, N.Y., 1945

Rellich, F. (1953) "Uber das asymptotische verhalten der Losungen von du + ly = 0 in unendlichen gebieten", Jahrsbericht der Deutschen Mathematiker Vereinigung, 53, pp 57-65

Remmers, G.M. & Belsheim, R.O. (1964) "Effects of technique on the reliability of mechanical impedance measurement", SVB, 34(3), 1964

Salvesen, N., Tuck, E.O. & Faltinsen, O. (1970) " Ship motions and sea loads", Trans. SNAME, 78, pp 250-287

Schenck, H.A. (1968) "Improved integral equation formulation for acoustic radiation problems", J. Acoust. Soc. Am., 44(1), pp 41-58

Seybert, A.F., Soenarko, B., Rizzo, F.J. & Shippy, D.J. (1985) "An advanced computational method for radiation and scattering of acoustic waves in three dimensions", J. Acoust. Soc. Am., 77(2), pp 362-368

Shen, S.F. (1977) "Finite element methods in fluid mechanics", Ann. Rev. Fluid Mech., pp 421-425

Sommerfeld, A. (1949) "Partial differential equations in physics", Academic Press, NY, p 189

Squire, J.J. (1987) "An investigation of the pressure loading effects on the dynamic behaviour of a thin walled cylinder", RNEC-RR-87003

Stokes, G.G. (1843) "On some cases of fluid motion", Proc. Camb. Phil. Soc., 8, pp 105-137

Turner, M.J., Clough, R.W., Martin, H.C. & Topp, L.J. (1956) "Stiffness and deflection analysis of complex structures", J. Aero. Sci., 23, pp 805-823

van Oortmerssen, G. (1972) "Some aspects of very large offshore structures", Proc. 9th. Symp. Naval Hydrodynamics, Paris, pp 957-975

Vasudevan, R. & DiMaggio, F.L. (1981) "Transient response of submerged shells using improved acoustic approximations", Computers & Structures, 14(3-4), pp 187-194

Vugts, J.H. (1971) "The hydrodynamic forces and ship motions in oblique waves", Neth. Res. Centre TNO Rept. 150S

Warburton, G.B. (1961) "Vibration of a cylindrical shell in an acoustic medium", J. Mech. Engr. Sci., 3, p 69

Wehausen, J.V. & Laitone E.V. (1960) "Surface waves", Handbuch der Physik, 9, pp 446-778, Springer-Verlag, Berlin

Wellstead, P.E. (1983) "Frequency response analysis", Tech. Rpt. No. 010/83, Solartron Instruments, Schlumberger Electronics (UK) Ltd.

Wu, Yousheng (1984) "Hydroelasticity of floating bodies", Ph.D. thesis, Dept. Mech. Eng., Brunel University

Zienkiewicz, O.C. & Bettes, P. (1975) "Infinite elements in the study of fluid-structure interaction problems", 2nd. Int. Symp. Computing Meth. Appl. Sci. and Engng, IRIA, Versailles

Zienkiewicz, O.C. & Bettes, P. (1978) "Fluid-structure dynamic interaction and wave forces. An introduction to numerical treatment", Int. J. num. Meth. Engng., 13(1), pp 1-16

Zienkiewicz, O.C. & Newton, R.E. (1969) "Coupled vibrations of a structure immersed in a compressible fluid", Proc. Symp. Finite Element Techniques, Institut fur Statik und Dynamik der Luft-und Baum-fahrt-konstruktionen, University of Stuttgart

Zienkiewicz, O.C. & Taylor, R.L. (1985) "Coupled problems - a simple time-stepping procedure", Comm. Appl. Num. Meth., 1( ), pp 233-239

APPENDICES

A - "Modal Analysis of a cylindrical structure immersed in water" by R.J.Randall presented at the 3rd International Modal Analysis Conference held at Orlando, Florida in January 1985.

B - "Underwater shock Trials on a plain, unreinforced cylinder" by R.J.Randall presented at the 56th Shock and Vibration Symposium held at Monterey, California in October 1985.

C - "Problems of modelling shell type structures for fluid-structure interaction problems" by R.J.Randall. Research report No. RNEC-RR-88001 January 1988

D - "Fluid-structure interaction of submerged shells" by W.G.Price, R.J.Randall and P.Temarel presented at the Stress Determination and Strain Measurement in Aeronautics, Naval Architecture and Offshore Engineering Conference held at the University of Surrey, Guildford in September 1988.

E - "Responses of a flexible non-uniform circular beam in a bounded, viscous fluid" by R.Hosoda, W.G.Price and R.J.Randall published in the Journal of Sound and Vibration Vol.128(1) January 1989.

Proceedings of the

3rd International Modal Analysis Conference

January 28-31, 1985
Orlando Marriott Inn
International Drive
Orlando, Florida

DIRECTOR:

Dominick J. DeMichele

UNION COLLEGE

Aaron Feinsot, Dean, Graduate and Continuing Studies

Rae D'Amelio, Administrator

Volume II

Sponsored by:

Union College

Schenectady, New York 12308

Appendix A

Proceedings of the

3rd International Modal Analysis Conference

January 28-31, 1985
Orlando Marriott Inn
International Drive
Orlando, Florida

DIRECTOR:
Dominick J. DeMichele
UNION COLLEGE
Aaron Feinsot, Dean, Graduate and Continuing Studies
Rae D'Amelio, Administrator

Volume II

Sponsored by:
Union College
Schenectady, New York 12308

MODAL ANALYSIS OF A CYLINDRICAL STRUCTURE IMMERSED IN WATER

Lieutenant R RANDALL Royal Navy
Royal Naval Engineering College
Plymouth Devon England

ABSTRACT

A common problem in a marine environment is associated with the interaction of a vibrating structure with the surrounding fluid. A variety of analytical and numerical solutions have been proposed for this situation often employing approximations as analytical solutions only exist for very straightforward geometrics. However, very little experimental data are available for comparison in this field.

The paper describes a series of dynamic studies conducted upon a cylindrical structure tested in air and totally immersed in water. Modal analysis techniques have been used to identify the natural frequencies and mode shapes under both conditions.

Good correlation has been obtained between experimental results and an analytical model.

NOMENCLATURE

a	Mean radius of cylinder.
C_0, C_1	Parameters defined in equation (1).
E	Youngs Modulus.
$H_n^{(2)}(x) \equiv J_n(x) - iY_n(x)$	Hankel function of the second kind.
$H_n^{(2)'}(x) = \frac{d}{dx}\left[H_n^{(2)}(x)\right]_{x = ka}$	
h	thickness of cylinder
$I_n(x)$, $K_n(x)$	Bessel functions of first and second kinds.
K_0, K_1, K_2	Parameters defined in equation (1).
$[K]$	Stiffness matrix.
L	Axial half wavelength.
$[M]$	Mass matrix.
m	Number of axial half waves.
N	Number of degrees of freedom.
n	Number of circumferential waves.
P_3	Disturbing force (radial direction)
t	time.
W	Radial component of amplitude of vibration of the cylinder
$\{x\}$, $\{\ddot{x}\}$	Vectors of displacement and acceleration.

$x \equiv ka \equiv \sqrt{(\Omega a/c)^2 - \lambda^2}$, $\Omega a/c > \lambda$

$x_1 \equiv k_1 a \equiv \sqrt{\lambda^2 - (\Omega a/c)^2}$, $\lambda > \Omega a/c$

α	Receptance.
$\beta \equiv h^2/12a^2$	
$\Delta = \rho_s \frac{a^2\Omega^2(1-\nu^2)}{E}$	
$\lambda = \pi a/L$	
ν	Poisson's Ratio.
ρ	Density of fluid medium.
ρ_s	Density of cylinder.
$[\Phi]$	Eigenvector ma matrix.
Ω	Frequency (circular).
ω	Natural frequency (circular) of shell in vacuo.

NOMENCLATURE (Contd)

$[\omega_r^2]$ Eigenvalue matrix.

1. Introduction

This is a record of experiments carried out in the laboratories of the RN Engineering College, Manadon on the dynamic response of a plain round cylinder. The cylinder was tested separately in air and underwater and the resonant frequencies and mode shapes were compared with those predicted by an analytical method.

This work forms part of an overall programme on the transient response of ship structures when subjected to shock being undertaken by the Structural Dynamics Division at RNEC.

2. Apparatus

The Flexural Vibrations of thin cylinders and the vibration of a cylindrical shell in an acoustic medium have been analysed by amongst others Arnold & Warburton[1,2]. In order to make the problem tractable there are several idealised conditions imposed. The thickness of the cylinder considered, is small compared to the least radius of curvature and the shell deformation is small and linear and assumed to be described by the middle surface deflection. The most obvious single limitation and one that is not practically realisable is in the length of the cylinder; analytical solutions for submerged shells only exist for infinitely long cylinders.

From previous studies[3] it was appreciated that geometrical irregularities in the cylinder such as large tolerances of the diameter around the circumference and non-uniform wall thickness cause poor definition or even split-peak at resonance. Therefore a finely manufactured cylinder was obtained from Research Models Equipment of Reading UK which was a scaled model of a much larger cylinder that had previously been measured at ARE Portland. The total length of the cylinder was limited by the physical dimensions of the laboratory and the need to place accelerometers inside the shell.

Measurement and excitation points were located at 15 points within the structure. Each point was instrumented with accelerometers to record vertical motion; the accelerometers were mounted on studs which were glued inside the cylinder. Single point excitation was applied in either the vertical or the horizontal direction using an electromagnetic shaker driving through a push-rod and force gauge.

The measurement sites were chosen to obtain the mode shapes in both the axial and circumferential planes. Eight accelerometers were spaced at 45° intervals around the circumference and the remaining seven accelerometers were arranged in line along the length of the cylinder. Signals from the accelerometers and force gauge were sent by cable through a watertight gland in one end into two conditioning amplifiers. The ends of the cylinder were closed, a finite element analysis of the structure confirming earlier results which showed that the presence or absense of ends had no noticeable effect on experimental measurements. Signals from the amplifiers could be fed into the measuring equipment.

3. Experimental Procedure

3.1 Calibration

Before any experiments were conducted upon the structure a calibration test was performed. The force gauge and accelerometer were attached to a known mass and a frequency response test carried out. Excitation was provided using the multi-sine (M-S) generator on a Solartron 1200 Signal Processor driving the electro-magnetic shaker through the force gauge. Force and acceleration signals were monitored using the Solartron 1200 and displayed as an apparent mass (Force/Acceleration) transfer function for the range 0 to 2000 Hz. The scale factor on the accelerometer channel was then adjusted so that the apparent mass corresponded to the mass of the inertia block. These calibration factors were retained during the complete set of trials and rechecked on completion.

3.2 Testing

Several alternative arrangements of testing were experimented with before the final test programme commenced. The purpose of this was to determine what influence different loading and support conditions had on the measurements. Two methods of support were used; with the cylinder freely supported on foam strips on a laboratory bench and suspended from a gantry with rubber "bungee" supports acting as mechanical low pass filters. The electromagnetic shaker was either mounted on the bench alongside the cylinder or suspended on 'soft' springs on the same gantry above the cylinder. There was no appreciable difference in the measured transfer functions whatever support or loading condition was used.

Two types of continuous excitation were used in the testing, multi-sine (M-S) and pseudo-random binary sequence (PRBS) noise. No significant differences could be noted between these two types of excitation except that M-S gave more pronounced peaks at resonance whereas PRBS gave better definition elsewhere but with less well defined coherence functions.

The measured response over the frequency range 100-600 Hz (in air) and 0-500 Hz (submerged) given in the form of receptance (x/f) curves obtained directly from the Solartron 1200, the data was also stored on magnetic tape using an HP85, for subsequent analysis. Transfer functions were also obtained for the same cylinder submerged in water. These measurements took place near the centre of a 7.5 m long × 1.7 m wide tank. The total depth of water was 1.6 m and the top of the cylinder was held 500 mm below the free surface. The cylinder was placed across the tank so that boundary effects such as wave reflections were minimised. The tank is lined with ceramic tiles.

As the sealed cylinder is positively buoyant it was necessary to secure it in position using rubber "bungees" attached to sinkers. The tank could be readily filled or drained in order to make adjustments to the supports. When the cylinder was level in the correct position the electromagnetic shaker was lowered on to the push rod which projected out of the water surface.

4. Theory & Analysis

4.1 Theoretical Model

The general theory for the forced response of an infinitely long cylindrical shell is given in the references. Three equations of motion are obtained in terms of the axial, tangential and radial displacements of the middle surface of the shell. When the effects of an acoustic medium are included, the equation describing radial displacement will have extra terms related to the pressures on the shell. The equations of motion of the tangential components are assumed to remain unaltered.

From Warburton[2] the radial component of amplitude of vibration of the shell is given by

$$W = \frac{-P_3(\Delta^2 - C_1\Delta + C_0)}{\Delta^3 - K_2\Delta^2 + K_1\Delta - K_0 + f(x)\Delta(\Delta^2 - C_1\Delta + C_0)} \quad (1)$$

At a resonant frequency the real part of the denominator of equation (1) is zero. Therefore resonant frequencies are given by

$$\Delta^3 - K_2\Delta^2 + K_1\Delta - K_0 + \Delta(\Delta^2 - C_1\Delta + C_0).\ \mathrm{Re}|f(x)| = 0 \quad \ldots\ldots (2)$$

The function $f(x)$ contains Bessels functions and their derivatives and takes different forms depending on whether the acoustic medium surrounds the shell, is contained with it or is present both inside and out. In the case in question ie an external fluid

$$f(x) = -\frac{\rho}{\rho_s}\frac{a}{h}\frac{1}{x}\frac{H_n^{(2)}(x)}{H_n^{(2)\prime}(x)} \quad \ldots\ldots (3)$$

for $\frac{\Omega a}{c} > \lambda$ and $x = \left[(\Omega a/_c)^2 - \lambda^2\right]^{\frac{1}{2}}$

and

$$f(x_1) = -\frac{\rho}{\rho_s}\frac{a}{h}.\frac{1}{x_1}\frac{K_n(x)}{K_n'(x)} \quad \ldots\ldots (4)$$

for $\frac{\Omega a}{c} < \lambda$ and $x_1 = \left[\lambda^2 - \left(\frac{\Omega a}{c}\right)^2\right]^{\frac{1}{2}}$

To solve equation (2) it is convenient to rewrite it as

$$SF(\Delta) - \gamma_n(x) = 0 \quad \ldots\ldots (5)$$

where

$$S = \frac{\rho_s}{\rho}.\frac{h}{a}$$

$$F(\Delta) = \frac{\Delta^3 - K_2\Delta^2 + K_1\Delta - K_0}{\Delta(\Delta^2 - C_1\Delta + C_0)}$$

$$\gamma_n(x) = \frac{1}{x}\frac{J_n(x)J_n'(x) + Y_n(x)Y_n'(x)}{\left[J_n'(x)\right]^2 + \left[Y_n'(x)\right]^2}$$

for $\Omega a/_c > \lambda$

Because both Δ and the argument of the Bessels function, x, depend of the resonant frequency, Ω, an iterative solution to equation (5) is required.

4.2 Modal Analysis

The receptance curves produced by the Solartron 1200 show the resonant frequencies at a glance. The information can also be used to calculate modal constants using a multi-mode curve fitting method based upon the technique described by Gleeson(4).

As it is not possible to analyse each point on the surface of a complicated structure a number of co-ordinate points or degrees of freedom are determined which will adequately describe the movement of the structure. The problem is thus discretized and can be represented in matrix form. The free response of an idealised undamped system can be written as

$$[M]\{\ddot{x}\} + [K]\{x\} = 0 \quad \ldots\ldots (6)$$

in which $[M]$ and $[K]$ are $N \times N$ mass and stiffness matrices where N is the number of degrees of freedom and $\{x\}$ and $\{\ddot{x}\}$ are $N \times 1$ displacement and acceleration vectors. If the displacement is of the form

$$\{x\} = \{X\}e^{i\omega t} \quad \ldots\ldots (7)$$

then equation (6) can be rewritten

$$-\omega^2[M]\{X\} + [K]\{X\} = 0 \quad \ldots\ldots (8)$$

which is a standard eigenvalue problem which has N solutions. The r^{th} mode is characterised by an eigenvalue ω_r^2 and an eigenvector $\{X_r\}$. If all N solutions are pulled together into a diagonal eigenvalue matrix $[\omega_r^2]$ and the eigenvector, or shape, matrix $[\phi]$, these constitute a modal model of the system.

The mode shape matrix is orthogonal and may be scaled (or mass-normalised) so that

$$[\phi]^T[M][\phi] = [I]$$
$$[\phi]^T[K][\phi] = [\omega_r^2] \quad \ldots\ldots (9)$$

therefore

$$[M] = [\phi]^{-T}[\phi]^{-1}$$
$$[K] = [\phi]^{-T}[\omega_r^2][\phi]^{-1} \quad \ldots\ldots\ldots\ldots (10)$$

substituting into the equations of motion for an undamped, sinusoidally excited N degree of freedom system

$$(|K| - \omega^2|M|)\{X\}e^{i\omega t} = \{F\}e^{i\omega t} \quad \ldots\ldots (11)$$

gives after rearranging, the response at the j^{th} co-ordinate caused by force input at the k^{th} co-ordinate

$$\frac{X_j(\omega)}{F_k(\omega)} = \alpha_{jk}(\omega) = \sum_{r=1}^{N} \frac{r\phi_j r\phi_k}{(\omega_r^2 - \omega^2)} \quad \ldots\ldots\ldots\ldots (12)$$

The product of elements in the mode shape matrix $r\phi_j r\phi_k$ is termed $_rA_{jk}$, a modal constant. In order to determine the individual elements the point receptance

$$\alpha_{kk}(\omega) = \sum_{r=1}^{N} \frac{r\phi_k^2}{(\omega_r^2 - \omega^2)} \quad \ldots\ldots\ldots\ldots\ldots (13)$$

is required and using this and the transfer receptances α_{jk} the full modal matrix can be constructed. Equation 12 can then be used to regenerate a curve for comparison with that obtained experimentally.

DISCUSSION

During the trials complete sets of receptance plots for the 15 transducers were obtained with the cylinder either in air or underwater. In this paper only the two point receptance curves (figs 2 & 3) have been reproduced. The regenerated curves are overlaid in each case and from these modal constants and resonant frequencies were obtained.

Table 1 - Comparison of results

In-air

Mode shape m	n	Predicted frequency (Hz)	Measured frequency (Hz)
1	2	193.4	194
1	3	197.2	198
1	4	339.0	336
2	3	381.8	387
2	4	399.6	403
1	5	540.7	537
3	4	559.4	565
2	5	567.0	569

Undermeter

Mode shape m	n	Predicted frequency (Hz)	Measured frequency (Hz)
1	2	98.2	96
1	3	109.6	107
1	4	203.7	199
2	3	215.6	214
2	4	242.0	239
2	2	338.4	338
3	4	342.7	341
1	5	345.2	-
2	5	363.6	359
3	3	410.5	401
3	5	412.3	411

From the above table the good correlation between predicted and measured data can be seen. The only difficulties are not due to the analytical model but are concerned with the problems of measuring several closely separated resonances and differentiating between n = 3 and n = 5 mode shapes with the transducers as situated.

CONCLUSIONS

A comprehensive set of results for the frequency response of a plain round cylinder vibrating in air and underwater have been obtained. Difficulties associated with the instrumentation and location of transducers has been highlighted. Good correlation has been obtained between the resonant frequencies and mode shapes predicted by an analytical method for an infinitely long ideal cylinder which have borne comparison with the measured values on the cylinder under test. Further trials are continuing using other models and comparing different methods of analysis.

REFERENCES

1. ARNOLD, R N & WARBURTON, G B: The flexural vibrations of thin cylinders. Proc. Instn Mech. Engrs, A, Vol 167, pp62-80, 1953.

2. WARBURTON, C B: Vibration of a cylindrical Shell in an acoustic medium. Jrnl. Mech. Engng. Sci., Vol 3, No 1, pp69-79, 1961.

3. RANDALL, R J & SQUIRE J J: Measurement of the dynamic response of a plain round cylinder in air and underwater. Mechanique Materiaux Electricite, No 404, pp59-67, March 1984.

4. GLEESON, P T: Spatial models of vibrating undamped beams. Mechanique Materiaux Electricite, No 389-390-391, pp210-217, May 1982.

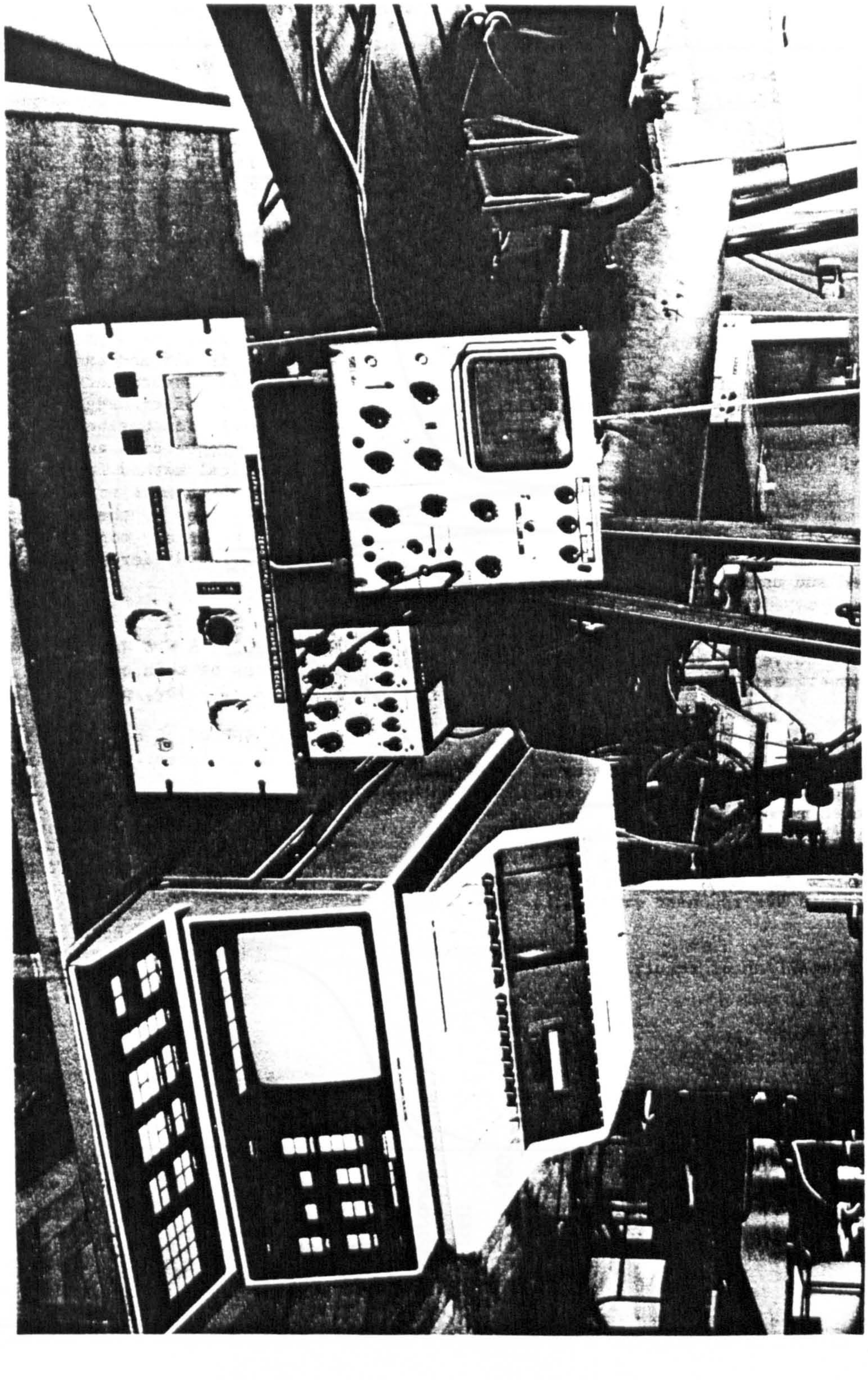

Figure 1 Apparatus

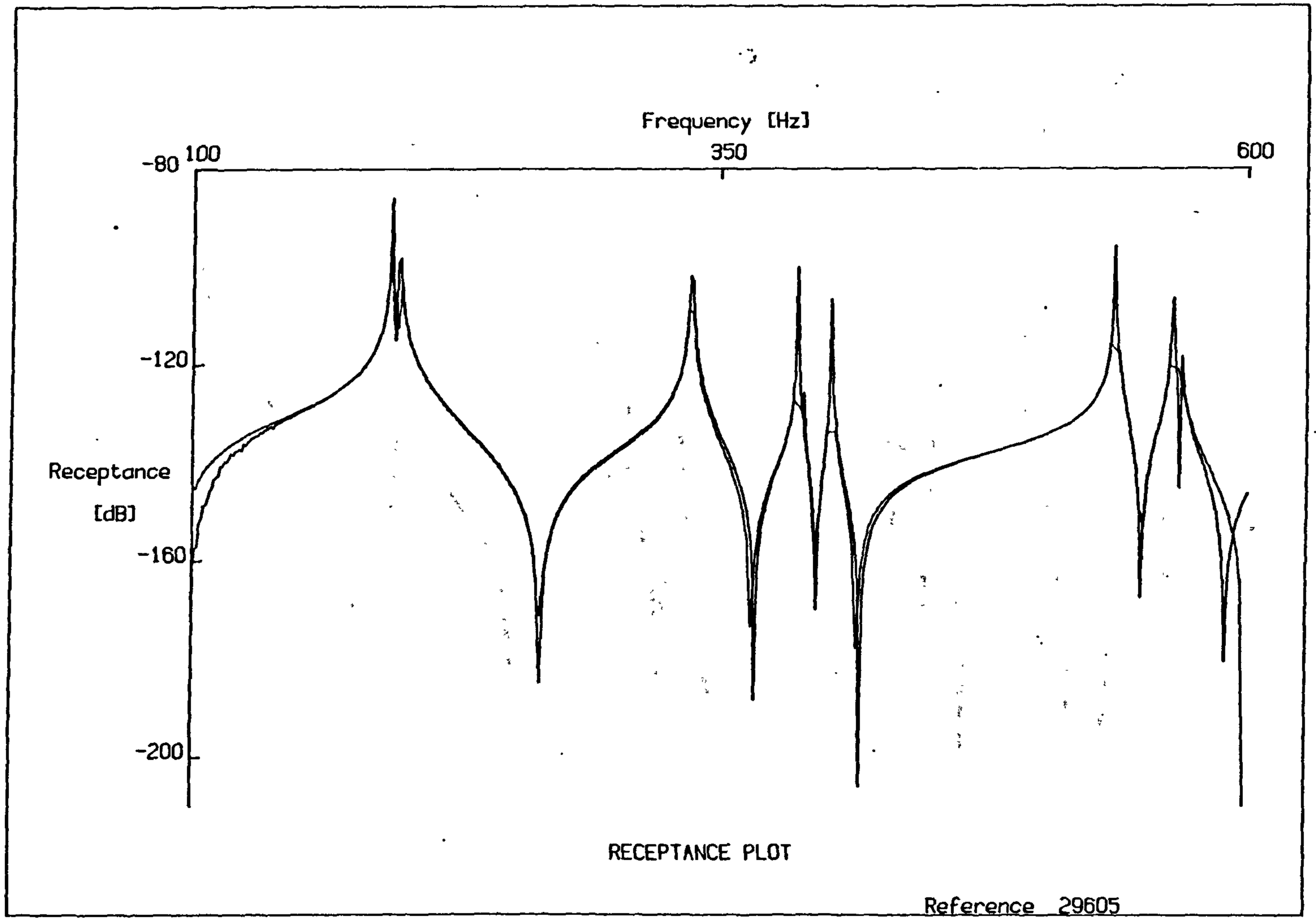

Figure 2 Measurements in Air

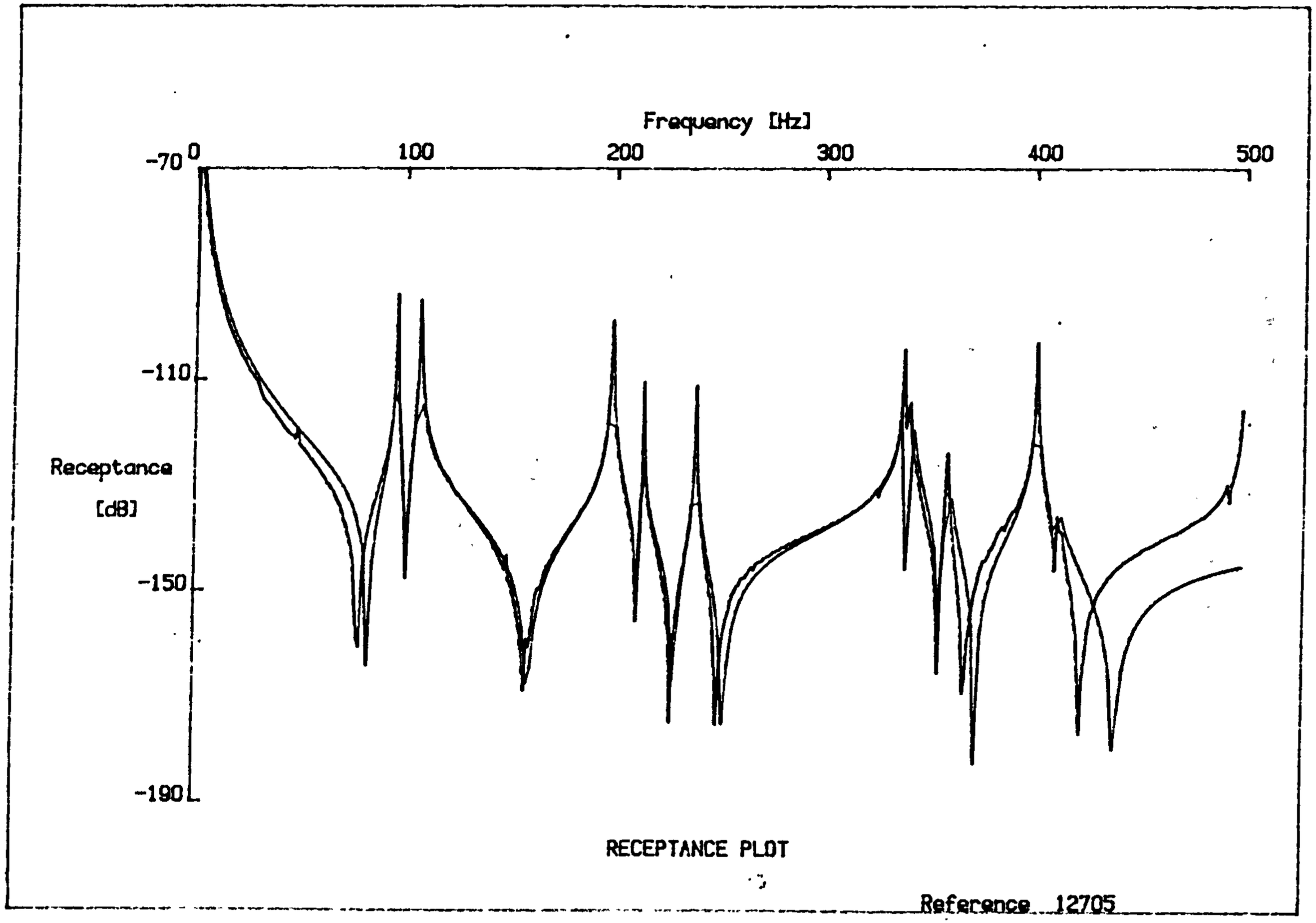

Figure 3 Measurements taken Underwater

Bulletin 56
(Part 1 of 3 Parts)

Reprinted From

THE SHOCK AND VIBRATION BULLETIN

Part 1
Welcome,
Invited Papers, Shipboard Shock,
Blast and Ground Shock,
Shock Testing and Analysis

AUGUST 1986

A Publication of
THE SHOCK AND VIBRATION
INFORMATION CENTER
Naval Research Laboratory, Washington, D.C.

Office of
The Under Secretary of Defense
for Research and Engineering

Bulletin 56
(Part 1 of 3 Parts)

Reprinted From

THE SHOCK AND VIBRATION BULLETIN

Part 1
Welcome, Invited Papers, Shipboard Shock, Blast and Ground Shock, Shock Testing and Analysis

AUGUST 1986

A Publication of
THE SHOCK AND VIBRATION
INFORMATION CENTER
Naval Research Laboratory, Washington, D.C.

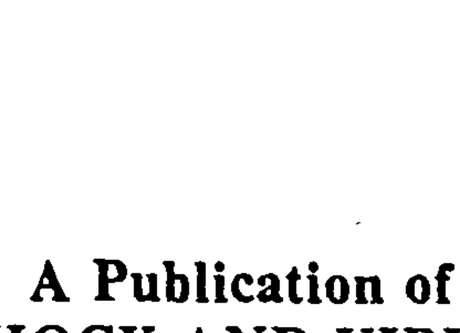

Office of
The Under Secretary of Defense
for Research and Engineering

UNDERWATER SHOCK TRIALS ON A PLAIN, UNREINFORCED CYLINDER

Lt R J RANDALL, RN
Admiralty Research Establishment
Portland Dorset

Strain was recorded at 14 locations on a submerged plain unreinforced cylinder when subjected to the blast from a small explosive charge. This work was carried out as part of a larger study into the topic of fluid-structure intersection. The cylinder was selected as a simple geometric shape which could be analysed theoretically so that the experimental results could validate the applicability of approximations in current use. Only the preliminary findings together with details of the testing environment and procedure are presented in this report. The results show how the hoop and meridonal strain levels vary with the angle of the incident shock wave, and how the shock is transferred from the fluid through the structure. Changes in the frequency response spectrum are also presented for the envelopment and post envelopment periods.

INTRODUCTION

In the latest reviews [1-4]assessing the developments in analytical techniques for dealing with the fluid-structure interaction problem, little or no evidence is given of experimental data than can be used to evaluate the analytical predictions. The reason for this, is probably that a good general formal method for dealing with the transient response of complex structures has not yet appeared. The most widely used approach is to adopt a decoupling scheme such as the 'doubly asymptotic approximation' [5]. This and later more refined schemes have been evaluated against the response of idealised structures for which an exact solution can be obtained. However all these schemes stem from an approximation which its author notes [6] is not satisfactory for situations involving prominent intermediate frequency components as it overestimates the radiation damping, and although they may prove adequate in certain circumstances they must be used with caution. Nevertheless computer codes are now being used and developed [7] which embody these approximations and therefore a more thorough validation should be performed.

As instrumentation and other practical considerations will introduce additional uncertainties into the problem it will assist the interpretation of results if the test structure retains a simplistic shape. There follows detailed information about a series of shock tests carried out on a simple test structure in collaboration with the staff of the Admiralty Research Establishment (ARE) Dunfermline in HM Naval Base, Rosyth.

The test structure was a plain unreinforced mild steel cylinder, whose geometry and dynamic characteristics were known from previous tests [8]. The cylinder was held in position underwater and subjected to a spherical shock wave caused by firing small explosive charges at a pre-determined stand-off. The only limitations on the size of the charge and the distance of the stand-off were that no permanent structure damage was to occur.

The charge size and stand-off were determined first and then remained unaltered for the remainder of the trial. The angle of incidence of the shock wave was varied, though, to investigate what effect this had on the maximum levels of stress recorded. The cylinder was maintained in position and for successive shots the location of the charge was altered in the same horizontal plane.

TESTING ENVIRONMENT

It is inevitable that there will be a compromise between the idealised system that is conceived for the sake of theoretical analysis and what can be physically set up to represent that system. The requirements, in this instance, are for a prescribed pressure to apply a force to a simple structure in a fluid environment.

The practical problems of representing this in the laboratory are evident from the photograph (Fig 1) of the structure suspended above the tank before testing.

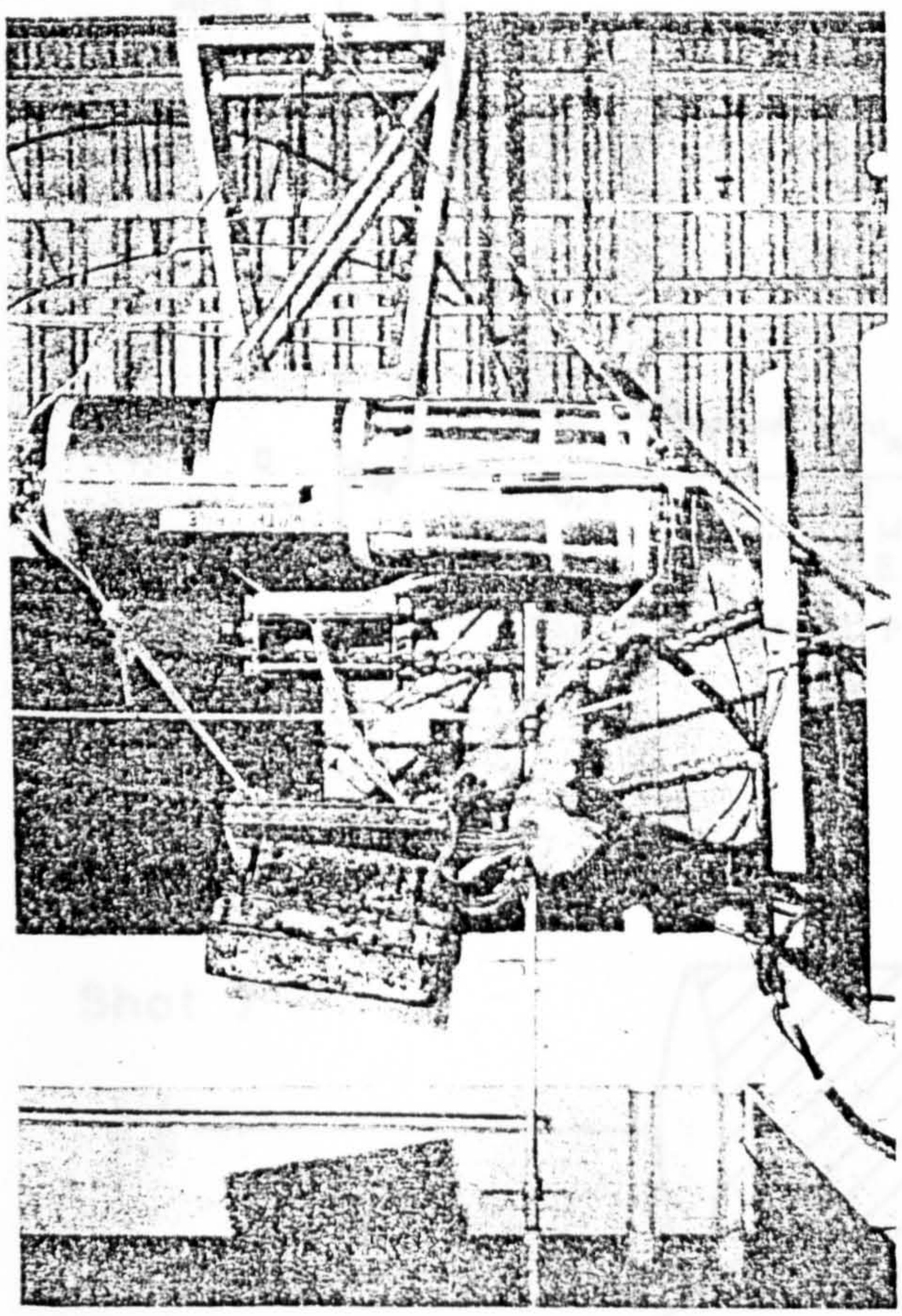

Fig 1 - General Arrangement

This arrangement is obviously divorced from the original concept of an idealised system. Hard reflective tank walls are clearly in close proximity to the structure. The cylinder itself is thin walled (3mm MS tube) with an aspect ratio of 120:1, but it is only 1.284m long and has flat ends. In addition ballast weights are needed to maintain the structure at the required depth (300mm below the free surface) and support arms have been welded to the ends to hold the explosive charge and pressure transducers.

The charges used in this trial were electric detonators, type N79, each containing 1 gm of plastic explosive. This small charge fixed relatively near to the structure produced a spherical shock wave but satisfied the requirements of the enclosed testing area and the limitation that no permanent damage was to be sustained by the structure. Each pressure time history has a unique signature but are characterised by a very brief duration.

A typical pressure time history is shown in Fig 2; the duration of the pulse is about 50 μs and the rise and decay of pressure is very rapid. Subsequently the pressure returns to zero.

A consequence of this characteristic pressure signature is that a very rapid sampling rate (1×10^6 sps) has to be employed on the ADC to prevent maxima being clipped. With this high sampling rate and the limitations of 32K of computer memory only the immediate response of the structure could be studied closely.

However five separate shocks and responses were measured and analysed. Fig 3 indicates the position of the charge relative to the structure for each individual firing (Shots 1 and 2 were calibration shots and are not included).

INSTRUMENTATION

Pressure Transducers

Two types of tourmaline underwater blast pressure transducer were used to record the pressure time history, one was manufactured by PCB Piezotronics Inc and the other was an ARE design. Both types have a volumetric sensitive tourmaline crystal element suspended in insulating oil and contain a built-in micro-electronic line driver amplifier which outputs a high voltage low impedance signal.

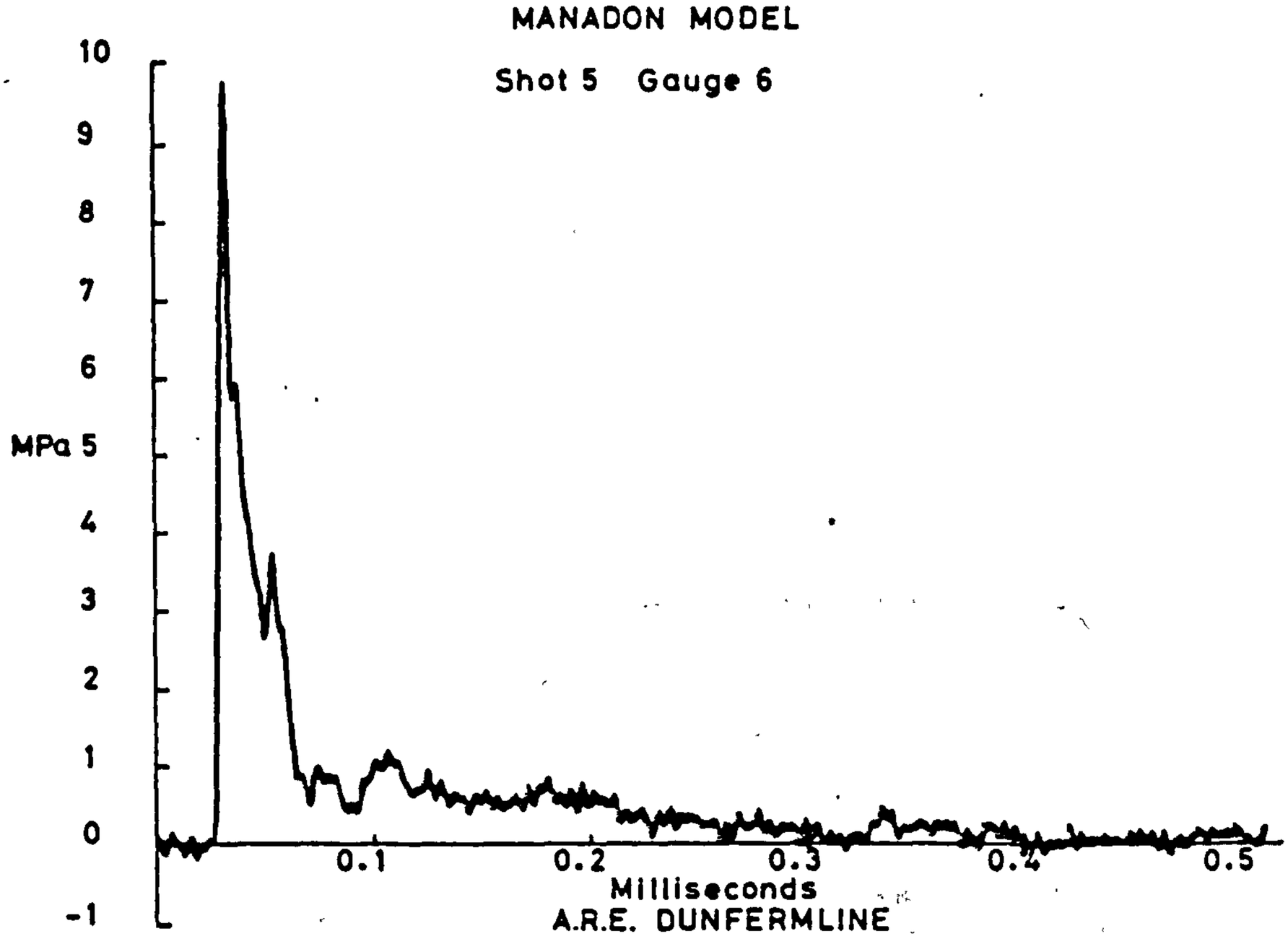

Fig 2 - Typical Pressure Time History

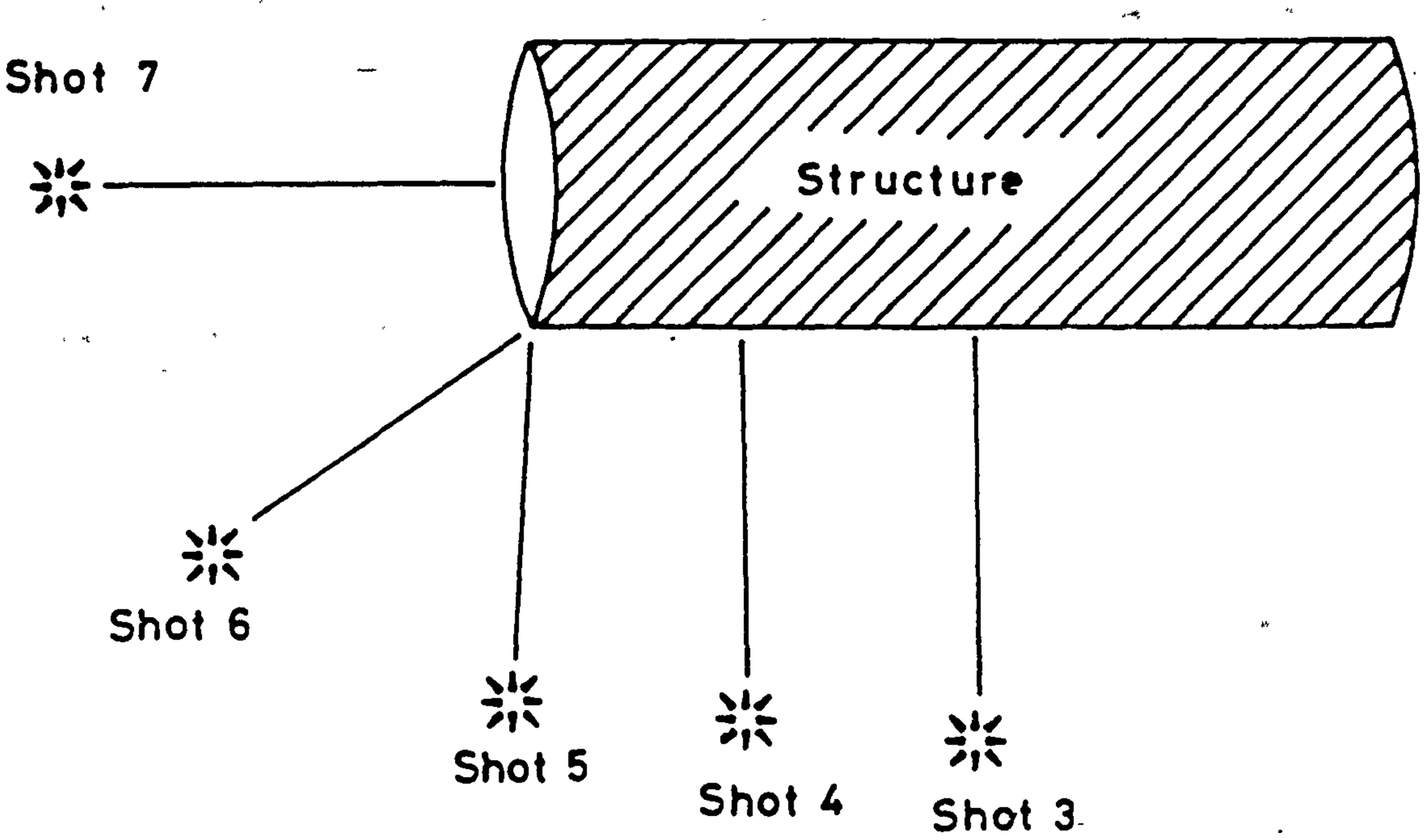

Fig 3 - Firing Sequence

Tourmaline gauges are not generally consistent or reliable and for this reason it would have been desirable to have a large number of transducers to measure the combined pressure field consisting of incident, reflected and radiated components. However, the presence of any pressure gauge and its associated cabling must interfere with the pressure field through shadowing and diffraction effects, therefore only 2 gauges were used to monitor 'free' field and 'near' field pressures.

The mounting arrangement for the 'free' field pressure sensor (Gauge No 6) is as shown (Fig 4). The 'near' field pressure sensor (Gauge No 5) was taped to the cylinder.

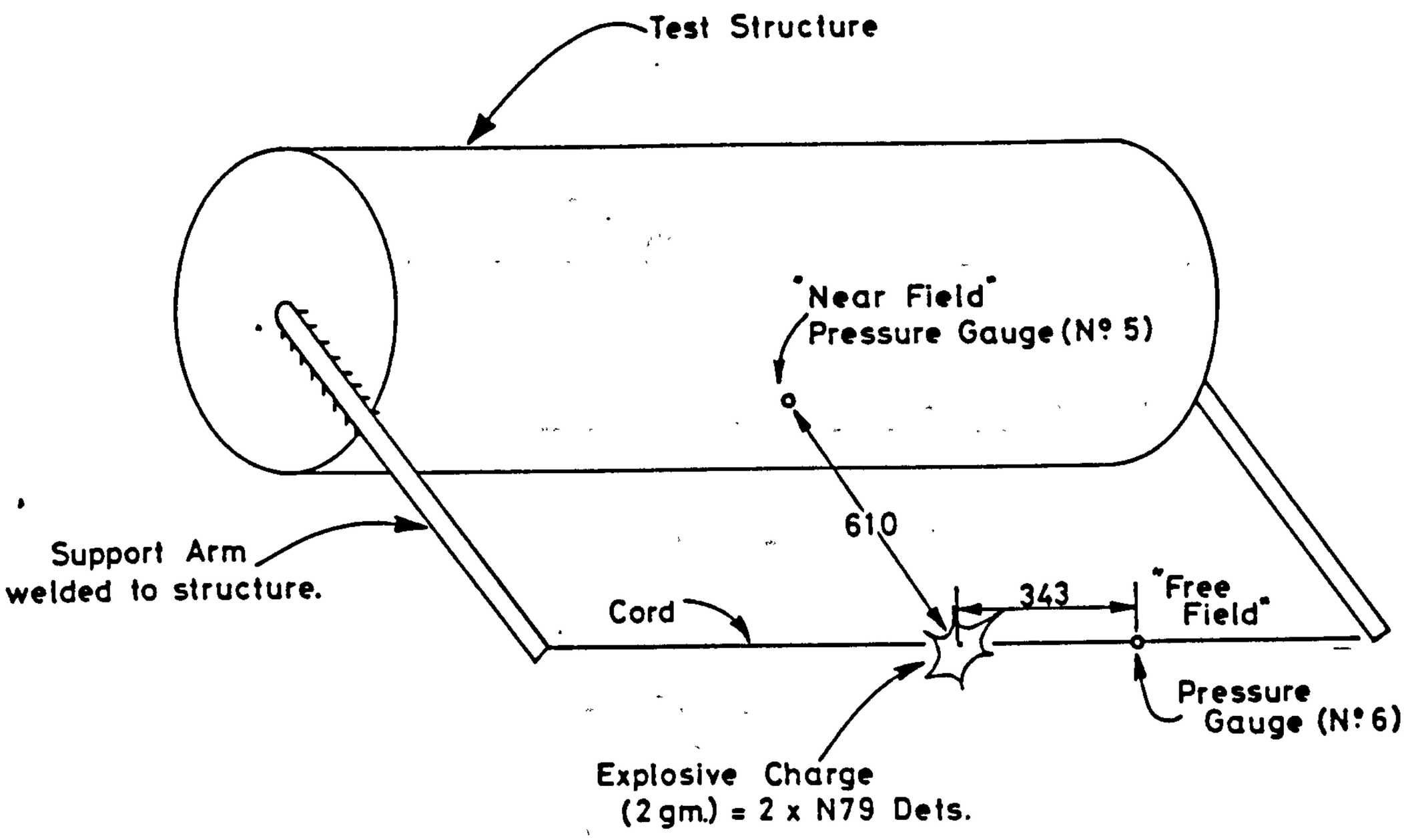

Figure 4 Charge handling Arrangement

Strain Gauges

The structural response was measured at 17 locations to obtain axial and circumferential (hoop) deformations (Fig 5). It was decided in this instance to use strain gauges rather than accelerometers. Each site was equipped with a right-angled pair of gauges set up to measure hoop and axial strain.

The advantages of obtaining strain as a structural response rather than accelerations were that:

(1) Strain is a direct measure of structural damage which is of prime importance.

(2) Less processing of data will be required as rigid body motions will not be recorded and zero shift, base strain and cross axis sensitivity problems encountered with accelerometers are largely done away with.

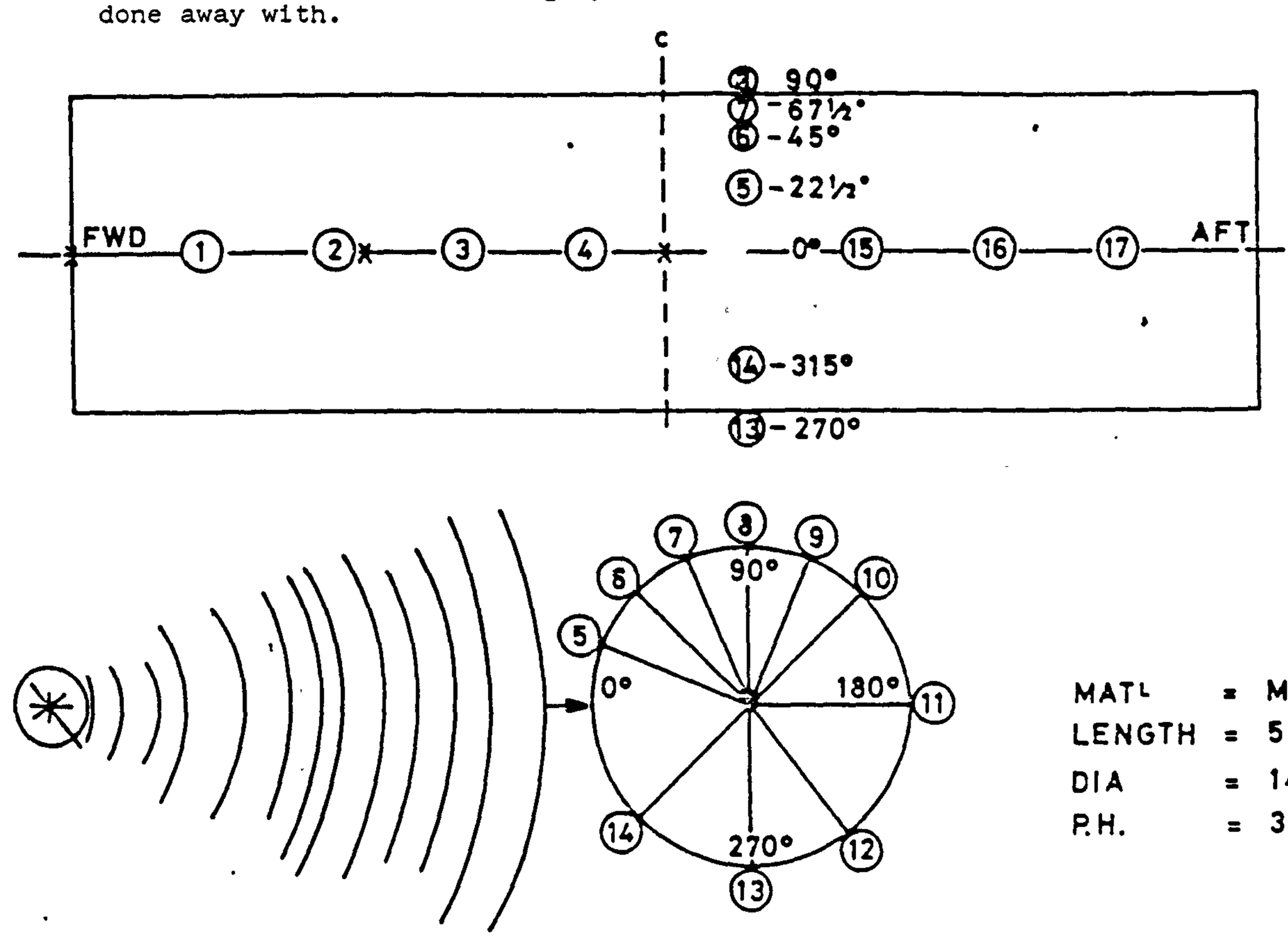

DEC 1984

R.N.E.C. MANADON S/M MODEL

Fig 5 - Strain Gauge Positions
(17 No right angled pairs)

RESULTS AND ANALYSIS

A representative selection of the results is included to demonstrate the major conclusions.

Shot 3 Channel 4C Time 0-8.191 ms

Fig 6 shows a typical pattern for the response at the centre of the structure subjected to a broadside shock wave. The peak response corresponds to the occurrance of the peak pressure and is followed by rapid, lightly damped, oscillations.

Each record was examined to assess the relationship between the onset of movement (as recorded by strain) and the arrival times of the pressure pulse. The shock wave can arrive at a point on the structure via two routes.

(1) directly through the field.

(2) by the most direct route between the charge and the structure and then through the structure to the point in question as a compression wave.

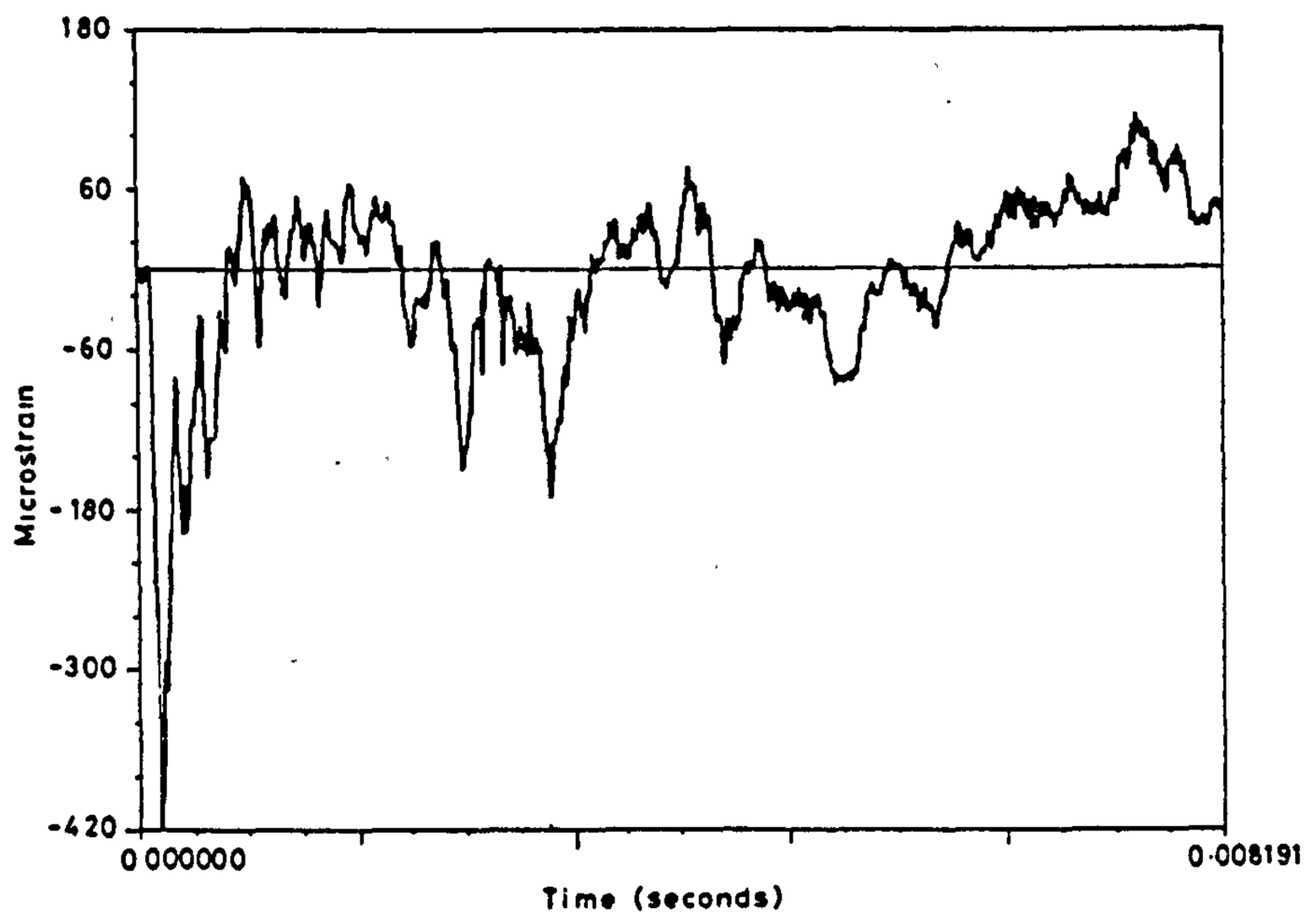

Fig 6 - Hoop Strain Time History
(Shot 3 Channel 4)

All recorded channels were measured simultaneously and then synchronised to a single event, namely the peak of the near field pressure pulse.

As stated previously the length of the signal was curtailed by the size of the processing unit but within this time window the maximum strain always occurs soon after the pressure pulse. Effects due to reflections and bubble collapse happen comparatively much later (circa 28 ms), therefore the period 0-1 millisecond is studied in greater detail.

The second route is longer but as the speed of sound is 3½ times faster in steel than it is in water this is more often the quicker route.

Shot 7 Channel 1C Time 0-1 ms (Fig 7)

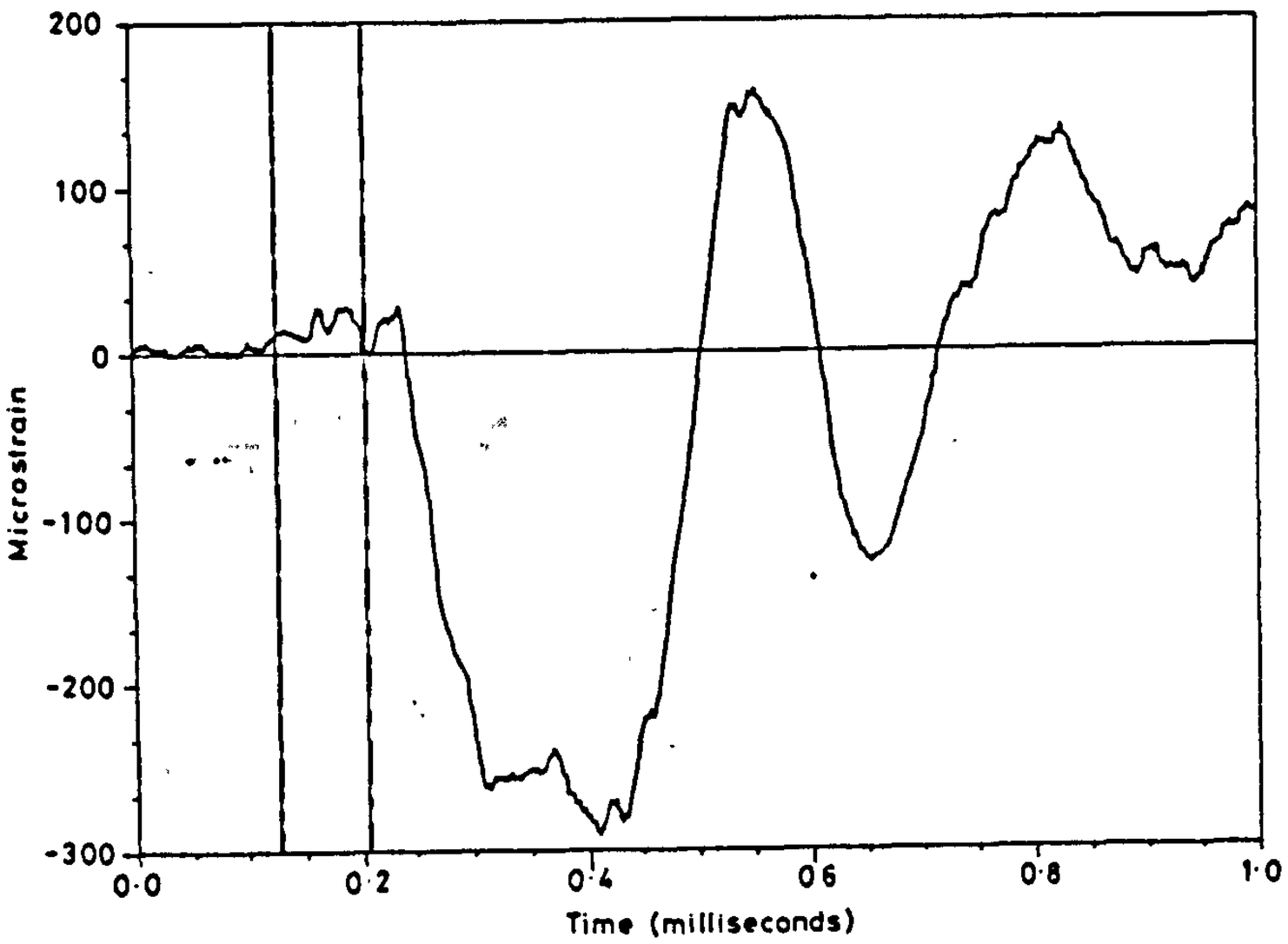

The two vertical lines signify the first arrival times of the shock wave travelling through the structure (shown dashed) and, secondly, directly through the water (shown chain-dotted). In this instance where variations in hoop strain are shown for the location nearest the charge causing an end-on attack, there is no correlation between these event times and the onset of strain.

Fig 7 - Hoop Strain Time History
(Shot 7 Channel 1)

Shot 7 Channel 1L Time 0-1ms (Fig 8)

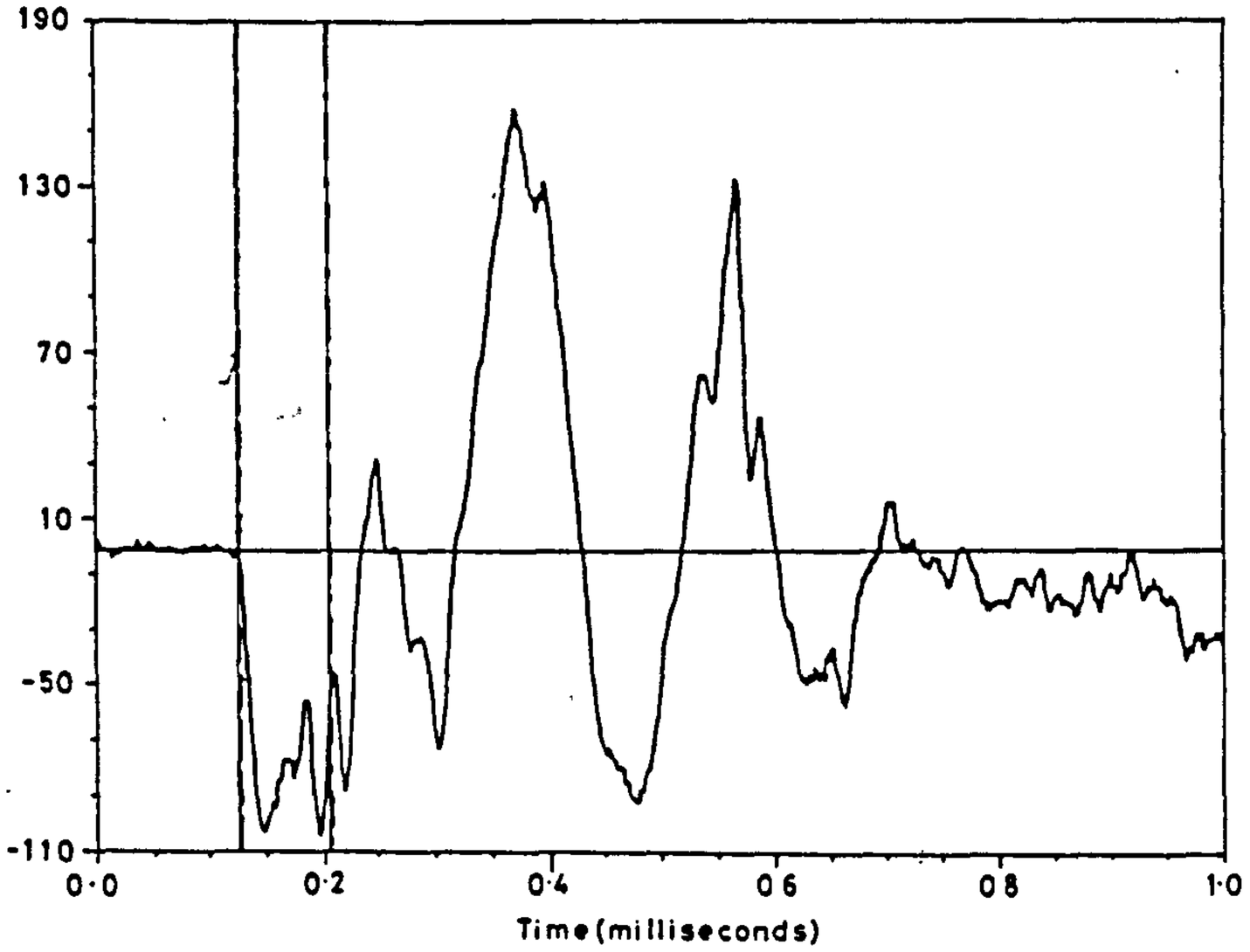

However Fig 8 shows the variation of axial strain at the same location and it can be seen that the onset of axial strain coincides very closely with the arrival of the shock wave which travels through the structure.

Fig 8 - Axial Strain Time History
(Shot 7 Channel 1)

Shot 7 Channel 17L Time 0-1ms (Fig 9)

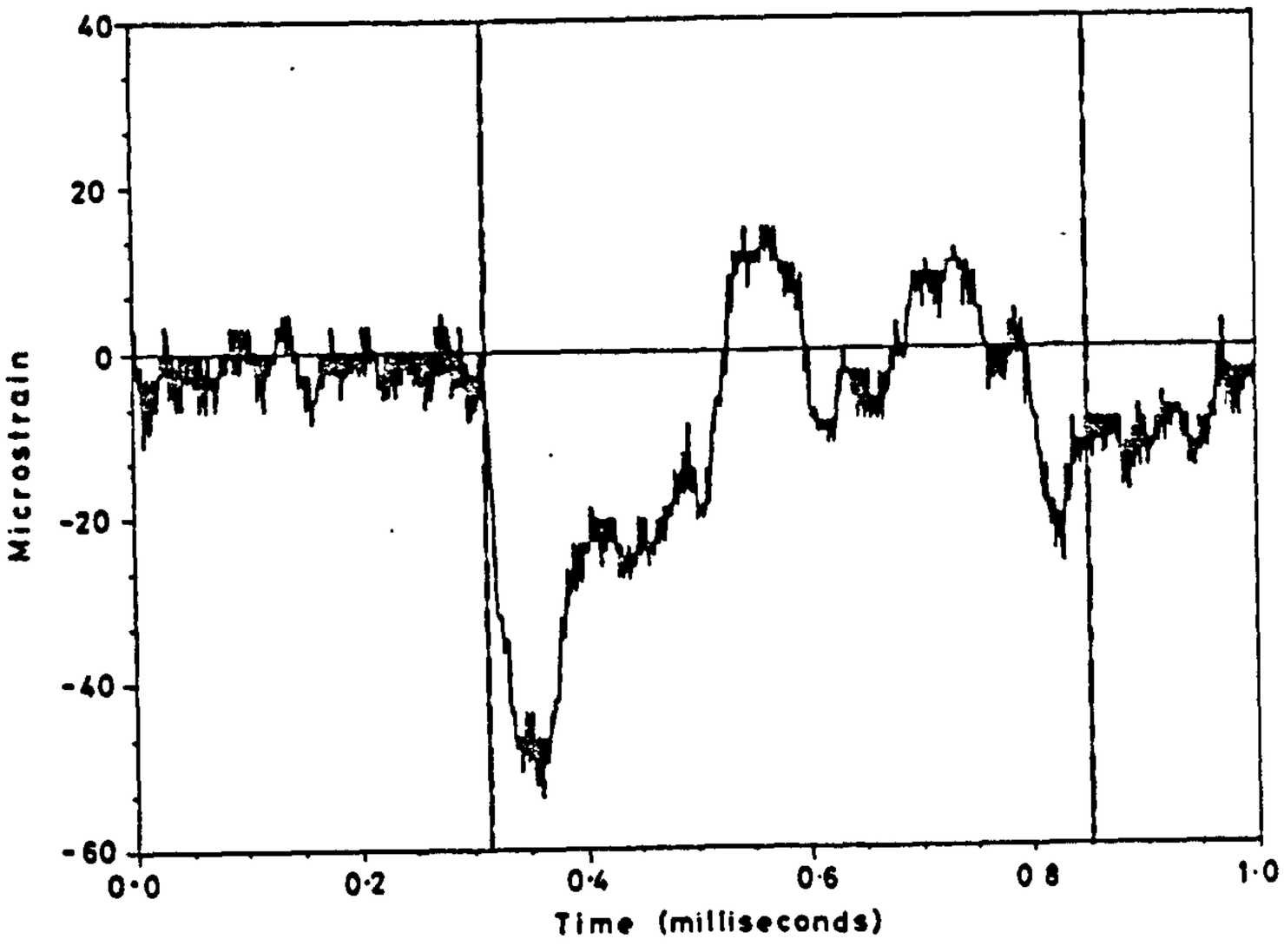

Fig 9 - Axial Strain Time History
(Shot 7 Channel 17)

Fig 9 shows the axial response at another point to the same shock. Location 17 is further away from the source and by the time the shock wave has travelled to the opposite end of the structure the gap between the two arrival times as shown by the vertical lines has widened due to the 3½ times difference in their rates. The intensity of the response has decreased as shown by the signal to noise ratio but the onset of axial strain clearly coincides with the shock wave travelling in steel.

Shot 4 Channel 12C Time 0-1ms (Fig 10)

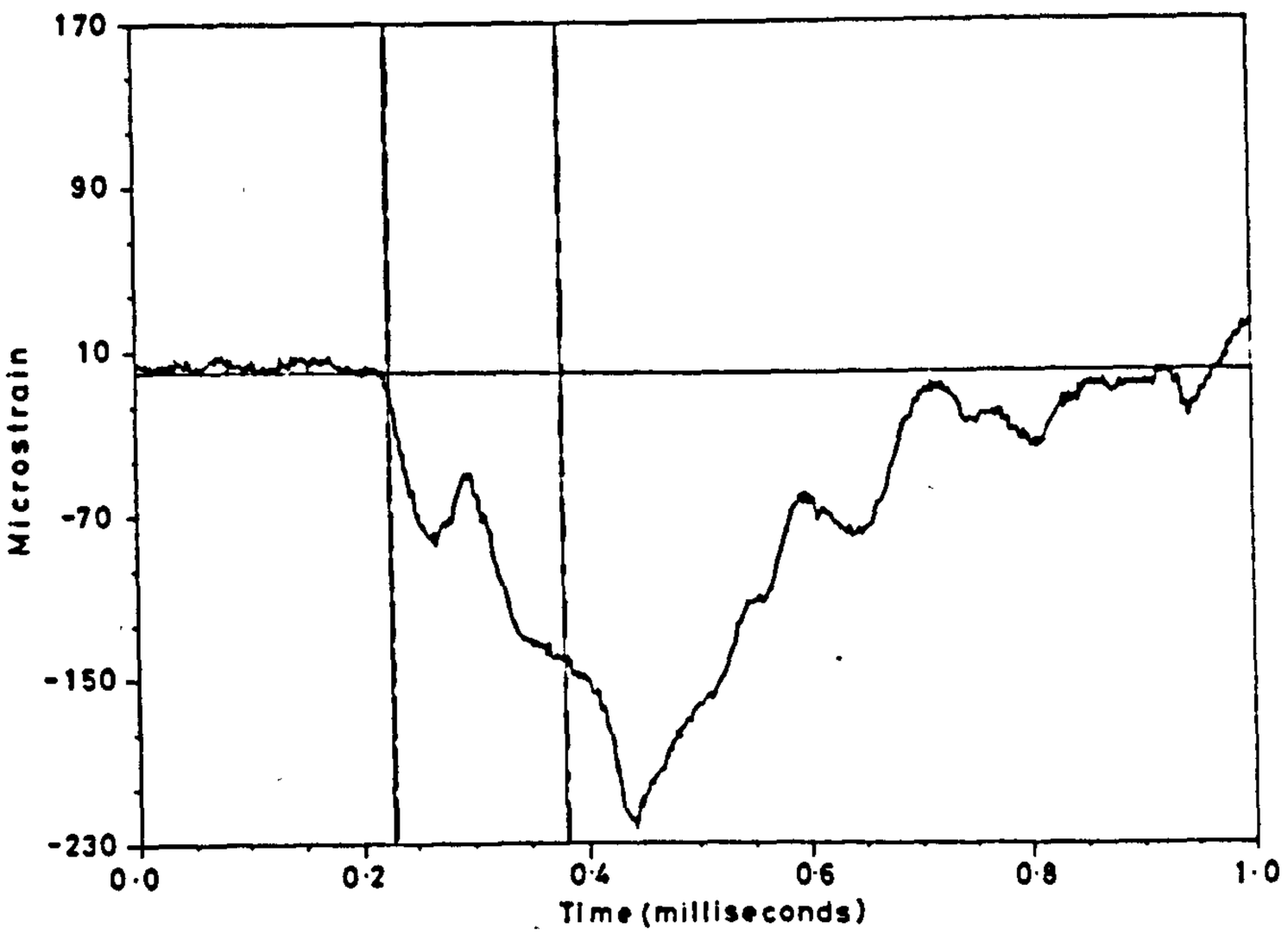

Fig 10 - Hoop Strain Time History
(Shot 4 Channel 12)

The variations in axial strain that were observed when the cylinder was acted upon by an end-on incident wave were also observed for hoop strain at locations under side-on attack. Fig 10 shows the response of a point on the opposite side of the structure from the source of a side-on attack.

Shot 4 Channel 6C Time 0-1ms (Fig 11)

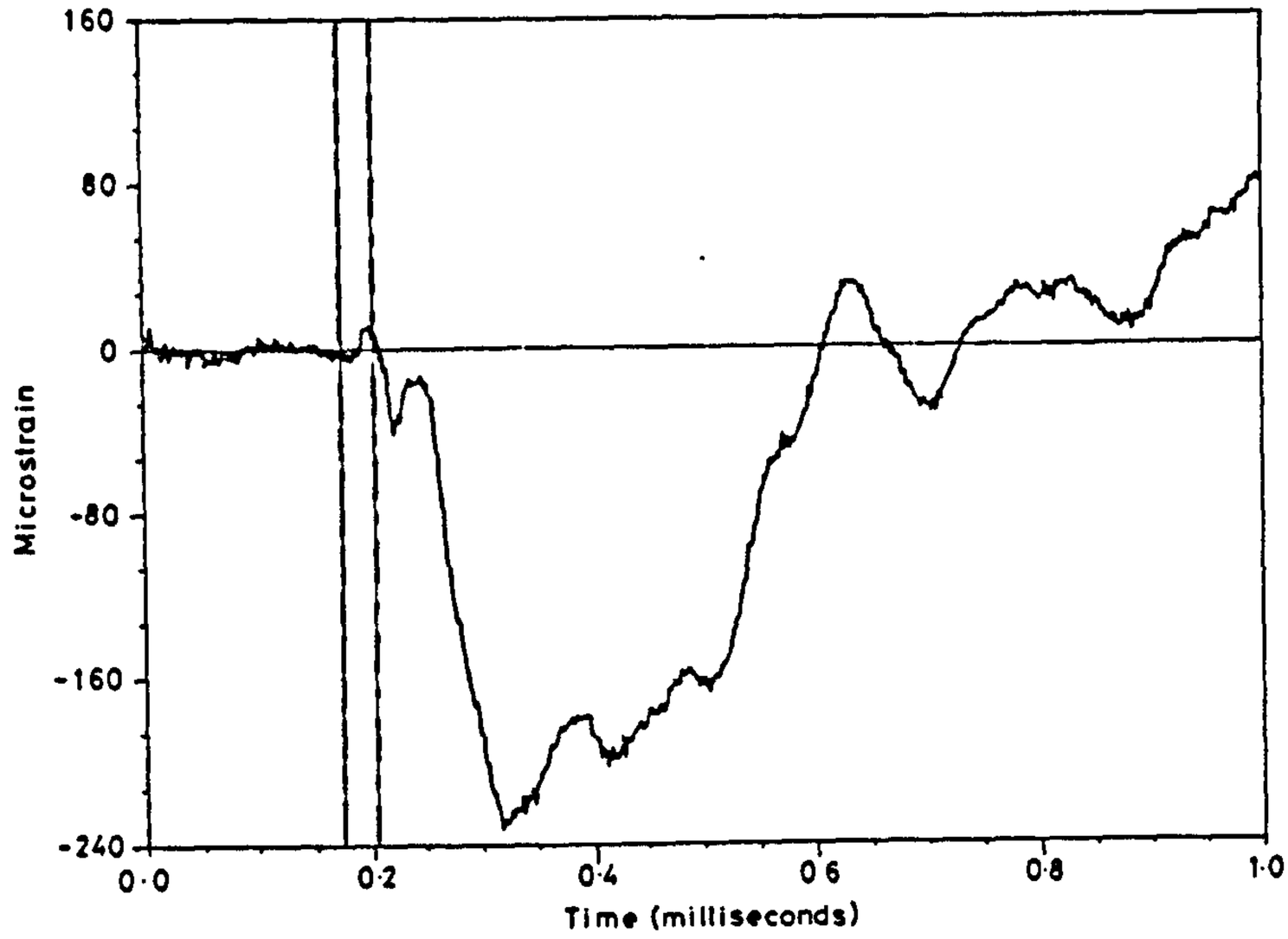

Fig 11 - Hoop Strain Time History
(Shot 4 Channel 6)

The response to Shot 4 at a different site on the same side of the cylinder as the source (directly opposite Channel 12), does not show what triggers movement; both arrival times are within 30 μs of each other. It does show however that the maximum strain recorded at two sites 180° apart varies by less than 10%.

None of the results of these trials support the view that the zone 'behind' the structure is sheltered from the shock wave. However having demonstrated that the compression wave that travels through the structure is an important event as far as the initiation of strain is concerned then it is not surprising that there is no sheltering as the forcing function is carried through the steel and all points on the structure are visible to the shock.

Further examination of Figs 10 and 11 does offer a possible explanation, as some of the evidence in support of a shadow zone is from large scale tests involving velocity meters and the rate of change of strain is always less for those points in the lee of the shock.

The importance of the shock wave travelling through the structure may also explain why the angle of incidence was not critical. The maximum response was always either nearest to the source of the shock or at the midpoint of the cylinder where the structure is most flexible. In retrospect it was not easy to determine what the effective angle of incidence was, as for many locations of the charge the extreme end of the structure will be disturbed first and initiate a shock wave which always travels to internal points by the same (most direct) route.

Shot 5 Channel 1C Time 0-1ms (Fig 12)

Shot 5 Channel 17C Time 0-1ms (Fig 13)

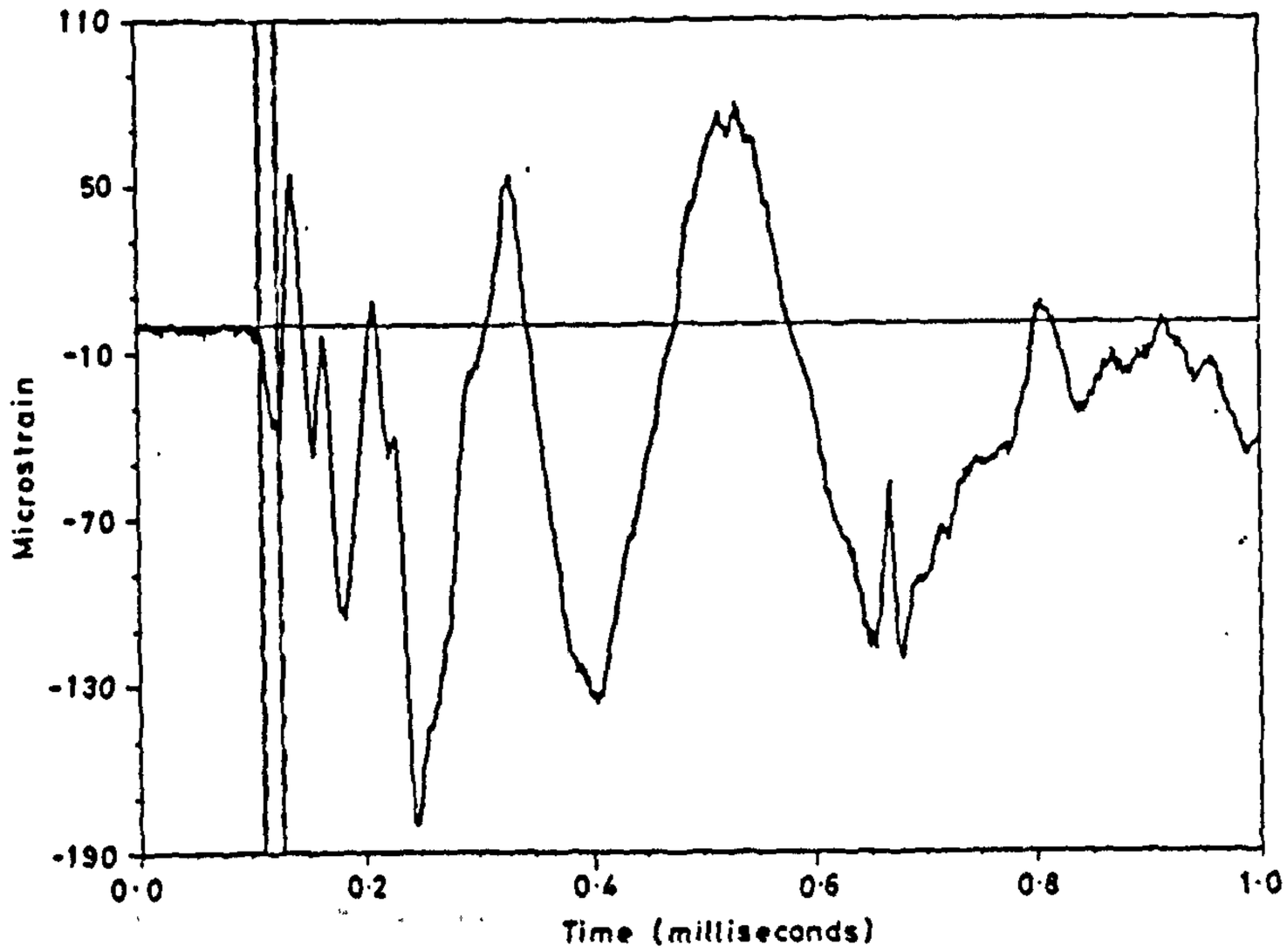

Fig 12 - Hoop Strain Time History
(Shot 5 Channel 1)

Figs 12 and 13 show hoop strain response at two points to a shot fired opposite the end of the cylinder. Fig 12 shows the response near the shock source where there are rapid oscillations in the level of strain and a high rate of change of strain. Whereas Fig 13 shows the time history at the other end of the structure and has less frequent oscillations and a lower rate of change of strain. The most significant difference however between the two locations is that there is considerable movement and the maximum strain level is achieved at the one site before the other side records anything.

Therefore one is lead to the conclusion that for a flexible structure such as this, initial movement is not in recognised modes but rather as local deformations.

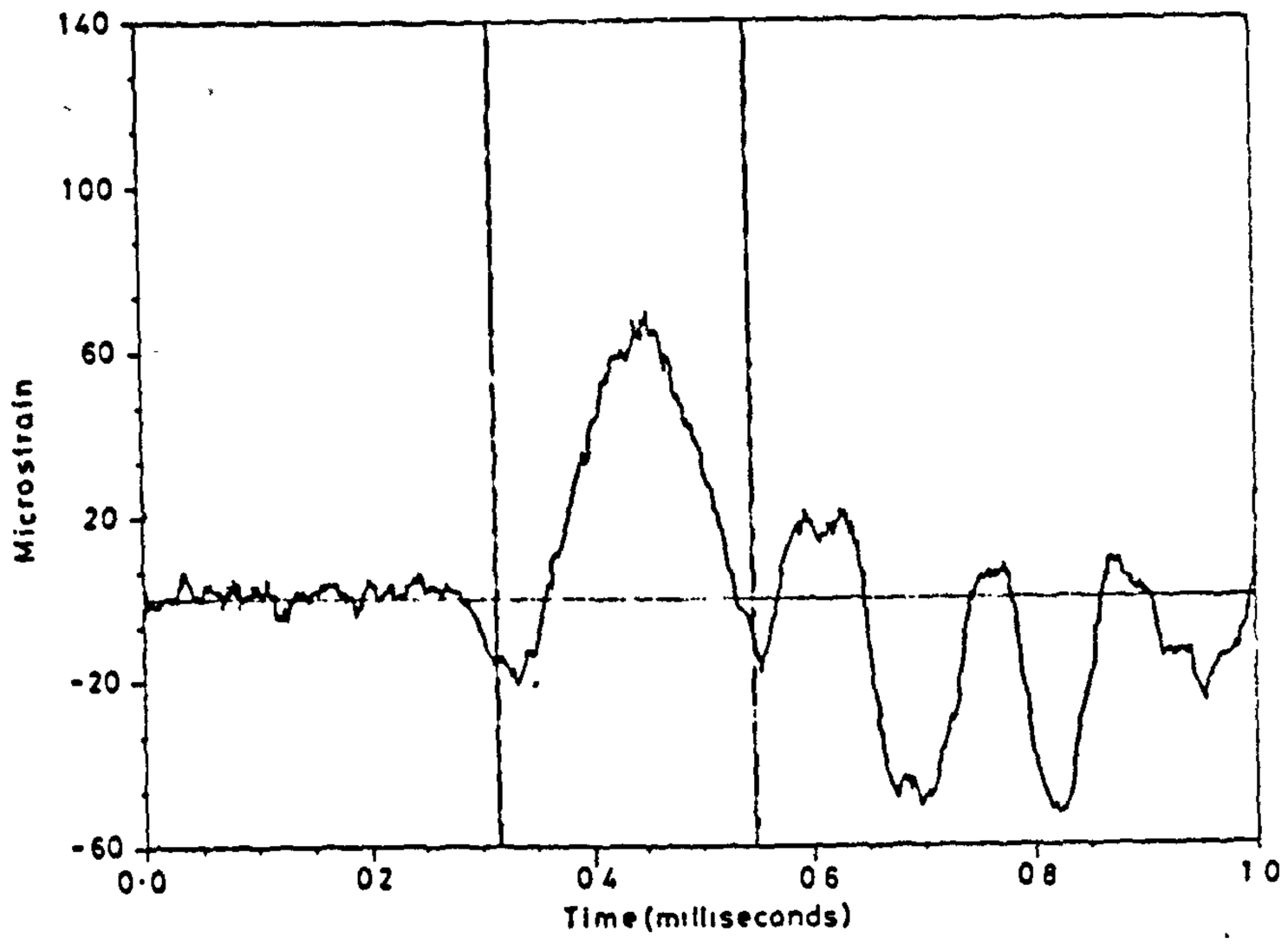

Fig 13 - Hoop Strain Time History
(Shot 5 Channel 17)

Shot 3 Channel 6C Time 0-1.024 secs
(Fig 14)

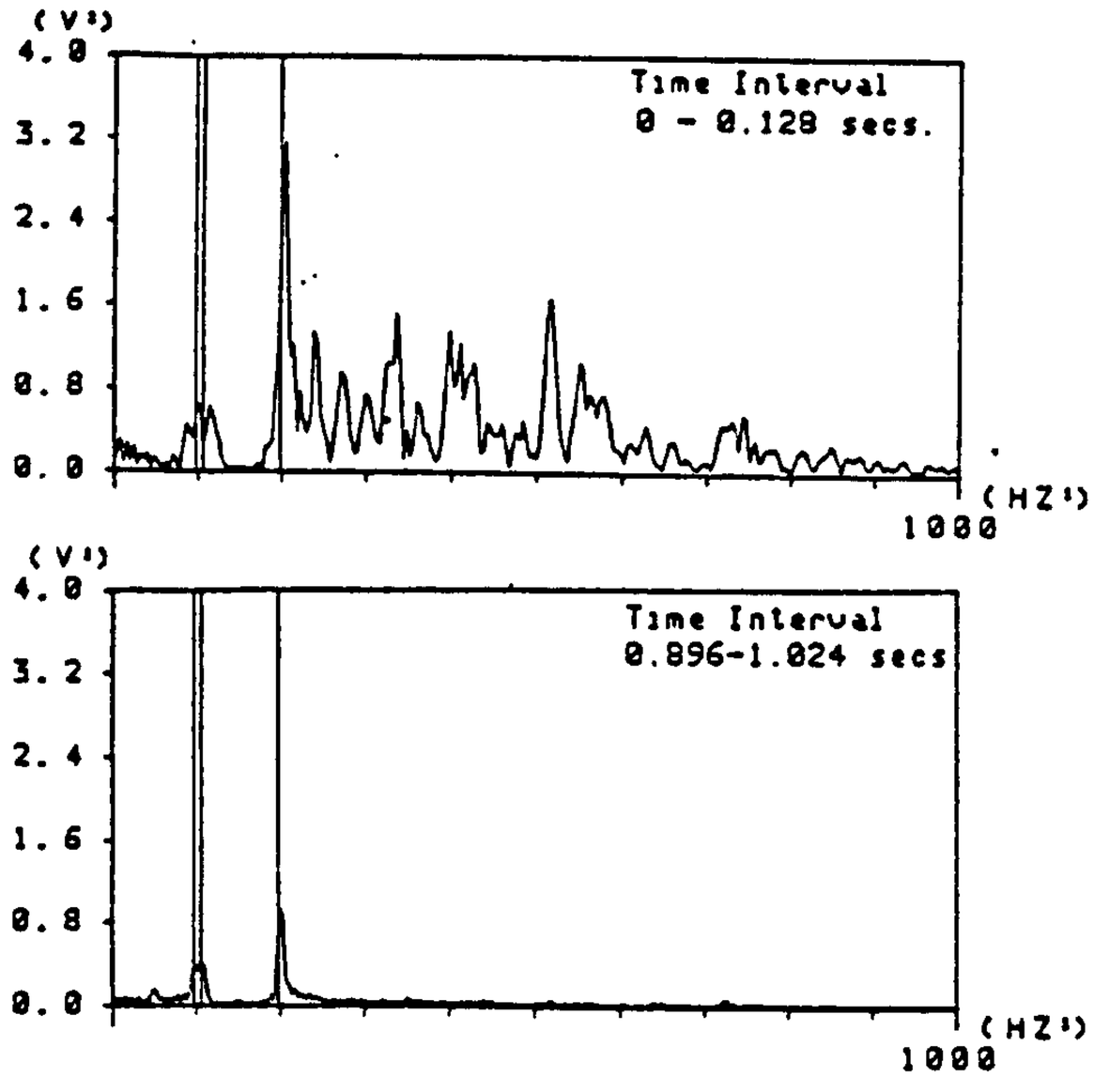

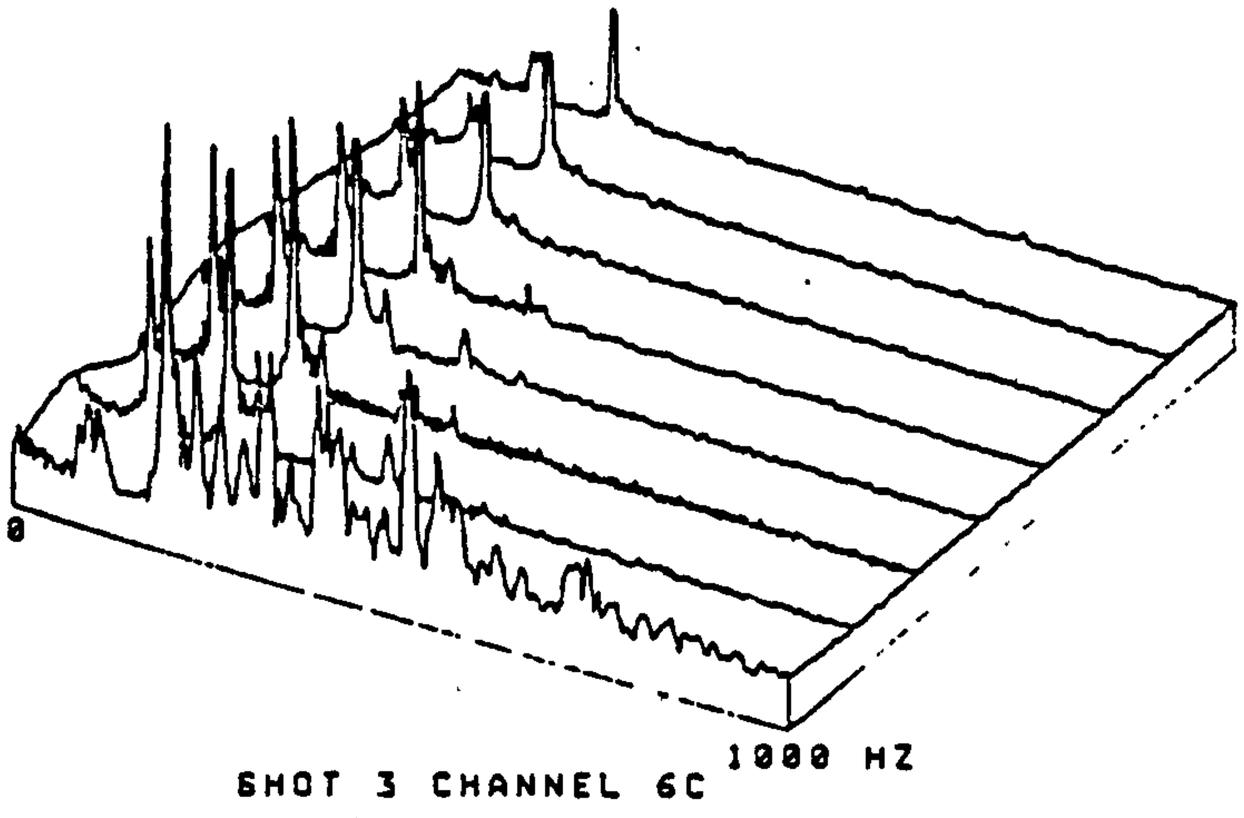

Fig 14 - Frequency Domain Analysis

The data from this series of tests was also analysed over a longer time period with an approach that considers the frequencies of vibration.

The response of each channel from 0-1.024 seconds was split into 8 equal increments and the frequency content of each increment compared. The resonant frequencies that were obtained from the shock data were readily identified with those obtained by steady-state testing and apart from the fact that certain modes increased in magnitude before eventually subsiding nothing extraordinary was observed.

SUMMARY

Although these are only preliminary findings and the results have yet to be compared with calculated values of strain several interesting points have been discovered or reaffirmed.

a. Strain gauges can be used to monitor the behaviour of a structure in the shock environment. Whether to assess damage, or to record deformations and stresses within the structure; strain is a good parameter to measure. However, most theoretical analyses are formulated in terms of displacements and although it is possible to establish strain from displacement there is no easy way of working back again.

b. The initial deformation of the cylinder when acted upon by the shock wave started a membrane or stretching wave which travelled through the structure at the speed of sound in steel. This is 3½ times faster than the speed of sound in water. Therefore the membrane or stretching wave arrives at points that are further away from the source of the explosion before the acoustic pulse. In these tests some strain gauges achieved their maximum values before the pressure pulse arrived. So although some points may be sheltered as far as the pressure pulse is concerned this is unimportant if the stress wave is causing maximum strain (or displacement) as all points of the structure will be visible to the stress wave.

c. On the other hand those locations on the opposite side of the structure from the source of the explosion were sheltered as far as the rate of change of strain was concerned.

d. It is unlikely that a theoretical analysis can produce accurate answers unless the effect of membrane forces is considered in derivations of the equations of motion.

e. From the tests as performed there was no evidence to support the view [9] that broadside loading is not the most severe condition for this type of structure.

f. Deformations of sections of the cylinder occurred at appreciable, sometimes maximum levels whilst other sections were undeformed. A structure that is undergoing local deformation is not particularly suited to modal analysis in the normal sense.

g. Modes corresponding to frequencies measured by steady-state testing [8] were readily identified from the shock data.

h. The structure is very lightly damped with very few dominant frequencies which persist for longer than 1 second after the shock event. As the structure rings down after all external loading has ceased, some modes were observed to increase in magnitude before subsiding again.

REFERENCES

1. "Underwater Fluid-Structure Interaction", LH Chen M Prerucci Shock and Vibration Digest, April 1977.

2. "Response of shells to acoustic shocks", J M Klosner, Shock Vib Digest 0 (5) pp 3-13, 1976.

3. "Interaction of Acoustic Pulses with Fluid Loaded Shell Structures", R T Menton, 2nd E B Magrab Shock Vib Digest, 5 (12), pp 1-12, 1973.

4. "Fluid-Structure Interaction", Ed P Bettess, Int J Num Meth Engng 13 (1) 1-201, 1978.

5. "Residual Potential and Approximate Methods for Three Dimensional Fluid-Structure Interaction Problems", Geers JASA Vol 49, Number 5 (part 2), 1970.

6. "Transient Response Analysis of Submerged Structures", T L Geers, ASME, AMD-Vol 14, 1975.

7. "Fluid-Structure Interaction". Shock and Vibration Computer Programs, Washington DC, Naval Research Laboratory, Shock and Vibration Information Centre, 1975.

8. "Modal Analysis of a Cylindrical Structure Immersed in Water", R J Randall. Proceedings of the 3rd Int modal Analysis Conf, Orlando, Florida, Jan 1985.

9. "Angle of Incidence Effects for Underwater Shock Using Generic Computational Models", C E Rosenkilde and V H Ginsberg, 55th Shock and Vibration Symposium Dayton, Ohio 1984.

10. "DATS 11 Help Manual" Data Analysis Centre, ISVR, University of Southampton. September 1978.

RNEC-RR-88001

Royal Naval Engineering College

Manadon, Plymouth

PROBLEMS OF MODELLING SHELL TYPE STRUCTURES FOR FLUID-STRUCTURE INTERACTION PROBLEMS

Lieut RJ Randall

Appendix C

Appendix C

FLUID-STRUCTURE INTER-ACTION OF A SUBMERGED CYLINDER

A unified hydroelasticity theory has been described by Bishop, Price and Wu (1) for a floating structure moving in a seaway. This general method has been used by Price and Fu (2) to investigate the variations in fluid loading parameters for a submerged plate which is near the free surface. Work is currently underway to study the behaviour of a thin cylindrical shell in a similar regime; the aim of this paper is to outline the method to be used particularly the distinction between 'wet' and 'dry' analyses. In the second part the problems of modelling shell-type structures using finite elements is presented.

This work relates to a particular scale model which has been extensively tested and for which experimental data is available from tests carried out at the RNEC, Manadon, these have been shown to compare well with an analytical solution assuming simply supported and conditions at the positions where the bulkheads exist on the physical model.

Following the approach of previous studies a finite element analysis of the dry structure is used to determine natural frequencies and mode shapes. These are then used with a singularity distribution method to obtain the fluid loading which together with structural damping and any other external loading are combined as forcing functions on the previously freely vibrating dry structure. Reductions in amplitude and magnitude of resonant frequencies and coupling between modes of vibration can then be observed for the wet structure.

Some of the novel aspects in the determination of the behaviour of a submerged shell as opposed to a solid structure are described below.

a. Dry Analysis

The general equations of motion fo plates and shells can be established in curvilinear co-ordinates by invoking Hamiltons' Variational principle

$$\int_{t_2}^{t_1} (\pi - K)dt = 0$$

Certain assumptions are made in the formulation of the equations of motion; the principal ones being that the shells are thin with respect to their radii of curvature, deflections are reasonably small and that transverse shear deflections are negligible. However allowing for these assumptions the equations are quite universal and apply to any arbitrary shape. In practice however, meaningful results can only be obtained for certain well defined geometries such as the sphere, the conical shell or the case which is of interest here, the circular cylindrical shell.

For a cylinder the Lame parameters are

$$A_1 = 1, \quad A_2 = a$$

and substituting these into Love's equations the equations of motion in the three polar directions become:

$$\frac{\partial N_{xx}}{\partial x} + \frac{1}{a}\frac{\partial N_{\theta x}}{\partial \theta} + q_x = \rho h \frac{\partial^2 u_x}{\partial t^2}$$

$$\frac{\partial N_{x\theta}}{\partial x} + \frac{1}{a}\frac{\partial N_{\theta\theta}}{\partial \theta} + \frac{Q_{\theta 3}}{a} + q_\theta = \rho h \frac{\partial^2 u_\theta}{\partial t^2}$$

$$\frac{\partial Q_{x3}}{\partial x} + \frac{1}{a}\frac{\partial Q_{\theta 3}}{\partial \theta}\frac{N_{\theta\theta}}{a} + q_3 = \rho h \frac{\partial^2 u_3}{\partial t^2}$$

where transverse shear forces are

$$Q_{x3} = \frac{\partial M_{xx}}{\partial x} + \frac{1}{a}\frac{\partial M_{\theta x}}{\partial \theta}$$

$$Q_{\theta 3} = \frac{\partial M_{x\theta}}{\partial x} + \frac{1}{a}\frac{\partial M_{\theta\theta}}{\partial \theta}$$

$$x = \frac{u_3}{x}$$

these equations relate to a thin shell whose neutral surface is a surface of revolution about the x-axis. If the cylinder is considered to be simply supported at its ends, ie there are node lines at these positions. Then boundary conditions

$$u_3 = u_\theta = M_{xx} = N_{xx} = 0$$

are established for all θ and t at x = 0 and x = L.

These equations provide an analytical solution with which to compare experimental and approximate solution techniques (see Table 1).

The numerical method most frequently used is finite element analysis. Three types of finite element analysis are possible for a uniform cylindrical shape; flat facet shell elements, curved (semi-Loof) shell elements and thin shell of revolution elements.

The latter are the most efficient and are used as a benchmark against which to compare the other solutions. The PAFEC suite of programs have been used in this analysis and the particular three noded shell of revolution element used is based on theory due to Novozhilov. Membrane effects are incorporated together with bending effects which corresponds approximately to Kirchoff plate theory. The displacement assumptions are in three orthogonal directions, with the order of the displacement polynomial in the radial direction twice that for the axial and circumferential directions. Consequently normal effects are catered for rather more accurately that effects in the other two directions. The element has 3 degrees of freedom at each of the nodes which vary with θ such that:

$$\text{axial displacement} = u_X \cos m\theta$$

$$\text{radial displacement} = u_Y \cos m\theta$$

$$\text{circum displacement} = u_Z \sin m\theta$$

for each value of m a set of mode shapes and frequencies is derived.

Facet Shell Elements

The facet approach to shell analysis is less exact introducing a number of factors whose effects cannot be readily quantified. The facet shell element used is one which has five degrees of freedom at each node with the extra freedom ϕ_Z introduced after the transformation to global co-ordinates. The first assumption of an approximate displacement (or shape function) relates displacements within the element to nodal displacements. This produces errors in the element stiffness relationship but is one of the basic assumptions upon which all finite element analyses are based. Secondly there is the obvious approximation caused by representing the smooth curved surface by a multifaced polyhedral surface. Finally there are other errors associated with the element itself. Plate elements assume that the effects of membrane and bending stresses are uncoupled and combine the two effects separately. The thin isotropic shell element used in this analysis combines plate bending with a constant strain membrane element. The bending element has three degrees of freedom at each node, w, dw/dx and dw/dy. The radial displacement, w, is defined by a cubic expression in terms of area co-ordinates and this degree of variation ensures compatability between elements. The normal slope varies quadratically on an edge and since only two end values are available to define the normal slope its variation is not uniquely specified by the end values: thus a discontinuity of normal slope will occur between adjacent elements in general. The in-plane displacements, u and v, are accounted for by an assumption of constant stress throughout the element.

Curved (Semi-Loof) Elements

Finally a curved element is considered; the semi-Loof element was used which has a curvilinear quadrilateral shape. There are 32 degrees of freedom associated with the element in its final form and it is noted that the rotational freedoms are applied at different points to the translational freedoms. The element freedoms are displacements u, v, w at corner and midside points and normal rotation values at two Gauss points along each side. The 32 degrees of freedom of this element should be sufficient to define linear stress fields for both membrane and bending behaviour. The theory and philosophy of the semi-Loof element are very complex and its application must be considered with caution.

The element can give spurious mechanisms on elements which store little or no strain energy and particular attention is paid to the order of integration used over the mid-surface of the element. There are three options; 4-point (ie 2*2), a special 5-point and 9-point (3*3) Gaussian integration. At each integrating point discrete Kirchoff assumptions are made so that normals to the mid-surface remain approximately normal, this is effected by imposing zero lateral strains. From the published results the

benefits of using reduced integration appear to be only predictable on a trial and error basis. However flexible structures such as thin cylinders are considered suitable for reduced integration and this has been practiced here.

b. Wet Analysis

The fluid loadings on the submerged cylinder are specified by means of the linear velocity potential:

$$\Phi(x, y, z, t) = [\phi_0(x, y, z) + \phi_0(x, y, z) + \sum_{r=1}^{n} P_r\phi_r(x, y, z)]e^{i\omega t}$$

which is a combination of incident, diffracted and radiated waves acting on the cylinder. If the cylinder is vibrating in still water, the first two terms are eliminated.

The remaining term for the radiation velocity potential is obtained by considering the following boundary conditions:

(1) At the free surface (by combining kinematic and dynamic boundary conditions).

$$\frac{\partial\phi_r}{\partial} - \frac{\omega^2}{g}\phi_r = 0 \text{ on } z = 0$$

(2) The seabed, which is horizontal, acts as a rigid boundary

$$\frac{\partial\phi_r}{\partial z} = 0 \text{ on } z = -d$$

where d is the depth of water which may be infinite.

(3) A radiation condition which ensures that the radiation potential is zero at an infinite distance from the vibrating cylinder satisfying the energy conservation law

$$\lim_{R\to\infty} \sqrt{R\left[\frac{\partial\phi_r}{\partial R} + i\omega\phi_r\right]} = 0$$

where $R = \sqrt{x^2 + y^2}$

(4) Continuity of motion such that the fluid and body velocities match at the interface. That is there is no cavitation and the radiation potential can be written as:

$$\frac{\partial\phi_r}{\partial n} = i\omega(u_r n_1 + v_r n_2 + w_r n_3)$$

On the mean wetted surface S for each mode r=1, 2, ..., n. In this expression $\underset{\sim}{n}$ denotes the outward drawn unit normal vector to the wetted surface with components (n_1, n_2, n_3) and transpose $\underset{\sim}{n}^T$.

A solution for this boundary value problem is obtained from potential flow theory, with a pattern of sources of unknown strength, $\delta(\underset{\sim}{r}_0, t)$ distributed over the wetted surface of the structure. The velocity potential at any position r in the fluid is given by

$$\phi(\underset{\sim}{r}, t) = \frac{1}{4\pi} \iint_S \delta(\underset{\sim}{r}_0, t) . G(\underset{\sim}{r}, \underset{\sim}{r}_0) . ds$$

The fluid loading is derived by use of the linearised Bernouilli's equation to obtain the fluid pressure on the instantaneous wetted surface of the cylinder and

$$Z_t(t) = \rho \iint_S \underset{\sim}{n}^T . \underset{\sim}{u}_r \; i\omega \sum_{k=1}^{n} P_K . \phi_K . ds$$

$$= \sum_{k=1}^{n} P_k (\omega^2 A_{rk} - i\omega B_{rk})$$

where Ark and Brk are the generalised added mass and damping coefficients.

Part II

Modelling their shells using Finite Elements

As discussed previously there are three elements that can be used to determine modes and frequencies of a circular cylindrical shell.

The first of these is the three noded thin shell of revolution element (PAFEC 42130).

Table 1. Natural frequencies using PAFEC 42130) (length = 0.892, radius = 0.121, thickness = 0.0025).

Axial No	Harmonic number =	2	3	4	5
1		287	353	631	1010
2		910	593	709	1049
3		1691	1050	918	1146
4		2459	1601	1250	1321

The hierarchy of modes can be deduced and it is noted there is no pre-ordained order but that it is governed by the dimensions of the cylinder. The first seven natural frequencies are compared in Table 2 with experimentally derived results, which are the average of two independant tests.

Table 2. Comparison of measured and predicted results

Mode M		1	1	2	1	2	3	1
Shape N		2	3	3	4	4	4	5
Measured		284	352	595	616	708	926	982
Predicted	(43210)	287	353	593	631	709	918	1010

The default of 60 automatically selected master degrees of freedom and 8 axial elements were used in this analysis, which was subsequently compared with facet shell (44210) and semi-loof element (43210) analyses.

To save computer time, the number of loadcases was limited to ten, this gave no more than 5 natural frequencies as a two orthogonal mode shapes are predicted at each frequency. The reason being that with an exactly circular cross-section the mode shape can occur in which can be given by using combinations of the orthogonal any plane mode shapes.

In the first 5 modes the highest circumferential harmonic number is 4. This implies a minimum of 8 elements because there are 8 changes of direction and as this is unnecessarily coarse a mesh with 16 elements circumferentially was chosen.

A straightforward convergency test was then performed using both element types varying 44210 and 43210 the number of elements axially. The number of automatically selected degrees of freedom was set at 100, initially.

Table 3. Convergency test using PAFEC 44210

Mode	No of Elements	32	64	128	256
1 (1, 2) 287 Hz		140	295	290	292
2 (1, 3) 353 Hz		143	376	365	368
3 (2, 3) 593 Hz		-	-	618	633
4 (1, 4) 631 Hz		-	-	662	678
5 (2, 4) 709 Hz		-	-	753	777

Despite the reservations concerning use of this element it is demonstrated that acceptable results can be obtained. The derived mode shapes, greatly exagerated, amplify the figures in Table 3. Crude and inaccurate mode shapes when the mesh is too coarse (Figure 1) or at higher modes for more refined mesh (Figure 2) are eventually replaced by accurate mode shapes which are symmetrical for all 5 modes (Figure 3).

The situation with regard to the curved shell element (43210), the sum-loof is complimented by the option for the order of integration used over the mid-surface of the element. For completeness all three options are included in Table 4.

Table 4. Convergency using PAFEC 43210.

Mode	Order of integration	No of Elements	32	64	128	256
1 (1, 2) 287 Hz	4		287	290	292	293 (291)
	5		290	290	291	292
	9		295	290	290	292
2 (1, 3) 353 Hz	4		353	366	368	375 (368)
	5		358	365	368	372
	9		364	363	365	372
3 (2, 3) 593 Hz	4		-	606	644	643 (638)
	5		-	612	639	635
	9		633	616	618	636
4 (1, 4) 631 Hz	4		500	672	684	710 (683)
	5		610	674	682	707
	9		652	660	668	700
5 (2, 4) 709 Hz	4		-	728	753	>800 (>800)
	5		676	744	791	>800
	9		-	751	763	796

Initially it appears that the results are an improvement over the PAFEC 44210 results. There is good agreement especially for lower modes even for the coarsest mesh. There appears to be little differences whichever integration order is used but the results do not seem to be converging as the mesh size reduces, particularly for higher modes.

Examination of the mode shapes reveals that the results are not quite as good as they first appeared. Excessive displacements of mid-side nodes, albeit greatly exagerated, produces distorted mode shapes (Figure 4) a situation that is improved as the integration order increases (Figure 5). As in the previous analysis using 44210 better solutions are obtained as the mesh size decreases (Figures 6, 7, 8) but only up to a point. At the highest number of axial lengths used, the solutions appeared to be divergent and some of the mode shapes were no longer symmetrical (Figure 9). Increasing the number of automatic masters (from 100 to 150) produced the improved results shown in brackets in Table 4 but the asymmetric mode shape was still produce. Unfortunately no firm conclusions can be drawn from the preceeding results except that facet shell elements can be used to give acceptable results and that sum-loof elements will give good results but must be used cautiously both regarding order of integration and shell geometry. In both instances a prior knowledge of the solution although not essential certainly greatly enhances the degree of certainty with which the results are viewed.

References

1. Bishop, R E D, Prince, W G & Yousheng Wu. 1986, A general linear hydroelasticity theroy of floating structures moving in a seaway. Phil. Trans.R.Soc. Lond. A316, 375-426.

2. Price, W G & Yuning Fu. 1987, Fluid-structure interactions between a vibrating cantilever plate partially or totally immersed within a fluid. To be published.

JSC

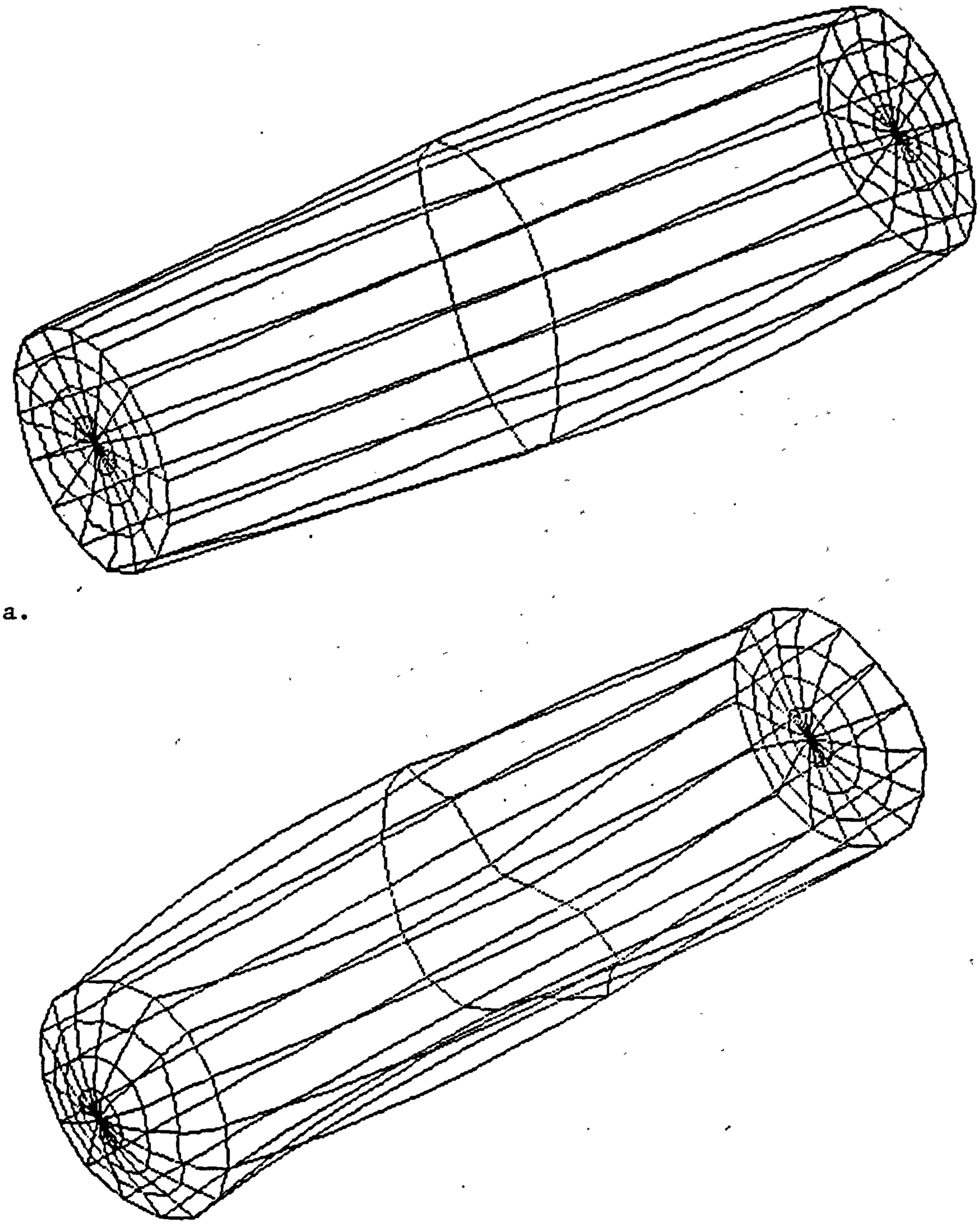

a.

b.

Figure 1. Mesh Size 32. Element Type 44210

a. 1st distortion mode.

b. 2nd distortion mode.

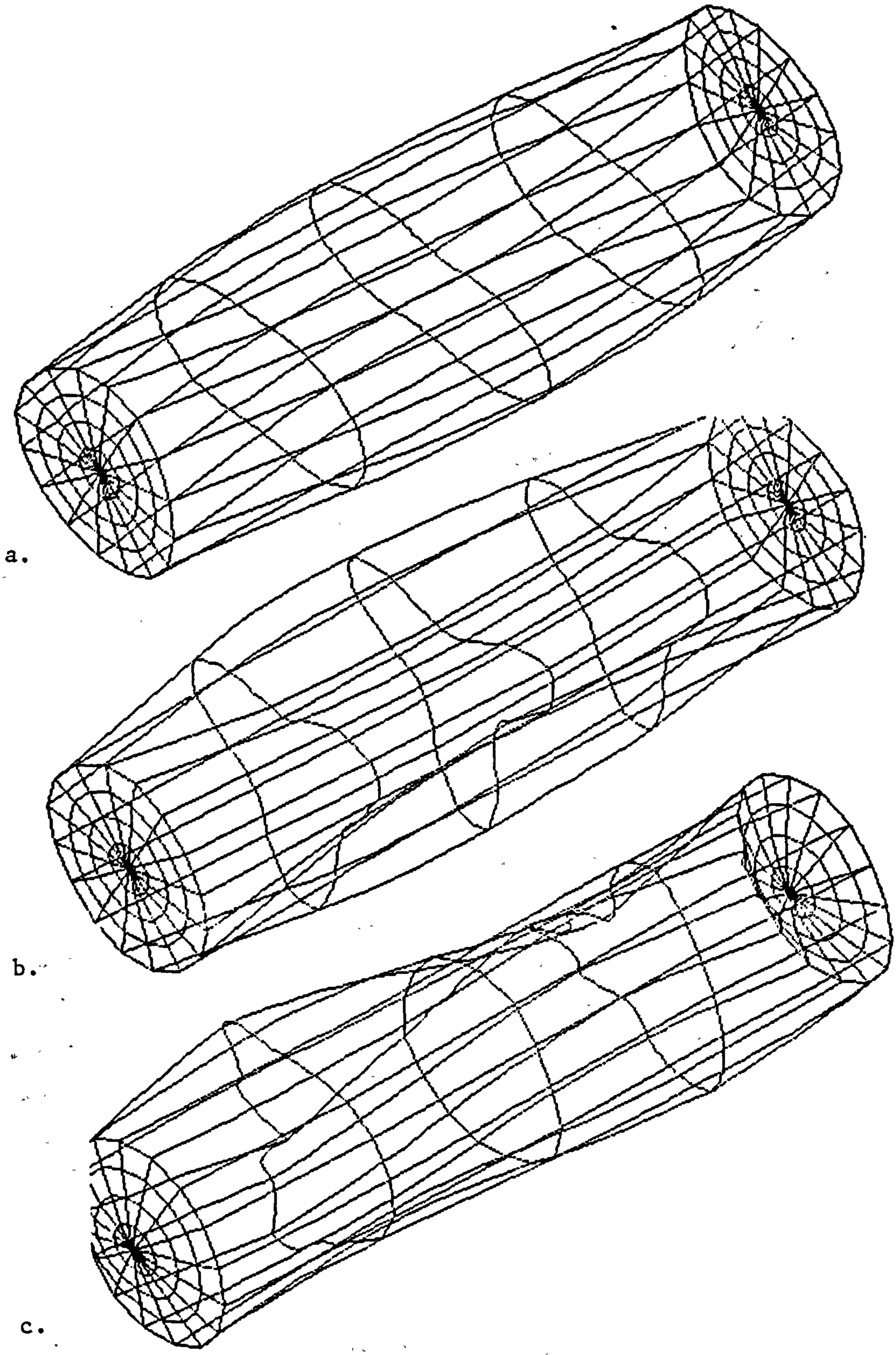

a.

b.

c.

Figure 2. Mesh Size 64. Element Type 44210

a. 1st distortion mode.

b. 2nd distortion mode.

c. 3rd distortion mode.

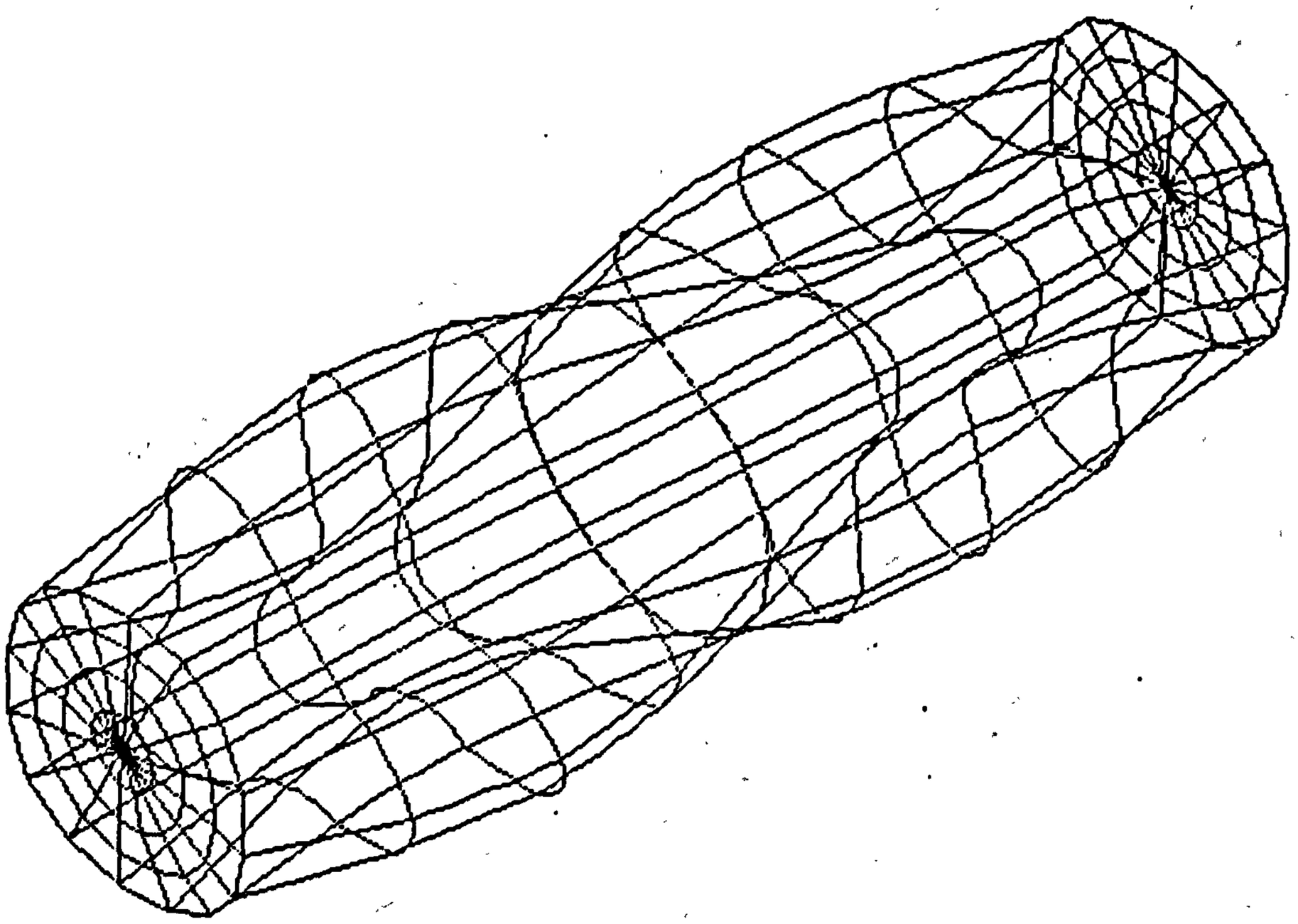

a.

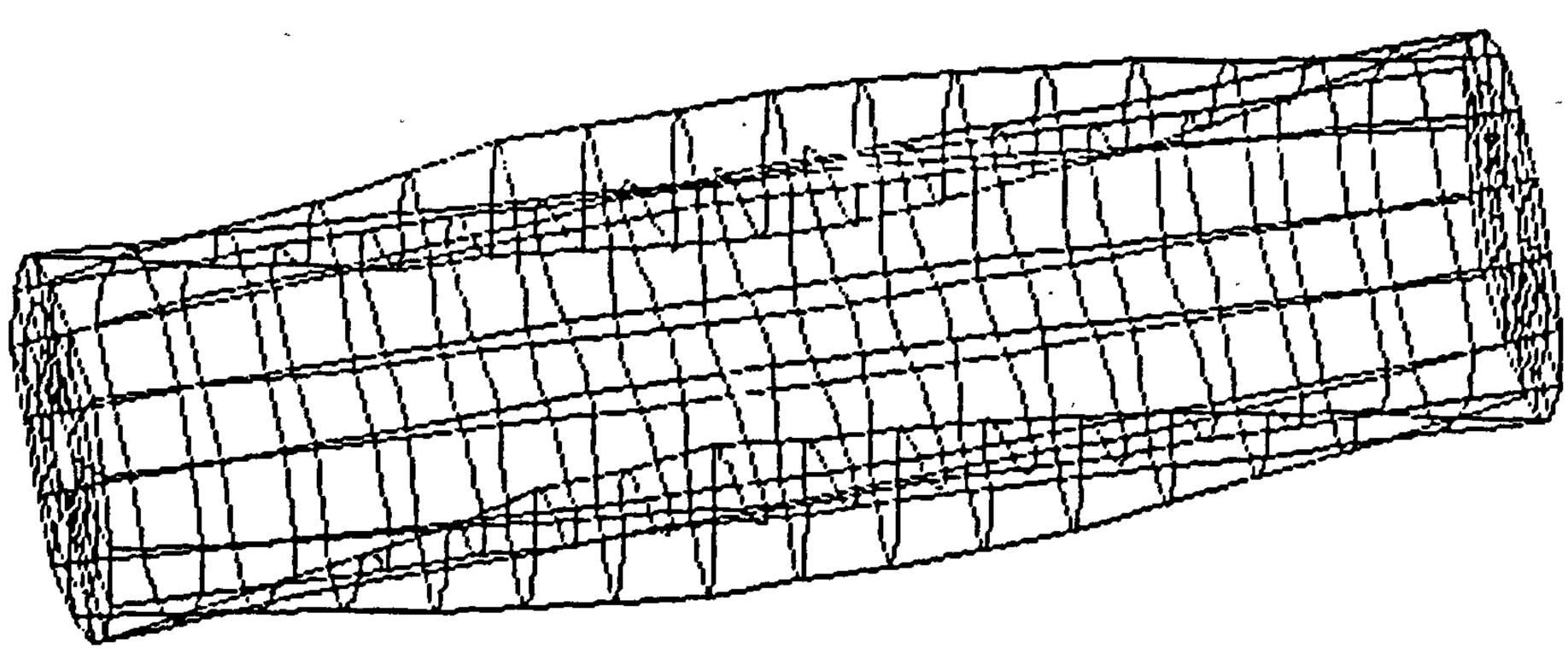

b.

Figure 3. Element Type 44210

a. Mesh size 128. 3rd distortion mode.

b. Mesh size 256. 4th distortion mode.

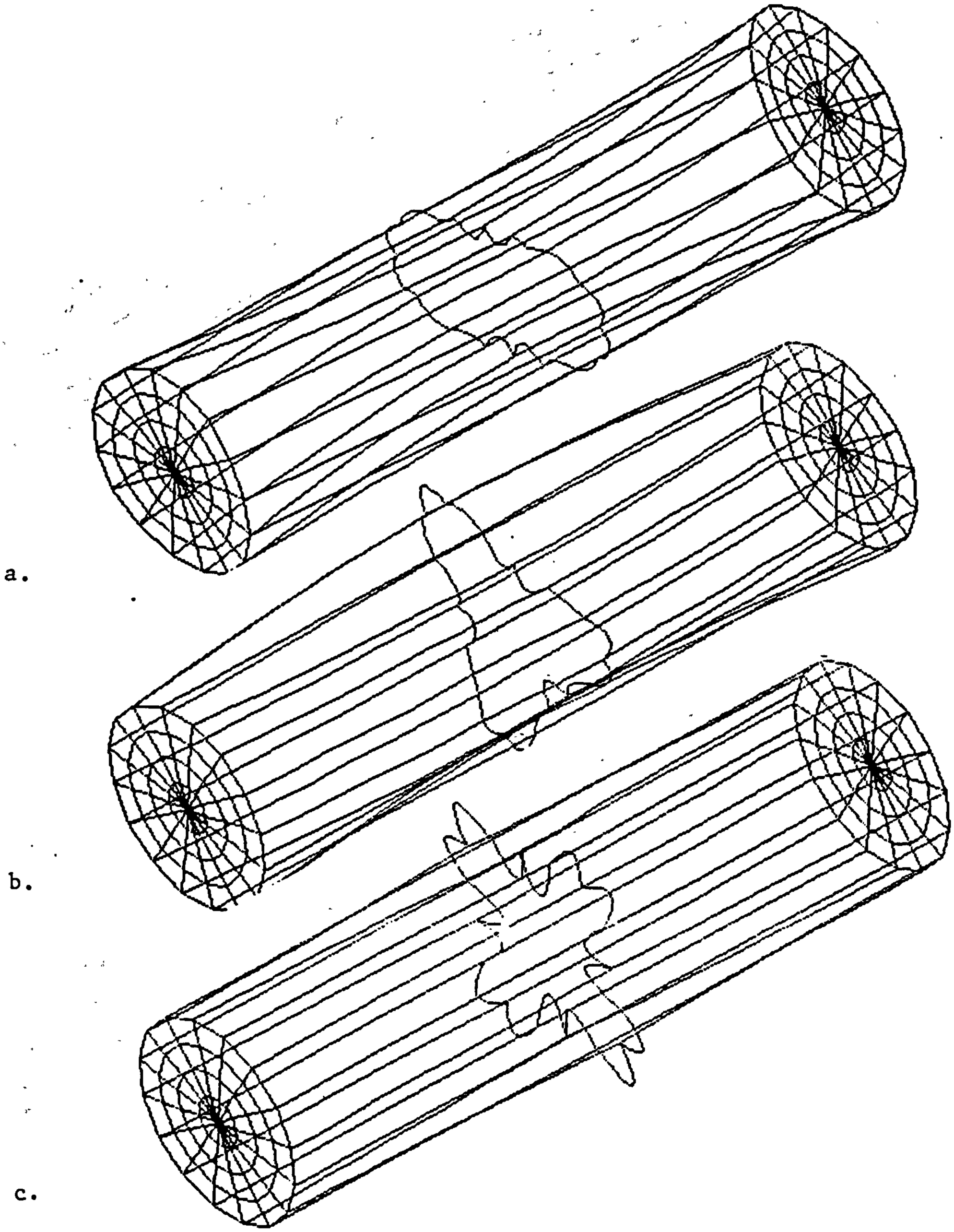

a.

b.

c.

Figure 4. Mesh size 32. Element type 43210.
Gauss integration 2 x 2.

a. 1st distortion mode.

b. 2nd distortion mode.

c. 3rd distortion mode.

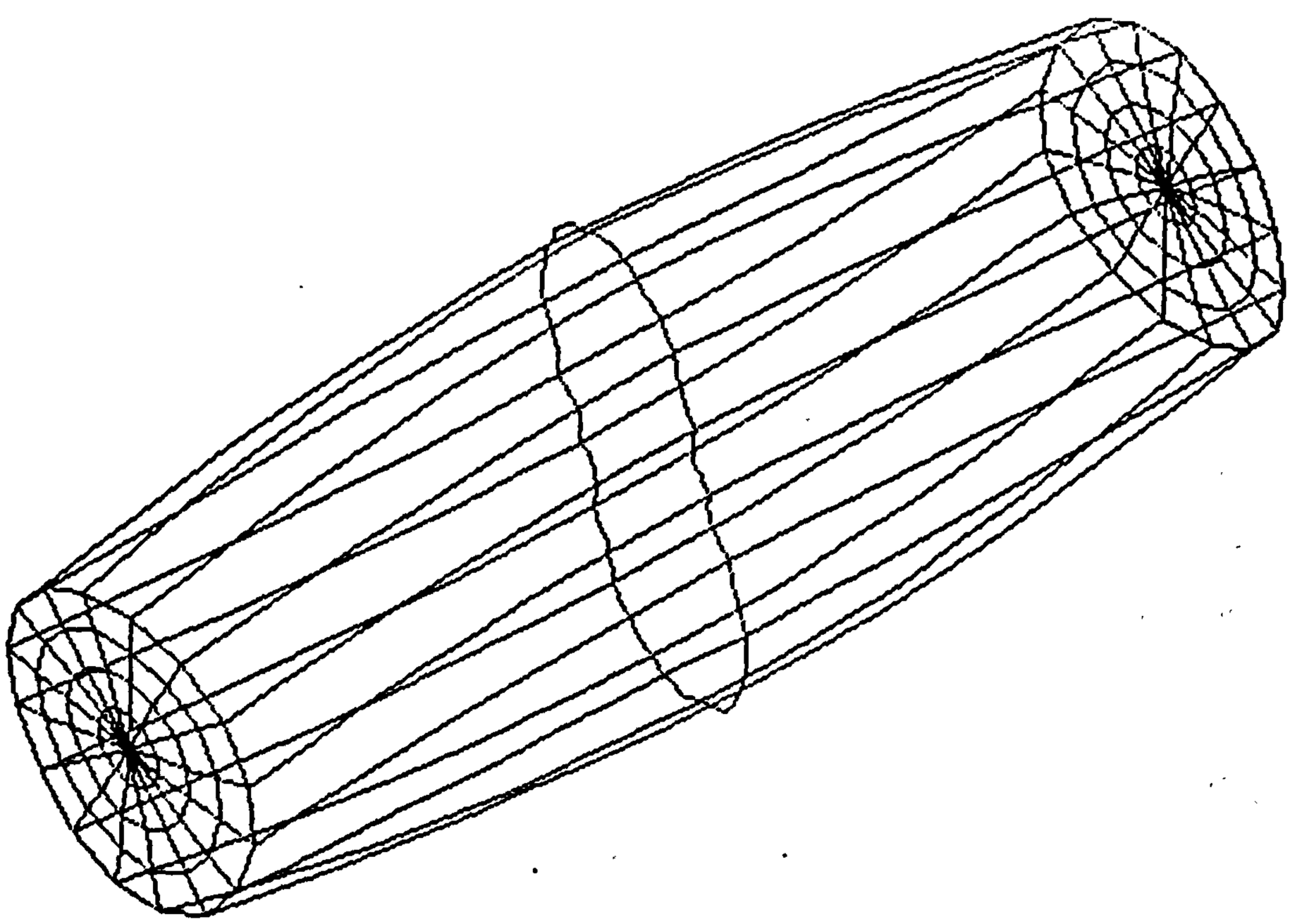

a.

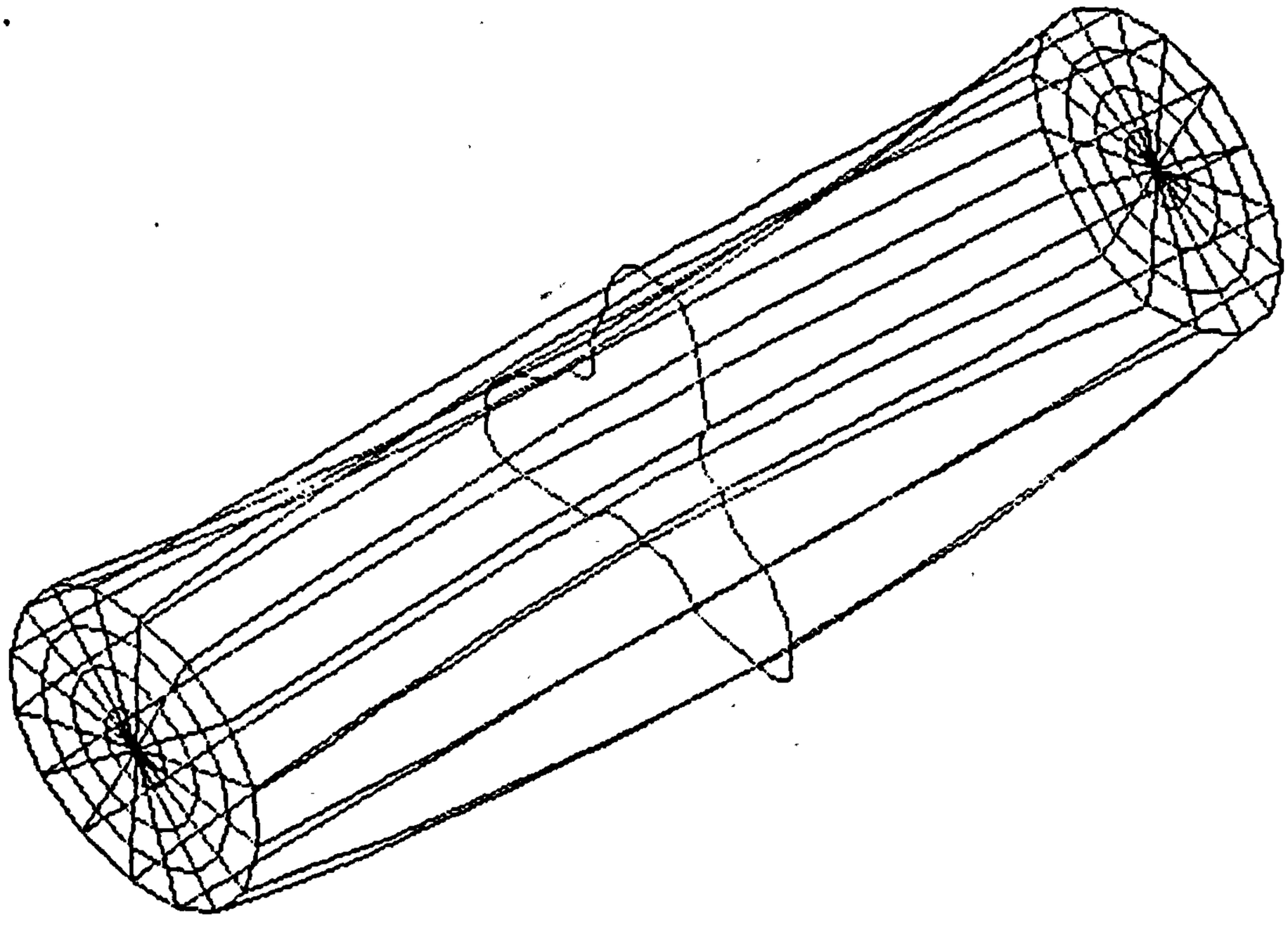

b.

Figure 5. Mesh size 32. Element type 43210. Gauss integration 5 pts

a. 1st distortion mode.

b. 2nd distortion mode.

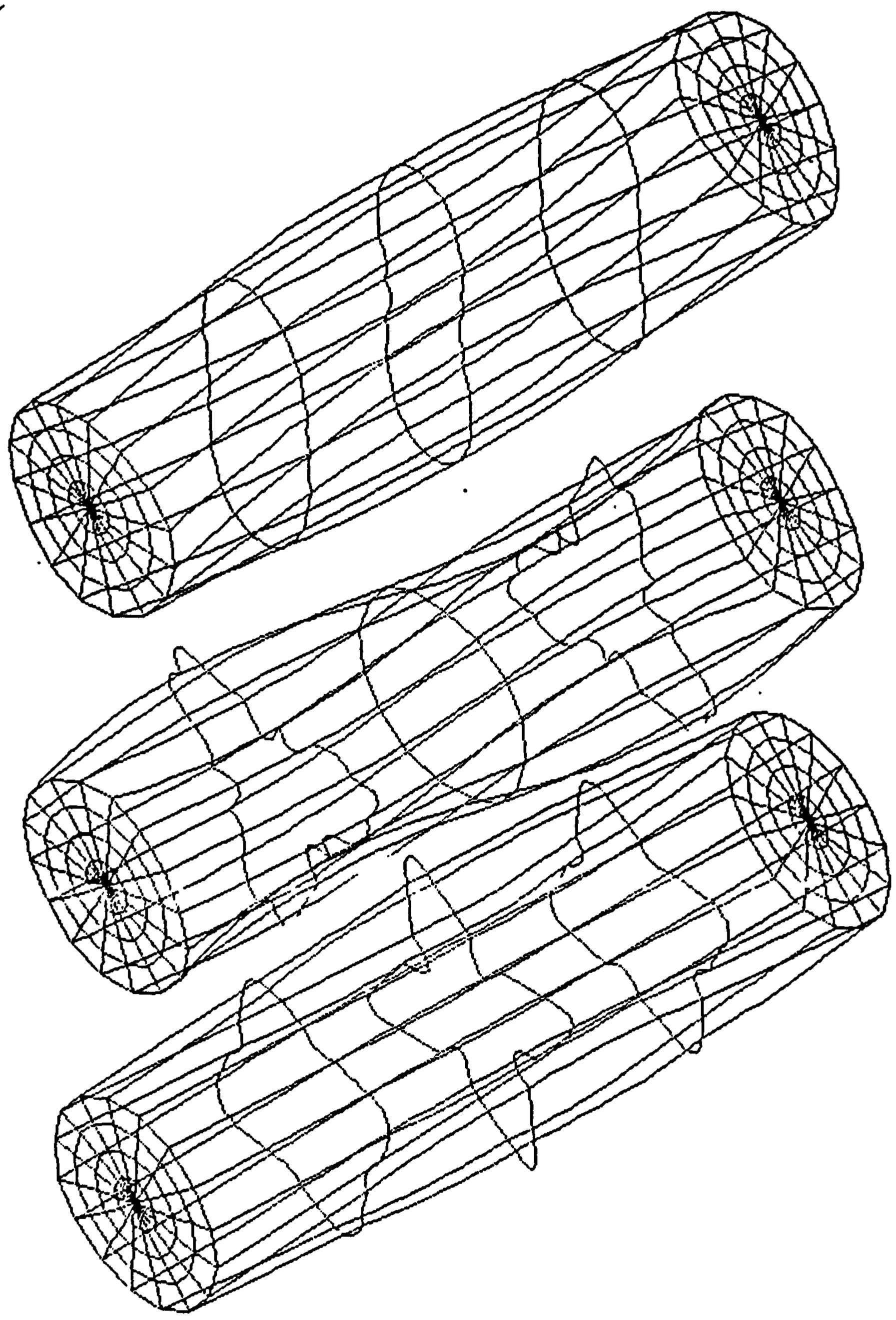

a.

b.

c.

Figure 6. Mesh size 64. Element type 43210.
Gaussin integraion 2 x 2.

a. 1st distortion mode.

b. 3rd distortion mode.

c. 4th distortion mode.

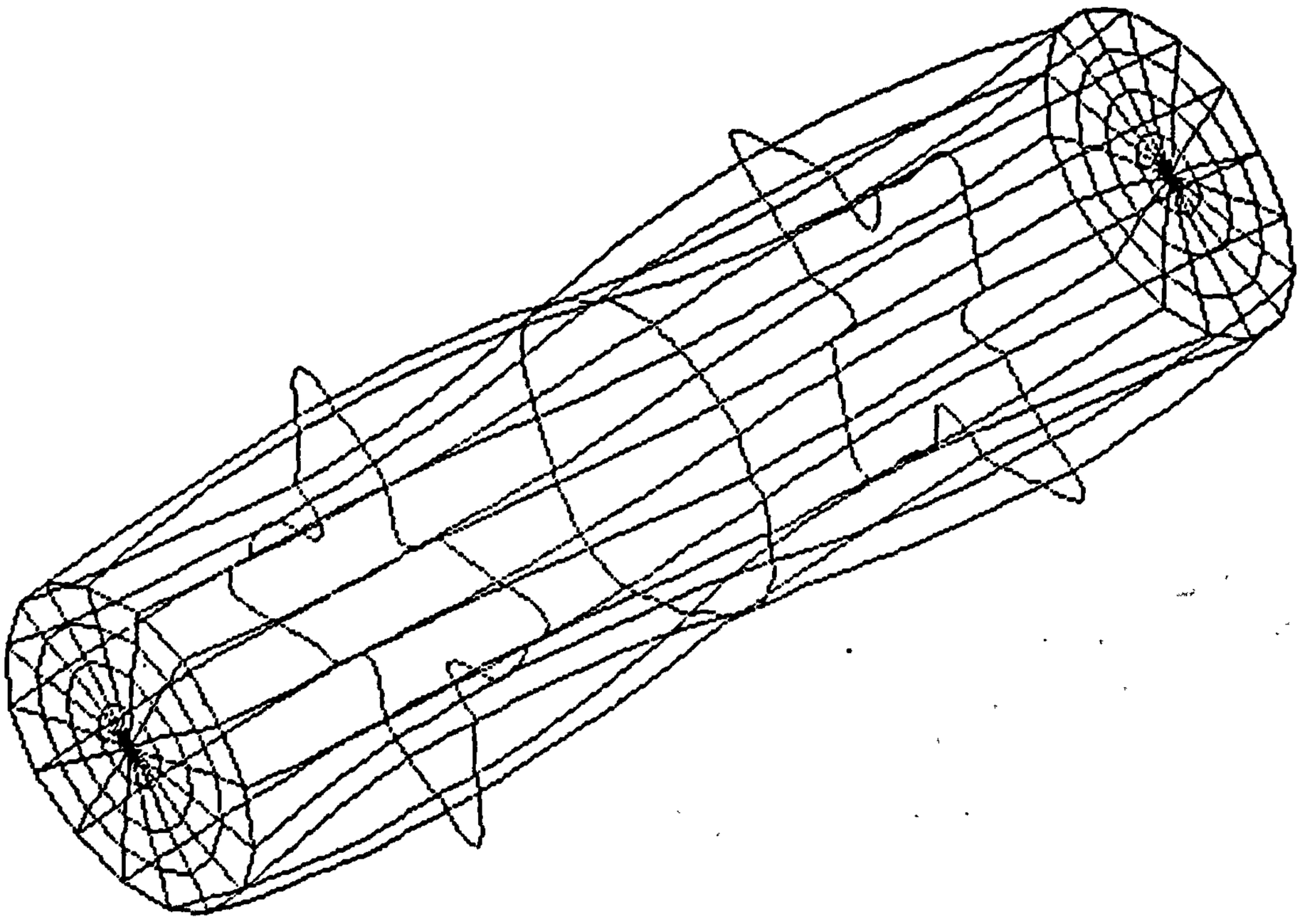

a.

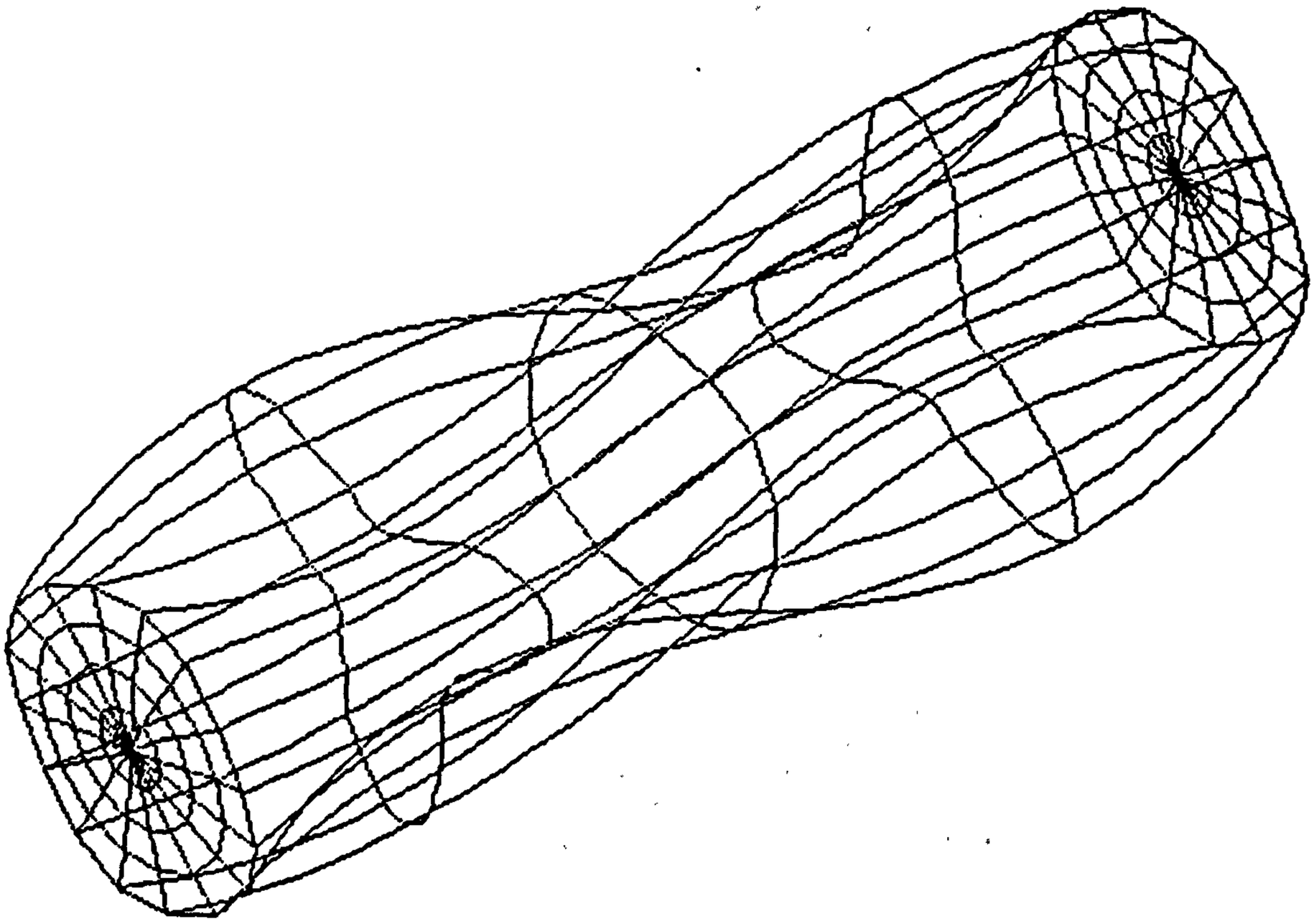

b.

Figure 7. Mesh size 64. Element type 43210

a. Gauss integration 5 pts. 5th distortion mode.

b. Gauss integration 3 x 3. 3rd distortion mode.

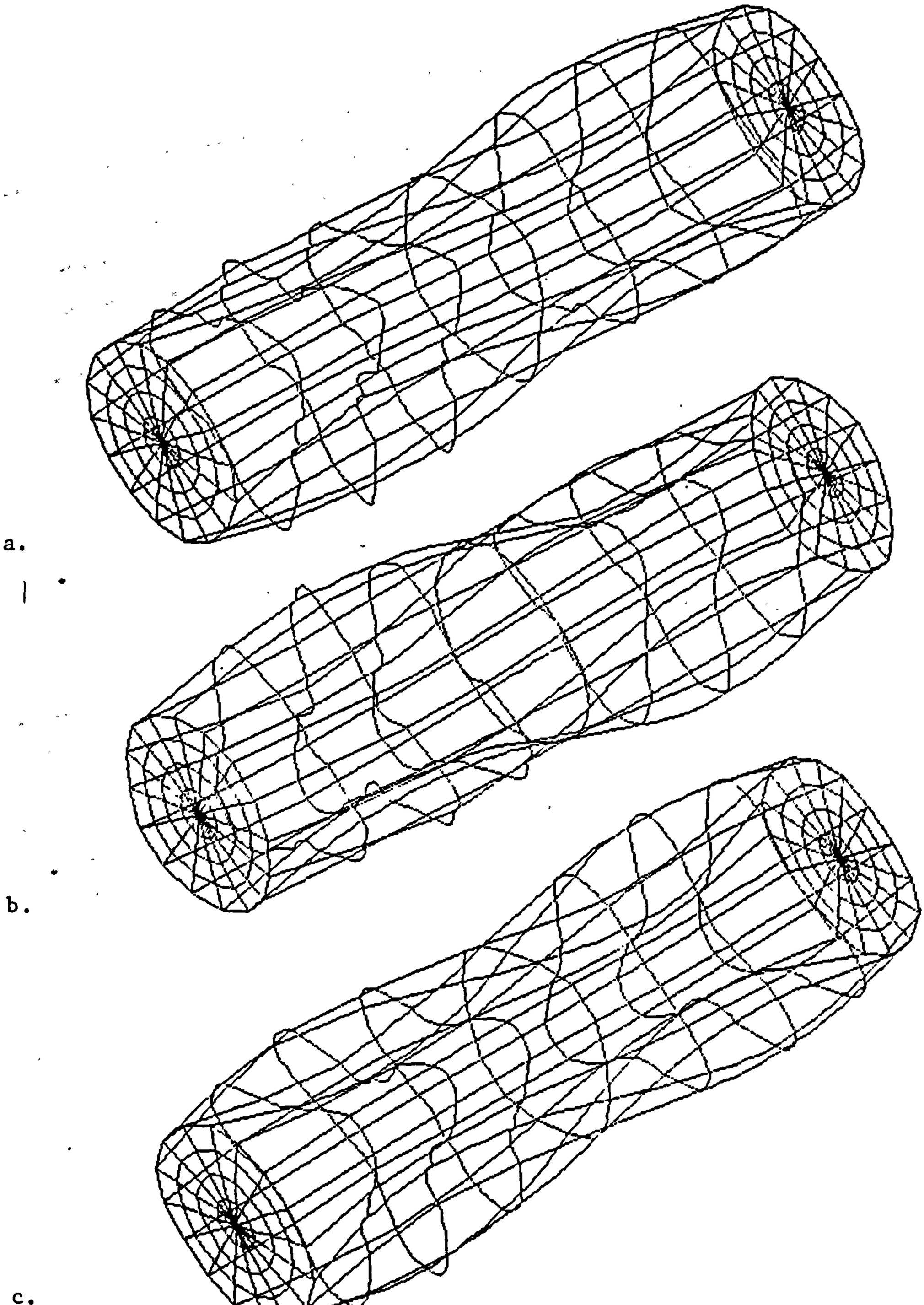

a.

b.

c.

Figure 8. Mesh size 128. Element type 128. 3rd distortion mode.

a. Gauss integration 2 x 2

b. Gauss integration 5 pts

c. Gauss integration 3 x 3

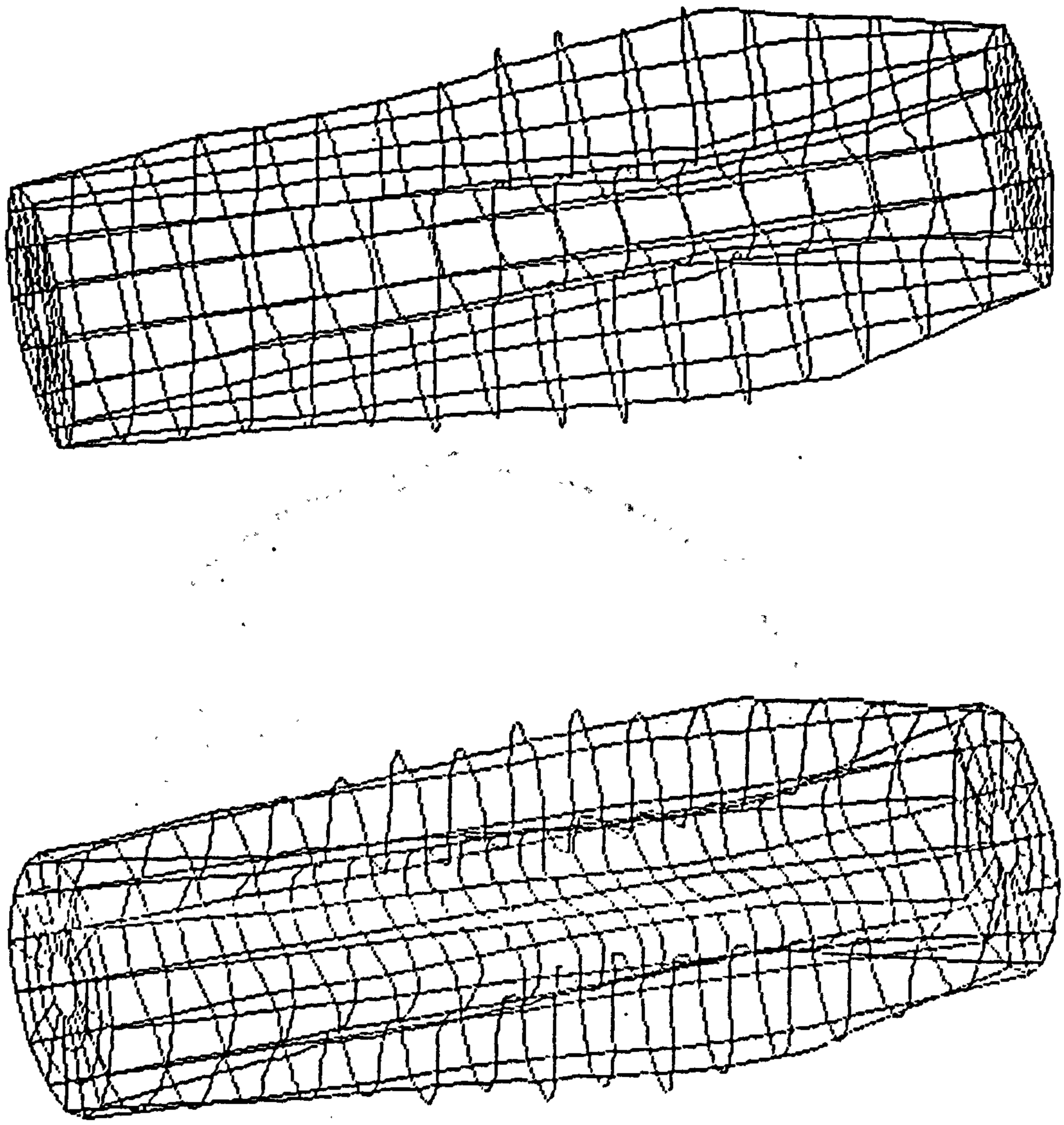

Figure 9. Mesh size 256. Element type 43210. Gauss integration 2 x 2 4th distortion mode.

STRESS DETERMINATION AND STRAIN MEASUREMENT IN AERONAUTICS, NAVAL ARCHITECTURE AND OFFSHORE ENGINEERING

6 - 8 SEPTEMBER 1988

UNIVERSITY OF SURREY, GUILDFORD

Organised by the Joint Aero Marine Group of the Royal Aeronautical Society, Royal Institution of Naval Architects and the Society for Underwater Technology in conjunction with the British Society for Strain Measurement

FLUID-STRUCTURE INTERACTION OF SUBMERGED SHELLS

by

W.G. PRICE[+], R. RANDALL[*] and P. TEMAREL[+]

A hydroelasticity theory approach to the dynamic response of a submerged structure is presented, incorporating both "dry" and 'wet' structural analyses. The chosen submerged structure is a typical pressure hull with ring stiffness, bulkheads and variable geometry.

To calculate natural frequencies and principal mode shapes of the structure in vacuo a finite element method is adopted, but the choice of elements demands expertise even for an unreinforced cylinder. This is assessed by comparing with experimental data the performance of facet and curved shell elements and thin shell of revolution elements.

The experimental tests were performed on a horizontal, unreinforced cylinder in air and submerged to a depth of 1.5 diameters. That is the centre of mass is 1.5 diameters below the calm free water surface. At this depth hydrostatic pressure is not significant but the influence of free surface is included in the mathematical model describing the dynamics of the neutrally buoyant cylinder. A singularity distribution method is employed to determine the generalised hydrodynamic coefficients, being functions of the principal modes of vibration of the dry structure. Fluid-structure interactions are evaluated and the influence of submergence on the 'wet' dynamic characteristics assessed.

[+] Department of Mechanical Engineering
Brunel The University of West London
Uxbridge.

[*] Royal Naval Engineering College
Manadon
Plymouth.

FLUID-STRUCTURE INTERACTION OF SUBMERGED SHELLS

by

W.G. PRICE[+], R. RANDALL[*] and P. TEMAREL[+]

A hydroelasticity theory approach to the dynamic response of a submerged structure is presented, incorporating both "dry" and 'wet' structural analyses. The chosen submerged structure is a typical pressure hull with ring stiffness, bulkheads and variable geometry.

To calculate natural frequencies and principal mode shapes of the structure in vacuo a finite element method is adopted, but the choice of elements demands expertise even for an unreinforced cylinder. This is assessed by comparing with experimental data the performance of facet and curved shell elements and thin shell of revolution elements.

The experimental tests were performed on a horizontal, unreinforced cylinder in air and submerged to a depth of 1.5 diameters. That is the centre of mass is 1.5 diameters below the calm free water surface. At this depth hydrostatic pressure is not significant but the influence of free surface is included in the mathematical model describing the dynamics of the neutrally buoyant cylinder. A singularity distribution method is employed to determine the generalised hydrodynamic coefficients, being functions of the principal modes of vibration of the dry structure. Fluid-structure interactions are evaluated and the influence of submergence on the 'wet' dynamic characteristics assessed.

+ Department of Mechanical Engineering
Brunel The University of West London
Uxbridge.

* Royal Naval Engineering College
Manadon
Plymouth.

1. Introduction

The description of the dynamic behaviour of a structure in an acoustic medium such as water and the analysis of the resultant induced stresses in the structure constitute a complex problem of immense practical significance. When the submerged structure is a thin shell, exact analytical solutions exist to describe the dynamic behaviour of a sphere and an infinitely long cylinder in an infinite acoustic domain[1,2]. The thin cylindrical shell is a commonly encountered shape in underwater structures such as submarine pressure hulls, offshore pipelines, etc. It is, therefore, an ideal starting point for the development of new analytical/numerical methods to examine the dynamic behaviour of submerged structures of arbitrary shape in water of finite or infinite depth.

This paper brings together results derived by classical analytical, experimental and numerical methods, each purporting to describe the dynamic behaviour of a thin cylindrical shell of finite length sealed at both ends. The numerical method adopted is the three dimensional hydroelasticity analysis developed for non-beamlike structures such as SWATHS (i.e. Small Waterplane Area Twin Hulls), jack-up rigs etc. floating in water[3,4,5,6]. The method, unlike classical analytical procedures, can be applied to structures of arbitrary shape and it has been shown to predict accurately the dynamic behaviour, as well as, the induced loadings and stresses at any position in the structure. Consequently, it can be used at any stage during the design process, being suitable for crude and refined representations of the structure and the surrounding acoustic medium.

The thin cylindrical shell to be investigated has the following properties:-

Overall length L=1284 mm
External radius r=180 mm
Shell thickness t=3 mm

and is sealed at both ends with flat plates. The cylinder is made of mild steel and the aspect ratios L/r and t/r were selected to be representative of a particular class of submarine hull, though in no way does the shell truly model a real submarine structure.

2. Experimental Predictions

The thin cylindrical shell was constructed to exacting tolerances as geometrical irregularities, such as large variations in the circularity of the cross section or non-uniform wall thickness, tend to affect the accuracy of the measured frequency response data at or near resonance.

Fifteen measurement sites were selected at positions where the vibration patterns of a cylindrical shell consisting of standing waves in both the axial and circumferential directions could be adequately defined. Eight measurement sites were located at 45° intervals around the circumference at a cross section where the majority of the mode shapes display significant amplitudes of motion, i.e. at a distance of 552 mm from one end. The remaining seven measurement sites were located at equal intervals on a straight line along the cylinder. Each site was fitted with an accelerometer, mounted on a stud inside the shell, recording radial motion. (No accelerometers were placed on the end plates).

A single point excitation was applied in a vertical direction in the plane of the eight accelerometers using an electro-magnetic shaker driving through a flexible push rod into a piezoelectric force gauge.

The tests were carried out with the thin cylindrical shell freely supported in vacuo and suspended near the centre of a tank of length 7.5m, width 1.7m and depth 1.6m. The top of the shell was 0.5m below the free water surface and the shell placed across the width of the tank to minimise wave reflections[7]. The shell was not neutrally buoyant and was lightly tethered to eliminate bodily motions. Receptances were obtained over the frequency range 100-600 Hz. in air and 0-500 Hz. in water. The corresponding results are shown in Fig. 1(a,b) respectively and also in Table 1 where the natural and resonance (water) frequencies for the first 8 modes shapes are tabulated. As can be seen, the value of the first natural frequency is halved when the shell is immersed in water, however, this decrease is not uniform for all the mode shapes. Modal dynamic properties (i.e. resonance frequency, damping factors, etc) were extracted from the experimental data using a straight line technique which is particularly accurate in separating closely spaced modes[8].

3. Analytical Predictions

Bleich and Baron[1] and Warburton[2] investigated the vibrations of infinitely long cylindrical shells in an infinite acoustic medium. They also considered finite values of the axial wave length, so that provided

the boundary conditions are satisfied at circumferential nodal positions the derived equations of motion are valid, and the solutions are applicable to simply supported cylindrical shells of finite length with open ends.

Assumptions were made in order to restrict the problem to the linear domain, thus ensuring no variation of displacement or stress across the thickness of the shell. These assumptions are known as the Kirchoff hypothesis and require:-

(a) The thickness of the shell to be large compared to the displacement but small compared to the radius of the shell.

(b) The fibres of the shell initially perpendicular to the middle surface remain so after deformation and are not subject to elongation.

(c) Normal stresses acting on planes parallel to the shell's middle surface are negligible compared to other stresses.

The displacements of the shell in the axial, tangential and radial directions are assumed to vary harmonically and three equations of motion are derived by solving the strain-displacement relationships in conjunction with the wave equation. When the acoustic medium is a fluid the solutions obtained range from the free vibrations of a cylinder in vacuo to the vibrations of the cylinder surrounded by an unbounded fluid. The fluid is assumed inviscid, irrotational and incompressible such that the fluid flow can be described by a velocity potential function.

Using Warburton's method[2], natural frequencies in vacuo and resonance frequencies in water were calculated for the cylindrical shell for a selection of m and n values which denote the number of axial half- and circumferential wave lengths respectively. These analytical results are shown in Table I and they are readily comparable with the experimental data. As can be seen, there appears excellent correlation between both sets of predictions in either acoustic medium. The analytical results also confirm that the missing in vacuo frequency (m=2,n=2) was outside the range of the experiments; on the other hand the frequency (m=1,n=5) in water was not picked up during the experiments.

At first sight this comparison provides confidence in the theoretical approach though it must be emphasised that the experimental data relate to a cylinder vibrating in a bounded fluid whereas the analytical results correspond to an unbounded fluid. Because of the increased influence of water in the bounded case, it would be expected that the resonance frequencies of the cylinder would be lower than those excited in the unbounded medium[9].

4. Numerical Analysis

The theoretical background to the general linear three dimensional hydroelasticity analysis adopted here has been discussed in detail elsewhere[3] and is therefore omitted. The equations of motion describing the responses of an arbitrary shaped, floating or submerged structure are given by

$$\mathbf{M\ddot{U} + B_d\dot{U} + KU = P} \tag{1}$$

where

M Mass matrix,

$\mathbf{B_d}$ Structural damping matrix,

K Stiffness matrix,

U Structural displacement vector,

P External force vector describing all fluid actions, imposed forces, etc.

The analysis consists of the following two parts:-

(i) The *dry* or *in vacuo* analysis in which the structure vibrates freely in vacuo in the absence of any structural damping or external forces. This motion is described by the equation

$$\mathbf{M\ddot{U} + KU = 0.} \tag{2}$$

The structure is discretised using finite elements and the natural frequencies and principal mode shapes of the structure are determined. To each principal mode shape a principal coordinate can be assigned and equation (1) rewritten in terms of the principal coordinates of the structure, namely

$$a\ddot{p} + b\dot{p} + cp = Z(t) \tag{3}$$

where

a Generalised mass matrix,

b Generalised structural damping matrix,

c Generalised stiffness matrix,

p Principal coordinate vector,

Z Generalised external force vector describing the fluid actions, etc.

(ii) The *wet* analysis introduces the fluid actions which are applied as an external loading to the flexible structure i.e. the cylindrical shell. A three dimensional velocity potential theory is employed and the wet surface of the structure discretised by panels with a source situated at the centre of each panel.[3] This part of the analysis produces the fluid structure interaction effects which are usually described by added mass, fluid damping, restoring force coefficients and additional fluid or other external excitations. Consequently it may be shown that equation (3) takes the form

$$(a+A)\ddot{p} + (b+B)\dot{p} + (c+C)p = \Xi(t) \tag{4}$$

where

A Generalised added mass matrix,

B Generalised fluid damping matrix,

C Generalised restoring matrix,

Ξ Generalised excitation vector describing wave actions, imposed forces, etc.

These equations of motion can now be solved for the principal coordinates of the structure which are subsequently used to evaluate the loadings and stresses associated with the structure[6], which in the present case is a flexible cylindrical shell.

5. Dry or In Vacuo Analysis

The most important aspect in the idealisation and modelling of the structure by finite elements is the selection of the appropriate element type. For the case of the thin cylindrical shell three types of finite element are available in the software package employed[10]. Namely,

- a thin shell of revolution (3 noded),
- a flat facet shell element (8 noded),
- a semi-loof curved shell element (8 noded) able to describe the exact curvature of the shell.

The thin shell of revolution is based on the theory due to Novozhilov[11] and incorporates membrane as well as bending effects. This model corresponds approximately to the Kirchoff plate theory and the element provides a highly efficient and accurate solution often used as a benchmark for comparison with other predictions. However, applications are limited to structures with simple geometries. Table 2 illustrates the *in vacuo* natural frequencies obtained using a finite element model consisting of 16 such elements with a total of 33 nodes. Unfortunately at present this element is not entirely suitable to use in the wet analysis theory.

Both the facet and semi-loof shell elements can carry membrane and bending loads. However, both require much larger computational efforts compared to that needed in the thin shell of revolution calculation, and their predictions are not as accurate. Studies carried out on thin cylindrical shells revealed interesting deviations regarding the use of these elements[12]. For the facet shell elements convergence of solution is achieved rather slowly, at the expense of a large number of elements, although, where applicable, symmetry of mode shape is maintained. For the semi-loof shell elements a more rapid convergence is attained producing good estimates with rather crude idealisations. However, caution is required when using these elements as there is some evidence of subsequent divergence, especially at higher modes. Closer examination of the results also revealed distorted mode shapes. These drawbacks of the semi-loof elements can be overcome by using refined idealisations, but this greatly reduces their advantage in comparison to the simpler facet shell elements.

Table 2 also includes predictions for the natural frequencies of the thin cylindrical shell using 288 facet and 384 semi-loof shell elements - 16 elements around the circumference and 18 along the shell as can be seen in Fig.2. Both element types produce two orthogonal mode shapes, at slightly different frequencies, for each natural frequency; the reason being that for a perfectly circular cross section the prescribed mode shape can occur in any plane between 0° and 360° and this infinite variation can be given using a linear combination of the two orthogonal mode shapes. Examples of these orthogonal mode shapes are illustrated in Figs. 2-7.

The correlation between the predicted and experimental results is not as good as the one observed in Table 1. The current finite element idealisation tends to overestimate the *in vacuo* natural frequencies. However, the idealisations with either the facet or semi-loof shell elements provide additional mode shapes relating to the end seals. The classical analysis[2] cannot account for these mode shapes and regrettably, at the time, the experiments were not set up to measure them[7].

6. Wet Analysis

The wet surface of the thin cylindrical shell was discretised using 384 panels, producing a one to one correspondence between the fluid panel and the semi-loof finite element idealisation. This one to one correspondence is not a necessary requirement since the fluid and structural idealisations are independent of one another, depending on the complexity of the structure and its wetted area hull shape. During the evaluation of the hydrodynamic properties the composite source method was used; taking advantage of the port/starboard symmetry of the structure and thus reducing the computational effort. This method requires that the mode shapes are port/starboard symmetric (or antisymmetric as the case may be). Of each pair of orthogonal mode shapes, shown in Figs. 2,3,6,7 , the one closest to satisfying port/starboard symmetry was selected in the wet analysis.

In general, the resonances of a structure in a fluid are determined by observing the peaks of the principal coordinates, i.e. the solution to equation (4), as the hydrodynamic matrices **A** and **B** are frequency dependent. However, in this particular example of a relatively "deeply" submerged shell the expected resonance frequencies are high; hence the free surface has negligible influence, the generalised hydrodynamic

damping coefficients are zero and the generalised added mass coefficients are of constant values over the frequency range[13]. Therefore, one can easily obtain the eigenvalues of the structure in water from the following equation:-

$$(\mathbf{a} + \mathbf{A})\ddot{\mathbf{p}} + (\mathbf{c} + \mathbf{C})\mathbf{p} = \mathbf{0} \tag{5}$$

provided the generalised structural damping is ignored.

The eigenvalues obtained from equation (5) describe the coupled behaviour of the system. On the other hand, the classical analysis[2] treats the mode shapes as uncoupled; that is to say, the resonance frequencies shown in Table 1 are derived from the expression

$$(\bar{\omega}_r)_{wet} = \left[\frac{(\omega_r)^2_{dry} a_{rr}}{(a_{rr} + A_{rr})}\right]^{\frac{1}{2}} \tag{6}$$

The results in water of infinite depth are summarised in Table 3. As can be seen the correlation between these values and the predictions shown in Table 1 is not good. Corresponding results obtained in water of 1.6 m finite depth are illustrated in Table 4. These predictions have a better correlation with the experimental results of Table 1. This is due to the increase in the value of the generalised added mass coefficient A_{rr} caused by the proximity of the tank's bottom. A comparison of the A_{rr} values in Tables 3 and 4 clearly illustrates the effect of finite water depth.

7. Conclusions

The results illustrated in Table 4 are very encouraging and demonstrate the applicability of the three dimensional hydroelasticity theory to structures such as submarine pressure hulls with considerable success; furthermore this method can provide the stresses in such structures[6].

It is surprising, to say the least, that the analytical predictions[2] based on cylindrical shells of infinite length in an infinite fluid domain correlate rather well with the experimental results. On the other hand, the corresponding predictions in Table 3 do not display such a good agreement.

Clearly the disagreement between the numerical and experimental results is mostly due to the inadequate discretisation of the structure. More elements are required around the circumference of the shell in

order to evaluate the hydrodynamic properties with sufficient accuracy, particularly for the higher mode shapes as can be seen from Tables 3 and 4. A more refined mesh should be created using facet shell elements rather than semi-loof shell elements due to the risk of obtaining spurious results in the latter. This would also create a better geometric description of the shell's curvature, further decreasing the geometric advantage of semi-loof elements. From the evidence presented, the latter should only be used as a last resort.

For the thin cylindrical shell under consideration each cross section possesses an infinite number of planes of symmetry. This results in two orthogonal mode shapes per natural frequency. The introduction of a negligible asymmetry either at the top or the bottom of the shell might result in the creation of port-starboard symmetric mode shapes without significantly affecting the dynamic behaviour of the structure.

8. References

1. H. H. Bleich and M. L. Baron, "Free and forced vibrations of an infinitely long cylindrical shell in an infinite acoustic medium," *Journal of Applied Mechanics*, pp. 167-177 (1954).

2. G. B. Warburton, "Vibration of a cylindrical shell in an acoustic medium," *Journal of Mechanical Engineering Science* 3(1) pp. 69-79 (1961).

3. R. E. D. Bishop, W. G. Price, and Wu Yousheng, "A general linear hydroelasticity theory of floating structures moving in a seaway," *Phil. Trans. Royal Soc. London* **A316** pp. 375-426 (1986).

4. Yuning Fu, W. G. Price, and P. Temarel, "The 'dry' and 'wet' towage of a jack-up rig in regular and irregular waves," *Trans. RINA* 129 pp. 147-159 (1987).

5. W. G. Price, P. Temarel, and Yongshu Wu, "Responses of a SWATH travelling in unidirectional irregular seas," *Underwater Technology* 13(4) pp. 2-10 (1987).

6. W. G. Price, P. Temarel, and Yongshu Wu, "Predictions of global stresses in floating structures excited by a seaway," in *Proc. Conf. Stress Determination and Strain Measurement in Aeronautics, Naval Architecture and Offshore Engineering, University of Surrey*, (1988).

7. R. Randall, "Modal analysis of a cylindrical structure immersed in water," *Proc. 3rd Int. Modal Analysis Conf. IMAC* 2 pp. 738-744 (1985).

8. B. J. Dobson, "A straight line technique for extracting modal properties from frequency response data," *Mechanical Systems and Signal Processing* 1(1) pp. 29-40 (1987).

9. R. Hosoda, W. G. Price, and R. Randall, "Responses of a flexible non-uniform circular beam in a bounded, viscous fluid.," *Journal of Sound and Vibration* (To be published)(1988).

10. Pafec, "Pafec Data Preparation User Manual," in *Pafec Limited*, (1986).

11. V. V. Novozhilov, "Theory of shells," in *Nordhoff*, (1959).

12. R. Randall, "Problems of modelling shell type structures for fluid structure interaction problems," *Royal Naval Engineering College, Manadon* RNEC-RR-88001(1988).

13. Yuning Fu and W. G. Price, "Interactions between a partially or totally immersed vibrating cantilever plate and the surrounding fluid," *Journal of Sound and Vibration* 118(3) pp. 495-513 (1987).

		Experimental			Analytical		
m	n	in vacuo	in water	α	in vacuo	in water	α
1	2	194	96	0.49	198	98	0.49
1	3	198	107	0.54	199	109	0.55
1	4	336	199	0.59	342	204	0.60
2	3	387	214	0.55	391	215	0.55
2	4	403	239	0.59	405	241	0.60
1	5	537	---	----	545	346	0.63
2	2	---	338	----	660	329	0.50
3	4	565	341	0.60	571	340	0.60

Table 1. Natural frequencies (Hz) in vacuo and resonance frequencies (Hz) in water of the thin cylindrical shell as predicted by experimental and analytical methods.

(α = resonance frequency in water/natural frequency in vacuo)

m	n	FE1	FE2	FE3	Experimental
1	2	197.6	198.1	199.1	194
1	2		198.8	200.1	
1	3	201.3	206.3	202.9	198
1	3		207.0	203.3	
+		---	207.8	209.2	---
+		---	216.6	218.0	---
1	4	344.4	364.0	352.5	336
1	4		366.1	353.7	
2	3	391.3	407.8	413.3	387
2	3		410.8	415.9	

Table 2. *In vacuo* natural frequencies (Hz) of the thin cylindrical shell using three different types of finite elements, namely a thin shell of revolution (FE1), a flat facet shell element (FE2) and a semi-loof curved shell element (FE3). (+ denotes vibrations of the end seals, as seen in Figs. 4,5)

r	$(\omega_r)_{dry}$ (Hz)	a_{rr} ($kg\ m^2$)	A_{rr} ($kg\ m^2$)	$(\bar{\omega}_r)_{wet}$ (Hz)	α	$(\omega_r)_{wet}$ (Hz)	
7	200.1	12.4	29.2	109.2	0.55	106.0	1,2
8	202.9	7.6	14.1	120.1	0.59	122.5	1,3
9	209.2	0.9	3.9	90.6	0.43	91.8	e1
10	218.0	0.8	2.9	101.4	0.47	101.2	e2
11	353.7	8.7	10.6	237.5	0.67	253.4	1,4
12	413.3	5.9	8.5	264.6	0.64	265.8	2,3
				from Eq.(6)		from Eq.(5)	

Table 3. Wet resonance frequencies of the thin cylindrical shell in water of infinite depth.

$(\alpha = (\bar{\omega}_r)_{wet} / (\omega_r)_{dry})$

r	$(\omega_r)_{dry}$ (Hz)	a_{rr} ($kg\ m^2$)	A_{rr} ($kg\ m^2$)	$(\bar{\omega}_r)_{wet}$ (Hz)	α	$(\omega_r)_{wet}$ (Hz)
7	200.1	12.4	44.0	93.8	0.47	90.7
8	202.9	7.6	18.1	110.3	0.54	114.4
9	209.2	0.9	6.3	74.0	0.35	75.3
10	218.0	0.8	4.7	83.1	0.38	83.3
11	353.7	8.7	10.0	241.3	0.68	245.3
12	413.3	5.9	10.7	246.4	0.60	261.0
				from Eq.(6)		from Eq.(5)

Table 4. Wet resonance frequencies of the thin cylindrical shell in water of 1.6 m depth.

$(\alpha = (\bar{\omega}_r)_{wet} / (\omega_r)_{dry})$

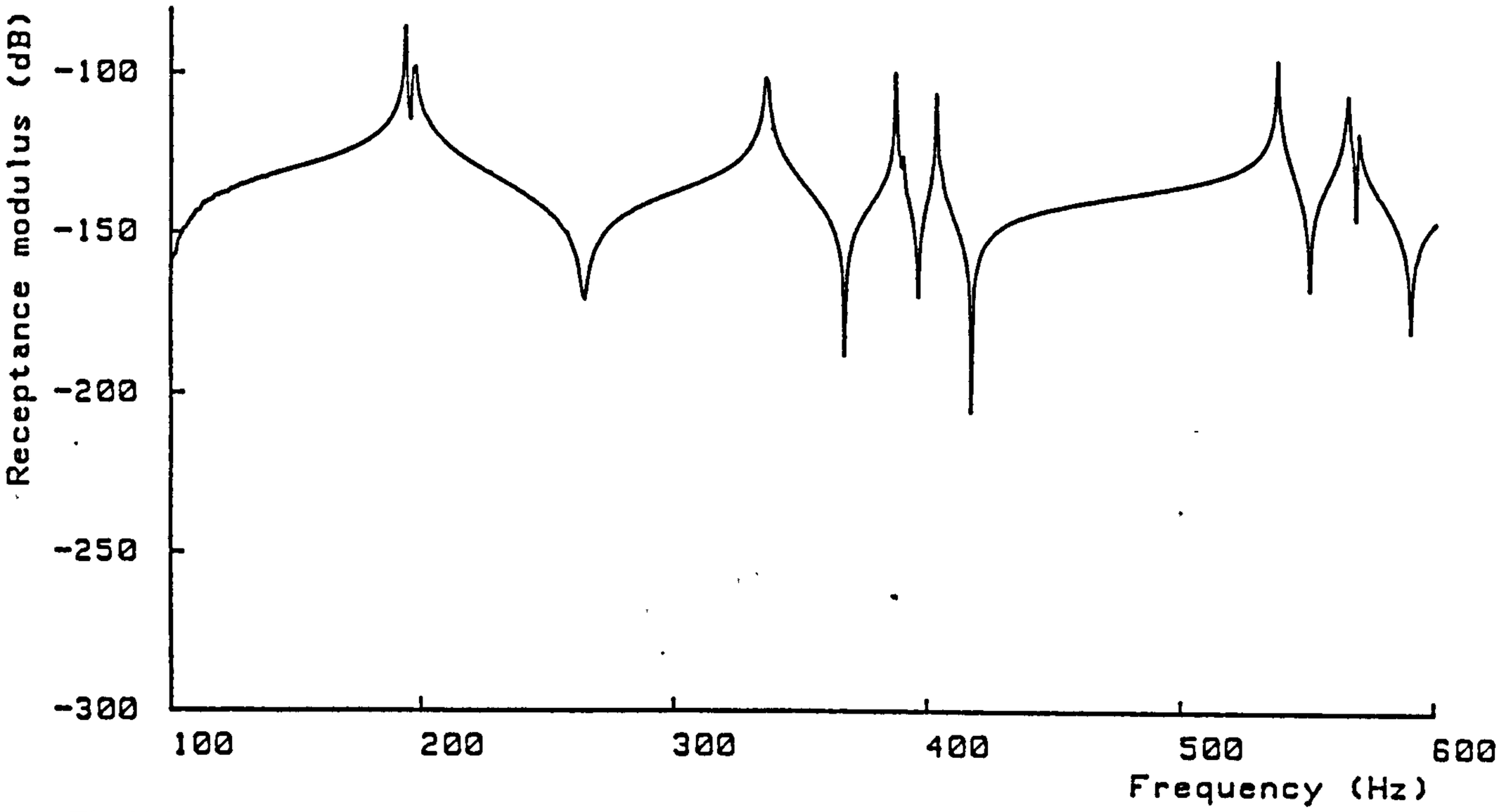

Fig.1(a)

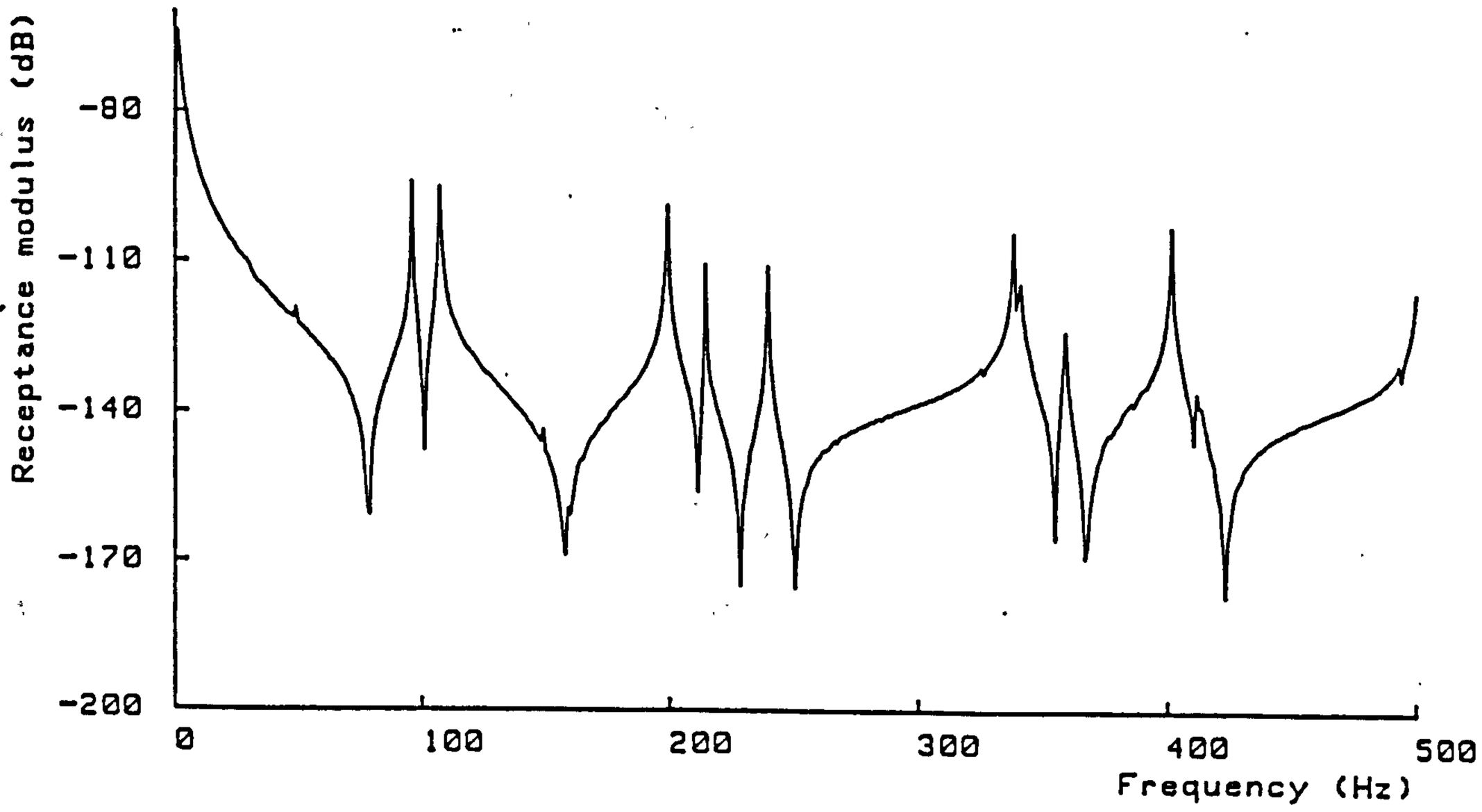

Fig.1(b)

Fig. 1 Receptance modulii obtained experimentally for the thin cylindrical shell (a) in vacuo and (b) in water.

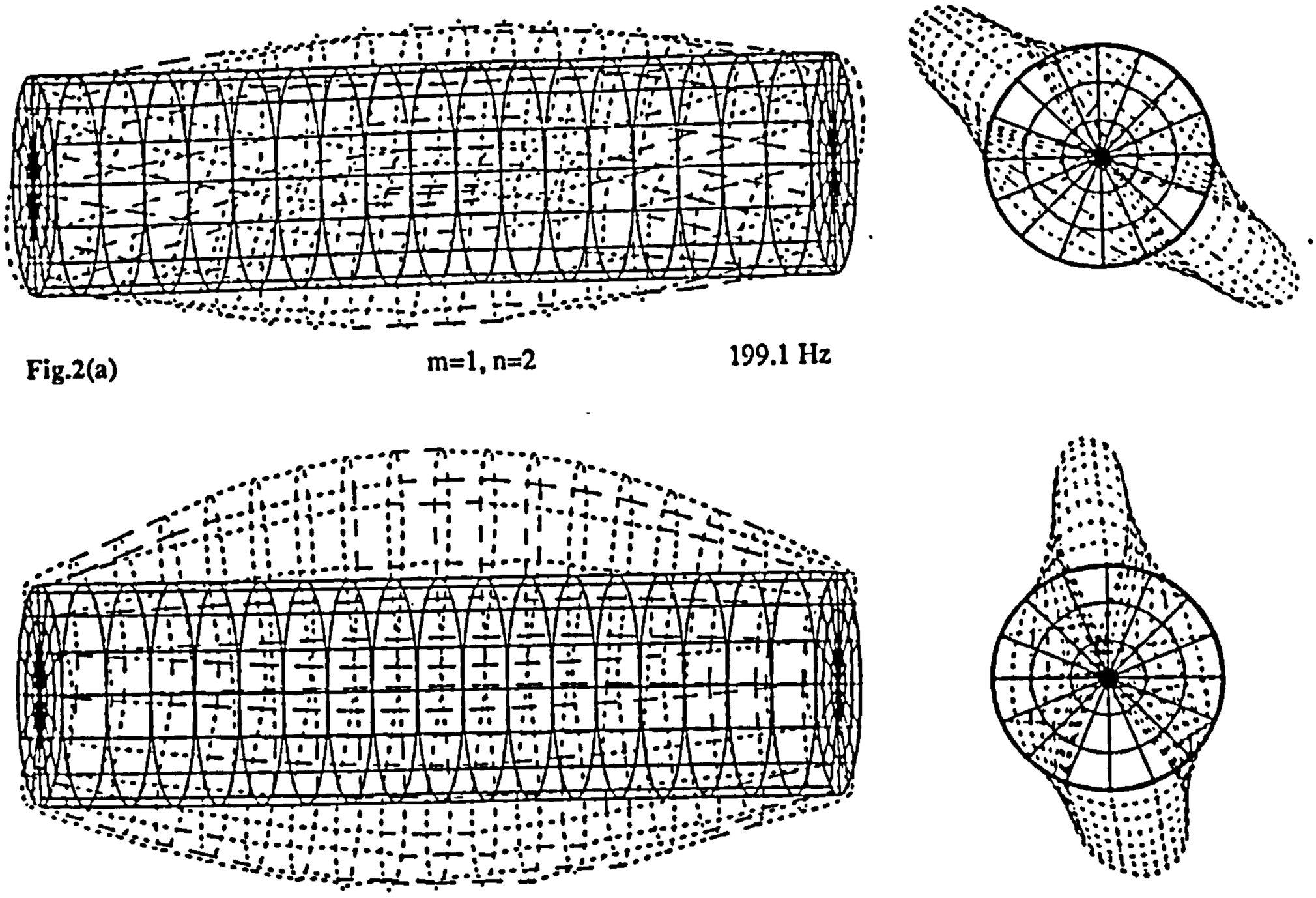

Fig.2(a) m=1, n=2 199.1 Hz

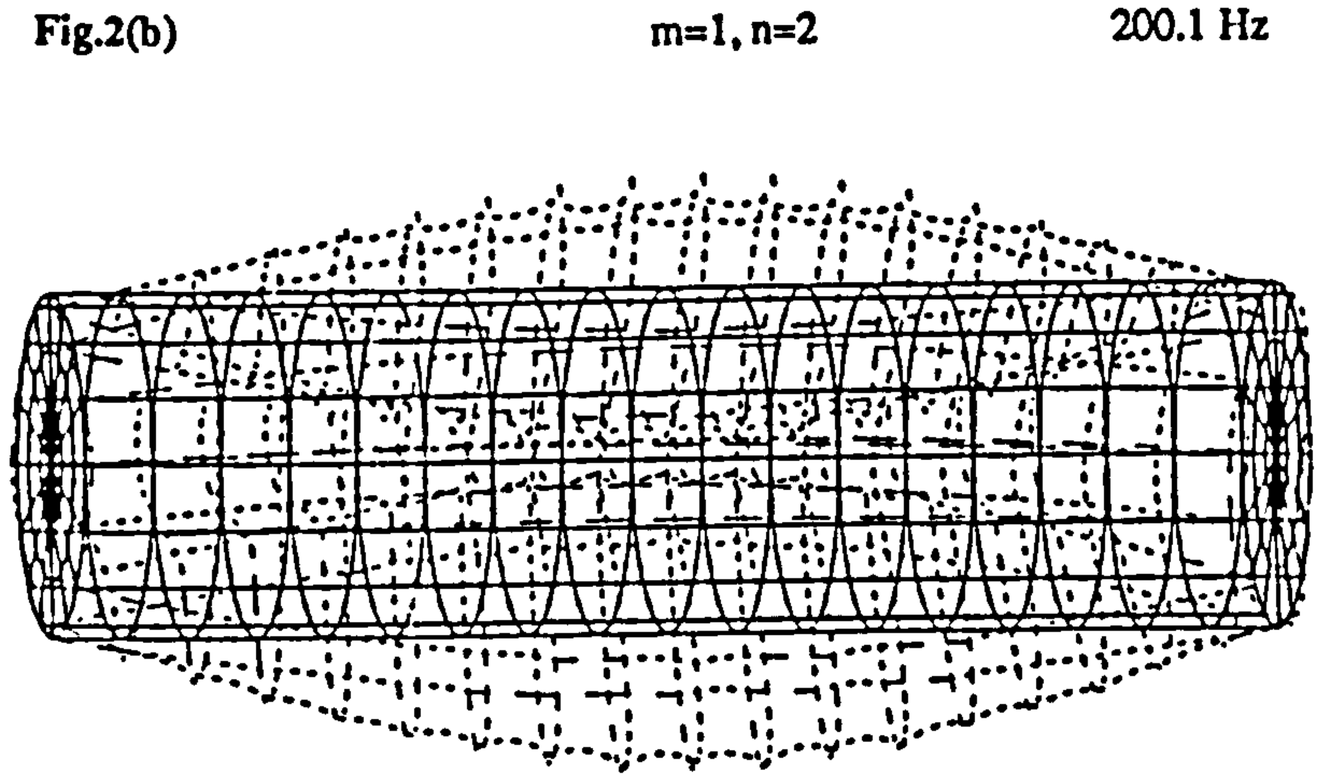

Fig.2(b) m=1, n=2 200.1 Hz

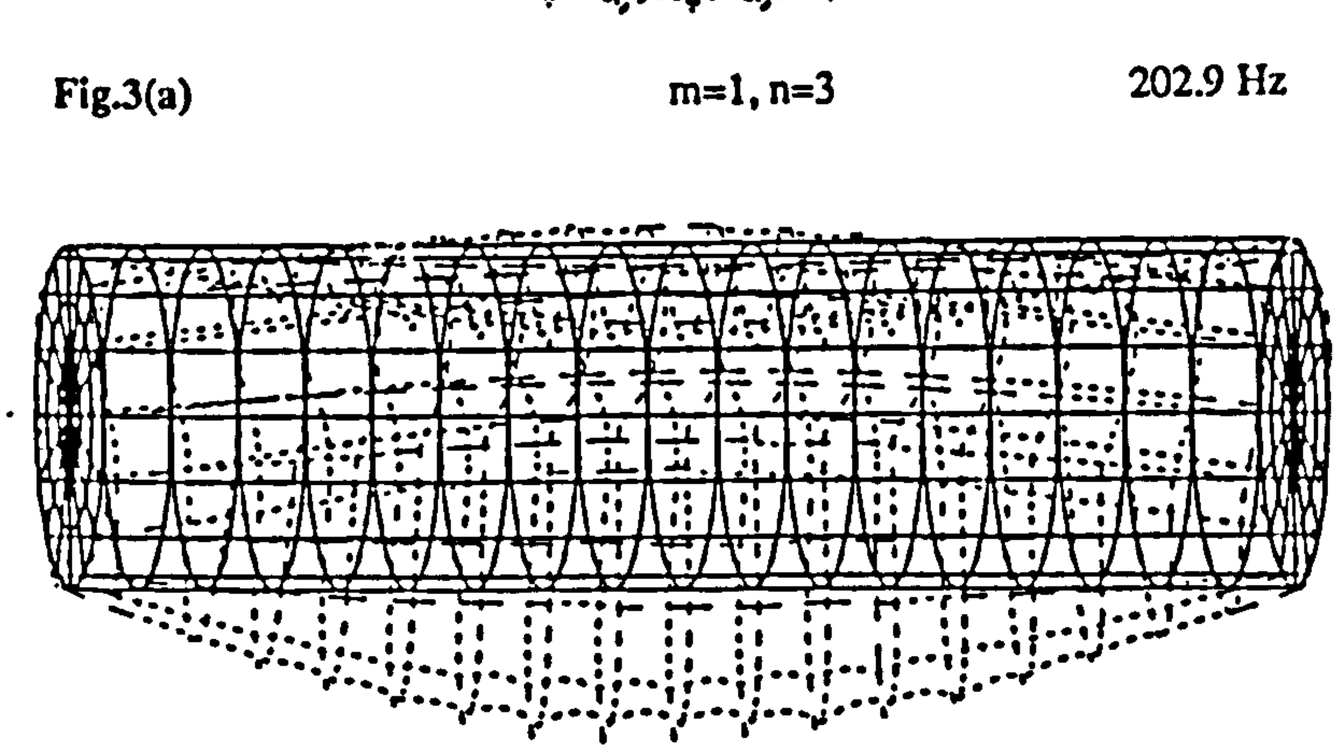

Fig.3(a) m=1, n=3 202.9 Hz

Fig.3(b) m=1, n=3 203.3 Hz

Figs.2,3 Distortion modes and natural frequencies of the thin cylindrical shell in vacuo using semi-loof curved shell elements.

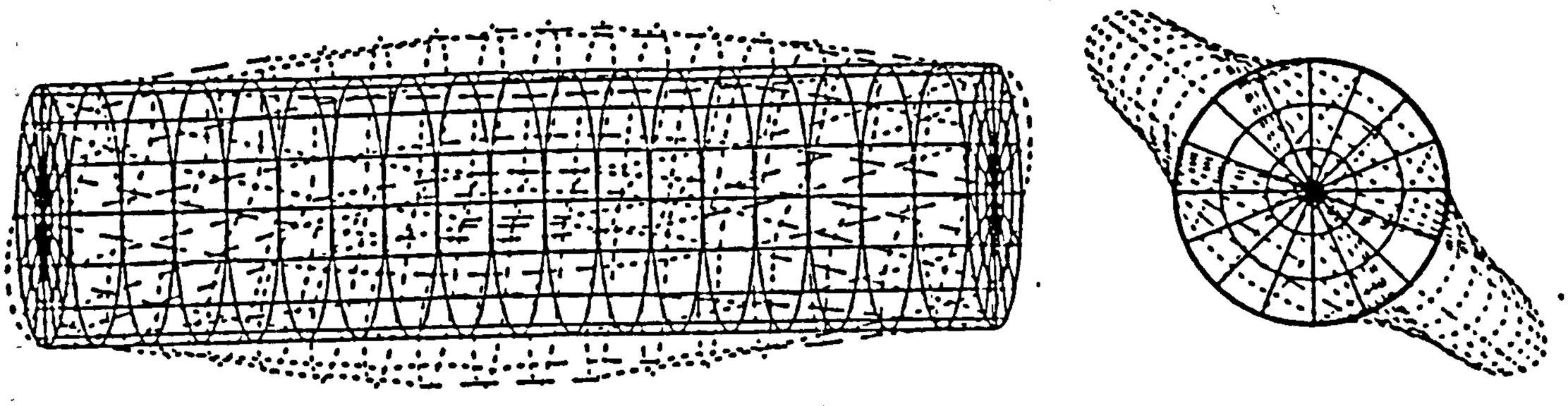

Fig.2(a) m=1, n=2 199.1 Hz

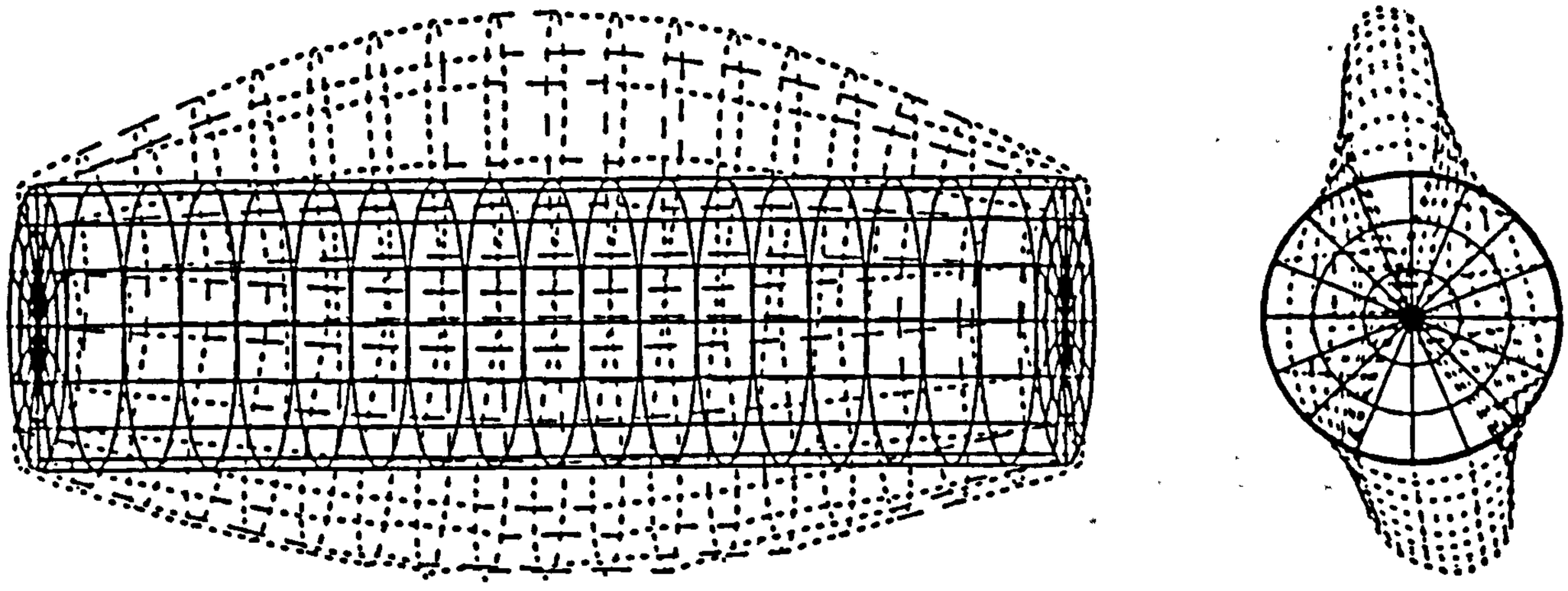

Fig.2(b) m=1, n=2 200.1 Hz

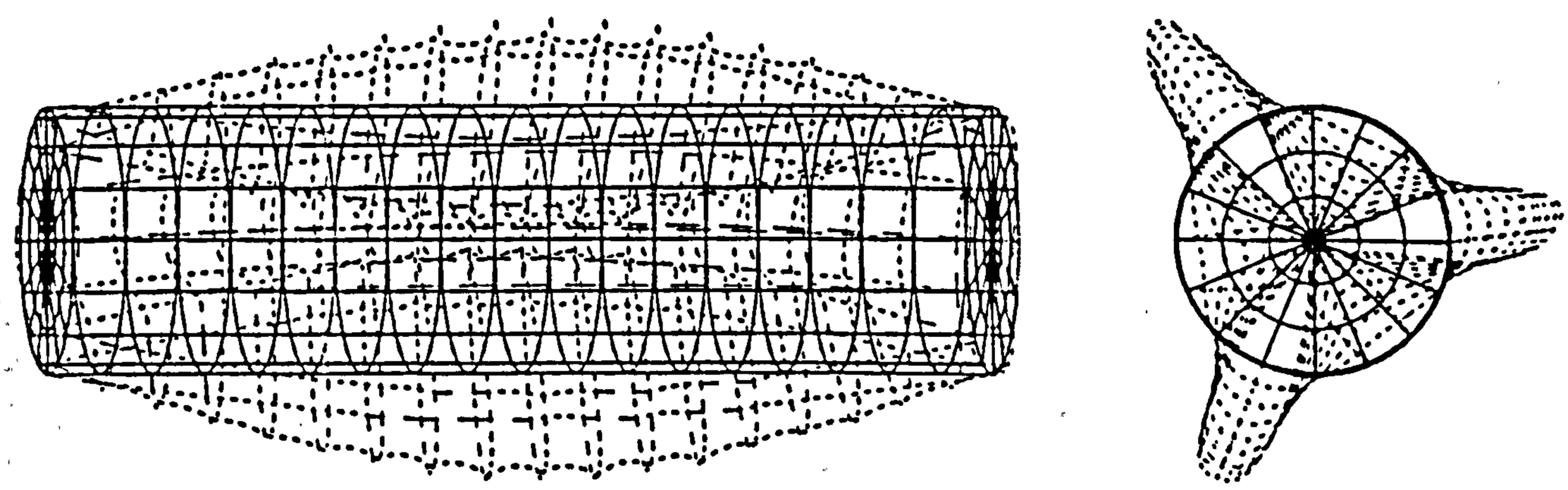

Fig.3(a) m=1, n=3 202.9 Hz

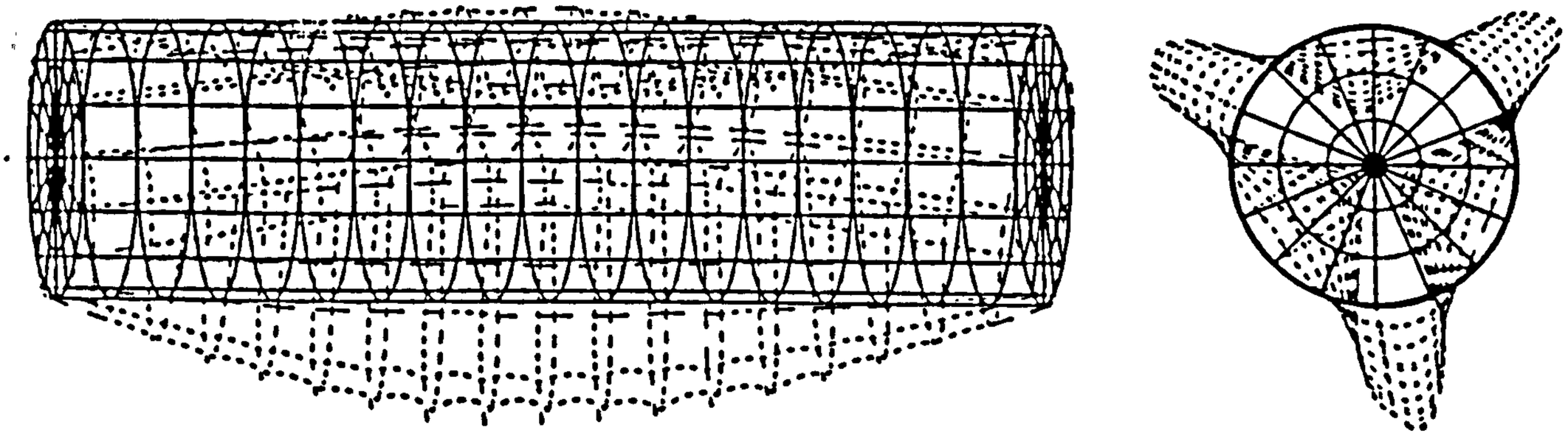

Fig.3(b) m=1, n=3 203.3 Hz

Figs.2,3 Distortion modes and natural frequencies of the thin cylindrical shell in vacuo using semi-loof curved shell elements.

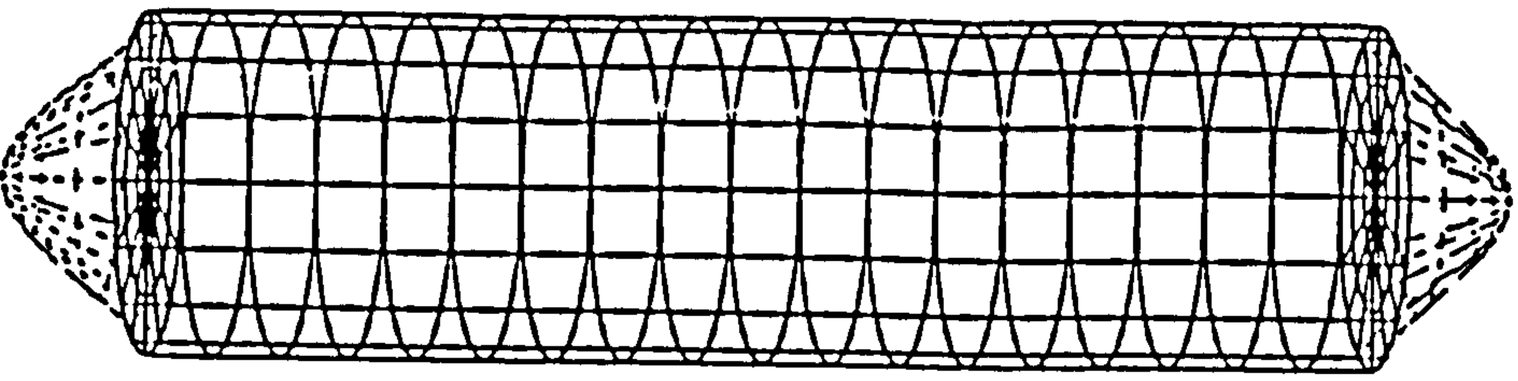

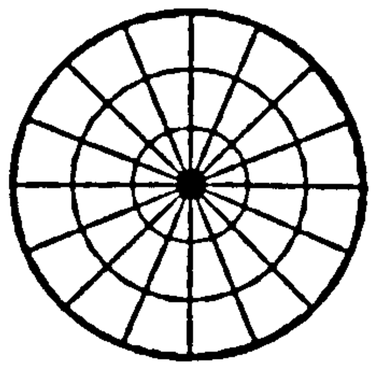

Fig.4 209.2 Hz

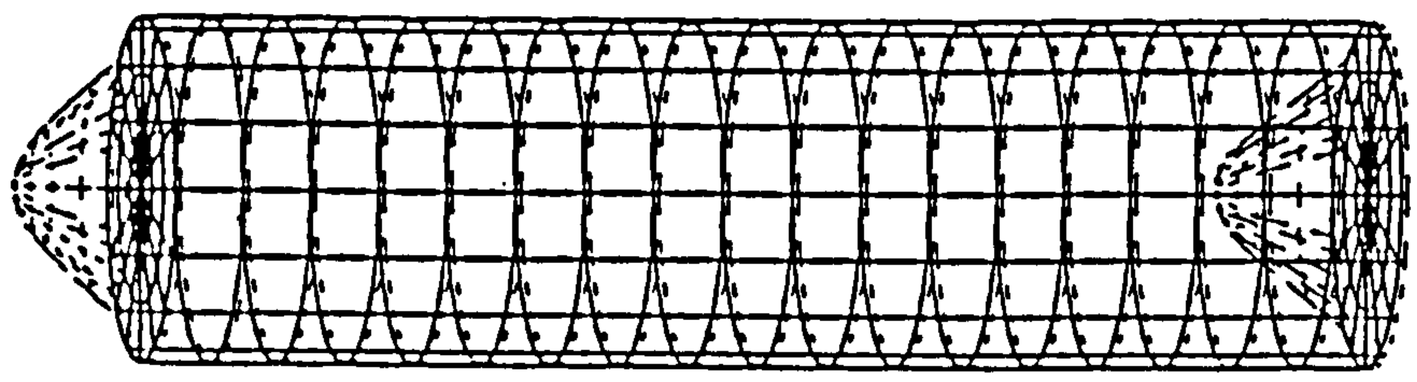

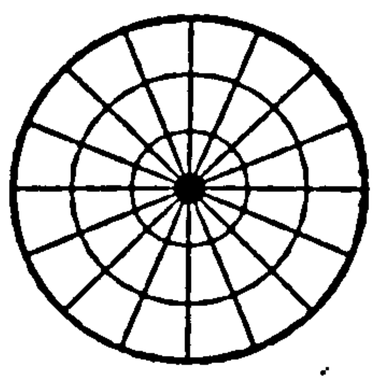

Fig.5 218.0 Hz

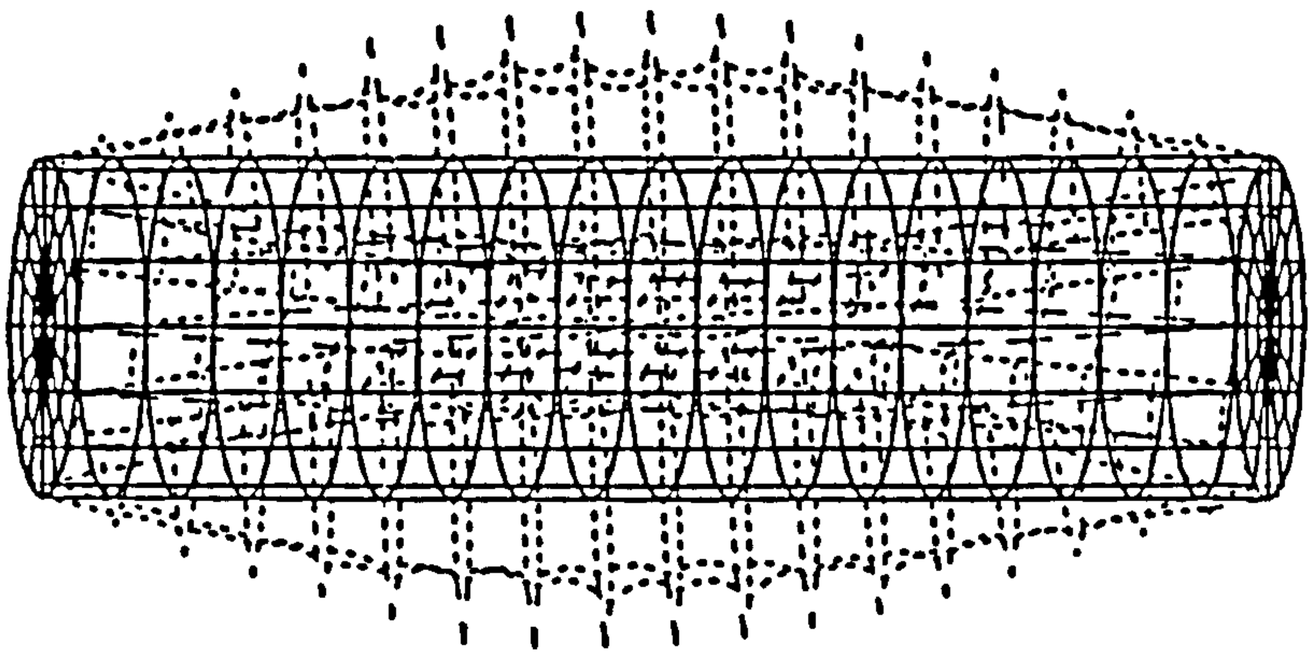

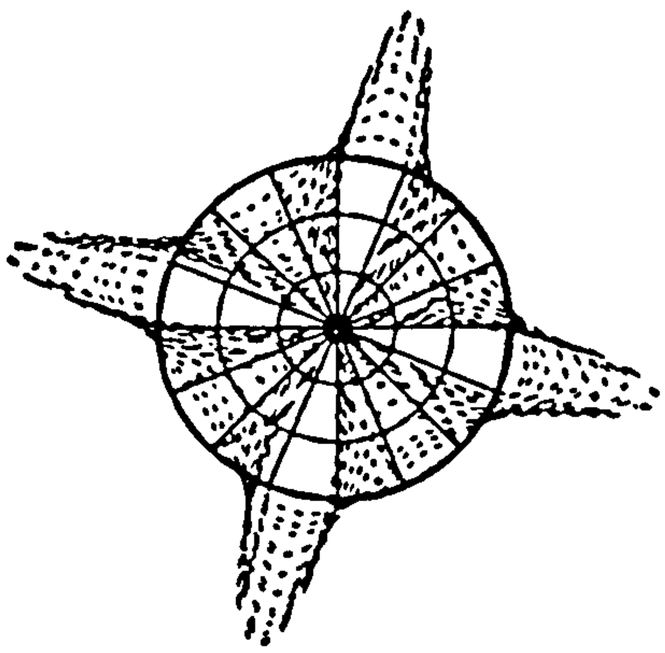

Fig.6(a) m=1, n=4 352.5 Hz

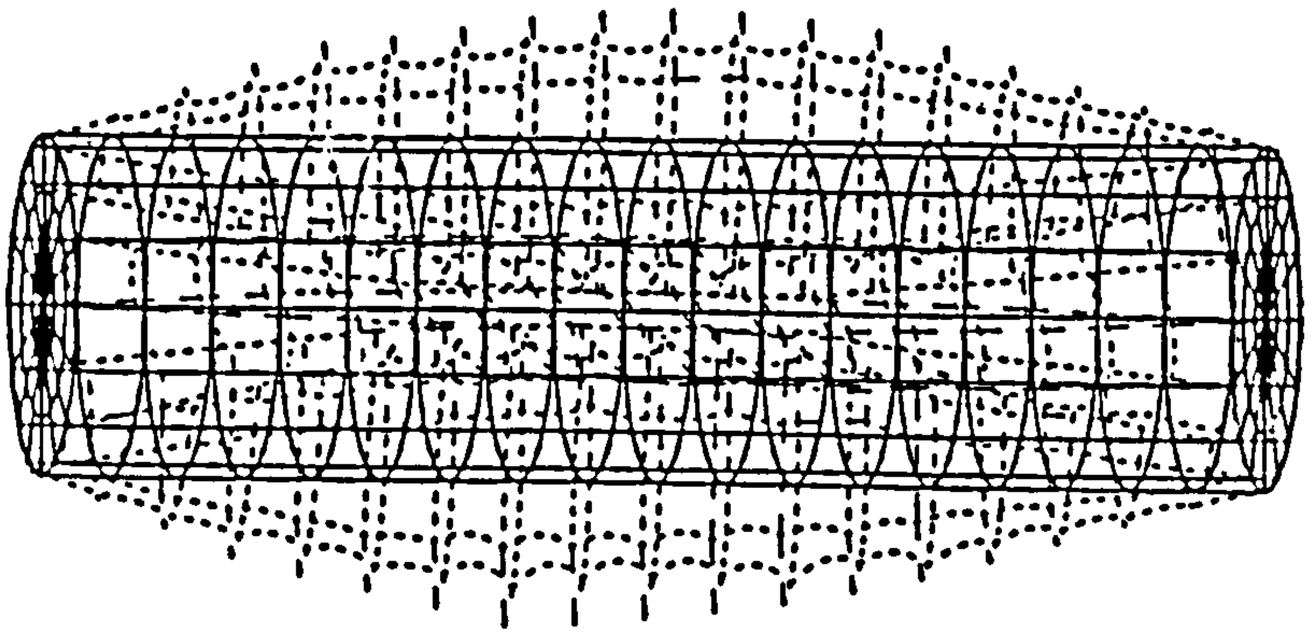

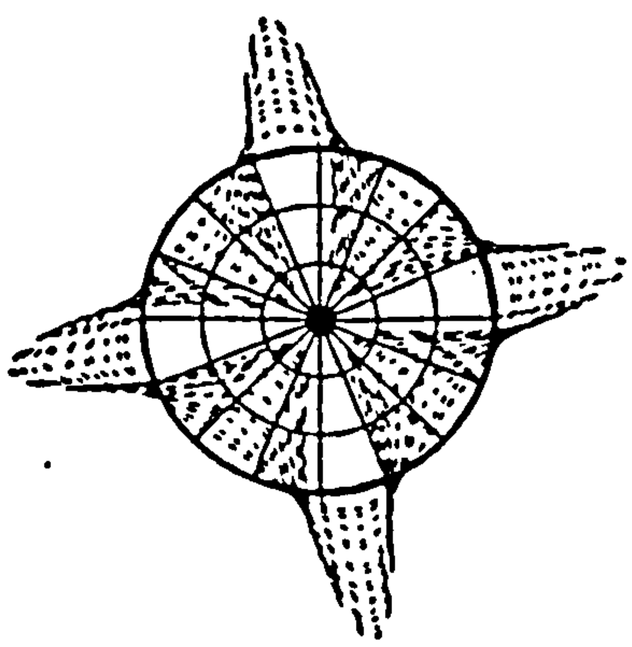

Fig.6(b) m=1, n=4 353.7 Hz

Figs.4-6 Distortion modes and natural frequencies of the thin cylindrical shell in vacuo using semi-loof curved shell elements.

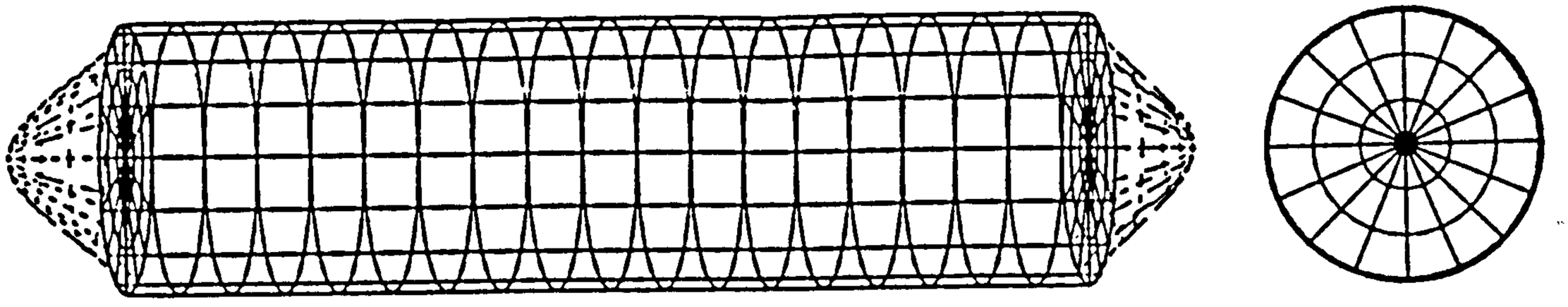

Fig.4 209.2 Hz

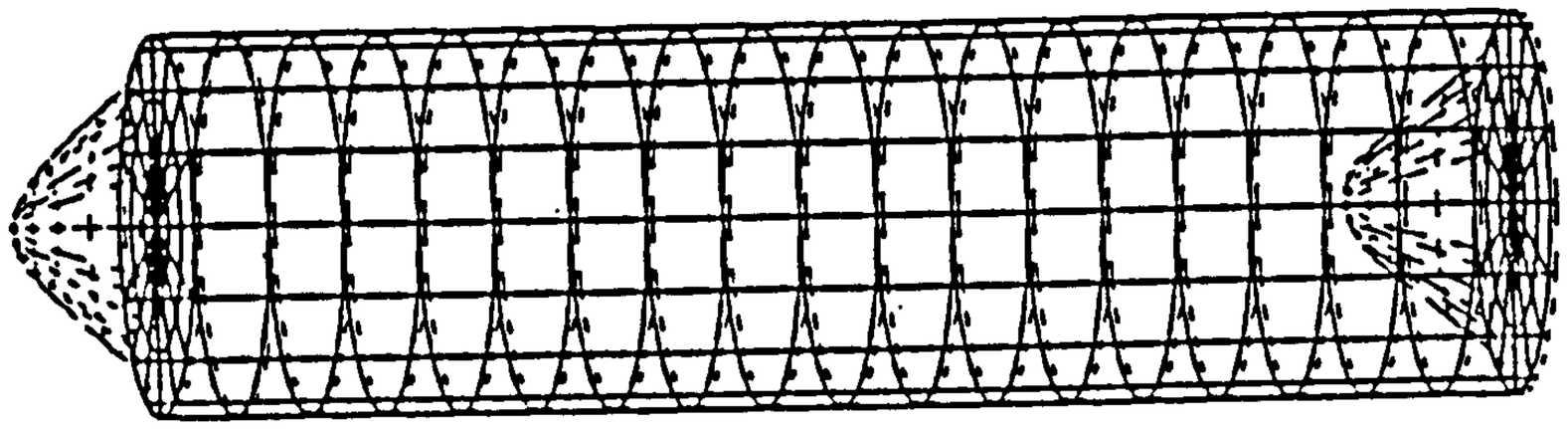

Fig.5 218.0 Hz

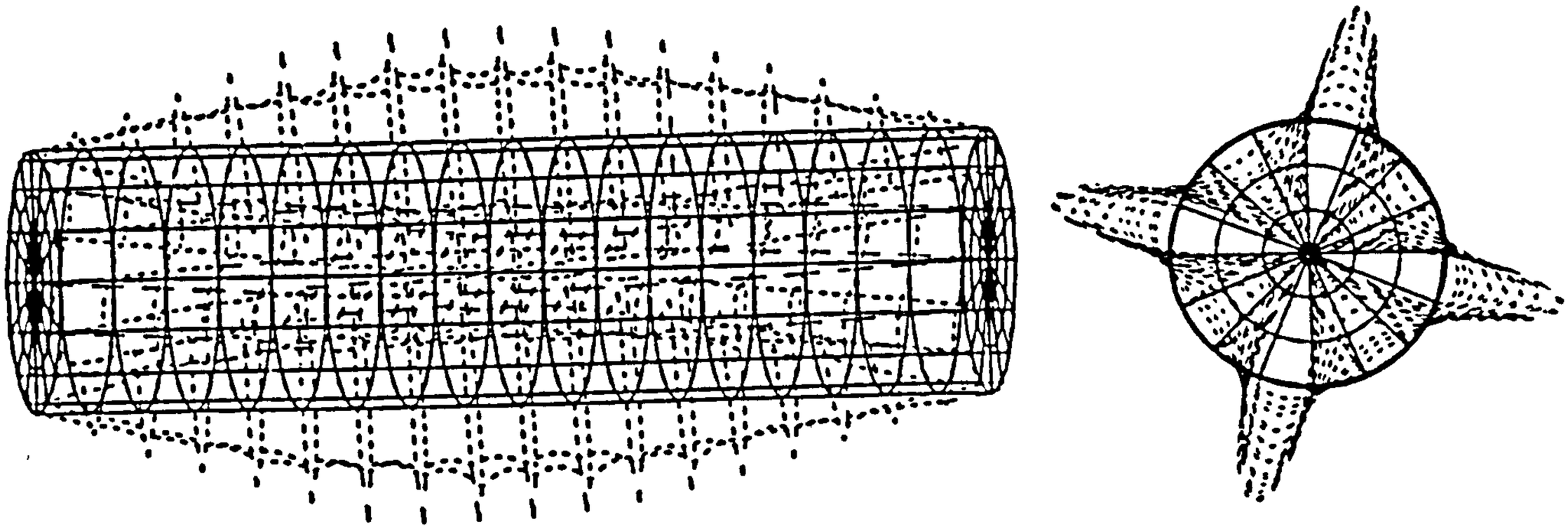

Fig.6(a) m=1, n=4 352.5 Hz

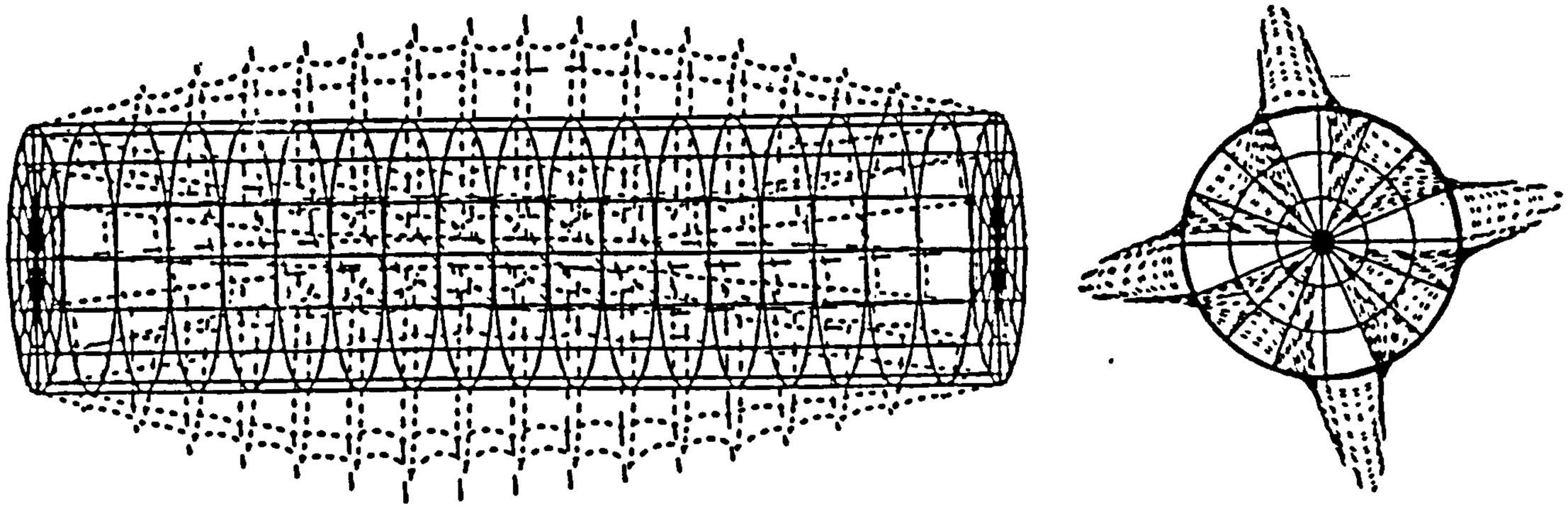

Fig.6(b) m=1, n=4 353.7 Hz

Figs.4-6 Distortion modes and natural frequencies of the thin cylindrical shell in vacuo using semi-loof curved shell elements.

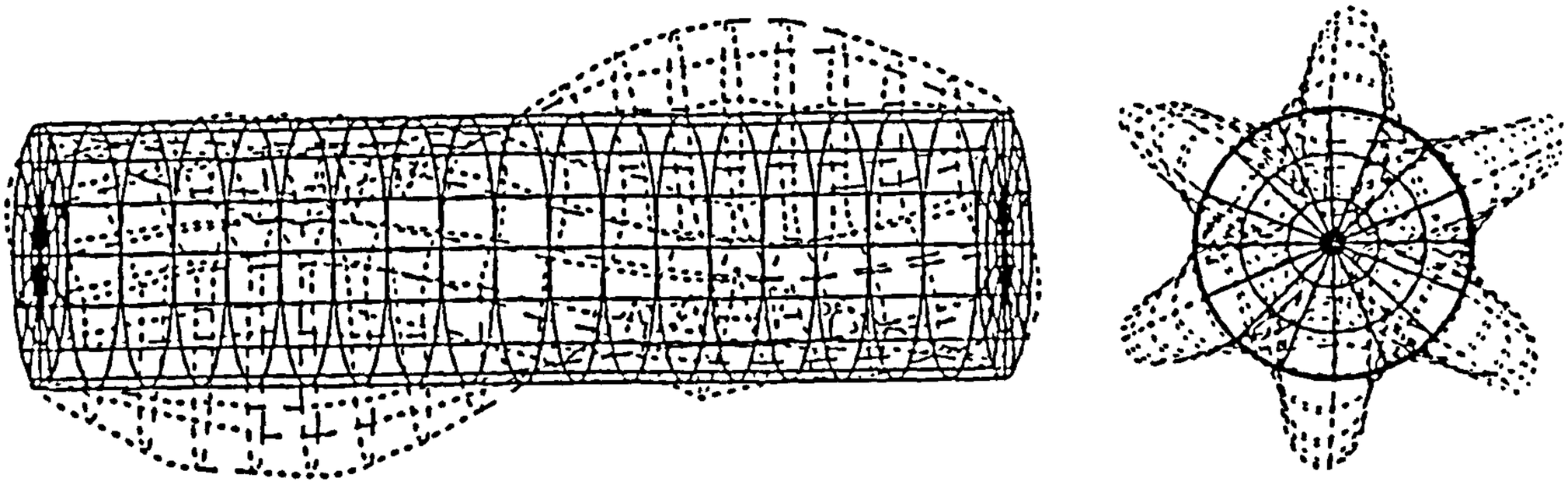

Fig.7(a) m=2, n=3 413.3 Hz

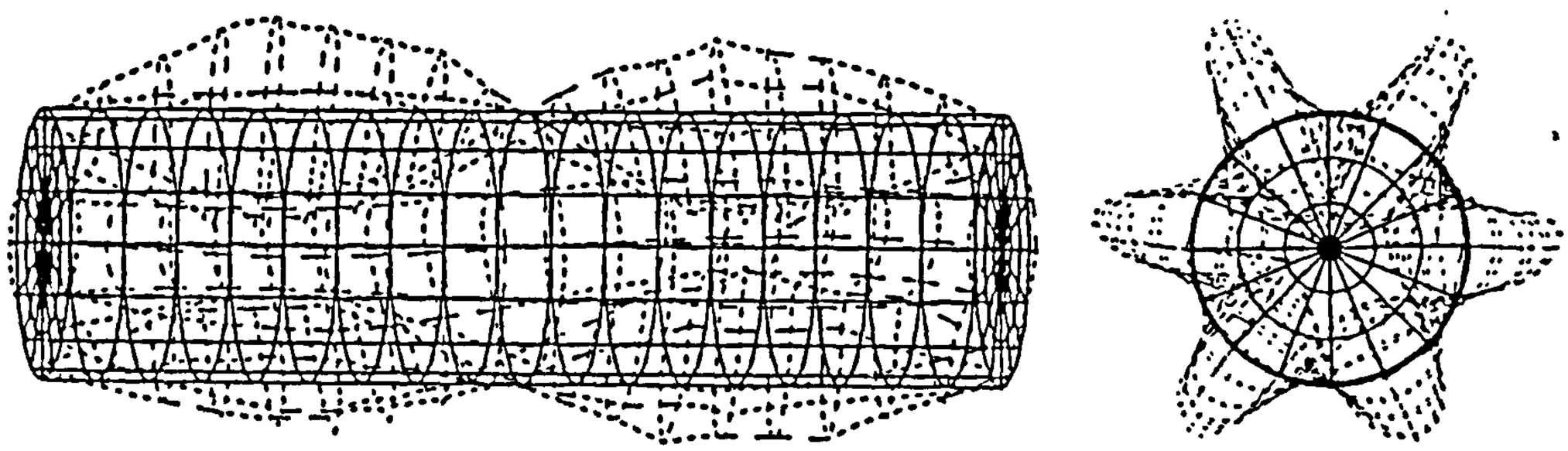

Fig.7(b) m=2, n=3 415.9 Hz

Figs.7 Distortion modes and natural frequencies of the thin cylindrical shell in vacuo using semi-loof curved shell elements.

Fig.7(a) m=2, n=3 413.3 Hz

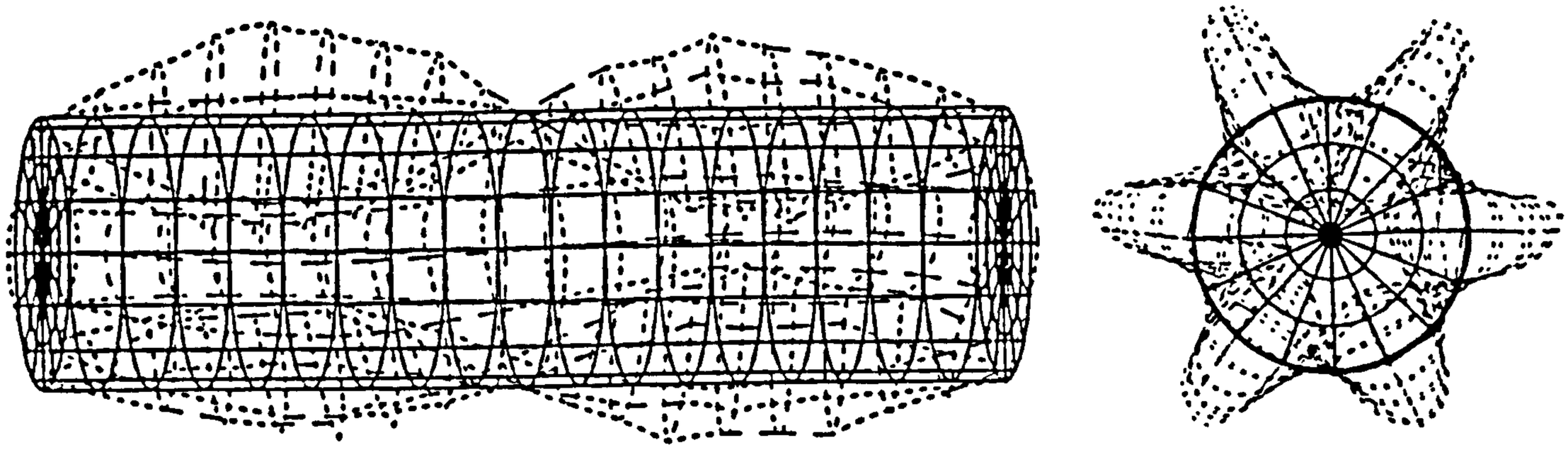

Fig.7(b) m=2, n=3 415.9 Hz

Figs.7 Distortion modes and natural frequencies of the thin cylindrical shell in vacuo using semi-loof curved shell elements.

Appendix E

Journal of Sound and Vibration (1989) **128**(1), 39–56

RESPONSES OF A FLEXIBLE NON-UNIFORM CIRCULAR BEAM IN A BOUNDED, VISCOUS FLUID

R. HOSODA

Department of Naval Architecture, University of Osaka Prefecture, Sakai, Osaka, Japan

W. G. PRICE

Department of Mechanical Engineering, Brunel University, Uxbridge UB8 3PH, UK

AND

R. RANDALL

Royal Naval Engineering College, Manadon, Plymouth, UK

(*Received* 13 *January* 1988, *and in revised form* 21 *June* 1988)

A hydroelasticity theory [1] and a hydroelastic analysis are presented to describe the dynamic characteristics of a circular non-uniform beam in a bounded, viscous fluid. *In vacuo*, the principal mode and natural frequency characteristics are uniquely defined but when the combined influences of fluid-structure-external boundary interactions are accounted for in the mathematical model, significant variations in the principal co-ordinates, resonance frequencies, responses, etc., occur. That is, resonance frequencies, etc., are not uniquely defined and reasons for this are found in the changes in the magnitudes of the generalized fluid actions. These are shown to be functions of the principal mode shapes, frequency of oscillation, the annular clearance between the cylinder and the rigid tube boundary and the viscosity of the fluid. The latter is mathematically modelled as an incompressible Stokes' fluid [2, 3] and the principal modes of the dry free-free non-uniform cylinder are determined by using a Prohl-Myklestad approach [1, 4].

1. INTRODUCTION

The hydroelasticity theory [1] developed to describe the responses of beam-like structures (e.g., ships) and the general linear three-dimensional hydroelasticity theory [5–7] of floating, arbitrary shaped structures (e.g., marine vehicles or structures) allow fluid-structure interactions to be assessed and analyzed. In these mathematical models the fluid is assumed inviscid and free surface effects are included in the description of the generalized external loadings.

In this paper the original hydroelasticity theory [1] is extended to include the influence of external boundaries and the fluid is assumed viscous. The latter is mathematically modelled as an incompressible Stokes' fluid [2, 3] and the structure, i.e., a cylinder, is assumed deeply submerged so that free surface wave effects are excluded from the analysis.

It is shown that both boundary and viscous effects alter the magnitudes of the generalized added mass or inertia coefficients and the generalized damping coefficients. These, in turn, significantly influence the resonance frequency values, produce couplings between the principal co-ordinates and introduce variations into the magnitudes of the responses. Whereas the principal modes and natural frequencies are uniquely defined in the dry analysis, the forced dynamic characteristics and responses are functions of the externally applied influences or loadings, and are therefore not uniquely defined quantities but

0022-460X/89/010039+18 $03.00/0

Journal of Sound and Vibration (1989) **128**(1), 39–56

RESPONSES OF A FLEXIBLE NON-UNIFORM CIRCULAR BEAM IN A BOUNDED, VISCOUS FLUID

R. HOSODA

Department of Naval Architecture, University of Osaka Prefecture, Sakai, Osaka, Japan

W. G. PRICE

Department of Mechanical Engineering, Brunel University, Uxbridge UB8 3PH, UK

AND

R. RANDALL

Royal Naval Engineering College, Manadon, Plymouth, UK

(*Received* 13 *January* 1988, *and in revised form* 21 *June* 1988)

A hydroelasticity theory [1] and a hydroelastic analysis are presented to describe the dynamic characteristics of a circular non-uniform beam in a bounded, viscous fluid. *In vacuo*, the principal mode and natural frequency characteristics are uniquely defined but when the combined influences of fluid-structure-external boundary interactions are accounted for in the mathematical model, significant variations in the principal co-ordinates, resonance frequencies, responses, etc., occur. That is, resonance frequencies, etc., are not uniquely defined and reasons for this are found in the changes in the magnitudes of the generalized fluid actions. These are shown to be functions of the principal mode shapes, frequency of oscillation, the annular clearance between the cylinder and the rigid tube boundary and the viscosity of the fluid. The latter is mathematically modelled as an incompressible Stokes' fluid [2, 3] and the principal modes of the dry free-free non-uniform cylinder are determined by using a Prohl–Myklestad approach [1, 4].

1. INTRODUCTION

The hydroelasticity theory [1] developed to describe the responses of beam-like structures (e.g., ships) and the general linear three-dimensional hydroelasticity theory [5–7] of floating, arbitrary shaped structures (e.g., marine vehicles or structures) allow fluid–structure interactions to be assessed and analyzed. In these mathematical models the fluid is assumed inviscid and free surface effects are included in the description of the generalized external loadings.

In this paper the original hydroelasticity theory [1] is extended to include the influence of external boundaries and the fluid is assumed viscous. The latter is mathematically modelled as an incompressible Stokes' fluid [2, 3] and the structure, i.e., a cylinder, is assumed deeply submerged so that free surface wave effects are excluded from the analysis.

It is shown that both boundary and viscous effects alter the magnitudes of the generalized added mass or inertia coefficients and the generalized damping coefficients. These, in turn, significantly influence the resonance frequency values, produce couplings between the principal co-ordinates and introduce variations into the magnitudes of the responses. Whereas the principal modes and natural frequencies are uniquely defined in the dry analysis, the forced dynamic characteristics and responses are functions of the externally applied influences or loadings, and are therefore not uniquely defined quantities but

0022-460X/89/010039+18 $03.00/0

change with circumstances. These findings are clearly demonstrated through an investigation of the dynamic behaviour of a flexible circular cylinder enclosed within a circular rigid tube filled with a viscous fluid (i.e., water).

2. MATHEMATICAL MODEL

The hydroelasticity theory developed to describe the responses (displacements, distortions, bending moments, shear forces, etc.) of two-dimensional beam-like structures and three-dimensional structures of arbitrary shape excited by a sinusoidal or irregular seaway relies on a "dry" structural analysis and a "wet" fluid analysis. In the former, where the structure is *in vacuo* in the absence of external fluid loadings and structural damping, natural frequencies and principal mode shapes are determined and these uniquely describe the dynamic characteristics of the structure. When the structure floats or is fixed in water, the fluid actions applied to the flexible structure are evaluated through a wet analysis, accounting for forward speed, free surface effects, distortions of the structure, fluid-structure interactions, etc. A combination of the dry and wet analyses permits the principal co-ordinates, resonance frequencies and responses at any point within the structure to be determined for prescribed external wave actions or any other source of excitation.

In Figure 1, the flexible non-uniform cylinder, denoted by AB, is completely surrounded by a viscous fluid and may be totally confined (a) within the rigid tube, (b) emerged partially or (c) completely emerged. At time $t=0$, the centres of the cylinder and tube coincide and a right-handed orthogonal equilibrium frame of axes $Oxyz$ is defined, with origin O at the centre of the cylinder and the Ox axis lying along the longitudinal axis. A symmetric cross-section of the tube and cylinder is shown in Figure 1(d) and their respective radii are denoted by d and $a(<d)$. In this problem external actions result from a combination of the interactions between the flexible cylinder, viscous fluid and the

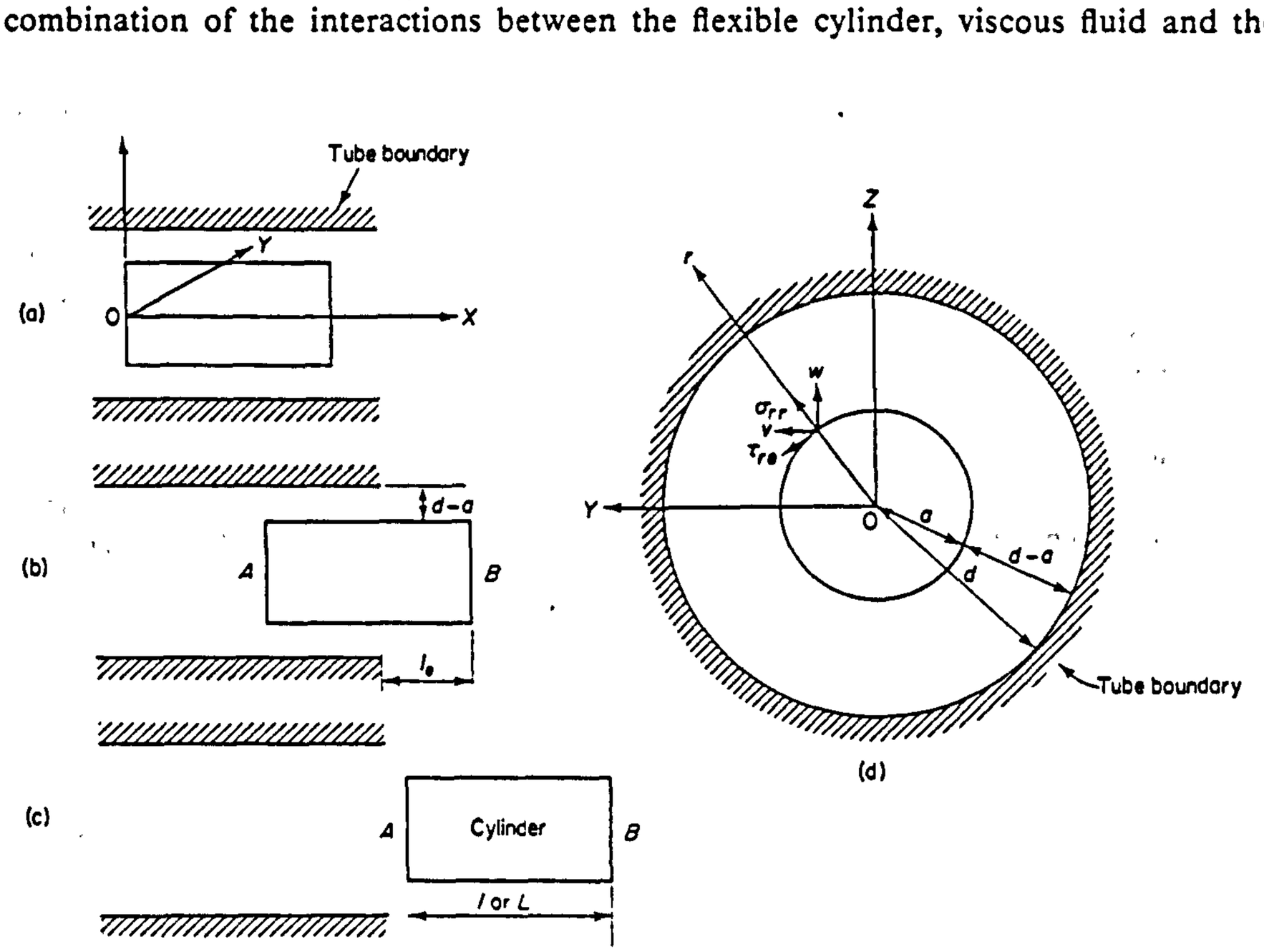

Figure 1. Schematic and co-ordinate system for cylinder vibrating in a fluid annulus.

presence or otherwise of the external tube boundary. Furthermore, it is assumed that the flexible non-uniform cylinder (or beam or projectile) is neutrally buoyant in the fluid.

2.1. DRY ANALYSIS

Since the non-uniform flexible cylinder is beam-like in form, beam theory may be used to determine the dynamic characteristics of the free-free dry structure [4]. To reduce mathematical complications, the cylinder is modelled as a simple Euler beam, but other more sophisticated theoretical models (e.g., Timoshenko [1, 4], Vlasov [8]) may be adopted.

It can be shown that if n denotes the number of principal co-ordinates required to describe the responses of the cylinder to a given external force, then the $(n \times 1)$ principal co-ordinate matrix $\mathbf{p}(t)$ is defined by the equation [1, 5-7]

$$\mathbf{a}\ddot{\mathbf{p}}(t)+\mathbf{b}\dot{\mathbf{p}}(t)+\mathbf{c}\mathbf{p}(t)=\mathbf{Z}(t). \tag{1}$$

Here, the $(n \times n)$ matrices $\mathbf{a}$, $\mathbf{b}$, $\mathbf{c}$ represent the generalized mass, damping and stiffness of the cylinder, respectively, with elements $c_{rr}=\omega_r^2 a_{rr}$ $(0 \leqslant r \leqslant n-1)$ and ω_r denotes the rth natural frequency associated with the rth principal mode $w_r(x)$ of the displacement $w(x, t)$ in the Oz direction. For the heave $(r=0)$ and pitch $(r=1)$ bodily modes of the free-free cylinder $\omega_r=0$, with non-zero natural frequencies associated with the higher modes $w_r(x)$, $r=2, 3, 4, \ldots$.

In theory the damping matrix $\mathbf{b}$ is not necessarily diagonal, but with no reliable information, it is assumed diagonal with elements defined as [4]

$$b_{rr}=2\nu_r\omega_r a_{rr}, \tag{2}$$

where ν_r is the rth modal damping factor associated with the non-uniform cylinder.

Apart from the principal co-ordinate matrix $\mathbf{p}(t)$ with elements $p_r(t)$, the remaining unknown in equation (1) is the generalized external force matrix $\mathbf{Z}(t)$ describing the interaction between cylinder, viscous fluid and tube wall.

2.2. WET ANALYSIS

In keeping with the dry analysis, the three-dimensional cylinder is assumed to be represented by a series of stripwise two-dimensional sections, as shown in Figure 1(d). The gap between the concentric cylinders is $(d-a)$, $0<d-a \leqslant \infty$, and the cylinder is of length $l(\gg a)$. The fluid surrounding the cylinder is assumed viscous and is mathematically described as an incompressible Stokes' fluid [2, 3]. At any section x $(0 \leqslant x \leqslant l)$ a two-dimensional fluid flow exists, defined by velocity components (v, w) along the axis directions Oy and Oz, respectively.

The Navier-Stokes equations of motion describing this two-dimensional fluid flow model are [2, 3]

$$\frac{\partial v}{\partial t}+v\frac{\partial v}{\partial y}+w\frac{\partial v}{\partial z}=\frac{1}{\rho}Y-\frac{1}{\rho}\frac{\partial p}{\partial y}+\nu\left(\frac{\partial^2 v}{\partial y^2}+\frac{\partial^2 v}{\partial w^2}\right),$$

$$\frac{\partial w}{\partial t}+v\frac{\partial w}{\partial y}+w\frac{\partial w}{\partial z}=\frac{1}{\rho}Z-\frac{1}{\rho}\frac{\partial p}{\partial z}+\nu\left(\frac{\partial^2 w}{\partial y^2}+\frac{\partial^2 w}{\partial z^2}\right) \tag{3}$$

and the equation of continuity is

$$\partial v/\partial y+\partial w/\partial z=0, \tag{4}$$

where Y, Z denote external potential forces, p represents pressure and ν is the coefficient of viscosity.

There exists a stream function $\psi(y, z, t)$ such that

$$v=-\partial\psi/\partial z, \qquad w=\partial\psi/\partial y, \tag{5}$$

and a vorticity

$$\zeta = \partial w/\partial y - \partial v/\partial z = (\partial^2/\partial y^2 + \partial^2/\partial z^2)\psi = \nabla^2\psi. \tag{6}$$

Substituting these last two relationships into equation (3) and eliminating the pressure components gives the equation describing the stream function as

$$\frac{\partial}{\partial t}\nabla^2\psi + \frac{\partial\psi}{\partial y}\frac{\partial}{\partial z}\nabla^2\psi - \frac{\partial\psi}{\partial z}\frac{\partial}{\partial y}\nabla^2\psi = \nu\nabla^4\psi. \tag{7}$$

For small amplitudes of motion, the product terms in ψ are assumed to be an order smaller than terms of order ψ and the linearized equation of motion is given in the form [2]

$$(\partial/\partial t)\nabla^2\psi - \nu\nabla^4\psi = 0. \tag{8}$$

For a sinusoidal disturbance of frequency ω a solution to this equation is sought in the form $\psi(y, z, t) = \psi(y, z)\,e^{i\omega t}$, and in terms of cylindrical co-ordinates (r, θ) it can be shown that this solution is given by (9, 10)

$$\psi(r, \theta, t) = U[A(a^2/r) + Br + Ca\,I_1(kr) + Da\,K_1(kr)]\sin\theta\,e^{i\omega t} = Uf(r)\sin\theta\,e^{i\omega t}. \tag{9}$$

In this expression $k = \sqrt{(i\omega/\nu)}$, U is the amplitude of the velocity of the oscillating beam section and I_1, K_1 are modified Bessel functions of the first and second kinds, respectively. The constants A, B, C, D are determined from the imposed boundary conditions at $r = a$ and $r = d$. That is, at $r = a$ the fluid velocity is in the direction of oscillation, while at $r = d$ the velocity of the fluid is zero.

By back substitution of these results into equation (3), the pressure on the surface of the cylinder at (a, θ) can be shown to be of the form

$$p(a, \theta)\,e^{i\omega t} = \rho g U k^2 (A - B)(1 - \cos\theta)\,e^{i\omega t} \tag{10}$$

and the corresponding normal stress σ_{rr} and shear stress $\tau_{r\theta}$ are defined as

$$\sigma_{rr} = -p + 2\rho\nu(\partial w/\partial r), \qquad \tau_{r\theta} = \rho\nu(\partial v/\partial r + \partial^2 w/\partial r\,\partial\theta - v/r). \tag{11}$$

These results allow the force component F_z acting at section x in the direction Oz to be expressed as

$$F_z(x, t) = \int_0^{2\pi} (\sigma_{rr}\cos\theta - \tau_{r\theta}\sin\theta)a\,d\theta, \tag{12}$$

which after much algebraic manipulation reduces to the expression

$$F_z(x, t) = -i\omega m U\{-A + B + C\,I_1(ka) + D\,K_1(ka)\}\,e^{i\omega t},$$

where the mass per unit length of the cylinder $m = \pi\rho a^2$ and the remaining constants associated with the section at x are given by

$$\begin{aligned}
A = [&-\alpha^2\{I_0(\alpha)K_0(\beta) - I_0(\beta)K_0(\alpha)\} + 2\alpha\{I_1(\alpha)K_0(\beta) + I_0(\beta)K_1(\alpha)\} \\
&-2\alpha\gamma\{I_0(\alpha)K_1(\beta) + I_1(\beta)K_0(\alpha)\} + 4\gamma\{I_1(\alpha)K_1(\beta) - I_1(\beta)K_1(\alpha)\}]/\Delta, \\
B = [&2\alpha\gamma\{I_1(\beta)K_0(\beta) + I_0(\beta)K_1(\beta)\} + \alpha^2\gamma^2\{I_0(\alpha)K_0(\beta) - I_0(\beta)K_0(\alpha)\} \\
&-2\alpha\gamma^2\{I_1(\alpha)K_0(\beta) + I_0(\beta)K_1(\alpha)\}]/\Delta, \\
C = [&-2\alpha K_0(\beta) - 4\gamma K_1(\beta) + \gamma^2\{2\alpha K_0(\alpha) + 4K_1(\alpha)\}]/\Delta, \\
D = [&-2\alpha I_0(\beta) + 4\gamma I_1(\beta) + 2\gamma^2\{\alpha I_0(\alpha) - 2\gamma I_1(\alpha)\}]/\Delta, \\
\Delta = &\alpha^2(1 - \gamma^2)\{I_0(\alpha)K_0(\beta) - I_0(\beta)K_0(\alpha)\} \\
&+2\alpha\gamma\{I_0(\alpha)K_1(\beta) - I_1(\beta)K_0(\beta) + I_1(\beta)K_0(\alpha) - I_0(\beta)K_1(\beta)\}
\end{aligned}$$

$$+2\alpha\gamma^2\{I_0(\beta)K_1(\alpha)-I_0(\alpha)K_1(\alpha)+I_1(\alpha)K_0(\beta)-I_1(\alpha)K_0(\alpha)\},$$

$$\alpha = ka, \qquad \beta = kd, \qquad \gamma = a/d, \qquad k^2 = i\omega/\nu.$$

(Note that for a cylinder and/or tube of varying cross-sectional circular shape the radii d and a are functions of x.)

Now the vertical displacement $w(x, t)$ in the direction Oz is given by [1, 4]

$$w(x, t) = \sum_{s=0}^{n-1} w_s(x)p_s(t) = \sum_{s=0}^{n-1} w_s(x)p_s\, e^{i\omega t}, \tag{14}$$

and the velocity by

$$\dot{w}(x, t) = \sum_{s=0}^{n-1} i\omega w_s(x)p_s\, e^{i\omega t} = U\, e^{i\omega t},$$

where the velocity amplitude is defined as

$$U = \sum_{s=0}^{n-1} i\omega w_s(x)p_s.$$

After substituting this result into equation (13), it follows that the vertical force per unit length at section x is given by

$$F_z(x, t) = \sum_{s=0}^{n-1} \omega^2 m w_s(x)\{-A+B+CI_1(ka)+DK_1(ka)\}p_s\, e^{i\omega t}$$

$$= -\sum_{s=0}^{n-1} w_s(x)\{H^R(x, \omega, \nu)\ddot{p}_s(t)+H^I(x, \omega, \nu)\dot{p}_s(t)\},$$

where H^R and H^I denote the real and imaginary components respectively, defined by the expression

$$\omega^2 H^R - i\omega H^I = \omega^2 m\{-A+B+CI_1(\mathrm{ka})+DK_1(ka)\} = \omega^2 mH, \tag{15}$$

and these are functions of the frequency of oscillation ω, coefficient of viscosity ν, radii d and a, etc.

In the conventional manner [1], the rth generalized vertical fluid force acting over the cylinder length $0 \leqslant x \leqslant l$ is given by

$$F_r(t) = \int_0^l w_r(x)F_z(x, t)\,dx = -\sum_{s=0}^{n-1} \int_0^l w_r(x)w_s(x)\{H^R\ddot{p}_s(t)+H^I\dot{p}_s(t)\}\,dx$$

$$= -\sum_{s=0}^{n-1} \{A_{rs}\ddot{p}_s(t)+B_{rs}\dot{p}_s(t)\}, \tag{16}$$

where the generalized hydrodynamic coefficient (i.e., generalized added mass) in phase with the acceleration is given by

$$A_{rs} = \int_0^l w_r(x)w_s(x)H^R(x, \omega, \nu)\,dx, \tag{17}$$

and the generalized damping in phase with the velocity is

$$B_{rs} = \int_0^l w_r(x)w_s(x)H^I(x, \omega, \nu)\,dx, \tag{18}$$

for each $r = 0, 1, \ldots, n-1$.

If further it is assumed that, in addition to this rth generalized fluid force $F_r(t)$, there exists an arbitrary rth generalized external force $\Xi_r(t)$, then the rth element or rth

generalized external force $Z_r(t)$, containing all sources of external excitation, is defined as $Z_r(t) = F_r(t) + \Xi_r(t)$. Substituting this result into equation (1) together with equations (15)-(18) it follows that the equation governing motion at p_r, the rth generalized co-ordinate, is given by

$$a_{rr}[\ddot{p}_r(t) + \omega_r^2 p_r(t)] + \sum_{s=0}^{n-1} [A_{rs}\ddot{p}_s(t) + (b_{rs} + B_{rs})\dot{p}_s(t)] = \Xi_r \, e^{i\omega t}, \tag{19}$$

for $r = 0, 1, 2, \ldots, n-1$.

In particular, for an oscillatory external point loading $P(x, t)$ of unit magnitude acting at position x', i.e., $P(x, t) = 1\delta(x - x') \, e^{i\omega t}$ where $\delta(\,)$ denotes the Dirac delta function, the rth generalized external force is given by

$$\Xi_r(t) = \int_0^l P(x, t) w_r(x) \, dx = \int_0^l 1 \, \delta(x - x') \, e^{i\omega t} w_r(x) \, dx = w_r(x') \, e^{i\omega t},$$

for $r = 0, 1, \ldots, n-1$. Upon substituting this result into equation (19), where $\Xi_r = w_r(x')$, the generalized co-ordinate matrix $\mathbf{p}(t)$ is found to be a solution to the matrix equation

$$(\mathbf{a} + \mathbf{A})\ddot{\mathbf{p}}(t) + (\mathbf{b} + \mathbf{B})\dot{\mathbf{p}}(t) + \mathbf{c}\mathbf{p}(t) = \boldsymbol{\Xi} \, e^{i\omega t}, \tag{20}$$

where the matrices $\mathbf{c}$ and $\boldsymbol{\Xi}$ have elements $\omega_r^2 a_{rr}$ and $w_r(x')$, respectively.

For a steady state solution $\mathbf{p}(t) = \mathbf{p} \, e^{i\omega t}$, the amplitude matrix $\mathbf{p}$ satisfies the equation $[-\omega^2(\mathbf{a} + \mathbf{A}) + i\omega(\mathbf{b} + \mathbf{B}) + \mathbf{c}]\mathbf{p} = \mathbf{D}\mathbf{p} = \boldsymbol{\Xi}$, or

$$\mathbf{I}\mathbf{p} = \mathbf{D}^{-1}\boldsymbol{\Xi} = \frac{\text{adj } \mathbf{D}}{\det \mathbf{D}} \boldsymbol{\Xi} = \mathbf{Q}(\omega)\boldsymbol{\Xi}, \tag{21}$$

where adj denotes the adjoint matrix and the determinant is $\det \mathbf{D} = |-\omega^2(\mathbf{a} + \mathbf{A}) + i\omega(\mathbf{b} + \mathbf{B}) + \mathbf{c}|$. A combination of this solution for the generalized principal co-ordinates and the principal modes allows the responses in the flexible cylinder to be determined (e.g., see equation (14)).

3. CALCULATIONS

3.1. DRY DYNAMIC CHARACTERISTICS

For the simple cylindrical beams under investigation a Prohl-Myklestad approach [1, 4] was found adequate to determine the mode shapes and natural frequencies of the free-free cylinders *in vacuo*. In all calculations, the continuous structure was idealized into 50 segments.

3.2. WET ANALYSIS OF UNIFORM BEAM

In general the quantities H^R and H^I in equation (15) vary with frequency of oscillation, coefficient of viscosity, and the radii d and a, and their variations are reflected in the generalized hydrodynamic coefficients A_{rs}, B_{rs} given in equations (17) and (18), respectively. However, for a uniform cylindrical beam of sufficient length so that end effects are negligible, H^R and H^I are constant for all x and, because of the orthogonality relationships [4] existing between the dry principal modes, the generalized hydrodynamic cofficients matrices $\mathbf{A}$ and $\mathbf{B}$ are diagonal in form with zero off-diagonal terms.

From equation (15) the added mass coefficient C_m and damping coefficient C_v may be defined as

$$C_m = \text{Real}\{-A + B + C\mathrm{I}_1(ka) + D\mathrm{K}_1(ka)\} = \text{Real}\{H\} = H^R/m,$$

$$C_v = -m\omega \, \text{Imag}\{-A + B + C\mathrm{I}_1(ka) + D\mathrm{K}_1(ka)\} = -m\omega \, \text{Imag}\{H\} = H^I.$$

In this form their variations with the non-dimensional parameter $RS = \omega a^2/\nu$ and the gap clearance can be assessed. Here R $(=\bar{U}a/\nu)$ and S $(=\omega a/\bar{U})$ denote the Reynolds number and Strouhal number, respectively, both based on a representative velocity $\bar{U}$.

3.2.1. *Inviscid model* ($\nu = 0$)

For the inviscid case it may be shown that $H = (1+\gamma^2)/(1-\gamma^2)$, $\gamma = a/d$, is a real number which tends to infinity as the annular gap vanishes. The added mass coefficient C_m is independent of frequency and Figure 2 illustrates its variation with annular gap clearance. As can be seen, for small gap clearances the inphase fluid loadings increase rapidly. In this model no hydrodynamic damping exists: i.e., $C_v = 0$.

3.2.2. *Viscid model* ($\nu \neq 0$)

When the outer boundary is moved to infinity, i.e., $d \to \infty$ so that $\beta = kd \to \infty$ and $\gamma = a/d \to 0$, it can be shown that,

$$H = 1 + 4K_1(\alpha)/\alpha K_0(\alpha), \qquad \alpha = ka, \qquad k^2 = i\omega/\nu,$$

which is a complex function.

Figure 3 shows that, for increasing values of RS, the real part of H tends to unity, which from Figure 2 is the limiting value when $\nu = 0$. Figure 4 shows the increasing magnitude of the damping coefficient with frequency, provided ν and a are kept constant.

In the general case $d \neq \infty$, Figure 5 illustrates a selection of curves displaying the combined influence of viscosity and annular clearance on the added mass coefficient C_m and damping coefficient C_v.

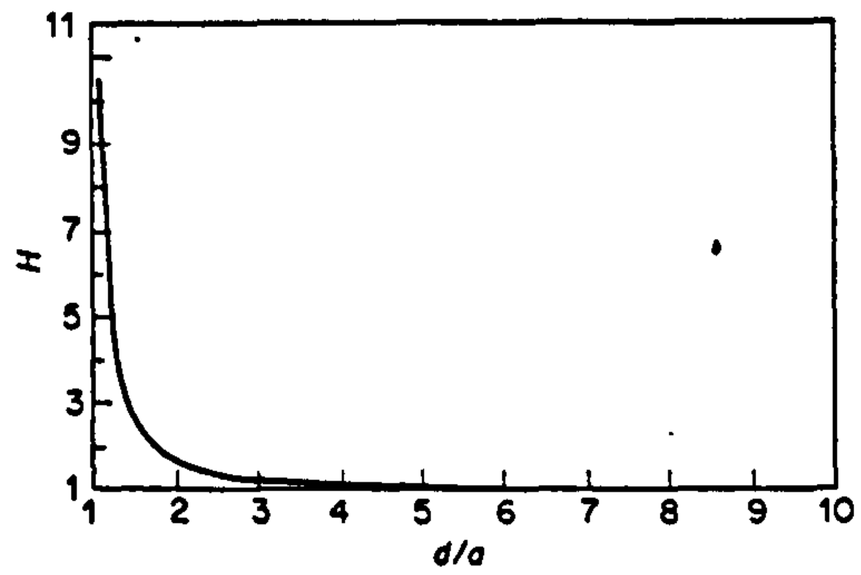

Figure 2. Changes in added mass coefficient, C_m, due to variation in annular clearance; inviscid fluid.

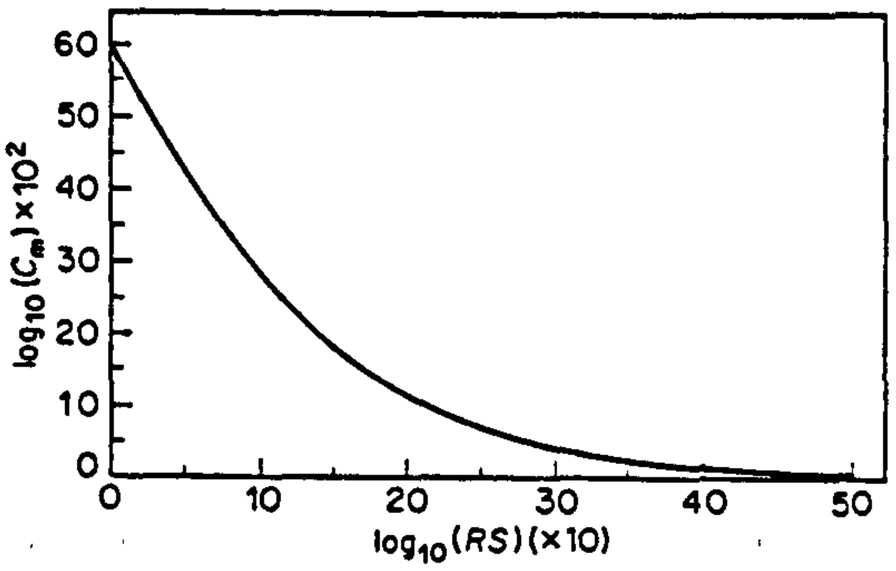

Figure 3. Variation of added mass coefficient, C_m, for viscous fluid ($d/a \to$ infinity); Reynolds number $R = \bar{U}a/\nu$; Strouhal number $S = \omega a/\bar{U}$.

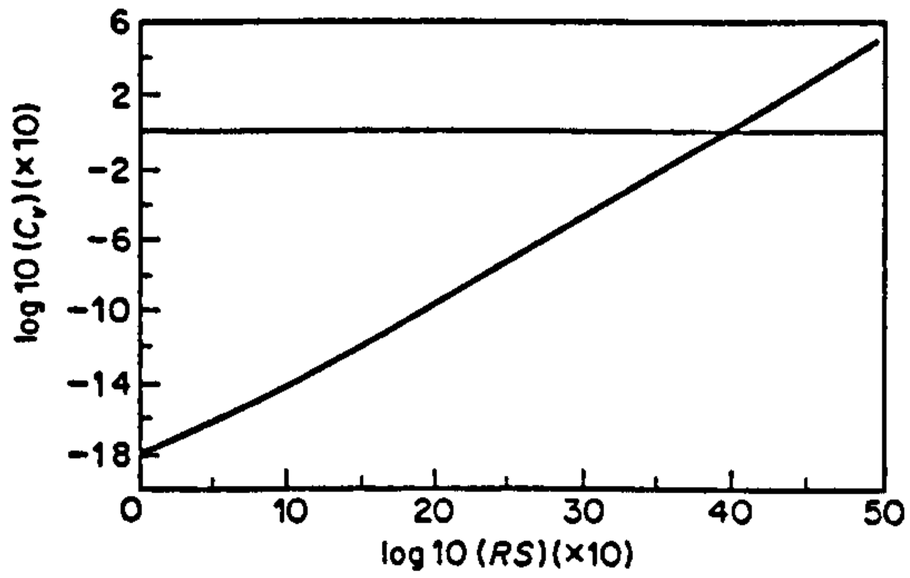

Figure 4. Variation of damping coefficient, C_v, for viscous fluid ($d/a \rightarrow$ infinity); R, S as Figure 3.

3.2.3. *Principal co-ordinates of uniform beam*

Figure 6 shows a selection of results for the principal co-ordinates $|p_r|$ for varying values of the aspect ratios l/a, d/a and coefficient of viscosity ($\nu = 0$, inviscid fluid; $\nu = 1{\cdot}14 \times 10^{-6}$ m^2/s, water). The uniform cylindrical beam is assumed lightly damped with a constant structural modal damping factor $\nu_r = 1 \times 10^{-4}$ for $r = 2, 3, 4$ and is excited by a point loading at $x' = 0{\cdot}65l$ measured from the stern. Where appropriate in the investigation the following fixed values are assumed for the beam radius $a = 0{\cdot}1$ m, tube radius $d = 2$ m and cylinder length $l = 1{\cdot}0$ m. Furthermore, the true fluid flows around the ends of the cylinder are not modelled and it is assumed that no fluid separation occurs.

From the evidence presented, the principal co-ordinates are uncoupled (as theory predicts) and the influence of viscosity and shift in resonance frequency values associated with principal co-ordinate $|p_2|$ becomes increasingly noticeable as the aspect ratio l/a increases (a, d fixed). This type of behaviour could produce an important effect in the description of the vibration characteristics of long flexible tubes or pipes. Similarly, the effect of annular clearance on the resonance frequency value of $|p_2|$ is also clearly demonstrated for fixed values of l, a and viscosity $\nu = 1{\cdot}14 \times 10^{-6}$ m^2/s.

3.3. PRINCIPAL CO-ORDINATES OF SIMPLE NON-UNIFORM BEAMS

Coupling between the principal co-ordinates arises when the beam is composed of non-homogeneous segments and/or the geometry of the beam varies relative to the outer boundary. To demonstrate the former the same data were adopted as in the previous calculation of $|p_4|$ in Figure 6, but now a 50% increase in the density of half (i.e. $0 \leqslant x \leqslant 0{\cdot}5l$) of the beam is assumed. Figure 7(a) illustrates the recalculated principal co-ordinate $|p_4|$ and this clearly displays the coupling associated with the co-ordinates $|p_2|$ and $|p_3|$.

To illustrate the effect of geometric variation a uniformly tapered beam ($a = 0{\cdot}1$ m, $x = 0$; $a = 0{\cdot}2$ m, $x = l$) of constant density was considered and the annular clearance varied from $0{\cdot}21$ m $\leqslant d \leqslant 2{\cdot}0$ m. The beam is surrounded by water ($\nu = 1{\cdot}14 \times 10^{-6}$ m^2/s) and Figure 7(b) summarizes the role of coupling in the principal co-ordinate $|p_4|$ for different values of the annular clearance. The coupling between the co-ordinates increases as the annular clearance decreases, and this is due to the increasing influence of the off-diagonal contributions arising in the generalized hydrodynamic coefficients A_{rs} and B_{rs} ($r, s = 0, 1, 2, 3, 4$).

3.4. INFLUENCE OF THE OUTER BOUNDARY

In the previous section it was demonstrated that significant changes in the principal co-ordinates are caused by comparatively minor changes in the proximity of the outer boundary. However, in each example the outer boundary was equidistant from the

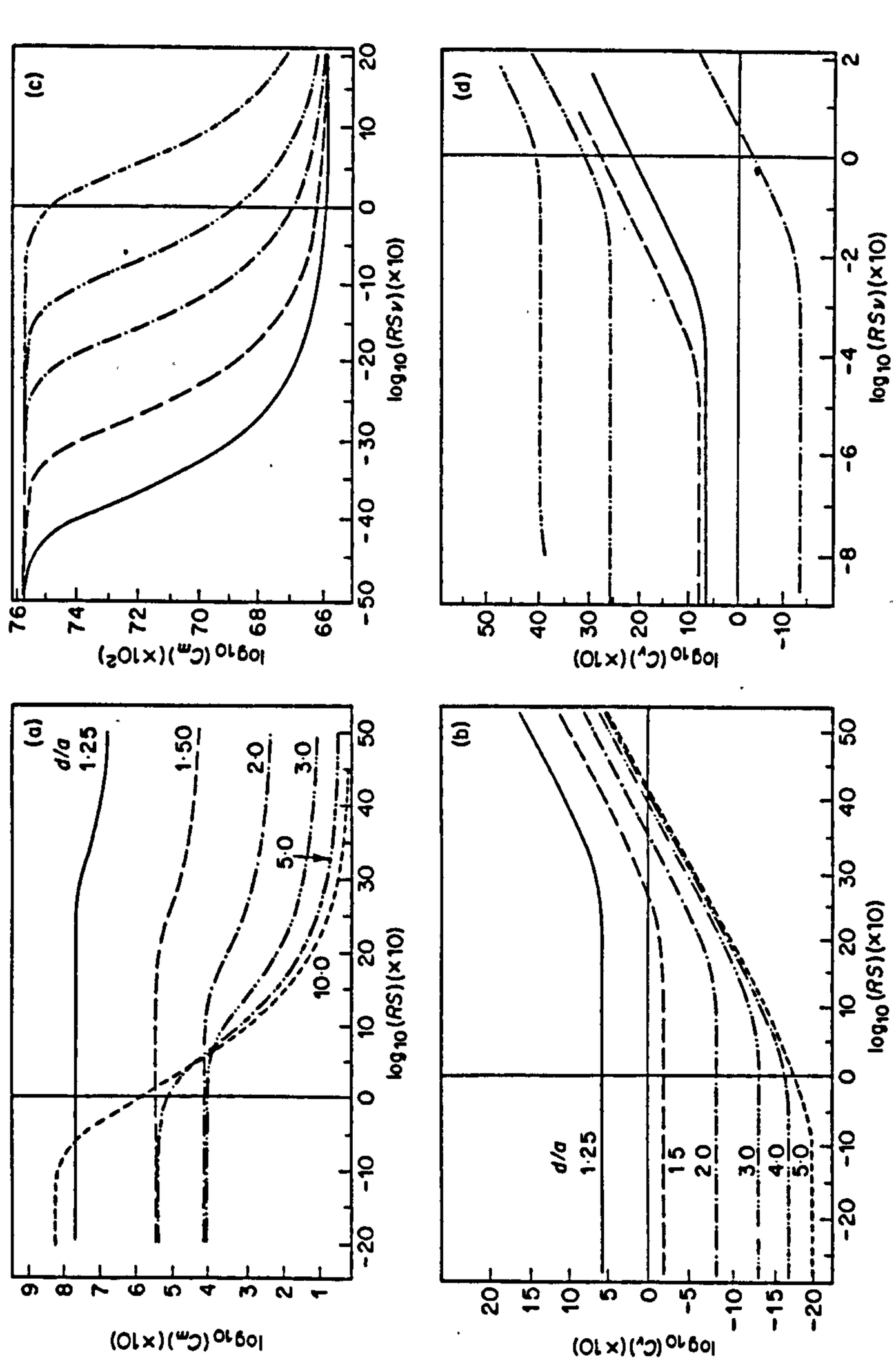

Figure 5. Changes in (a) added mass coefficient, C_m, and (b) damping coefficient, C_v, for different viscous fluids; $d/a = 1{\cdot}25$. Key for (c), (d): ——, water; – – –, mercury; – · –, air; – · · –, olive oil; — · —, glycerine. Variation of (c) added mass coefficient, C_m, and (d) damping coefficient, C_v, for selected values of d/a.

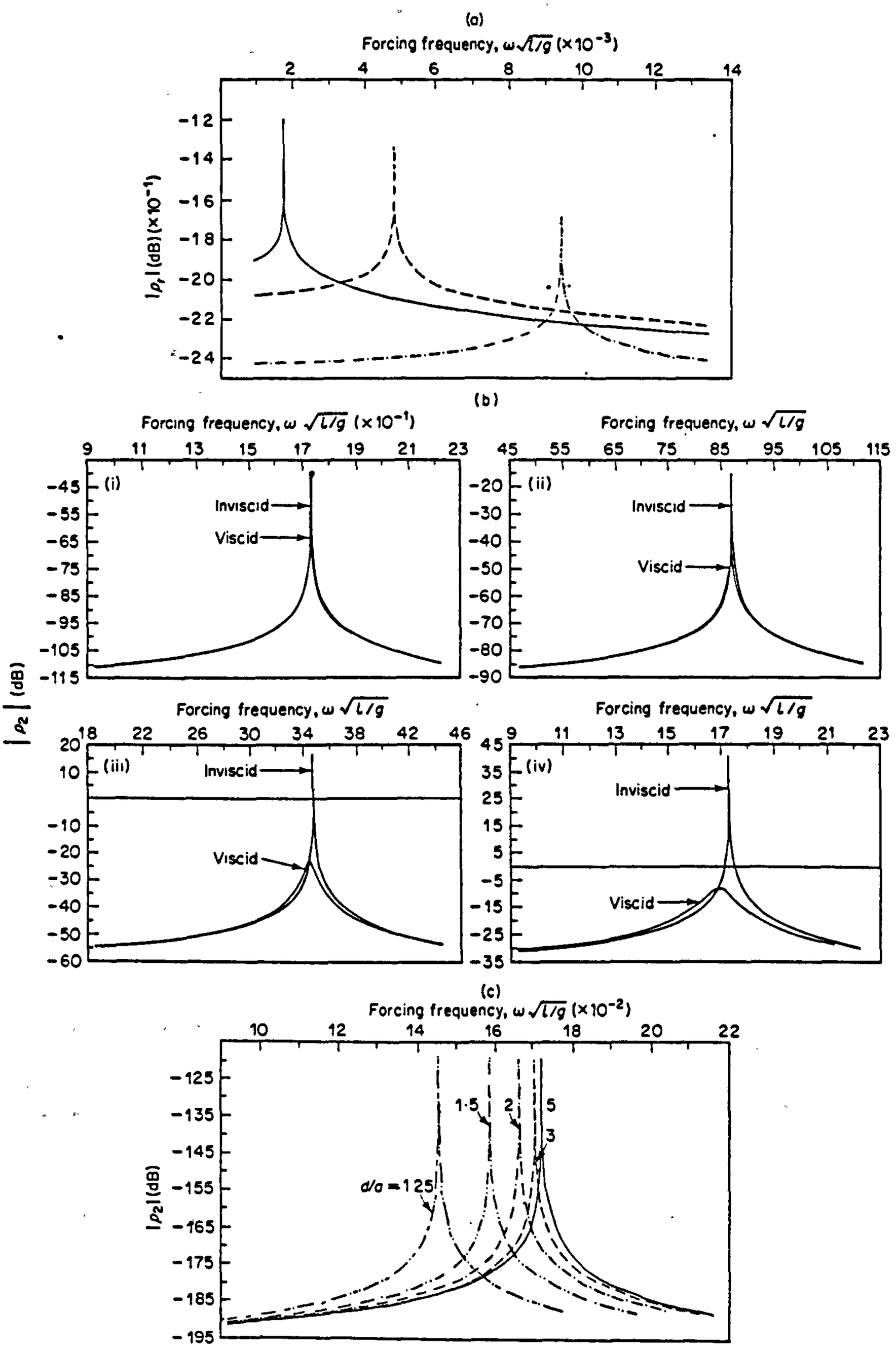

Figure 6. (a) Variation of principal co-ordinates $|p_r|$, $r = 2, 3, 4$, for uniform beam ($L/a = 10$, $d/a = 20$, $\nu =$ either 0 or $1{\cdot}14 \times 10^{-6}$ m^2/s (water)). ——, p_2; – – –, p_3; – · –, p_4. (b) Variation of principal co-ordinate $|p_2|$ showing effect of viscosity (L/a varies, $d/a = 20$); (i) $L/a = 100$; (ii) $L/a = 200$; (iii) $L/a = 500$; (iv) $L/a = 1000$. (c) Variation of principal co-ordinate $|p_2|$ of uniform beam for selected values of d/a ($L/a = 10$, $\nu =$ either 0 or $1{\cdot}14 \times 10^{-6}$ m^2/s (water)).

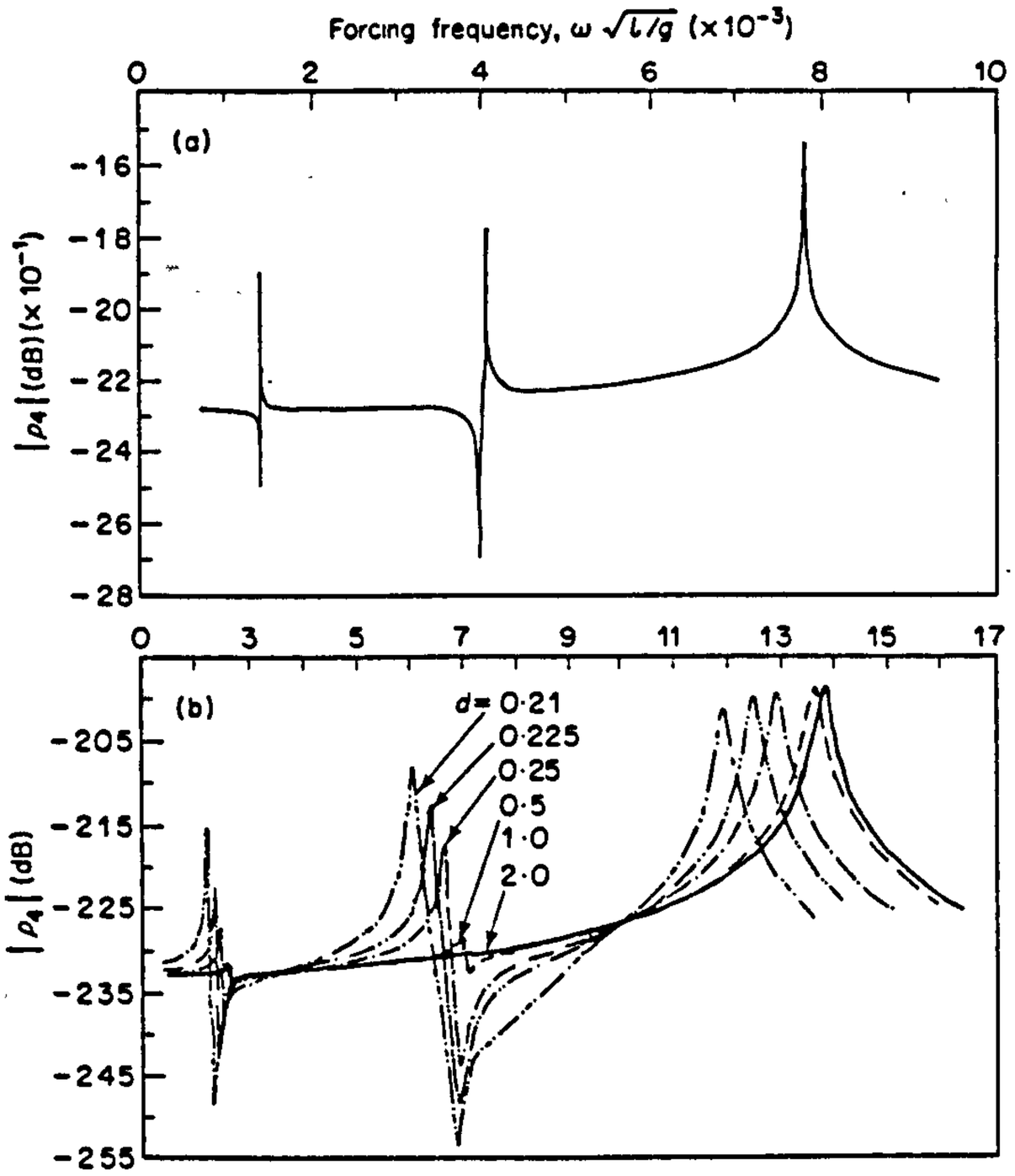

Figure 7. (a) Variation of principal co-ordinate $|p_4|$ of constant radius beam with non-uniform mass distribution ($L/a = 10$, $d/a = 20$, $\nu = 0$ or $1{\cdot}14 \times 10^{-6}$ m^2/s (water); $1{\cdot}0p$, $0 < x < 0{\cdot}5l$; $1{\cdot}5p$, $0{\cdot}5l < x < l$). (b) Variation of principal co-ordinate $|p_4|$ of non-uniform beam with decreasing annular clearance ($L/a = 10$, $x = 0$; $L/a = 5$, $x = L$; $\nu = 0$ or $1{\cdot}14 \times 10^{-6}$ m^2/s (water)).

longitudinal axis of the beam. With a tapered beam this gave rise to non-zero off-diagonal terms in the generalized hydrodynamic coefficients and, consequently, coupling between the principal co-ordinates. This will now be investigated further by considering a non-uniform beam surrounded by a discontinuous outer boundary.

Figure 8 provides a schematic illustration of a flexible projectile emerging from a circular tube. The projectile is assumed to be beam-like and of varying circular cross-section along its length. The projectile is surrounded by fluid and as the outer boundary is moved to the right, a crude simulation in a quasi-static manner of the launch of the projectile becomes possible. This allows the changes in the amplitude of the principal co-ordinate $|p_r|$ and the resonance frequencies ω_r to be monitored.

Figure 9 illustrates the change in $|p_r|$, $r = 2, 3, 4$, as the projectile moves from a state of enclosure within the tube to one of complete emergence. The resulting increase in resonance frequency values as the generalized hydrodynamic inertia coefficients reduce is evident, but what is slightly more unpredictable is the manner in which the resonance frequency values change with emerging length as shown in Figure 10 or the variation in the coupling between the principal co-ordinates. These variations are due to the interaction between the changing geometric shape of the projectile and the tube boundary influencing the generalized hydrodynamic coefficients.

When the surrounded water is treated as a viscous fluid no noticeable differences are observed in the resonance frequency values from those determined from the inviscid

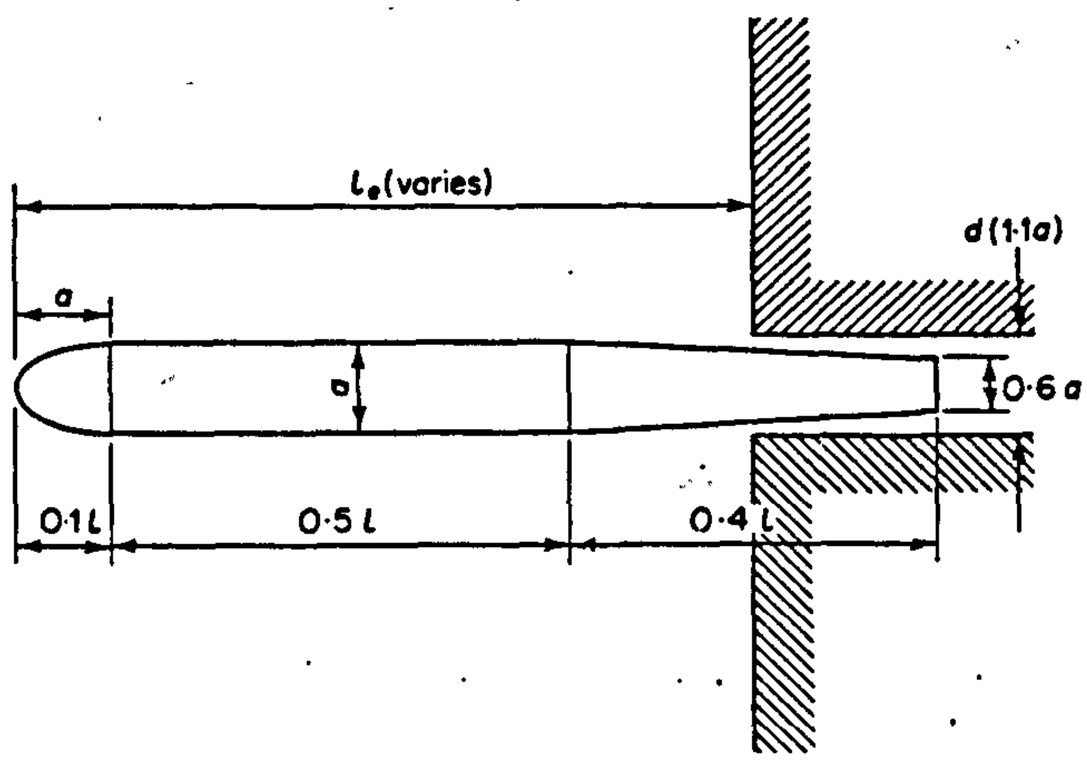

Figure 8. Non-uniform beam partially enclosed by rigid outer boundary.

model. The only change that occurs is an increase in the generalized hydrodynamic damping coefficient values, producing a reduction in the peak values of $|p_r|$. A mark is shown on each of the curves in Figure 9 to indicate the lower amplitude associated with the viscid fluid.

3.5. RESPONSES

The displacement and bending moment at any position x on the projectile excited by a sinusoidal generalized external loading are given by [1]

$$w(x,\ t) = \sum_{r=0}^{4} w_r(x) p_r\, e^{i\omega t}, \qquad M(x, t) = \sum_{r=2}^{4} M_r(x) p_r\, e^{i\omega t},$$

respectively, where for simplicity only five principal co-ordinates are admitted into the analysis. In these equations $M_r(x)$ denotes the rth principal bending moment mode and, as shown by the previous analysis, the amplitude p_r is a complex quantity.

In matrix form, the symmetrical vertical displacement at position x to an oscillatory applied unit amplitude force at position x' is given by [11]

$$w(x, x', t) = \mathbf{w}^{\mathrm{T}}(x)\mathbf{Q}(\omega)\mathbf{w}(x')\, e^{i\omega t};$$

where the complex valued function $\mathbf{Q}(\omega)$ is defined in equation (21) and $\mathbf{w}^{\mathrm{T}}(x)$ is the transpose of the column matrix $\mathbf{w} = \{w_0(x),\ w_1(x), \ldots, w_4(x)\}$.

A resonance condition is identified when $|\det \mathbf{D}(\omega)|$ in equation (21) is a minimum, at $\omega = \Omega$ (say), and the resonance displacement may be expressed as

$$w(x,\ x',\ t) = W(x,\ x',\ \Omega)\, e^{i\varepsilon(x,x',\Omega)}\, e^{i\Omega t}.$$

Here $W(x, x', \Omega)$ denotes the displacement amplitude associated with the "wet" resonance frequency Ω and $\varepsilon(x, x', \Omega)$ is the phase angle between the applied force at x' and the response at x measured from the stern.

If the complex receptance is expressed in the form $\mathbf{Q}(\Omega) = \mathbf{Q}^R(\Omega) + i\,\mathbf{Q}^I(\Omega)$, it follows that

$$W(x, x', \Omega) \cos \varepsilon(x, x', \Omega) = \mathbf{w}^{\mathrm{T}}(x) Q^R(\Omega) \mathbf{w}(x') = A_1 \quad \text{(say)},$$

$$W(x, x', \Omega) \sin \varepsilon(x, x', \Omega) = \mathbf{w}^{\mathrm{T}}(x) Q^I(\Omega) \mathbf{w}(x') = A_2,$$

where the phase angle satisfies the relationship $\tan \varepsilon(x, x', \Omega) = A_2/A_1$ and the vertical displacement amplitude is $W(x, x', \Omega) = (A_1^2 + A_2^2)^{1/2}$. In a full-scale measurement it is

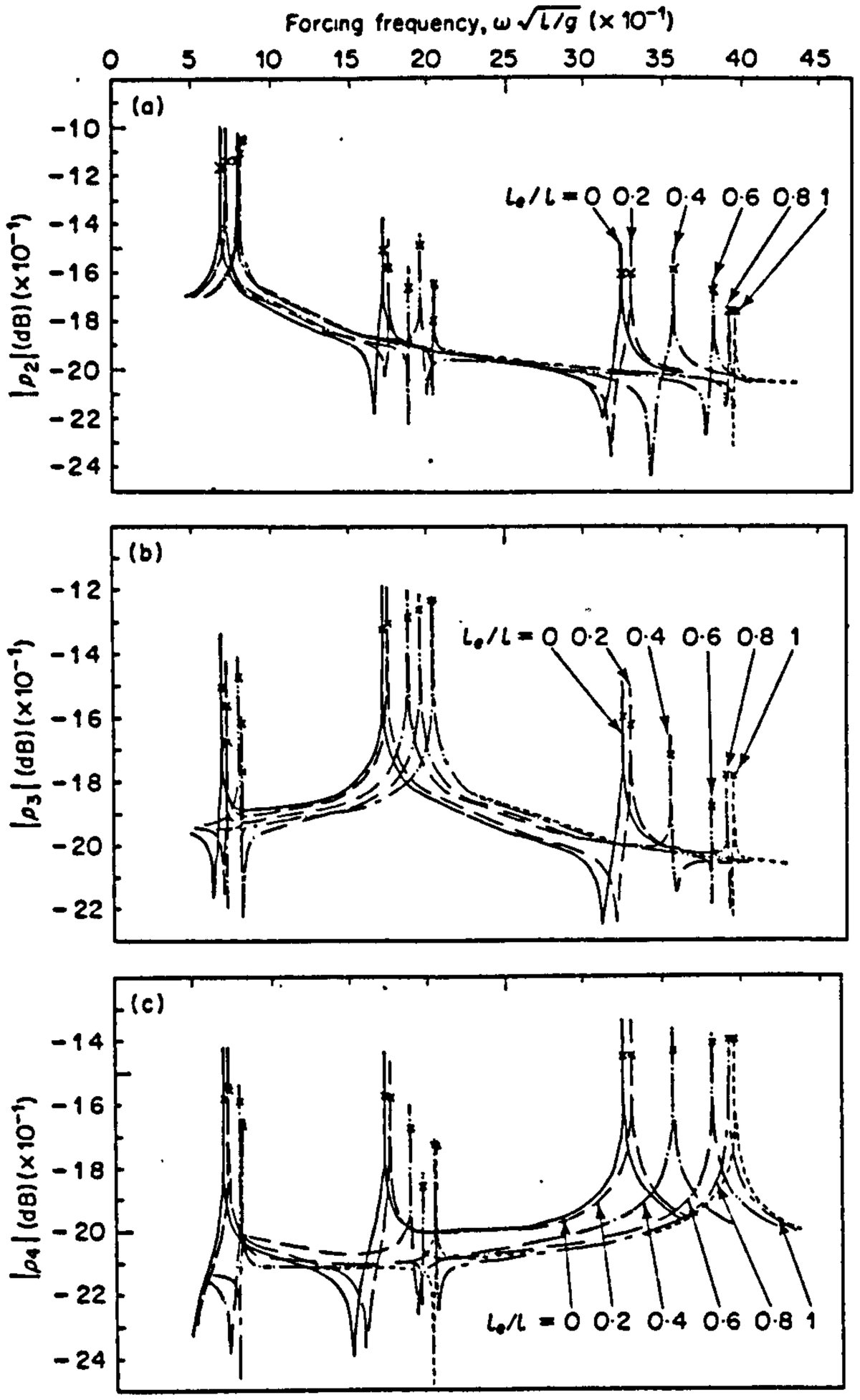

Figure 9. Variations of principal co-ordinates (a) $|p_2|$, (b) $|p_3|$ and (c) $|p_4|$ during simulated weapon launch, for various l_e/l (see Figure 8).

this displacement amplitude which is measured and this is commonly referred to as a "mode shape", being associated with a resonance condition. In particular, at $x=0$, $w(0, x', t) = W(0, x', \Omega)\, e^{i\varepsilon(0,x',\Omega)}\, e^{i\Omega t}$, and the resonance mode displacement at position x may be expressed in the normalized form

$$\frac{w(x, x', t)}{w(0, x', t)} = \frac{W(x, x', \Omega)}{W(0, x', \Omega)} \exp\left[i\{\varepsilon(x, x', \Omega) - \varepsilon(0, x', \Omega)\}\right],$$

where $W(x, x', \Omega)/W(0, x', \Omega)$ represents the normalized amplitude of the resonance mode shape of the cylinder in fluid and is independent of the amplitude of the input excitation. However, the dimensionless displacement is a complex quantity since there is a "space dependent" phase difference between the input and the output.

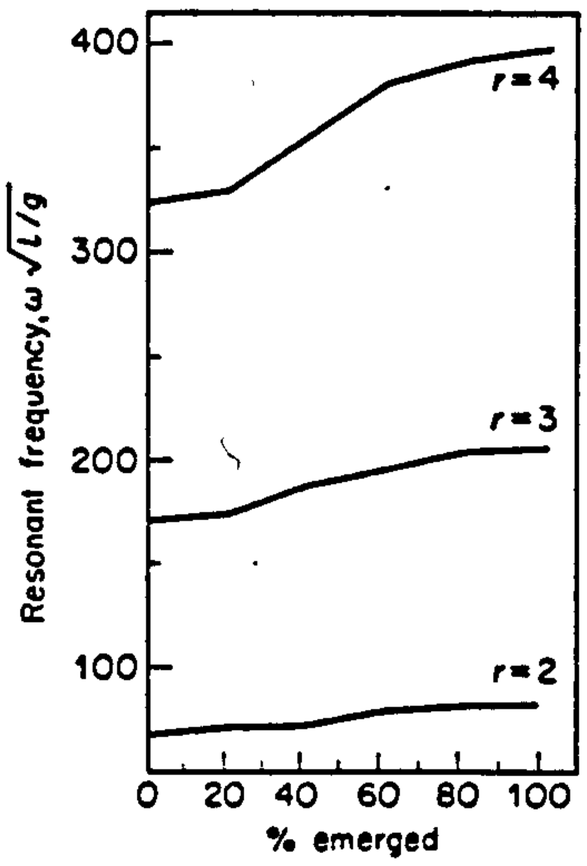

Figure 10. Variation in resonant frequencies during simulated projectile launch.

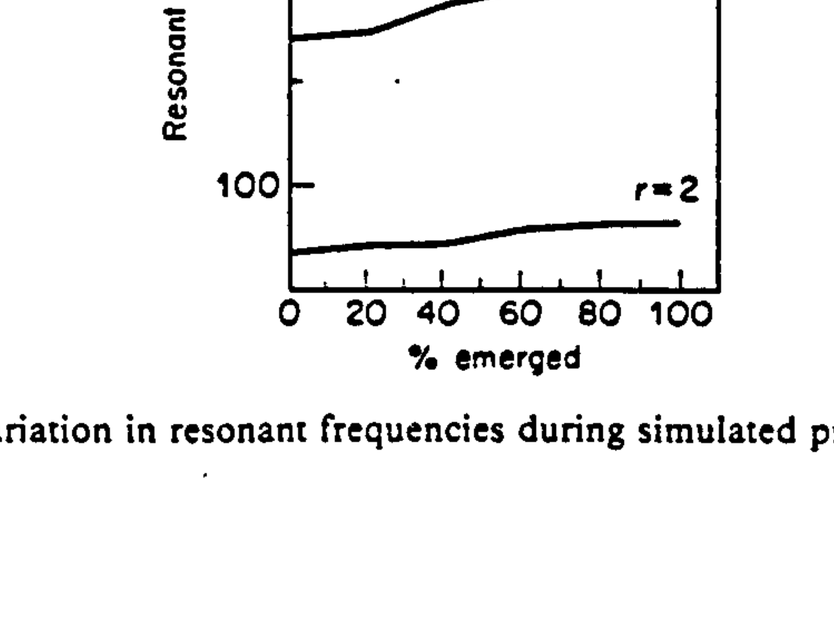

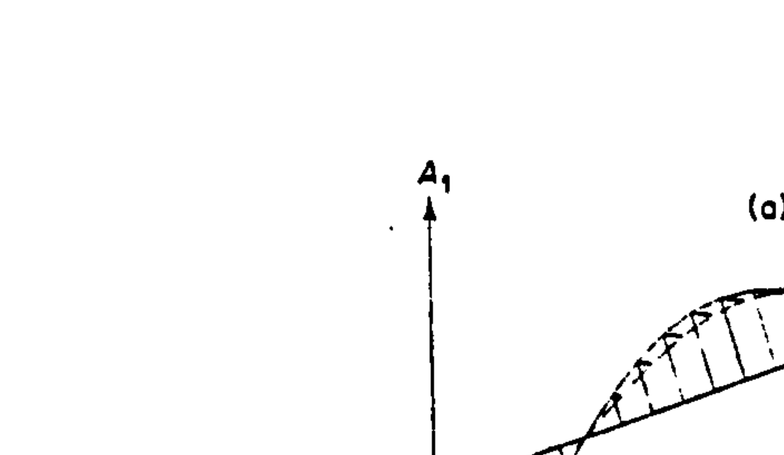

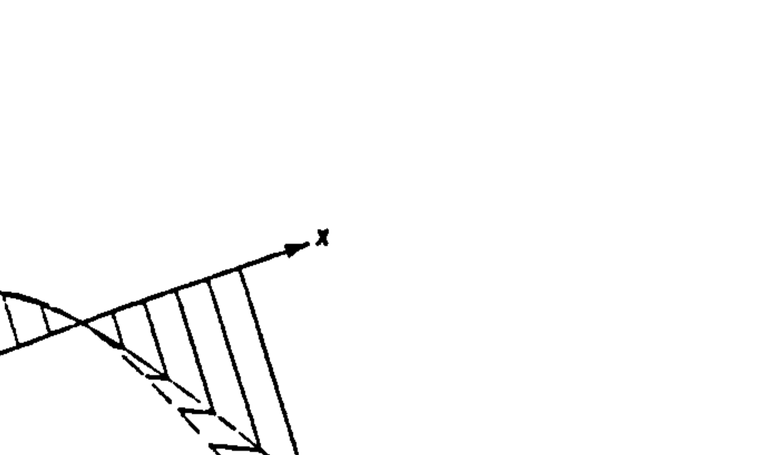

Figure 11. Mode shapes including phase relationships at (a) first, (b) second and (c) third resonant frequencies ($I_e/l = 0$).

The calculated results displayed in Figures 11 and 12 clearly demonstrate the complex characteristics of the vertical displacement at the first three lowest resonance frequencies. For the projectile in open water, Figure 11 illustrates the variation of the "mode shape" along the body as given by equation (24). The "twist" observed in the mode shape is due to the influence of the viscous fluid and structural damping. Figure 12 shows similar information but represented in terms of the normalized amplitude of the resonance mode shape and an accompanying phase angle, as defined by equation (28). The overall shapes of these normalized modes remain the same for both viscid and inviscid calculations, but

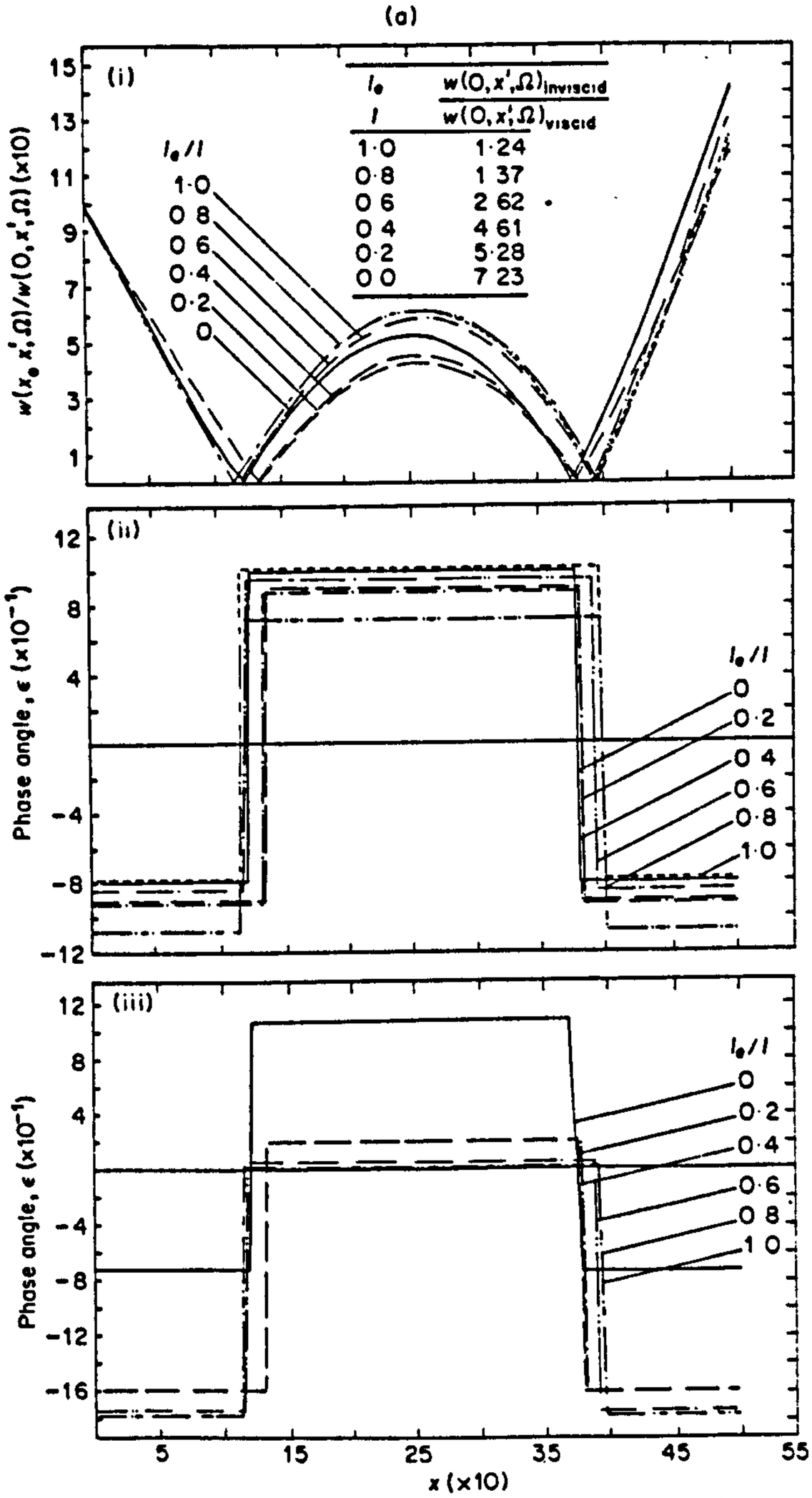

Figure 12. Normalized amplitudes and phase angles corresponding to (a) first, (b) second and (c) third resonant frequencies during simulated projectile launch; (i) amplitude; (ii) phase, angle, inviscid fluid; (iii) phase angle, viscous fluid ($\nu = 1{\cdot}14 \times 10^{-6}$ m^2/s (water)).

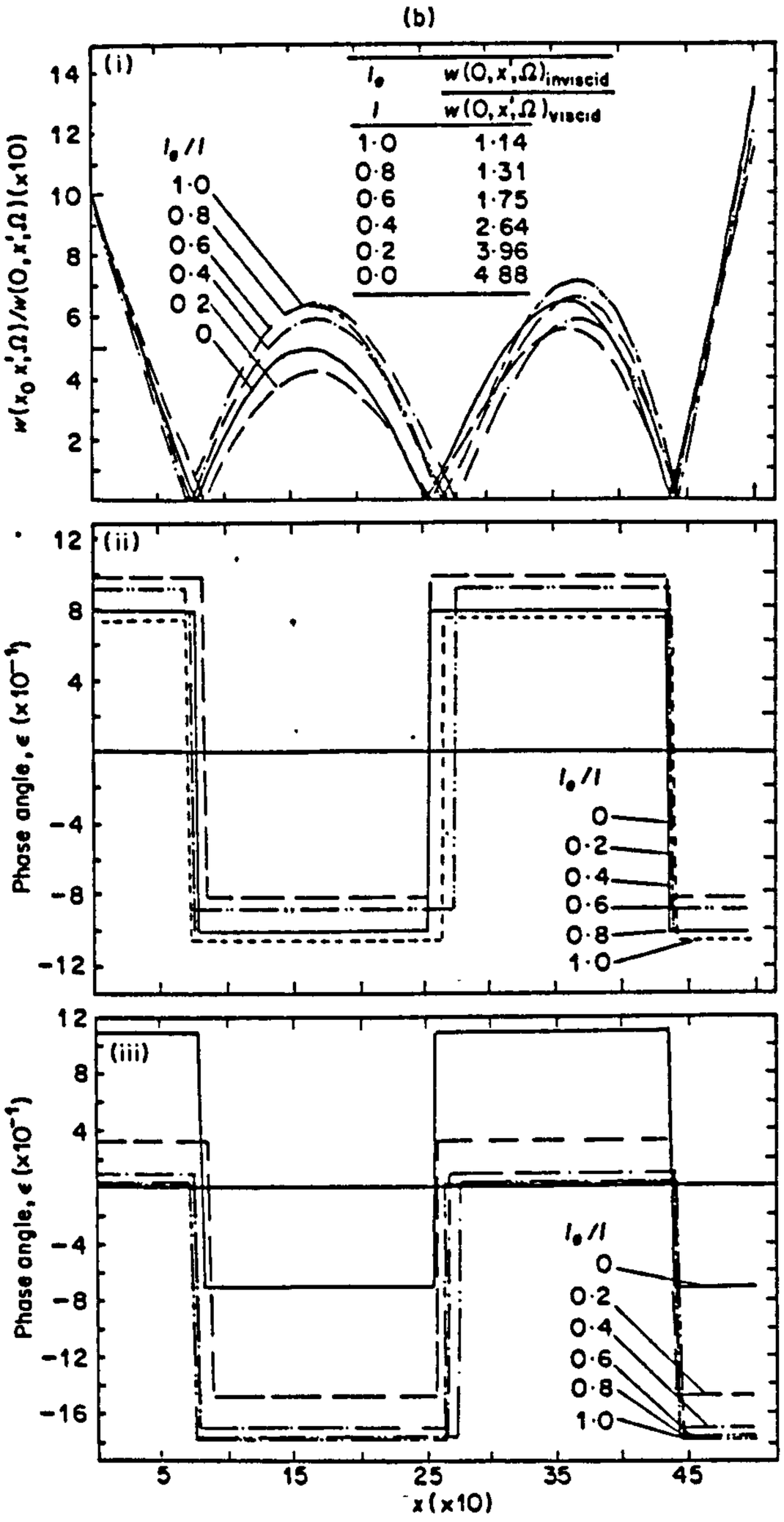

Figure 12—*continued.*

the magnitudes of the mode shapes differ because of the fluid description and the length of projectile emerging from the tube.

4. CONCLUSIONS

A modified hydroelasticity theory and hydroelastic analysis have been presented, accounting for the effect of fluid viscosity on the forced vibration characteristics of a cylindrical beam enclosed within a rigid tube. The influence of viscosity and annular clearance are clearly demonstrated by reference to their effects on resonance frequency values and on the characteristics of the principal coordinates. These are shown to depend

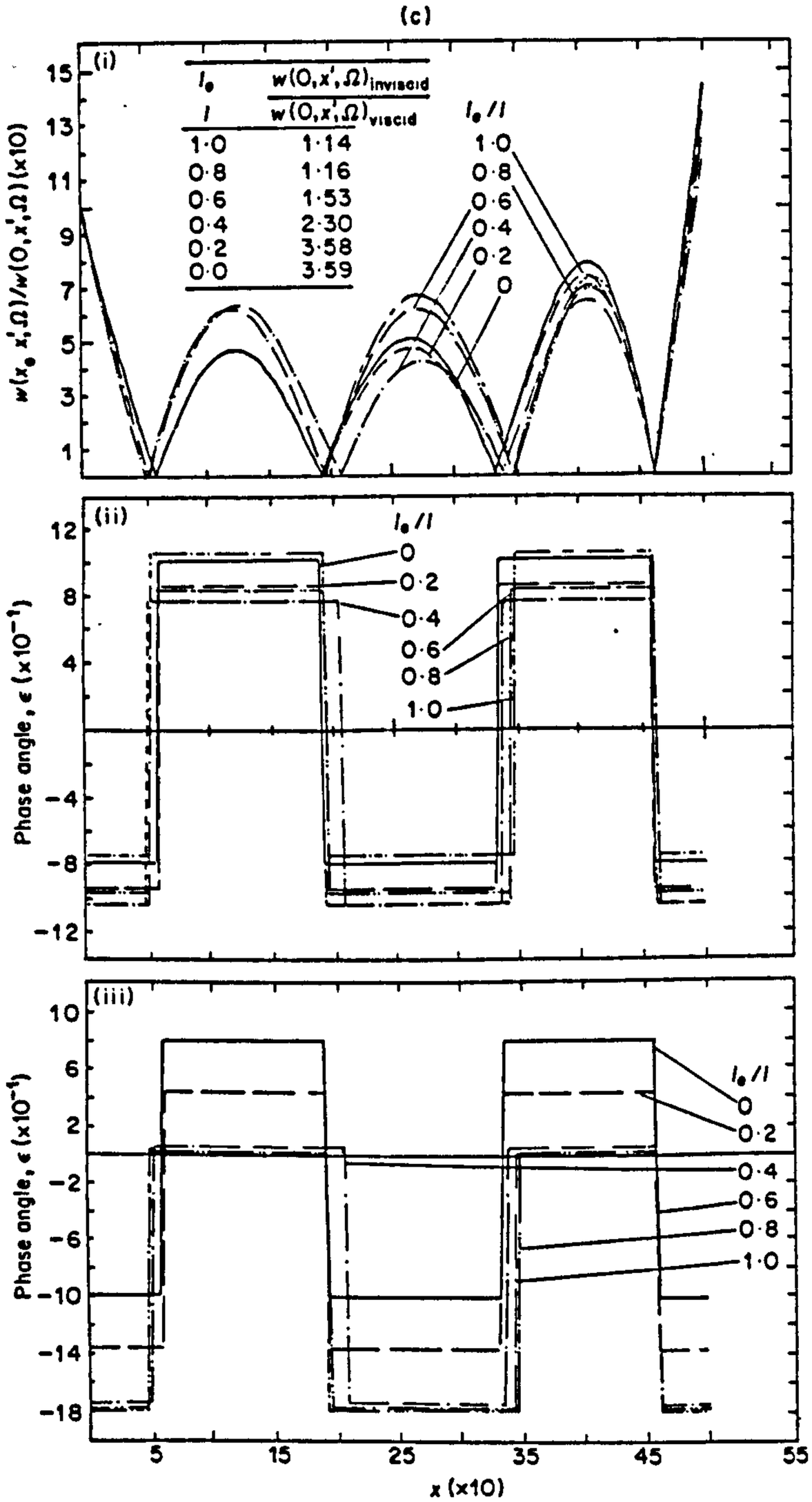

Figure 12—*continued.*

on the magnitude of the generalized external fluid loading which increases as the annular clearance decreases. Thus, the resonance frequency values decrease and stronger coupling is exhibited between the principal coordinates as the annular clearance value reduces. Only minor downward shifts in the resonance frequency values are observed when the viscid fluid (i.e., water) replaces the idealized inviscid fluid, but a decrease in the peak values of the principal co-ordinates occurs.

A simple representation of a projectile, as a non-uniform circular cylinder of varying cross-sectional radius along its length, allowed responses (i.e., displacement and bending

moment) to be evaluated for the projectile emerging from the tube. It is seen that the magnitudes of these responses are significantly diminished by assuming the fluid to be viscous, though similar trends are displayed in the results when the fluid is inviscid.

Although interest has been confined to the dynamical description of the interaction between a flexible cylinder and a rigid tube, analogous problems arise in naval architecture. For example, the dynamical behaviour of a long flexible pipe or slender structural member surrounded by a viscous medium (i.e., the case $\nu \neq 0$, $d \to \infty$); a propeller rotating in the vicinity of a hull or within a ring torus or shroud. In the last example, the generalized external fluid loading depends on tip clearance (i.e., annular clearance) and viscosity and by analogy with the idealized problem discussed, it is expected that the resonance frequency values of the propeller (or hull or shroud) and responses excited are greatly influenced by these two parameters (i.e. $d - a$ small and $\nu \neq 0$). In general, the surrounding or localized structure is also flexible (i.e., a non-rigid tube) and this dynamic influence must also be included in the description of the fluid-structure interactions arising between propeller and hull.

ACKNOWLEDGMENT

Professor Hosoda gratefully acknowledges the financial support of the Japan Society for the Promotion of Science (JSPS) during his stay in Brunel University.

REFERENCES

1. R. E. D. BISHOP and W. G. PRICE 1979 *Hydroelasticity of Ships.* Cambridge: Cambridge University Press.
2. G. G. STOKES 1843 *Proceedings of the Cambridge Philosophical Society* 8, 105–137. On some cases of fluid motion.
3. G. K. BATCHELOR 1967 *An introduction to Fluid Mechanics.* Cambridge: Cambridge University Press.
4. R. E. D. BISHOP and D. C. JOHNSON 1960 *The Mechanics of Vibration.* Cambridge: Cambridge University Press.
5. YOUSHENG WU 1984 *Ph.D. Thesis, Brunel University.* Hydroelasticity of floating bodies.
6. W. G. PRICE and YOUSHENG WU 1985 in *Theoretical and Applied Mechanics* (editors F. I. Niordson and N. Olhoff), 311–337. Hydroelasticity of marine structures. North Holland: Elsevier.
7. R. E. D. BISHOP, W. G. PRICE and YOUSHENG WU 1986 *Philosophical Transactions of the Royal Society London* A316, 375–426. A general linear hydroelasticity theory of floating structures moving in a seaway.
8. R. E. D. BISHOP, W. G. PRICE and ZHANG XICHENG 1983 *Proceedings of the Royal Society London* A388, 49–73. On the structural dynamics of a Vlasov beam.
9. S. S. CHEN, M. W. WAMBSGANSS and J. A. JENDRZEJCZYK 1976 *Journal of Applied Mechanics* 43(2), *Transactions of the American Society of Mechanical Engineers* 98, *Series E*, June 1976, 325–329. Added mass and damping of a vibrating rod in confined viscous fluids.
10. T. YEH and S. S. CHEN 1978 *Journal of Sound and Vibration* 59, 453–467. The effect of fluid viscosity on coupled tube/fluid vibrations.
11. R. E. D. BISHOP, W. G. PRICE and P. TEMAREL 1984 *CETENA, Genoa, Italy*, 1984, *Paper* 20. A study of mode shapes in hull vibration of low frequency.